ABSTRACT

Title of dissertation: ANALYSIS AND SYNTHESIS OF COLLECTIVE MOTION: FROM GEOMETRY TO DYNAMICS

Matteo Mischiati, Doctor of Philosophy, 2011

Dissertation directed by: Professor P. S. Krishnaprasad
Department of Electrical and Computer Engineering

The subject of this dissertation is collective motion, the coordinated motion of two or more individuals, in three-dimensional space. Inspired by the problems of understanding collective motion in nature and designing artificial collectives that can produce complex behaviors, we introduce mathematical methods for the analysis of collective motion data, and biologically-inspired algorithms for generating collective motion in engineered systems.

We explore two complementary approaches to the analysis and synthesis of collective motion. The first "top-down" approach consists in exploiting the geometry of n-body systems to identify certain elementary components of collective motion. A main contribution of this thesis is to reveal a new geometrical structure (fiber bundle) of the translation-reduced configuration space and a corresponding classification of collective motions alternative to the classical one based on reduction to shape space. We derive a mathematical framework for decomposing arbitrary collective motions into elementary components, which can help identify

the main modes of an observed collective phenomenon. We synthesize vector fields that implement some of the most interesting elementary collective motions, and suggest, whenever feasible, decentralized implementations.

The second "bottom-up" approach consists in starting from known biologically-plausible individual control laws and exploring how they can be used to generate collective behaviors. This approach is illustrated using the motion camouflage proportional guidance law as a building block. We show that rich and coordinated motion patterns can be obtained when two individuals are engaged in mutual pursuit with this control law. An extension of these dynamics yields coordinated motion for a collective of n individuals.

ANALYSIS AND SYNTHESIS OF COLLECTIVE MOTION: FROM GEOMETRY TO DYNAMICS

by

Matteo Mischiati

Dissertation submitted to the Faculty of the Graduate School of the
University of Maryland, College Park in partial fulfillment
of the requirements for the degree of
Doctor of Philosophy
2011

Advisory Committee:
Professor P. S. Krishnaprasad, Chair/Advisor
Professor Steven I. Marcus
Professor André L. Tits
Professor Alexander Barg
Professor William M. Goldman

Dedicated to my parents and to my wife

Acknowledgments

My advisor, Prof. Krishnaprasad, has provided me with invaluable guidance and support since the first day I stepped on campus. During the past five years, he has challenged me to improve my skills and stimulated me to explore new directions, while leaving significant research freedom. I am especially grateful to him for guiding me with patience through the fascinating world of differential geometry and for introducing me to a class of biologically-inspired problems that captured my imagination and became the underlying motivation for this dissertation. Furthermore, his standards of excellence in research and teaching, and his passion for science, have been a continuous source of inspiration.

I am grateful to Prof. Marcus, Prof. Tits, Prof. Barg and Prof. Goldman for their availability and useful feedback as members of my dissertation committee. The mentorship of Prof. Marcus, and the support of Prof. Martins, Prof. Papamarcou and Dr. Hassouneh when I served as their teaching assistant, have also greatly benefited my teaching skills.

I thank the staff of the Electrical and Computer Engineering Department and the Institute for Systems Research for their friendly and efficient assistance.

I am indebted to the research group of Dr. Cavagna in Rome for the flocking data used in section 3.6, and for sharing with me their experimental techniques during a very enjoyable field trip.

I want to thank my friends at the Intelligent Servosystems Lab with whom I shared research ideas, serious discussions or equally important laughs and jokes

(and the much awaited coffee trips to the faculty lounge), in particular Vishwa Reddy, Ermin Wei, Philip Twu, Graham Alldredge, Tetsuaki Nakano, Ben Flom, Biswadip Dey and Kevin Galloway. It was a pleasure sharing a big part of this "marathon" with fellow runner Kevin, and, in the final stretch, closely collaborating with Biswa on the analysis of starling flocks. Some of his algorithms and computational techniques were instrumental to the analysis of section 3.6.

Finally, I would not have made it this far without the love and support of my family, especially my parents and my wife. The encouragement and consistent engagement of my parents in my studies, as well as their help during the months following the birth of my daughter Ilaria, have been invaluable. My wife Lankika has been a great companion during these years, lovingly sharing with me all the sacrifices, ups and downs, and playing a leading role in our very own challenging and exciting n-body problem.

This research was supported in part by the Air Force Office of Scientific Research under AFOSR Grant Nos. FA95500410130, FA9550710446 and FA95501010250; by the Army Research Office under ARO Grant No. W911NF-0610325; by NIH-NIBIB grant 1 R01 EB004750-01, as part of the NSF/NIH Collaborative Research in Computational Neuroscience Program; by the ODDR&E MURI2007 Program Grant N000140710734 (through the Office of Naval Research); by a Graduate Fellowship from the Department of Electrical and Computer Engineering; and by a Future Faculty Fellowship from the School of Engineering of the University of Maryland.

Table of Contents

List of Tables

List of Figures

List of Symbols

$\cong$	diffeomorphic to
$T_m\mathcal{M}$	tangent space at m to manifold $\mathcal{M}$
$\langle ., . \rangle_m$	Riemannian metric evaluated at m
Fl_t^X	flow of vector field X
$[X, Y]$	Jacobi-Lie bracket of vector fields X, Y
Φ_g	group action associated to the group element g
$\mathcal{M}/G$	quotient space associated to action of group G on $\mathcal{M}$
$\mathrm{hor}(v_m)$	horizontal projection of a tangent vector v_m in total space
$\mathrm{lift}_m(v_b)$	horizontal lift at m of a tangent vector v_b in base space
ker	kernel (of a mapping)
dim	dimension (of a manifold)
tr	trace (of a matrix)
det	determinant (of a matrix)
$\mathrm{diag}(a, ..)$	diagonal matrix with elements a, ...
$\mathrm{sym}(A)$	symmetric part of matrix A
$\mathrm{skew}(A)$	skew-symmetric part of matrix A
$\mathbb{1}$	identity matrix
$\mathbb{0}$	zero matrix
$O(n)$	group of orthogonal matrices
$SO(n)$	group of special orthogonal matrices (with det $= 1$)
$SE(n)$	special euclidean group
$so(n)$	Lie algebra of $SO(n)$ (skew-symmetric matrices)
$\mathbb{R}^{3\times3}_{sym}$	space of symmetric matrices $\mathbb{R}^{3\times3}$
$\mathbb{R}^{3\times3}_{sym,>0}$	space of symmetric positive definite matrices $\mathbb{R}^{3\times3}$
$\mathcal{R}$	space of absolute collective configurations ($\cong \mathbb{R}^{3\times n}$)
$\mathcal{R}^{2^+d}$	absolute configurations that are at least $2d$ (not collinear)
$\mathcal{R}^{3d}$	absolute configurations that are $3d$ (not planar)
$\mathbf{r_i}$	absolute position of particle (agent) i
$\mathbf{r_{com}}$	absolute position of center of mass
$\mathbf{c_i}$	relative position of particle (agent) i (i.e. $\mathbf{r_i} - \mathbf{r_{com}}$)
$\mathcal{C}$	space of relative collective configurations (see (3.5))
$\mathcal{C}^{2^+d}$	relative configurations that are at least $2d$ (see (3.10))
$\mathcal{C}^{3d}$	relative configurations that are $3d$ (see (3.22))
$\mathcal{V}_{n,k}$	Stiefel manifold of orthonormal $\mathbb{R}^{n\times k}$ matrices
$\mathcal{K}$	space of full-rank coefficient of inertia tensors ($\cong \mathbb{R}^{3\times3}_{sym,>0}$)
$\mathbb{M}$	diagonal matrix of masses: $\mathbb{M} = \mathrm{diag}(m_1, m_2, ..., m_n)$
M	total mass (sum of masses)
W	fixed matrix in $\mathcal{V}_{n,n-1}$ orthogonal to $[\sqrt{m_1} \cdots \sqrt{m_n}]^T$
$f_{K,W}$	diffeomorphism between fiber over K and $\mathcal{V}_{n-1,3}$ (see (3.29))
$\mathcal{G}$	sensing network graph
$\mathcal{G}_\mathcal{C}$	communication network graph
$\mathrm{Rot}(\mathbf{e}, \alpha)$	rotation by an angle α about axis $\mathbf{e} \in \mathbb{R}^3$

Chapter 1

Introduction

Many observed phenomena in animal and human societies are characterized by the emergence of collective behavior from the individual actions of each member. Even though individuals typically have limited sensing and communication capabilities, and hence limited direct interaction with each other, large groups arise in which all the members appear to act in coordinated manner to achieve tasks that would be impossible or inefficiently performed by each member alone. Examples from biology include bird flocking and fish schooling, where moving collectively increases the individual chances of surviving a predator attack and to find food sources, or collective migration of cells within the body, such as platelets for wound-healing and, arguably, cancerous cells for metastasis [17]. From a biological perspective, there is great interest in finding the mechanisms that generate these collective behaviors, which are not yet fully understood.

Several simple mathematical models have been created over the years to reproduce some of the features displayed by natural collectives. For example in

[53] coordinated motion in a common direction is obtained when each individual adjusts its direction of motion based on the average direction of its neighbors. In [28] motion somewhat comparable to that of fish schools is achieved by combining, for each individual, attraction from far neighbors, repulsion from close neighbors, and velocity alignment with the neighbors that are within an intermediate range. A similar model presented in [24] was able to predict reasonably well the conditions for emergence of collective behavior among shoaling fish in a laboratory setting (but not in the field). While these models are useful to gain insight on the "ingredients" for obtaining collective behavior, and their simplicity is a virtue in this regard, they take only marginally into account the physical limitations of the animal species involved. As such, they are typically insufficient to postulate biologically-feasible models for the sensorimotor process guiding the actions of each individual of the collective. Moreover, there are recently discovered aspects of collective phenomena, such as the topological (as opposed to metric) interaction in flocks of starlings (see [3]), that violate some of the principles on which current models are based. In this context, a control-theoretical approach to modeling natural collectives, focused on searching feasible "control-laws" that each individual might be employing, could be very valuable to produce more realistic models.

Aside from the biological interest in collectives, in many engineering fields there has been a clear shift in emphasis from centralized and single-agent to distributed and multi-agent paradigms. For example, wireless sensor networks

and associated data fusion techniques have been developed to provide a cheaper and more robust alternative to centralized environmental monitoring. Similarly in robotics, multi-agent systems composed of simple robots are often preferred to systems based on a single sophisticated and expensive robot. The use of distributed algorithms permits decomposition of a complex task into simpler tasks that can be efficiently performed by simple agents; moreover the task execution is robust to failure or loss of some of the members of the team. In the quest for efficient distributed paradigms, it is sensible to search for inspiration in the natural world. Some natural collectives are in fact capable of robustly performing complicated tasks with limited sensing capabilities, in a way that is unmatched by even the most advanced artificial (robotic) multi-agent systems. For example the fascinating aerial displays of flocks of thousands of starlings are achieved despite the fact that each starling interacts directly with only a small number of its neighbors (estimated to be 6 or 7 in [3]). This justifies the growing interest in novel design paradigms for the cooperative control of robots that are inspired by the behavior of natural collectives, and aim at matching their performances.

The objective of this dissertation is to contribute to both the analysis of collective motion, especially in nature, and the synthesis of new biologically-inspired paradigms for the control of artificial formations. Towards this goal, we explore two complementary approaches.

The first approach consists in studying the geometry of multi-body systems, to identify motions that are elementary from a geometric point of view,

and methods for decomposing arbitrary collective motions into these elementary components. When dealing with very large and complex systems in motion, such as large flocks of birds, this "top-down" approach can help to uncover the underlying main "modes" of motion, which in turns can suggest efficient methods for analysis and modeling of these phenomena. Moreover, decomposition in elementary components can provide criteria for comparing different collective phenomena in nature.

The analysis of the geometry of multi-body systems in this thesis is based on the concepts of fiber bundle and connection, which are briefly recalled in chapter 2. These concepts have been used in the physics literature to precisely define *shape* and *shape transformations* of an n-body system. The rigid translation of such a system can be easily identified by isolating the motion of the center of mass from the relative particle motions with respect to the center of mass. It is more subtle, instead, to identify the rigid rotation of the system from other types of motion. This requires recognizing and exploiting the geometrical structure of a principal fiber bundle with principal connection induced by kinetic energy. The quotient space (shape space) in this bundle contains all the information on the n-body system that is invariant to rigid motions, and hence invariant to changes in the choice of the absolute reference frame; the fibers are instead diffeomorphic to the rotation group. Rigid rotations of the collective are the motions along the fibers, whereas shape transformations are the motions orthogonal to the fibers. One drawback of this fiber bundle is that the shape space is still high-dimensional

and has complicated topology.

In chapter 3, after introducing this classical fibering with a convenient notation (that does not require a choice of Jacobi vectors), we uncover an alternative geometric structure for the n-body problem. We show that the space of relative body positions (with respect to the center of mass) can also be interpreted as a fiber bundle with base space given by the set of full-rank coefficient of inertia tensors (closely related to the moment of inertia tensors). This base space is only 6-dimensional and is equivalent to the space of symmetric positive-definite 3×3 matrices. The fibers in this case are not diffeomorphic to a rotation group but to a Stiefel manifold, having non-trivial but well-known topology. The motions along the fibers are the "reshufflings" of individual positions which do not alter the coefficient of inertia tensor of the n-body system, whereas the motions orthogonal to the fibers are coefficient of inertia transformations.

Exploiting this geometric structure, it is possible to decompose any collective motion in terms of its effect on the coefficient of inertia tensor, the rigid motions it induces on the system, and the reshuffling of the particle positions (motion along the Stiefel manifold) it produces.

The knowledge of elementary collective motions also opens interesting opportunities in the design of artificial formations. An effective design approach can be to design implementations of the elementary motions, and then build more complicated motions, possibly mimicking natural collectives, by composi-

tion of elementary ones. Inspired by this consideration, we devote chapter 4 to the implementation of the new types of elementary motions that arise from the alternative fiber bundle uncovered in chapter 3. We focus, whenever possible, on distributed implementations based only on local sensing and communication between members of the collective.

The second approach explored in this dissertation consists in starting from known biologically-plausible individual control laws and analyzing how they can be combined to generate collective behaviors. Models of natural collective phenomena constructed with this "bottom-up" approach take inherently into account the biological limitations, and can therefore potentially produce improvements over the existing mathematical models, that are often too simplistic.

Control laws associated with pursuit strategies are natural candidates for use in the synthesis of collective motion. On the one hand, pursuit skills are highly developed in many animal species, as they are fundamental for critical tasks such as chasing prey or mates. On the other hand, it has been shown in mathematical models that local pursuit between neighboring members is a mechanism that can support the cohesive movement of multiple individuals. The cyclic pursuit scheme, in which the i-th element of a n-unit collective pursues the $(i+1)$-th element (modulo n), can produce for example coordinated motions for different choices of pursuit laws (see [20] and references therein).

A recurring pursuit strategy in nature is the one in which the pursuer

approaches a target while maintaining constant absolute direction of the baseline connecting the two positions. There is evidence that this strategy, referred to as *motion camouflage (with respect to infinity)* or *constant absolute target direction*, is used by hoverflies and dragonflies [41] [44] [50] as well as echolocating bats [21]. A steering law implementing this pursuit strategy in three-dimensional space has been postulated in [47], and its biological plausibility is supported, in the case of echolocating bats, by the experimental data in [46].

In chapter 5 we explore the use of this biologically-plausible control law as a "building block" to generate collective behaviors. We first investigate the case of two individuals engaged in mutual pursuit using this control law, and show that the resulting dynamics (called *mutual motion camouflage*) yields rich and coordinated motion patterns. We then suggest an extension of these dynamics to the case of multiple agents. The fact that this control law is biologically plausible also means that it can be implemented with limited sensing, computation and communication capabilities of each individual. This is a highly desired feature in the control of artificial formations, such as teams of unmanned air vehicles. Motivated by this observation, in recent papers [38] [40] we have adapted the mutual motion camouflage system, to make it a useful tool for the design of artificial formations that can perform spatial coverage tasks with limited individual resources.

We conclude the dissertation summarizing the key results and suggesting possible future directions of research in chapter 6.

Chapter 2

Mathematical background

In this chapter, we briefly introduce the concepts of fiber bundle, connection, and horizontal lift, used extensively in chapter 3. Understanding of these concepts requires a certain familiarity with the basic concepts of manifold, vector field, Riemannian metric, Lie group and group action, that are assumed to be already familiar to the reader. Nevertheless we describe in some detail a specific manifold, the *Stiefel manifold*, which is important for the analysis of chapter 3. The material in this chapter is based on [27], [1], [10], [37] (for fiber bundles and connections), [56](for mechanical connection) and [19](for the Stiefel manifold).

2.1 Fiber bundles

Definition 2.1.1 (Fiber bundle) Let P, F, B be smooth manifolds, referred to as *total space*, *fiber* and *base space* respectively. Let $\pi : P \to B$ be a smooth surjective submersion, i.e. a smooth onto mapping whose derivative $d\pi_p$ is onto $\forall p \in P$, referred to as the *bundle projection*. Then the tuple (P, π, B, F) is a

(smooth) fiber bundle if $\forall b \in B$ the inverse image $\pi^{-1}(b)$, called the *fiber over* b, is a diffeomorphic copy of the fiber F, and each $b \in B$ has a neighborhood $U \subset B$ and a *fiber-respecting* diffeomorphism $\varphi : \pi^{-1}(U) \to U \times F$ which completes the following diagram (here $\mathrm{pr}_1(u, f) \triangleq u,\ \forall u \in U, f \in F$):

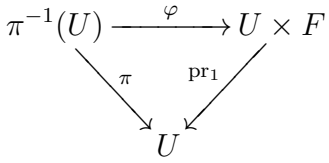

Hence $\pi^{-1}(U)$ is diffeomorphic to $U \times F$, and every point $p \in \pi^{-1}(U)$ can be uniquely identified by a pair $(b, f), b \in U, f \in F$. This property is called *local triviality* of a fiber bundle, and if it holds globally (i.e. $P \cong B \times F$) the fiber bundle is called *globally trivial*.

We will sometimes denote the fiber bundle with just the triple (P, π, B), when we are not interested in specifying the fiber manifold.

The pair (U, φ) is called a *fiber chart*, and a collection of fiber charts $(U_\alpha, \varphi_\alpha)$ such that $\{U_\alpha\}$ is an open cover of P is called a *fiber bundle atlas*.

A smooth injective mapping that associates to each $b \in B$ an element of the fiber over b, is called a *cross section* of the fiber bundle. Choosing a cross section for a fiber bundle corresponds to choosing a "reference element" on each fiber.

The following lemma from [37] gives sufficient conditions for a fiber bundle. Notice that in the proof of the lemma, $\mathfrak{X}$ is the space of vector fields and Fl_t^X is the flow of a vector field $X \in \mathfrak{X}$.

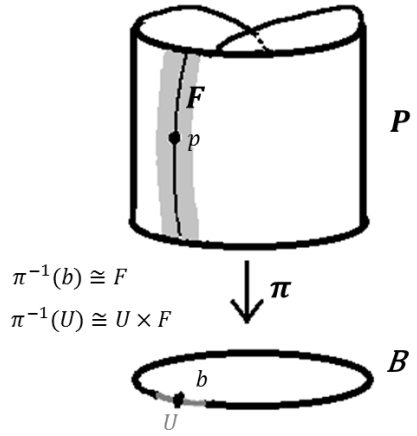

Figure 2.1: Graphical representation of a fiber bundle. The black line passing through $p \in P$ is the fiber over $b = \pi(p)$. The shaded region is $\pi^{-1}(U)$, where U is an open neighborhood of $b \in B$.

Lemma 2.1.2 (**[37], Lemma 17.2).** *Let $\pi : P \to B$ be a surjective submersion which is proper, so that $\pi^{-1}(K)$ is compact in P for each compact $K \subset B$, and let B be connected. Then (P, π, B) is a fiber bundle.*

Proof. We have to produce a fiber chart at each $b_0 \in B$. So let (U, u) be a manifold chart centered at b_0 on B such that $u(U) \cong \mathbb{R}^m$ (m being the dimension of manifold B). For each $b, y \in U$ let $\xi_b(y) := (T_y u)^{-1} u(b)$; then we have $\xi_b \in \mathfrak{X}(U)$ which depends smoothly on $b \in U$, such that $u(\mathrm{Fl}_t^{\xi_b} u^{-1}(z)) = z + tu(b)$. Thus each ξ_b is a complete vector field on U. Since π is a submersion, with the help of a partition of unity on $\pi^{-1}(U)$ we may construct vector fields $\eta_b \in \mathfrak{X}(\pi^{-1}(U))$ which depend smoothly on $b \in U$ and are π-related to $\xi_b : T_\pi \eta_b = \xi_b \circ \pi$. Thus $\pi \circ \mathrm{Fl}_t^{\eta_b} = \mathrm{Fl}_t^{\xi_b} \circ \pi$, so $\mathrm{Fl}_t^{\eta_b}$ is fiber-respecting, and since π is proper and ξ_b is complete, η_b

has a global flow too. Denote $\pi^{-1}(b_0)$ by F. Then $\varphi : U \times F \to \pi^{-1}(U)$, defined by $\varphi(b, f) = \mathrm{Fl}_t^{\eta_b}(f)$, is a diffeomorphism and is fiber-respecting, so (U, φ^{-1}) is a fiber chart. Since B is connected, the fibers $\pi^{-1}(b)$ are all diffeomorphic. $\square$

Remark 2.1.3 If the hypothesis of lemma 2.1.2 hold and $B \cong \mathbb{R}^m$ (for some m), then the fiber bundle is *globally trivial*, i.e. $P \cong B \times F$.

Another sufficient condition for a fiber bundle is the existence of a free and proper action of a Lie group on a manifold; the resulting fiber bundle is called *principal*.

Definition 2.1.4 (**Principal fiber bundle**) Let G be a Lie group acting freely and properly (say on the left) on the smooth manifold P, i.e. for each $g \in G$ there exists a mapping $\Phi_g : P \to P$ such that $\Phi_g(p) = p \Leftrightarrow g = e$, the identity of the group, $\Phi_{gh}(p) = \Phi_g(\Phi_h(p)) \forall g, h \in G, p \in P$, and moreover the mapping $(g, p) \mapsto (\Phi_g(p), p)$ is proper (the inverse image of every compact set is compact). Let B be the quotient space P/G, whose elements are the equivalence classes associated to the equivalence relation $p \sim p' \iff \exists g \in G \, s.t. \, p' = gp$, and let π be the (projection) map from each point of P into its equivalence class. Then (P, π, B, G) is a *principal fiber bundle*. The fibers are in this case diffeomorphic to the Lie group G, and the choice of a cross section can be thought of as the choice of which element is diffeomorphic to the identity within each fiber.

2.2 Connections and horizontal lifts

Given a fiber bundle (P, π, B, F) and a point $p \in P$, the derivative of the projection at p (denoted as $d\pi_p$) maps every tangent vector $v_p \in T_pP$ into a corresponding tangent vector $v_{\pi(p)} \in T_{\pi(p)}B$. If $v_p \in \ker(d\pi_p)$, the tangent vector is along the fiber direction; we call tangent vectors of this type as *vertical* and $V_p \triangleq \ker d\pi_p$ as the *vertical space* at p.

Definition 2.2.1 (**Ehresmann connection**) An *Ehresmann connection* A is a vertical valued one-form on P made of linear vertical projections: $\forall p \in P$, $A_p : T_pP \to V_p$ is a linear map and $A_p(v_p) = v_p \quad \forall v_p \in V_p$.

When an Ehresmann connection is specified, it is possible to define, $\forall p \in P$, an *horizontal space* $H_p \triangleq \ker A_p$ such that $T_pP = V_p \oplus H_p$. This allows to split uniquely any total space tangent vector into a vertical part and an horizontal part.

Notice that if the manifold P is equipped with a Riemannian metric $\langle ., . \rangle_p : T_pP \times T_pP \to \mathbb{R}$, then an Ehresmann connection can be defined by taking the orthogonal projection:

$$A_p(v_p) \triangleq \arg \min_{w_p \in V_p} \langle w_p - v_p, w_p - v_p \rangle_p, \forall v_p \in T_pP. \tag{2.1}$$

Given a tangent vector $v_p \in T_pP$, there exists a unique horizontal vector $\mathrm{hor}(v_p) \triangleq v_p - A_p(v_p)$, which we call the *horizontal projection* of v_p (for a given choice of connection). When the connection is defined as in (2.1), then $\langle \mathrm{hor}(v_p), A_p(v_p) \rangle_p = 0$. Conversely, given a tangent vector $v_b \in T_bB$ and a point

$p \in \pi^{-1}(b)$, there exist many tangent vectors in T_pP that project to v_b under $d\pi_p$, but only one that is horizontal (for the given choice of connection). We refer to this vector as the *horizontal lift* of v_b to T_pP, or as $\text{lift}_p(v_b)$, and we obtain it as: $\text{lift}_p(v_b) = \text{hor}(w_p)$, where $w_p \in T_pP$ is any tangent vector that projects to v_b under $d\pi_p$.

The *curvature* of an Ehresmann connection is the vertical-valued two-form acting on two vector fields X, Y on P as follows:

$$B(X,Y) \triangleq -A([\text{hor}(X), \text{hor}(Y)]), \tag{2.2}$$

where the bracket on the right-hand side is the Jacobi-Lie bracket of vector fields. The curvature two-form is a measure of the vertical displacement (along the fiber) that is obtained upon following a trajectory in total space produced by horizontal lift of a closed curve in base space.

In the context of principal fiber bundles, the splitting of tangent vectors into horizontal and vertical components is performed with respect to a *principal connection*, defined as follows.

Definition 2.2.2 (Principal connection) A *principal connection* $\mathcal{A}$ on the principal bundle $(P, \pi, P/G, G)$ is an equivariant $\mathfrak{g}$-valued one form $\mathcal{A} : TP \to \mathfrak{g}$ that satisfies, $\forall p \in P$, the "projection property": $\mathcal{A}(\xi_P(p)) = \xi \quad \forall \xi \in \mathfrak{g}$. Here $\mathfrak{g}$ is the Lie algebra of the Lie group G and ξ_P is the infinitesimal generator corresponding to $\xi \in \mathfrak{g}$:

$$\xi_P(p) \triangleq \left.\frac{d}{dt}\right|_{t=0} \Phi_{exp(t\xi)}(p). \tag{2.3}$$

As in the case of the Ehresmann connection, the vertical and horizontal spaces at $p \in P$ can be defined as $V_p \triangleq \ker d\pi_p$ and $H_p \triangleq \ker \mathcal{A}_p$ respectively. Indeed the two definitions of connection are strictly related for principal fiber bundles, and an Ehresmann connection A can be obtained from a principal connection $\mathcal{A}$ as: $A(v_p) = (\mathcal{A}(v_p))_P(p)$.

The equivariance property of $\mathcal{A}$ requires that: $\mathcal{A}(T_p\Phi_g(v_p)) = Ad_g\mathcal{A}(v_p)$, $\forall v_p \in T_pP, g \in G$, where Ad_g is the adjoint action of G, which is the derivative at the origin of the map $\Psi_g : G \to G, h \mapsto \Psi_g(h) \triangleq ghg^{-1}$; this property guarantees that horizontal vectors get mapped into horizontal vectors by the derivative of the group action.

The curvature of a principal connection form $\mathcal{A}$ is defined similarly to (2.2): $\mathcal{B}(X, Y) \triangleq -\mathcal{A}([\text{hor}(X), \text{hor}(Y)])$.

Given a principal fiber bundle and a metric that is invariant under the action of the group, the principal connection that gives orthogonal splitting of tangent vectors with respect to the metric is called *mechanical connection* and is obtained as follows.

Definition 2.2.3 (**Mechanical connection**) The *mechanical connection* $\mathcal{A}$ on the principal fiber bundle $(P, \pi, P/G, G)$, associated to metric $\langle ., . \rangle$ on P, is given by:

$$\mathcal{A} : TP \to \mathfrak{g}, \quad \mathcal{A}_p(v_p) \triangleq I_p^{-1} J(v_p), \tag{2.4}$$

where J is the equivariant *momentum map*:

$$J : TP \to \mathfrak{g}^*, \quad (J(v_p))(\xi) \triangleq \langle v_p, \xi_P(p) \rangle, \quad \forall \xi \in \mathfrak{g}, \tag{2.5}$$

and I is the *locked inertia tensor* defined, $\forall p \in P$, as:

$$I_p : \mathfrak{g} \to \mathfrak{g}^*, \quad (I_p(\eta))(\xi) \triangleq \langle \eta_P(p), \xi_P(p) \rangle, \quad \forall \eta, \xi \in \mathfrak{g}. \tag{2.6}$$

Here I_p is just a compact notation for $I(p)$; the two notations will be used interchangeably in this dissertation.

Notice that the horizontal vectors associated to connection (2.4) are those in the kernel of the momentum map (2.5). The motivation for using the term *mechanical connection* is that if the principal fiber bundle is associated to a *simple mechanical system with symmetry* [48], where $G = SO(3)$ acts from the left on the configuration space P and the Riemannian metric is the kinetic energy ($SO(3)$-invariant), then the momentum map is the angular momentum, and horizontal vectors have the clear mechanical meaning of zero angular momentum value.

To see that this connection is the one giving orthogonal splitting of tangent vectors, observe that:

$$\begin{aligned}
(J(v_p - (I_p^{-1} J(v_p))_P(p)))(\xi) &= \langle v_p - (I_p^{-1} J(v_p))_P(p), \xi_P(p) \rangle_p = \\
&= \langle v_p, \xi_P(p) \rangle_p - \langle (I_p^{-1} J(v_p))_P(p), \xi_P(p) \rangle_p = \\
&= (J(v_p))(\xi) - (I_p(I_p^{-1} J(v_p)))(\xi) = 0 \ \forall \xi \in \mathfrak{g},
\end{aligned}$$

hence, $\forall v_p \in T_p P$:

$$\langle v_p - (I_p^{-1} J(v_p))_P(p), (I_p^{-1} J(v_p))_P(p) \rangle_p = (J(v_p - (I_p^{-1} J(v_p))_P))(I_p^{-1} J(v_p)) = 0.$$

Given a principal fiber bundle with a Riemannian metric invariant under the group action, and given the corresponding mechanical connection, then one can define an induced metric on the base (quotient) space as follows:

$$\langle v_b, w_b \rangle_b = \langle \text{lift}_p v_b, \text{lift}_p w_b \rangle_p \quad \forall b \in B,\ v_b, w_b \in T_b B, \tag{2.7}$$

where p is any point belonging to the fiber over b.

Similarly, let a fiber bundle (not principal) and the Ehresmann connection which gives orthogonal splitting of tangent vectors (with respect to a Riemannian metric) be given. Then (2.7) can still be used to define an induced metric on base space, provided that the Riemannian metric on total space is "bundle-like" i.e. it satisfies: $\langle v_p, w_p \rangle_p = \langle v_q, w_q \rangle_q\ \forall p, q \in \pi^{-1}(b),\ \forall v_p, w_p \in H_p,\ v_q, w_q \in H_q$ such that $d\pi_p(v_p) = d\pi_q(v_q) = v_b,\ d\pi_p(w_p) = d\pi_q(w_q) = w_b$.

2.3 Stiefel manifold

Definition 2.3.1 (**Stiefel manifold**) The *Stiefel manifold* $\mathcal{V}_{n,k}$ is the smooth manifold composed of "thin" orthonormal matrices:

$$\mathcal{V}_{n,k} \triangleq \{V \in \mathbb{R}^{n \times k} : \quad V^T V = \mathbb{1}\}, \tag{2.8}$$

where $k \leq n$ and $\mathbb{1}$ is the $k \times k$ identity matrix.

The Stiefel manifold is also equal to the quotient space $O(n)/O(n-k)$, with equivalence relation on $O(n)$:

$$O_1 \sim O_2 \Leftrightarrow \exists Q \in O(n-k)\ s.t.\ O_2 = O_1 \begin{bmatrix} \mathbb{1} & \mathbb{0} \\ \mathbb{0} & Q \end{bmatrix}. \tag{2.9}$$

From (2.8), it's easy to verify that the tangent space to an element V of the Stiefel manifold is given by:

$$T_V\mathcal{V}_{n,k} = \{\Delta \in \mathbb{R}^{n\times k} : \quad V^T\Delta + \Delta^T V = \mathbb{O}\}. \tag{2.10}$$

Hence tangent vectors must be such that $\Delta^T V$ is skew, and for this to be the case they must have the form: $\Delta = VA + V^\perp B$, for $A \in \mathbb{R}^{k\times k}$ skew, $V^\perp \in \mathbb{R}^{n\times(n-k)}$ s.t. $V^T V^\perp = \mathbb{O}$ and $B \in \mathbb{R}^{(n-k)\times k}$ arbitrary.

Lemma 2.3.2. *The* **canonical metric on the Stiefel manifold** *induced by the Frobenius metric for $O(n)$ is given by:*

$$\langle \Delta_1, \Delta_2\rangle_V = \frac{1}{2}\mathrm{tr}(A_1^T A_2) + \mathrm{tr}(B_1^T B_2) = \mathrm{tr}(\Delta_1^T(\mathbb{1} - \frac{1}{2}VV^T)\Delta_2) \tag{2.11}$$

Proof. We proceed in the way explained at the end of Section 2.2, exploiting the definition of the Stiefel manifold as the quotient space $O(n)/O(n-k)$, with equivalence relation (2.9). We start with tangent vectors to $Q \in O(n)$, which have the form $\Lambda = QE$ for E skew-symmetric. The flows of vertical vector fields leave unchanged the first k columns of Q, and therefore the vertical tangent vectors are those of the form $\Lambda = Q\begin{bmatrix} \mathbb{O} & \mathbb{O} \\ \mathbb{O} & C \end{bmatrix}$ with $C \in \mathbb{R}^{(n-k)\times(n-k)}$ skew-symmetric.

The Frobenius (Riemannian) metric on $O(n)$ is defined as: $\langle \Lambda_1, \Lambda_2\rangle_Q = \mathrm{tr}(\Lambda_1^T\Lambda_2) = \mathrm{tr}(E_1^T E_2)$ and does not depend on Q. If we consider the orthogonal splitting of tangent vectors to $O(n)$ with respect to this metric, it is easy to see that horizontal vectors are those of the form $\Lambda = Q\begin{bmatrix} A & -B^T \\ B & \mathbb{O} \end{bmatrix}$ for $A \in \mathbb{R}^{k\times k}$

skew, and $B \in \mathbb{R}^{(n-k)\times k}$ arbitrary (in fact it must be $\Lambda = Q\,E$, with $E \in \mathbb{R}^{n\times n}$ skew-symmetric).

The horizontal lift of any tangent vector $\Delta = VA + V^{\perp}B \in T_V\mathcal{V}_{n,k}$ is therefore given by $\Lambda = Q \begin{bmatrix} A & -B^T \\ B & \mathbb{O} \end{bmatrix}$ at each Q belonging to the equivalence class of V (i.e. each Q whose first k columns are equal to V). Since the Frobenius metric does not depend on Q, we can induce the following metric on $\mathcal{V}_{n,k}$:

$$\langle \Delta_1, \Delta_2 \rangle_V = \langle \mathrm{lift}_Q \Delta_1, \mathrm{lift}_Q \Delta_2 \rangle_Q = \mathrm{tr}\left(\begin{bmatrix} A_1^T & B_1^T \\ -B_1 & \mathbb{O} \end{bmatrix} \begin{bmatrix} A_2 & -B_2^T \\ B_2 & \mathbb{O} \end{bmatrix} \right)$$

$$= \mathrm{tr}(A_1^T A_2) + 2\,\mathrm{tr}(B_1^T B_2).$$

Instead of using exactly this metric, we multiply everything by $1/2$ to obtain the more convenient expression (2.11). □

We conclude this section with a constructive proof of the expression of the **gradient of a function on the Stiefel manifold**, with respect to the canonical metric. The gradient of a function $F : \mathcal{V}_{n,k} \to \mathbb{R}$ at $V \in \mathcal{V}_{n,k}$ is defined as the tangent vector $\nabla F(V)$ that satisfies:

$$\langle \nabla F(V), \Delta \rangle_V = \mathrm{tr}(F_V^T(V)\Delta) \quad \forall \Delta \in T_V\mathcal{V}_{n,k}, \tag{2.12}$$

where $F_V \in \mathbb{R}^{n\times k}, (F_V)_{ij} \triangleq \frac{\partial F(V)}{\partial V_{ij}}$ and $\langle ., . \rangle$ is the canonical metric on the Stiefel manifold given by (2.11).

Lemma 2.3.3. *The gradient of $F : \mathcal{V}_{n,k} \to \mathbb{R}$ at $V \in \mathcal{V}_{n,k}$ can be computed as:*

$$\nabla F(V) = F_V(V) - V F_V^T(V) V \tag{2.13}$$

Proof. From the definition of gradient (2.12) and the expression of the tangent space to the Stiefel manifold (2.10), we have that ∇F must satisfy both of the following:

$$\begin{aligned} \mathrm{tr}(\nabla F^T(\mathbb{1} - \frac{1}{2}VV^T)\Delta) &= \mathrm{tr}(F_V^T\Delta) \quad \forall \Delta \in T_V\mathcal{V}_{n,k} && (2.14) \\ \nabla F^T V &= -V^T\nabla F && (2.15) \end{aligned}$$

Substituting (2.15) into (2.14), we obtain:

$$\mathrm{tr}(\nabla F^T\Delta - F_V^T\Delta + \frac{1}{2}V^T\nabla F V^T\Delta) = 0 \quad \forall \Delta \in T_V\mathcal{V}_{n,k}, \tag{2.16}$$

which is clearly satisfied by (2.13). □

Chapter 3

Decomposition and analysis of collective motion

In this chapter, we present a mathematical framework for decomposing collective motions into elementary components, derived from certain geometric structures (fiber bundles) in n-body systems.

The first step in the analysis of the geometry of multi-body problems, discussed in section 3.1, is to separate the information on the translation of the system, described by the center of mass motion, from the motion of each body with respect to the center of mass. In the "translation-reduced" configuration space, there are then at least two alternative fiber bundle structures that can be identified.

The classical approach is to consider the left-action of the group $SO(3)$, corresponding to rotations of the absolute reference frame, and show that the translation-reduced configuration space is a principal fiber bundle with respect to this action. We briefly recall some of the main results arising from this approach in section 3.2.

In section 3.3, we present the main contribution of this dissertation to the

analysis of the n-body problem, represented by an alternative fiber bundle structure on the translation-reduced configuration space. This alternative fibering is based on projecting each of the (translation-reduced) configurations to their corresponding coefficient of inertia tensor. The resulting base space is diffeomorphic to the six-dimensional space of symmetric positive definite 3×3 matrices. The fibers in this case are not groups but are diffeomorphic to Stiefel manifolds. Vertical vector fields generate rearrangements of body positions which do not alter the coefficient of inertia tensor of the n-body system (while also leaving the center of mass unchanged); if all the bodies have equal masses, these include the discrete family of permutations of body positions.

In section 3.4 we discuss the relevance of this work to the analysis of collective motion. In particular we introduce decompositions of vector fields for the n-body problem based on the classical and alternative fiber bundle structures. We also discuss in detail the characteristics of the elementary types of collective motions.

In section 3.6, the techniques developed in the chapter are applied to the analysis of experimental data obtained from a starling flock.

3.1 Reduction of the translational degree of freedom

We model a *collective* as n point particles moving in $\mathbb{R}^3$. Each particle has an associated value of mass $m_i > 0$, which can be thought of as the physical mass or alternatively as the "weight" that the individual has on the decisions of the

collective (for collectives of indistinguishable individuals, one can think of taking all the masses equal to each other).

We denote the position of the i-th particle with respect to an arbitrary absolute reference frame as $\mathbf{r_i} \in \mathbb{R}^3$. The overall configuration of the collective is $\mathbf{r} \triangleq [\mathbf{r_1}\ \mathbf{r_2}\ ...\ \mathbf{r_n}] \in \mathcal{R}$, where $\mathcal{R} \cong \mathbb{R}^{3\times n}$ is the configuration space. We choose to represent configurations as $3 \times n$ matrices, as opposed to $3n$-dimensional vectors; this choice will be convenient in the following derivations.

A tangent vector to $\mathcal{R}$ at $\mathbf{r}$ is denoted by $\mathbf{v_r} \triangleq [\mathbf{v_{r1}}\ \mathbf{v_{r2}}\ ...\ \mathbf{v_{rn}}] \in T_\mathbf{r}\mathcal{R}$. Notice that $T_\mathbf{r}\mathcal{R} \cong \mathbb{R}^{3\times n}$. The tangent bundle $T\mathcal{R}$, whose elements are pairs $(\mathbf{r}, \mathbf{v_r})$, is the *phase space* of the collective.

The *kinetic energy* is defined on phase space as:

$$E : T\mathcal{R} \to \mathbb{R}, \quad E(\mathbf{r}, \mathbf{v_r}) \triangleq \frac{1}{2}\sum_{i=1}^{n} m_i |\mathbf{v_{ri}}|^2, \tag{3.1}$$

which can be expressed as $E(\mathbf{r}, \mathbf{v_r}) = \frac{1}{2}\langle \mathbf{v_r}, \mathbf{v_r}\rangle_\mathbf{r}$ with respect to the following Riemannian metric on $\mathcal{R}$:

$$\langle ., . \rangle_\mathbf{r} : T_\mathbf{r}\mathcal{R} \times T_\mathbf{r}\mathcal{R} \to \mathbb{R}$$
$$\langle \mathbf{v_r}, \mathbf{w_r}\rangle_\mathbf{r} \triangleq \sum_{i=1}^{n} m_i \mathbf{v_{ri}^T w_{ri}} = \mathrm{tr}(\mathbf{v_r} \mathbb{M} \mathbf{w_r^T}), \tag{3.2}$$

where $\mathbb{M} = \mathrm{diag}(m_1, ..., m_n)$ is the diagonal matrix of the masses (we use this bolder script to distinguish from the total mass M defined below), and we have used the property of vectors $\mathbf{a}^T\mathbf{b} = \mathrm{tr}(\mathbf{a}\mathbf{b}^T)$. We will refer sometimes to (3.2) as the "metric associated to kinetic energy".

On $\mathcal{R}$, the action of $(\mathbb{R}^3, +)$ corresponding to translation of the abso-

lute reference frame: $[\mathbf{r_1}\ \mathbf{r_2}\ ...\ \mathbf{r_n}] \mapsto [\mathbf{r_1}+\mathbf{r_0}\ \mathbf{r_2}+\mathbf{r_0}\ ...\ \mathbf{r_n}+\mathbf{r_0}]$ for $\mathbf{r_0} \in \mathbb{R}^3$, is free and proper. The configuration space has therefore the geometrical structure of a principal fiber bundle $(\mathcal{R}, \pi, \mathcal{R}/\mathbb{R}^3, \mathbb{R}^3)$, where the quotient space is $\mathcal{R}/\mathbb{R}^3 \cong \mathbb{R}^{3\times n}/\mathbb{R}^3 \cong \mathbb{R}^{3\times(n-1)}$, and the projection π is defined by mapping each configuration into its equivalence class. To provide an explicit expression for the projection map, we introduce the *center of mass*:

$$\mathbf{r_{com}} = \sum_{i=1}^{n} \frac{m_i}{M} \mathbf{r_i}, \tag{3.3}$$

where $M = \sum_{i=1}^{n} m_i$ is the *total mass* of the system, and define:

$$\pi(\mathbf{r}) = [\mathbf{c_1}\ \mathbf{c_2}\ ...\ \mathbf{c_n}] \triangleq [\mathbf{r_1}-\mathbf{r_{com}}\ \mathbf{r_2}-\mathbf{r_{com}}\ ...\ \mathbf{r_n}-\mathbf{r_{com}}]. \tag{3.4}$$

The new variables $\mathbf{c_1}, \mathbf{c_2}, ..., \mathbf{c_n}$ are translation-invariant and provide a way of describing the quotient space $\mathcal{R}/\mathbb{R}^3$ as a $(3n-3)$-dimensional subspace of $\mathbb{R}^{3\times n}$, which we denote as $\mathcal{C}$:

$$\mathcal{C} \triangleq \{\mathbf{c} = [\mathbf{c_1}\ \mathbf{c_2}\ ...\ \mathbf{c_n}] \in \mathbb{R}^{3\times n}\ s.t.\ \sum_{i=1}^{n} m_i \mathbf{c_i} = \mathbf{0}\}. \tag{3.5}$$

The principal fiber bundle associated to translation is globally trivial, i.e. $\mathcal{R} \cong \mathcal{C} \times \mathbb{R}^3$, since every configuration $\mathbf{r} \in \mathcal{R}$ can be unambiguously identified by the pair $(\mathbf{r_{com}}, \mathbf{c})$, $\mathbf{r_{com}} \in \mathbb{R}^3$, $\mathbf{c} \in \mathcal{C}$, defined as in (3.3)-(3.4). Similarly, for each $\mathbf{r} \in \mathcal{R}$, $T_{\mathbf{r}}\mathcal{R} \cong T_{\mathbf{r_{com}}}\mathbb{R}^3 \times T_{\mathbf{c}}\mathcal{C}$ and each tangent vector $\mathbf{v_r}$ can be identified with the pair $(\mathbf{v_{com}}, \mathbf{v_c})$, where $\mathbf{v_c} = [\mathbf{v_{r1}}-\mathbf{v_{com}}\ \mathbf{v_{r2}}-\mathbf{v_{com}}\ ...\ \mathbf{v_{rn}}-\mathbf{v_{com}}]$ and $\mathbf{v_{com}} = \sum_{i=1}^{n} \frac{m_i}{M} \mathbf{v_{ri}}$. As in $\mathcal{C}$, elements of $T_{\mathbf{c}}\mathcal{C}$ are $3 \times n$ matrices with linearly

dependent columns:

$$T_{\mathbf{c}}\mathcal{C} \triangleq \{\mathbf{v_c} = [\mathbf{v_{c1}}\ \mathbf{v_{c2}}\ ...\ \mathbf{v_{cn}}] \in \mathbb{R}^{3\times n}\ s.t.\ \sum_{i=1}^{n} m_i \mathbf{v_{ci}} = \mathbf{0}\}. \tag{3.6}$$

Moreover, the metric (3.2) is invariant to translations of the reference frame and therefore the machinery of mechanical connection described in section 2.2 can be used to obtain orthogonal splitting of tangent vectors in $T\mathcal{R}$ and horizontal lifts of tangent vectors in $T\mathcal{C}$. In the interest of brevity (and because the results are quite straightforward in this case) we do not report the detailed derivation of the results, but only remark that the momentum map (in the definition of mechanical connection) corresponds to the (scaled) linear momentum $\mathbf{J} = \sum_{i=1}^{n} m_i \mathbf{v_i} = M\mathbf{v_{com}}$.

The resulting splitting of tangent vectors into horizontal and vertical components is given by:

$$\mathbf{v_r} = \mathbf{v_c} + [\mathbf{v_{com}}\ \mathbf{v_{com}}\ ...\ \mathbf{v_{com}}]. \tag{3.7}$$

Clearly horizontal tangent vectors are those that leave invariant the position of the center of mass ($\mathbf{v_{com}} = \mathbf{0}$), and the horizontal lift of a tangent vector $\mathbf{v_c} \in T_{\mathbf{c}}\mathcal{C}$ is trivially $\mathrm{hor}(\mathbf{v_c}) = \mathbf{v_c}$. The metric induced on $\mathcal{C}$ by (3.2) and by the mechanical connection is:

$$\langle ., . \rangle_{\mathbf{c}} : T_{\mathbf{c}}\mathcal{C} \times T_{\mathbf{c}}\mathcal{C} \to \mathbb{R}$$

$$\langle \mathbf{v_c}, \mathbf{w_c} \rangle_{\mathbf{c}} \triangleq \sum_{i=1}^{n} m_i \mathbf{v_{ci}^T} \mathbf{w_{ci}} = \mathrm{tr}(\mathbf{v_c} \mathbb{M} \mathbf{w_c^T}). \tag{3.8}$$

The kinetic energy can be broken down into a vertical component E_{com} (due to the center of mass motion) and a horizontal component E_{rel} (due to the relative

motion of the particles with respect to the center of mass) as follows:

$$E(\mathbf{r}, \mathbf{v_r}) = \frac{1}{2}\langle \mathbf{v_r}, \mathbf{v_r} \rangle_{\mathbf{r}} = \frac{1}{2} M |\mathbf{v_{com}}|^2 + \frac{1}{2}\langle \mathbf{v_c}, \mathbf{v_c} \rangle_{\mathbf{c}} \triangleq E_{com} + E_{rel}. \tag{3.9}$$

In the next two sections, we focus on the translation-reduced configuration space $\mathcal{C}$, as defined in (3.5), equipped with metric (3.8).

Remark 3.1.1 In the physics literature on the n-body problem (see for example [35]) the translation-reduced configurations are not usually described by the positions of the bodies with respect to the center of mass $(\mathbf{c_1}, \mathbf{c_2}, ..., \mathbf{c_n})$ but rather by the mass-weighted *Jacobi vectors*. The latter are $n-1$ vectors $\boldsymbol{\rho_1}, \boldsymbol{\rho_2}, ..., \boldsymbol{\rho_{n-1}} \in \mathbb{R}^3$ constructed to be invariant to translations of the absolute reference frame, and in such a way that the kinetic energy is simply expressible as: $E = E_{com} + E_{rel} = \frac{1}{2} M |\mathbf{v_{com}}|^2 + \sum_{i=1}^{n-1} |\mathbf{v}_{\rho \mathbf{i}}|^2$ for $(\mathbf{v}_{\rho \mathbf{1}}, \mathbf{v}_{\rho \mathbf{2}}, ..., \mathbf{v}_{\rho \mathbf{n-1}}) \in T_{\rho_1, \rho_2, ..., \rho_{n-1}} \mathcal{R}/\mathbb{R}^3$. The advantages of Jacobi vectors are that they are actual coordinates for the $(3n-3)$-dimensional quotient space $\mathcal{R}/\mathbb{R}^3$ (hence there are no dependencies between them, as opposed to the linearly-dependent $\mathbf{c_i}$'s) and they produce simpler expressions for the kinetic energy and the Riemannian metric (in which the masses do not explicitly appear). Nevertheless, the definition of Jacobi vectors depends on an arbitrary choice of clustering of the particles into disjoint sets. Hence there is no unique way of defining these vectors, and different choices can lead to very different equations describing the translation-invariant evolution of the n-body system. This, together with the fact that Jacobi vectors are much harder to visualize than the relative positions of the particles with re-

spect to the center of mass, makes us prefer (3.5) as the representation of the translation-invariant configuration space. However we remark that it is always possible to go from one representation to the other with appropriate (admittedly cumbersome) algebraic transformations.

3.2 A classical fibering: reduction to shape space

Consider the following left-action of $SO(3)$ on the (translation-reduced) configuration space $\mathcal{C}$ (defined in (3.5)): $[\mathbf{c_1}\ \mathbf{c_2}\ ...\ \mathbf{c_n}] \mapsto [Q\mathbf{c_1}\ Q\mathbf{c_2}\ ...\ Q\mathbf{c_n}]$, where $Q \in SO(3)$ can be thought of as a rotation of the absolute reference frame. This group action is free and proper on the following subset of configuration space, called *pre-shape space*, which includes all the configurations that are at least 2-dimensional (planar):

$$\mathcal{C}^{2^+d} \triangleq \{\mathbf{c} = [\mathbf{c_1}\ \mathbf{c_2}\ ...\ \mathbf{c_n}] \in \mathbb{R}^{3\times n}\ s.t.\ \sum_{i=1}^{n} m_i\mathbf{c_i} = \mathbf{0},\ \mathrm{rank}(\mathbf{c}) \geq 2\}. \tag{3.10}$$

The 1-dimensional (i.e. collinear) configurations have to be excluded from the configuration space, because the action fails to be free; if all $\mathbf{c_i}$'s are in the same direction, then the rotations about the common direction form an isotropy subgroup of $SO(3)$, leaving invariant the configuration of the system.

After excluding the thin set of collinear configurations, the remaining space $\mathcal{C}^{2^+d}$ has the geometrical structure of a principal fiber bundle ($\mathcal{C}^{2^+d}$, π, $\mathcal{C}^{2^+d}/SO(3)$, $SO(3)$), where the projection π maps every configuration in total space into its equivalence class. The quotient space $\mathcal{S} \triangleq \mathcal{C}^{2^+d}/SO(3)$ is called the *(Jacobi)*

shape space.

By the local triviality of fiber bundles, each configuration $\mathbf{c} \in \mathcal{C}^{2+d}$ can be locally identified with a pair $(\mathbf{s}, Q)$, $\mathbf{s} \in \mathcal{S}$, $Q \in SO(3)$. The shape space $\mathcal{S}$ is $(3n-6)$ dimensional, and the actual mapping $\mathbf{s} = \pi(\mathbf{c})$ depends on the choice of the representation of elements of $\mathcal{S}$, which must be of course translation and rotation invariant. Except for small n, there is no established method of choosing shape coordinates that have clear physical interpretation and easy visualization. In practice, one can settle for a sufficiently rich family of dot products and triple products of the $\mathbf{c_i}$'s (or of the Jacobi vectors). The high dimensionality and difficult coordinatization of the shape space are the main drawbacks in using this "classical" fibering approach when dealing with a large number of particles.

In order to identify each of the configurations $\mathbf{c} = \pi^{-1}(\mathbf{s})$ with a corresponding $Q \in SO(3)$, one needs to define a (locally) smooth cross section of the principal fiber bundle. This means choosing, smoothly for each shape $\mathbf{s}$, a reference configuration $\tilde{\mathbf{c}}(\mathbf{s}) \in \pi^{-1}(\mathbf{s})$ to be identified as $(\mathbf{s}, \mathbb{1})$, where $\mathbb{1}$ here stands for the 3×3 identity matrix. Then each $\mathbf{c} = \pi^{-1}(\mathbf{s})$ can be mapped into the pair $(\mathbf{s}, Q)$, where Q is such that $\mathbf{c} = Q\tilde{\mathbf{c}}$. The choice of the reference configurations $\tilde{\mathbf{c}}(\mathbf{s})$ (also called *gauge convention*) can also be thought of as the choice of the body frame associated to each shape, and Q as the rotation needed to make the body frame overlap with the absolute frame. When this terminology is used, then $\tilde{\mathbf{c}}(\mathbf{s})$ is the *configuration in the body frame.* Notice that for $n \geq 4$ it is impossible to find a globally smooth gauge convention [35], i.e. the fiber bundle is not trivial.

The Riemannian metric (3.8) is invariant under the left action of $SO(3)$: $\langle Q\mathbf{v_c}, Q\mathbf{w_c}\rangle_{Q\mathbf{c}} = \mathrm{tr}(Q\mathbf{v_c}\mathbb{M}\mathbf{w_c}^T Q^T) = \mathrm{tr}(\mathbf{v_c}\mathbb{M}\mathbf{w_c}^T) = \langle \mathbf{v_c}, \mathbf{w_c}\rangle_{\mathbf{c}}, \ \forall Q \in SO(3)$. Therefore the mechanical connection can be used to define the orthogonal splitting of tangent vectors and of the kinetic energy. In this case it is interesting to show some of the explicit derivations.

The Lie algebra of the Lie group $SO(3)$ is $so(3)$, the space of 3×3 skew-symmetric matrices. Given $\xi \in so(3)$, the infinitesimal generator of the group action Φ_g on $\mathcal{C}^{2^+d}$ induced by ξ is defined as:

$$\xi_{\mathcal{C}^{2^+d}}(\mathbf{c}) = \left.\frac{d}{dt}\right|_{t=0} \Phi_{exp(t\xi)}(\mathbf{c}) = \left.\frac{d}{dt}\right|_{t=0} (exp(t\xi))\mathbf{c} = \xi\mathbf{c}, \tag{3.11}$$

which can also be expressed as:

$$\xi_{\mathcal{C}^{2^+d}}(\mathbf{c}) = [\boldsymbol{\xi} \times \mathbf{c_1} \ \boldsymbol{\xi} \times \mathbf{c_2} \ ... \ \boldsymbol{\xi} \times \mathbf{c_n}] \tag{3.12}$$

where $\boldsymbol{\xi} \in \mathbb{R}^3$ is the vector associated to $\xi \in so(3)$ so that $\xi\mathbf{v} = \boldsymbol{\xi} \times \mathbf{v}$, $\forall \mathbf{v} \in \mathbb{R}^3$. Then the locked inertia tensor can be computed as follows, $\forall \mathbf{c} \in \mathcal{C}^{2^+d}$:

$$\begin{aligned}
(I_{\mathbf{c}}(\eta))(\xi) \triangleq & \langle \eta_{\mathcal{C}^{2^+d}}(\mathbf{c}), \xi_{\mathcal{C}^{2^+d}}(\mathbf{c})\rangle = \\
&= \sum_{i=1}^{n} m_i((\boldsymbol{\xi} \times \mathbf{c_i})^T(\boldsymbol{\eta} \times \mathbf{c_i})) = \\
&= \sum_{i=1}^{n} m_i \boldsymbol{\xi}^T(\mathbf{c_i} \times (\boldsymbol{\eta} \times \mathbf{c_i})) = \\
&= \boldsymbol{\xi}^T \sum_{i=1}^{n} m_i(|\mathbf{c_i}|^2 \mathbb{1} - \mathbf{c_i}\mathbf{c_i}^T)\boldsymbol{\eta} \quad \forall \eta, \xi \in so(3),
\end{aligned} \tag{3.13}$$

where we have used the triple product formulae for vectors in $\mathbb{R}^3$: $\mathbf{a} \times \mathbf{b} \cdot \mathbf{c} = \mathbf{b} \times \mathbf{c} \cdot \mathbf{a}$, $\mathbf{a} \times (\mathbf{b} \times \mathbf{c}) = \mathbf{b}(\mathbf{a} \cdot \mathbf{c}) - \mathbf{c}(\mathbf{a} \cdot \mathbf{b})$. Hence the locked inertia tensor is

nothing else than the *moment of inertia tensor* (with respect to the center of mass):

$$I(\mathbf{c}) = \sum_{i=1}^{n} m_i(|\mathbf{c_i}|^2 \mathbb{1} - \mathbf{c_i}\mathbf{c_i}^T), \tag{3.14}$$

or alternatively $I(\mathbf{c}) = (\mathrm{tr}(K(\mathbf{c}))\mathbb{1} - K(\mathbf{c}))$ where $K(\mathbf{c}) = \sum_{i=1}^{n} m_i \mathbf{c_i}\mathbf{c_i}^T$ is the *coefficient of inertia tensor*, which will be important in the next section.

A similar computation specializing (2.5) yields the momentum map, $\forall(\mathbf{c}, \mathbf{v_c}) \in T\mathcal{C}^{2^+d}$:

$$\begin{aligned}(\mathbf{J}(\mathbf{c}, \mathbf{v_c}))(\xi) \triangleq &\langle \mathbf{v_c}, \xi_{\mathcal{C}^{2^+d}}(\mathbf{c})\rangle = \\ &= \sum_{i=1}^{n} m_i((\boldsymbol{\xi} \times \mathbf{c_i})^T \mathbf{v_{ci}}) = \\ &= \sum_{i=1}^{n} m_i \boldsymbol{\xi}^T(\mathbf{c_i} \times \mathbf{v_{ci}}) = \\ &= \boldsymbol{\xi}^T \sum_{i=1}^{n} m_i(\mathbf{c_i} \times \mathbf{v_{ci}}) \quad \forall \xi \in so(3),\end{aligned} \tag{3.15}$$

which is simply the $\boldsymbol{\xi}$-component of the *angular momentum* (with respect to the center of mass):

$$\mathbf{J}(\mathbf{c}, \mathbf{v_c}) = \sum_{i=1}^{n} m_i(\mathbf{c_i} \times \mathbf{v_{ci}}). \tag{3.16}$$

The mechanical connection is therefore:

$$\mathcal{A}_\mathbf{c}(\mathbf{v_c}) \triangleq I_\mathbf{c}^{-1}\mathbf{J}(\mathbf{c}, \mathbf{v_c}), \tag{3.17}$$

and the Ehresmann connection that projects every tangent vector $\mathbf{v_c} \in T_\mathbf{c}\mathcal{C}^{2^+d}$ to its vertical component is:

$$A_\mathbf{c}(\mathbf{v_c}) = [\mathcal{A}_\mathbf{c}(\mathbf{v_c})]_{\mathcal{C}^{2^+d}} = [I_\mathbf{c}^{-1}\mathbf{J}(\mathbf{c}, \mathbf{v_c}) \times \mathbf{c_1} \ ... \ I_\mathbf{c}^{-1}\mathbf{J}(\mathbf{c}, \mathbf{v_c}) \times \mathbf{c_n}]. \tag{3.18}$$

Horizontal tangent vectors with respect to this connection are those with zero angular momentum, while vertical vector fields leave the shape invariant and only produce rigid rotations of the collective. Given an arbitrary $\mathbf{v_c} \in T_{\mathbf{c}}\mathcal{C}^{2+d}$, it can be split (orthogonally with respect to (3.8)) into a vertical component $A_{\mathbf{c}}(\mathbf{v_c})$ and a horizontal component $\mathrm{hor}(\mathbf{v_c}) = \mathbf{v_c} - A_{\mathbf{c}}(\mathbf{v_c})$; the latter can also be expressed as the horizontal lift of a tangent vector $\mathbf{v_s} \in T_{\mathbf{s(c)}}\mathcal{S}$. Of course the explicit expressions of the horizontal lift and of the metric induced on shape space by the mechanical connection depend on the choice of shape coordinates and gauge convention; we refer the reader to [35] and [57] for more on these aspects.

The splitting of the kinetic energy E_{rel} (which is the component of the total kinetic energy due to the relative motion with respect to the center of mass, as defined in (3.9)) into a vertical part due to rotation and a horizontal part due to change of shape, can instead be done independently on the choice of shape coordinates and gauge conventions, as follows:

$$\begin{aligned} E_{rel}(\mathbf{c}, \mathbf{v_c}) = \frac{1}{2}\langle \mathbf{v_c}, \mathbf{v_c} \rangle_{\mathbf{c}} = \frac{1}{2}\langle A_{\mathbf{c}}(\mathbf{v_c}), A_{\mathbf{c}}(\mathbf{v_c}) \rangle_{\mathbf{c}} + \frac{1}{2}\langle \mathrm{hor}(\mathbf{v_c}), \mathrm{hor}(\mathbf{v_c}) \rangle_{\mathbf{c}} \\ \triangleq \qquad E_{rot}(\mathbf{c}, \mathbf{v_c}) \qquad + \qquad E_{shape}(\mathbf{c}, \mathbf{v_c}) \end{aligned} \tag{3.19}$$

The following formula can be derived for the rotational component E_{rot} using

(3.8), (3.18) and the triple vector products formulae:

$$\begin{aligned} E_{rot}(\mathbf{c}, \mathbf{v_c}) =& \frac{1}{2} \sum_{i=1}^{n} m_i (I_{\mathbf{c}}^{-1} \mathbf{J}(\mathbf{c}, \mathbf{v_c}) \times \mathbf{c_i})^T (I_{\mathbf{c}}^{-1} \mathbf{J}(\mathbf{c}, \mathbf{v_c}) \times \mathbf{c_i}) = \\ =& \frac{1}{2} \sum_{i=1}^{n} m_i (\mathbf{J}(\mathbf{c}, \mathbf{v_c})^T I_{\mathbf{c}}^{-1} (|\mathbf{c_i}|^2 \mathbb{1} - \mathbf{c_i} \mathbf{c_i}^T) I_{\mathbf{c}}^{-1} \mathbf{J}(\mathbf{c}, \mathbf{v_c})) = \\ =& \frac{1}{2} \mathbf{J}(\mathbf{c}, \mathbf{v_c})^T \ I_{\mathbf{c}}^{-1} \ \mathbf{J}(\mathbf{c}, \mathbf{v_c}). \end{aligned} \tag{3.20}$$

From (3.9), (3.19) and (3.20), we have therefore the following more detailed breakdown of kinetic energy:

$$\begin{aligned} E(\mathbf{r}, \mathbf{v_r}) =& E_{com} + E_{rot} + E_{shape} = \\ =& \frac{1}{2} M |\mathbf{v_{com}}|^2 + \frac{1}{2} \mathbf{J}(\mathbf{c}, \mathbf{v_c})^T \ I_{\mathbf{c}}^{-1} \ \mathbf{J}(\mathbf{c}, \mathbf{v_c}) + E_{shape}. \end{aligned} \tag{3.21}$$

Remark 3.2.1 Several control problems inspired by this classical fibering of the n-body problem have been studied in the past. For example [57] studies controlled Lagrangians dynamics in which the control has only authority on the shape space. The controllability and optimal control problems when the control authority is limited to shape space have been studied in [56] for a kinematic system composed of a rigid body with two oscillators. This system is different from the n-body one studied here, but shares with it the principal fiber bundle structure associated to the left action of $SO(3)$. The same is true for many other problems related to control of nonholonomic mechanical systems (a monograph on this subject is [9]).

Remark 3.2.2 Another symmetry group for the Riemannian metric (3.8) that is discussed in the literature on the n-body problem is the *democracy group*.

Consider the translation-invariant configuration space, represented in terms of Jacobi vectors: $\mathcal{C} = \{[\boldsymbol{\rho_1}\ \boldsymbol{\rho_2}\ ...\ \boldsymbol{\rho_{n-1}}] \in \mathbb{R}^{3\times(n-1)}\}$. The democracy group ($\mathcal{D}$) is defined as the group of $O(n-1)$ orthogonal matrices acting on the right on $\mathcal{C}$ as follows: $[\boldsymbol{\rho_1}\ \boldsymbol{\rho_2}\ ...\ \boldsymbol{\rho_{n-1}}] \mapsto [\boldsymbol{\rho_1}\ \boldsymbol{\rho_2}\ ...\ \boldsymbol{\rho_{n-1}}]D$, where $D \in \mathcal{D} \cong O(n-1)$. Notice that upon action of a democracy group element (often referred to as "democracy transformation" or "kinematic rotation"), each Jacobi vector $\boldsymbol{\rho_i}$ gets mapped into $\boldsymbol{\rho'_i} = \sum_{j=1}^{n-1} D_{ij}\boldsymbol{\rho_j}$, a linear combination of the original Jacobi vectors. The democracy group includes the set of permutations of the Jacobi vectors; moreover any two different choices of Jacobi vectors (constructed from different choices of clustering of the particles) are related by a democracy transformation [35].

Only quantities that are "democracy invariant" are independent of the particle clustering used in the definition of Jacobi vectors. It is easy to verify that the kinetic energy $E_{rel} = \sum_{i=1}^{n-1} |\mathbf{v}_{\rho\mathbf{i}}|^2$ is one of these quantities (invariant to the democracy group action).

Since democracy transformations commute with the left actions by $SO(3)$ corresponding to rotations of the absolute reference frame, there is a well-defined induced action of the democracy group on shape space. Unfortunately this action is not free, hence it is not possible to identify the shape space as a principal fiber bundle. It is possible instead to decompose the shape space into the family of orbits of the democracy group, and to choose appropriately some of the shape coordinates to be democracy invariant, as described in [33] and [34] for the case of three and four bodies.

3.3 An alternative fibering: reduction to the space of coefficient of inertia tensors

3.3.1 Fiber bundle formulation

In this section we consider only configurations with respect to the center of mass that are "three-dimensional", i.e. for which $\text{rank}([\mathbf{c_1}\ \mathbf{c_2}\ ...\ \mathbf{c_n}]) = 3$. We denote this subset of the configuration space $\mathcal{C}$ as $\mathcal{C}^{3d}$:

$$\mathcal{C}^{3d} \triangleq \{\mathbf{c} = [\mathbf{c_1}\ \mathbf{c_2}\ ...\ \mathbf{c_n}] \in \mathbb{R}^{3\times n}\ s.t.\ \sum_{i=1}^{n} m_i \mathbf{c_i} = \mathbf{0},\ \text{rank}(\mathbf{c}) = 3\}. \tag{3.22}$$

$\mathcal{C}^{3d}$ is an open subset of the manifold $\mathcal{C} \cong \mathbb{R}^{3\times(n-1)}$, obtained removing from $\mathcal{C}$ the closed set of planar configurations, hence it is a manifold. Notice that $\mathcal{C}^{3d} \subset \mathcal{C}^{2^+d}$, the subset of configuration space considered in the previous section, but both differ from $\mathcal{C}$ (and from each other) by only a "thin set". We also remark that all the configurations composed of 3 or fewer particles are planar, hence $\mathcal{C}^{3d}$ is empty if $n < 4$. Thus the results of this section are useful only for collectives composed of at least 4 individuals (just as the results of the previous section are useful only for 3 or more particles).

The objective of this section is to present a fiber bundle description of $\mathcal{C}^{3d}$ which is alternative to that in section 3.2 based on the left action of $SO(3)$. At the heart of this alternative fibering is the map that projects each configuration

$\mathbf{c} \in \mathcal{C}^{3d}$ to the corresponding coefficient of inertia tensor:

$$\pi : \mathcal{C}^{3d} \to \mathcal{K}$$
$$\mathbf{c} \mapsto K \triangleq \pi(\mathbf{c}) = \sum_{i=1}^{n} m_i \mathbf{c_i} \mathbf{c_i}^T = \mathbf{c}\mathbb{M}\mathbf{c}^T. \tag{3.23}$$

Here $\mathbb{M} = \text{diag}(m_1, ..., m_n)$ and we have used the symbol $\mathcal{K}$ for the space of coefficient of inertia tensors associated to three-dimensional configurations.

We aim to show that (3.23) is a bundle projection that defines a smooth fiber bundle $(\mathcal{C}^{3d}, \pi, \mathcal{K}, \mathcal{V}_{n-1,3})$ with fibers diffeomorphic to the Stiefel manifold $\mathcal{V}_{n-1,3}$ (whose elements are matrices $V \in \mathbb{R}^{(n-1)\times 3}$ s.t. $V^T V = \mathbb{1}$). Towards this goal, we need to introduce the following lemmas.

Lemma 3.3.1. *$\mathcal{K} = \mathbb{R}^{3\times 3}_{sym,>0}$, the space of symmetric, positive definite, 3×3 matrices, and therefore is a connected manifold.*

Proof. Part I: $\mathcal{K} \subseteq \mathbb{R}^{3\times 3}_{sym,>0}$

Since $\mathbb{M}$ is diagonal (hence symmetric), every $K = \mathbf{c}\mathbb{M}\mathbf{c}^T \in \mathcal{K}$ is certainly symmetric. For any $\mathbf{x} \in \mathbb{R}^3$, $\mathbf{x}^T K \mathbf{x} = \mathbf{x}^T \mathbf{c}\mathbb{M}\mathbf{c}^T \mathbf{x} = \sum_{i=1}^{n} m_i |\mathbf{x}^T \mathbf{c_i}|^2 \geq 0$ which proves that every $K \in \mathcal{K}$ is positive semidefinite. To prove that indeed each K is positive definite, we show that $\text{rank}(K) = 3$. For the latter, observe that $K = \mathbf{c}\mathbb{M}\mathbf{c}^T = (\mathbb{M}^{\frac{1}{2}}\mathbf{c}^T)^T(\mathbb{M}^{\frac{1}{2}}\mathbf{c}^T)$, where $\mathbb{M}^{\frac{1}{2}} = \text{diag}(\sqrt{m_1}, \sqrt{m_2}, ..., \sqrt{m_n})$. Hence $\text{rank}(K) = \text{rank}(\mathbb{M}^{\frac{1}{2}}\mathbf{c}^T) = \text{rank}(\mathbf{c}^T) = \text{rank}(\mathbf{c}) = 3$, where we used the fact that $\text{rank}(A) = \text{rank}(A^T) = \text{rank}(A^T A)$ for each matrix A, and the fact that $\mathbb{M}^{\frac{1}{2}}$ is full rank.

Part II: $\mathbb{R}^{3\times 3}_{sym,>0} \subseteq \mathcal{K}$

We prove this by constructing, for any $K \in \mathbb{R}^{3\times3}_{sym,>0}$, a $\mathbf{c} \in \mathcal{C}^{3d}$ s.t. $K = \mathbf{c}\mathbb{M}\mathbf{c}^T$. Since K is symmetric positive definite, there exist $Q \in SO(3)$ (matrix of eigenvectors of K) and $\lambda_1, \lambda_2, \lambda_3 \in \mathbb{R}^+$ (eigenvalues of K) such that $QKQ^T = \Lambda = \text{diag}(\lambda_1, \lambda_2, \lambda_3)$. Now $K = \mathbf{c}\mathbb{M}\mathbf{c}^T \Leftrightarrow \Lambda = \tilde{\mathbf{c}}\tilde{\mathbf{c}}^T$ where $\tilde{\mathbf{c}} = Q\mathbf{c}\mathbb{M}^{\frac{1}{2}}$, i.e. the three rows of $\tilde{\mathbf{c}}$ are orthogonal to each other and have norms $\sqrt{\lambda_1}$, $\sqrt{\lambda_2}$ and $\sqrt{\lambda_3}$ respectively. Moreover the condition $\mathbf{c}[m_1\, m_2 \ldots m_n]^T = \mathbf{0}$, which is a compact way of expressing $\sum_{i=1}^n m_i\mathbf{c_i} = \mathbf{0}$, implies the following condition on $\tilde{\mathbf{c}}$: $\tilde{\mathbf{c}}[\sqrt{m_1}\,\sqrt{m_2} \ldots \sqrt{m_n}]^T = \mathbf{0}$. So the problem of finding $\mathbf{c}$ such that $K = \mathbf{c}\mathbb{M}\mathbf{c}^t$ reduces to finding 3 n-dimensional vectors (the rows of $\tilde{\mathbf{c}}$) which are orthogonal to each other and to the vector $[\sqrt{m_1}\,\sqrt{m_2} \ldots \sqrt{m_n}]$ and have norms $\sqrt{\lambda_1}, \sqrt{\lambda_2}, \sqrt{\lambda_3}$. It is easy to verify algebraically that one possible choice (as sparse as possible) is to take $\tilde{\mathbf{c}}$ equal to the following:

$$\begin{bmatrix} \frac{\sqrt{\lambda_1 m_1}}{\mu_1} & 0 & 0 & -\frac{\sqrt{\lambda_1 m_4}}{\mu_1}\left(\frac{m_1}{m_4}\right) & 0\cdots0 \\ \frac{\sqrt{\lambda_2 m_1}}{\mu_2} & -\frac{\sqrt{\lambda_2 m_2}}{\mu_2}\left(\frac{m_1+m_4}{m_2}\right) & 0 & \frac{\sqrt{\lambda_2 m_4}}{\mu_2} & 0\cdots0 \\ \frac{\sqrt{\lambda_3 m_1}}{\mu_3} & \frac{\sqrt{\lambda_3 m_2}}{\mu_3} & -\frac{\sqrt{\lambda_3 m_3}}{\mu_3}\left(\frac{m_1+m_2+m_4}{m_3}\right) & \frac{\sqrt{\lambda_3 m_4}}{\mu_3} & 0\cdots0 \end{bmatrix}$$

where μ_1, μ_2, μ_3 are normalizing factors given by:

$$\begin{aligned} \mu_1 &= \sqrt{\frac{m_1(m_1+m_4)}{m_4}}, \quad \mu_2 = \sqrt{\frac{(m_1+m_4)(m_1+m_2)}{m_2}} \\ \mu_3 &= \sqrt{\frac{(m_1+m_2+m_4)(m_1+m_2+m_3+m_4)}{m_3}}. \end{aligned} \tag{3.24}$$

Therefore, by taking $\mathbf{c} = Q^T\tilde{\mathbf{c}}\mathbb{M}^{-\frac{1}{2}}$, we have that the following configuration $\mathbf{c} \in \mathcal{C}^{3d}$ has the specified symmetric positive definite matrix K as its coefficient

of inertia tensor:

$$\mathbf{c} = Q^T \begin{bmatrix} \frac{\sqrt{\lambda_1}}{\mu_1} & 0 & 0 & -\frac{\sqrt{\lambda_1}}{\mu_1}\left(\frac{m_1}{m_4}\right) & 0\cdots 0 \\ \frac{\sqrt{\lambda_2}}{\mu_2} & -\frac{\sqrt{\lambda_2}}{\mu_2}\left(\frac{m_1+m_4}{m_2}\right) & 0 & \frac{\sqrt{\lambda_2}}{\mu_2} & 0\cdots 0 \\ \frac{\sqrt{\lambda_3}}{\mu_3} & \frac{\sqrt{\lambda_3}}{\mu_3} & -\frac{\sqrt{\lambda_3}}{\mu_3}\left(\frac{m_1+m_2+m_4}{m_3}\right) & \frac{\sqrt{\lambda_3}}{\mu_3} & 0\cdots 0 \end{bmatrix}, \tag{3.25}$$

where we remind that $Q \in SO(3), \lambda_1, \lambda_2, \lambda_3 \in \mathbb{R}^+$ are obtained from an eigenvalue decomposition of K, and μ_1, μ_2, μ_3 are given by (3.24). Notice that (3.25) proves that any desired coefficient of inertia tensor can be obtained by a configuration in which only 4 particles are located away from the center of mass.

Hence Part I and Part II of this proof guarantee that $\mathcal{K} = \mathbb{R}^{3\times3}_{sym,>0}$. Finally, $\mathbb{R}^{3\times3}_{sym,>0}$ is diffeomorphic to $\mathbb{R}^{3\times3}_{sym}$, with diffeomorphism given by the matrix logarithm, and clearly $\mathbb{R}^{3\times3}_{sym} \cong \mathbb{R}^6$. Hence $\mathbb{R}^{3\times3}_{sym,>0} \cong \mathbb{R}^6$ is a connected manifold. □

Lemma 3.3.2. *The projection map* (3.23) *is a smooth surjective submersion.*

Proof. The surjectivity of the projection map has already been proved above, and its smoothness is trivial. Hence we only need to prove the surjectivity of the derivative $d\pi_{\mathbf{c}}$ at each $\mathbf{c} \in \mathcal{C}^{3d}$.

$d\pi_{\mathbf{c}} : T_{\mathbf{c}}\mathcal{C}^{3d} \to T_K\mathcal{K}$ is defined as follows:

$$\begin{aligned} d\pi_{\mathbf{c}}(\mathbf{v_c}) = \left.\frac{d}{dt}\right|_{t=0} \pi(\mathbf{c} + t\mathbf{v_c}) = \mathbf{c}\mathbb{M}{\mathbf{v_c}}^T + \mathbf{v_c}\mathbb{M}\mathbf{c}^T = \\ =(\mathbf{c}\mathbb{M}^{\frac{1}{2}})(\mathbf{v_c}\mathbb{M}^{\frac{1}{2}})^T + (\mathbf{v_c}\mathbb{M}^{\frac{1}{2}})(\mathbf{c}\mathbb{M}^{\frac{1}{2}})^T \\ =2\,\mathrm{sym}((\mathbf{c}\mathbb{M}^{\frac{1}{2}})(\mathbf{v_c}\mathbb{M}^{\frac{1}{2}})^T). \end{aligned} \tag{3.26}$$

From lemma 3.3.1, $\mathcal{K} = \mathbb{R}^{3\times3}_{sym,>0}$ and therefore $T_K\mathcal{K} = \mathbb{R}^{3\times3}_{sym}$, since the tangent

vectors to the space of symmetric positive definite matrices are themselves symmetric (not necessarily positive definite) matrices.

Given any $C_K \in \mathbb{R}^{3\times 3}_{sym}$ we need to prove that there is a $\mathbf{v_c} \in T_{\mathbf{c}}\mathcal{C}^{3d}$ such that $2\,\mathrm{sym}((\mathbf{c}\mathbb{M}^{\frac{1}{2}})(\mathbf{v_c}\mathbb{M}^{\frac{1}{2}})^T) = C_K$. We can guarantee that $(\mathbf{c}\mathbb{M}^{\frac{1}{2}})(\mathbf{v_c}\mathbb{M}^{\frac{1}{2}})^T = C_K/2$, satisfying the above, by taking $(\mathbf{v_c}\mathbb{M}^{\frac{1}{2}})^T$ to be the product of the pseudo-inverse of $\mathbf{c}\mathbb{M}^{\frac{1}{2}}$ (which exists since the matrix is full rank) and $C_K/2$:

$$\begin{aligned}(\mathbf{v_c}\mathbb{M}^{\frac{1}{2}})^T =&(\mathbf{c}\mathbb{M}^{\frac{1}{2}})^T((\mathbf{c}\mathbb{M}^{\frac{1}{2}})(\mathbf{c}\mathbb{M}^{\frac{1}{2}})^T)^{-1}C_K/2 = \\ =&(\mathbf{c}\mathbb{M}^{\frac{1}{2}})^T K^{-1}C_K/2.\end{aligned}$$

So we have the following candidate for $\mathbf{v_c}$:

$$\mathbf{v_c} = \frac{1}{2}C_K K^{-1}\mathbf{c}, \tag{3.27}$$

and we only need to prove that $\mathbf{v_c} \in T_{\mathbf{c}}\mathcal{C}^{3d}$, i.e. $\mathbf{v_c}[m_1 m_2 ... m_n]^T = \mathbf{0}$ (equivalently $\sum_{i=1}^n m_i \mathbf{v_{ci}} = \mathbf{0}$). The latter is immediately verified: $\mathbf{v_c}[m_1 m_2 ... m_n]^T = \frac{1}{2}C_K K^{-1}\mathbf{c}[m_1 m_2 ... m_n]^T = \mathbf{0}$, since $\mathbf{c}[m_1 m_2 ... m_n]^T = \mathbf{0}$. □

By the pre-image theorem (see [23]), the previous lemma also guarantees that for all $K \in \mathcal{K}$ the inverse image $\pi^{-1}(K)$ is a smooth manifold of dimension $\dim(\mathcal{C}^{3d}) - \dim(\mathcal{K}) = (3n-3) - 6 = 3n - 9$. By showing that the projection map is proper and that the fibers $\pi^{-1}(K)$ are diffeomorphic to the Stiefel manifold $\mathcal{V}_{n-1,3}$, we can now conclude the proof that $(\mathcal{C}^{3d}, \pi, \mathcal{K}, \mathcal{V}_{n-1,3})$ is a fiber bundle (using lemma 2.1.2).

Theorem 3.3.3 (**The alternative fiber bundle).** *The projection* (3.23) *defines*

a smooth globally trivial fiber bundle $(\mathcal{C}^{3d}, \pi, \mathcal{K}, \mathcal{V}_{n-1,3})$*, with fibers diffeomorphic to the Stiefel manifold* $\mathcal{V}_{n-1,3}$*.*

Proof. Consider the subspace topologies on $\mathcal{C}^{3d} \subset \mathbb{R}^{3\times n}$ and $\mathcal{K} \subset \mathbb{R}^{3\times 3}$. Then the notion of compact set in $\mathcal{C}^{3d}$ and $\mathcal{K}$ corresponds to the notion of closed and bounded set. Since π is a continuous map, the inverse image of each closed set is closed. Now let C_K be a bounded set in $\mathcal{K}$; then there exists $\alpha < \infty$ s.t. $\mathrm{tr}(K^T K) \leq \alpha \ \forall K \in C_K$ (note that $\sqrt{\mathrm{tr}(K^T K)}$ is a legitimate norm in $\mathbb{R}^{3\times 3}$). The pre-image $\pi^{-1}(C_K)$ is given by:

$$\begin{aligned}
\pi^{-1}(C_K) &= \left\{ \mathbf{c} \in \mathcal{C}^{3d} s.t. \, \mathrm{tr}\left(\left(\sum_{i=1}^{n} m_i \mathbf{c_i} \mathbf{c_i}^T \right) \left(\sum_{j=1}^{n} m_j \mathbf{c_j} \mathbf{c_j}^T \right) \right) \leq \alpha \right\} = \\
&= \left\{ \mathbf{c} \in \mathcal{C}^{3d} s.t. \, \sum_{i=1}^{n} \sum_{j=1}^{n} m_i m_j |\mathbf{c_i}^T \mathbf{c_j}|^2 \leq \alpha \right\} = \\
&= \left\{ \mathbf{c} \in \mathcal{C}^{3d} s.t. \, \sum_{i=1}^{n} m_i^2 |\mathbf{c_i}|^4 + \sum_{i=1}^{n} \sum_{j=1, j\neq i}^{n} m_i m_j |\mathbf{c_i}^T \mathbf{c_j}|^2 \leq \alpha \right\}.
\end{aligned}$$

Hence $\forall \mathbf{c} \in \pi^{-1}(C_K)$ we have $\sum_{i=1}^{n} m_i^2 |\mathbf{c_i}|^4 \leq \alpha \Rightarrow \sum_{i=1}^{n} |\mathbf{c_i}|^4 \leq \alpha / m_{min}^2 \Rightarrow (\max_i |\mathbf{c_i}|)^4 \leq \alpha / m_{min}^2 \Rightarrow \max_i |\mathbf{c_i}| \leq (\alpha / m_{min}^2)^{1/4} < \infty$. Here m_{min} is the smallest mass. Since $\max_i |\mathbf{c_i}|$ is a legitimate norm in $\mathcal{C}^{3d}$, this proves that the inverse image of each bounded set is bounded, and completes the proof that π is a proper map. Therefore, by lemma 2.1.2, $(\mathcal{C}^{3d}, \pi, \mathcal{K})$ is indeed a fiber bundle. Since $\mathcal{K} = \mathbb{R}^{3\times 3}_{sym,>0} \cong \mathbb{R}^6$, the fiber bundle is globally trivial.

Finally we can show that, given any $K \in \mathcal{K}$, the fiber $\pi^{-1}(K)$ is diffeomor-

phic to $\mathcal{V}_{n-1,3}$. First of all, consider that:

$$\pi(\mathbf{c}) = K \Leftrightarrow \pi(Q\mathbf{c}) = \Lambda = \mathrm{diag}(\lambda_1, \lambda_2, \lambda_3)$$

$$\Leftrightarrow (\Lambda^{-\frac{1}{2}} Q\mathbf{c}\mathbb{M}^{\frac{1}{2}})(\Lambda^{-\frac{1}{2}} Q\mathbf{c}\mathbb{M}^{\frac{1}{2}})^T = \mathbb{1},$$

where $K = Q^T \Lambda Q$ is as usual an eigenvalue decomposition of K and $\Lambda^{-\frac{1}{2}}$ is the diagonal matrix $\mathrm{diag}(1/\sqrt{\lambda_1}, 1/\sqrt{\lambda_2}, 1/\sqrt{\lambda_3})$. Hence: $\pi^{-1}(K) = \{\mathbf{c} \in \mathcal{C}^{3d}\, s.t.\, (\Lambda^{-\frac{1}{2}} Q\mathbf{c}\mathbb{M}^{\frac{1}{2}})^T \in \mathcal{V}_{n,3}\}$.

Now: $\mathbf{c} \in \mathcal{C}^{3d} \Leftrightarrow \mathbf{c}[m_1 m_2 ... m_n]^T = \mathbf{0} \Leftrightarrow \mathbf{c}\mathbb{M}^{\frac{1}{2}}[\sqrt{m_1}\sqrt{m_2}...\sqrt{m_n}]^T = \mathbf{0} \Leftrightarrow \Lambda^{-\frac{1}{2}} Q\mathbf{c}\mathbb{M}^{\frac{1}{2}}[\sqrt{m_1}\sqrt{m_2}...\sqrt{m_n}]^T = \mathbf{0}$.

So we can also rewrite $\pi^{-1}(K)$ as: $\pi^{-1}(K) = \left\{\mathbf{c} \in \mathbb{R}^{3\times n}\, s.t.\, \tilde{V}(\mathbf{c}) \in \mathcal{V}_{n,4}\right\}$, where

$$\tilde{V}(\mathbf{c}) = \left[\begin{array}{c|c} & \sqrt{m_1/M} \\ \mathbb{M}^{\frac{1}{2}}\mathbf{c}^T Q^T \Lambda^{-\frac{1}{2}} & \vdots \\ & \sqrt{m_n/M} \end{array}\right].$$

Now observe that, given any fixed $\tilde{Q} \in O(n)$, $\tilde{V}(\mathbf{c}) \in \mathcal{V}_{n,4} \Leftrightarrow \tilde{Q}\tilde{V}(\mathbf{c}) \in \mathcal{V}_{n,4}$ (in fact $(\tilde{Q}\tilde{V})^T(\tilde{Q}\tilde{V}) = \tilde{V}^T\tilde{V} = \mathbb{1}$). In particular choose $\tilde{Q} \in O(n)$ in the form: $\tilde{Q} = \tilde{Q}_W \triangleq \begin{bmatrix} \sqrt{m_1/M} \cdots \sqrt{m_n/M} \\ W^T \end{bmatrix}$, where $W \in \mathcal{V}_{n,n-1}$ has columns orthogonal to the vector $[\sqrt{m_1/M} \cdots \sqrt{m_n/M}]^T$. Then: $\tilde{V}(\mathbf{c}) \in \mathcal{V}_{n,4} \Leftrightarrow \tilde{Q}_W\tilde{V}(\mathbf{c}) \in \mathcal{V}_{n,4} \Leftrightarrow W^T\mathbb{M}^{\frac{1}{2}}\mathbf{c}^T Q^T\Lambda^{-\frac{1}{2}} \in \mathcal{V}_{n-1,3} \Leftrightarrow \mathbb{M}^{\frac{1}{2}}\mathbf{c}^T Q^T\Lambda^{-\frac{1}{2}} = WV$, for some $V \in \mathcal{V}_{n-1,3}$. In the last step we have used the fact that $W^TW = \mathbb{1}$ and the columns of $\mathbb{M}^{\frac{1}{2}}\mathbf{c}^T Q^T\Lambda^{-\frac{1}{2}}$ are in the range of W (in fact they are orthogonal to $[\sqrt{m_1} \cdots \sqrt{m_n}]^T$, and thus to the kernel of W^T: $[\sqrt{m_1} \cdots \sqrt{m_n}]\mathbb{M}^{\frac{1}{2}}\mathbf{c}^T Q^T\Lambda^{-\frac{1}{2}} = [m_1 \cdots m_n]\mathbf{c}^T Q^T\Lambda^{-\frac{1}{2}} = \mathbf{0}$).

So we conclude that:

$$\pi^{-1}(K) = \left\{ \mathbf{c} \in \mathbb{R}^{3\times n} \, s.t. \, \mathbb{M}^{\frac{1}{2}} \mathbf{c}^T Q^T \Lambda^{-\frac{1}{2}} = WV, \, V \in \mathcal{V}_{n-1,3} \right\}, \tag{3.28}$$

where $K = Q^T \Lambda Q$ is an eigenvalue decomposition of K, and $W \in \mathcal{V}_{n,n-1}$ is a fixed matrix chosen among those having columns orthogonal to the vector $[\sqrt{m_1} \cdots \sqrt{m_n}]^T$.

We can now establish the following diffeomorphism between $\pi^{-1}(K)$ and the Stiefel manifold:

$$f_{K,W} : \pi^{-1}(K) \to \mathcal{V}_{n-1,3}$$

$$\mathbf{c} \in \pi^{-1}(K) \mapsto V = f_{K,W}(\mathbf{c}) = W^T \mathbb{M}^{\frac{1}{2}} \mathbf{c}^T Q^T \Lambda^{-\frac{1}{2}} \in \mathcal{V}_{n-1,3}, \tag{3.29}$$

with inverse:

$$f_{K,W}^{-1} : \mathcal{V}_{n-1,3} \to \pi^{-1}(K)$$

$$V \in \mathcal{V}_{n-1,3} \mapsto \mathbf{c} = f_{K,W}^{-1}(V) = Q^T \Lambda^{\frac{1}{2}} V^T W^T \mathbb{M}^{-\frac{1}{2}} \in \pi^{-1}(K). \tag{3.30}$$

The smoothness of mappings (3.29) and (3.30) is a consequence of their linearity in the arguments. Notice that these mappings vary not only with K but also with the choice of W (hence the double suffix). □

Remark 3.3.4 The choice of W defines a cross section of the fiber bundle, and plays the role that was played by the choice of gauge convention (body reference frame) in the case of the classical fibering of section 3.2. The Stiefel manifold is not a group (hence there is no concept of identity), but if we arbitrarily choose an element of the Stiefel manifold $\mathcal{V}_{n-1,3}$ as a "reference", then the choice of

W defines which configuration within each fiber $\pi^{-1}(K)$ gets mapped by $f_{K,W}$ to the reference. For example, assume that we consider $\hat{V} = [\mathbb{1}\,\mathbb{O}]^T$ as the reference; then the associated configuration $\hat{\mathbf{c}} \in \pi^{-1}(K)$ s.t. $f_{K,W}(\hat{\mathbf{c}}) = \hat{V}$ is given by (using (3.30)): $\hat{\mathbf{c}} = Q^T \Lambda^{\frac{1}{2}} (W_{1..3})^T \mathbb{M}^{-\frac{1}{2}}$, which depends on W (actually on the first 3 columns of W, denoted by $W_{1..3}$). Hence if we have a desired choice of configuration $\hat{\mathbf{c}}$ (within each fiber) that we want to be associated to the reference element of the Stiefel manifold $\hat{V} = [\mathbb{1}\,\mathbb{O}]^T$, all we need to do is to choose $(W_{1..3})^T = \Lambda^{-\frac{1}{2}} Q \hat{\mathbf{c}} \mathbb{M}^{\frac{1}{2}}$, and the remaining columns of W in such a way that $W \in \mathcal{V}_{n,n-1}$ and has columns orthogonal to the vector $[\sqrt{m_1} \cdots \sqrt{m_n}]^T$. For example if we want the "sparse" configurations given by (3.25) to be associated to the Stiefel manifold element $\hat{V} = [\mathbb{1}\,\mathbb{O}]^T$, we need to choose $W_{1..3}$ as follows:

$$W_{1..3} = \begin{bmatrix} \frac{\sqrt{m_1}}{\mu_1} & 0 & 0 & -\frac{m_1}{\mu_1\sqrt{m_4}} & 0 \cdots 0 \\ \frac{\sqrt{m_1}}{\mu_2} & -\frac{(m_1+m_4)}{\mu_2\sqrt{m_2}} & 0 & \frac{\sqrt{m_4}}{\mu_2} & 0 \cdots 0 \\ \frac{\sqrt{m_1}}{\mu_3} & \frac{\sqrt{m_2}}{\mu_3} & -\frac{(m_1+m_2+m_4)}{\mu_3\sqrt{m_3}} & \frac{\sqrt{m_4}}{\mu_3} & 0 \cdots 0 \end{bmatrix}. \tag{3.31}$$

Notice however that the cross section $K \mapsto \hat{\mathbf{c}}(K)$ described above is not smooth at the coefficient of inertia tensors that have repeated eigenvalues.

Remark 3.3.5 There is another way in which Stiefel manifolds appear in the description of n-body configurations. If the "thin" singular value decomposition is applied to the matrix of particle positions (with respect to the center of mass): $\mathbf{c} = Q_{svd} \Lambda_{svd} V_{svd}$, then the factors resulting from the decomposition are a matrix $Q_{svd} \in O(3)$, a diagonal matrix Λ_{svd} (containing the singular values) and a matrix V_{svd} in the Stiefel manifold $\mathcal{V}_{n,3}$ (not $\mathcal{V}_{n-1,3}$). Compared to this

algebraic decomposition, presented in [2], the geometric decomposition based on the novel fiber bundle formulation presented here provides additional insight and mathematical tools for the analysis and synthesis of collective motions. The following sections will be dedicated to elaborating on this insight and exploiting the geometric machinery associated to the fiber bundle formulation.

3.3.2 Interpretation of the fiber bundle

The base space for the fiber bundle $(\mathcal{C}^{3d}, \pi, \mathcal{K}, \mathcal{V}_{n-1,3})$ is the space of full-rank coefficient of inertia tensors ($\mathcal{K}$). The coefficient of inertia tensor associated to a configuration is important for several reason. The first obvious reason is that it unambiguously defines the moment of inertia tensor of the configuration, as already seen in section 3.2: $I_{\mathbf{c}} = \mathrm{tr}(K_{\mathbf{c}})\mathbb{1} - K_{\mathbf{c}}$. There is indeed a one-to-one correspondence between coefficient of inertia tensors and moment of inertia tensors, given by:

$$K \xrightarrow{f} I = \mathrm{tr}(K)\mathbb{1} - K \tag{3.32}$$

$$I \xrightarrow{f^{-1}} K = \frac{1}{2}\mathrm{tr}(I)\mathbb{1} - I. \tag{3.33}$$

If we consider only three-dimensional configurations, then the following holds (from eigendecomposition of K):

$$QKQ^T = \mathrm{diag}(\lambda_1, \lambda_2, \lambda_3) \Leftrightarrow QIQ^T = \mathrm{tr}(K)\mathbb{1} - QKQ^T = \mathrm{diag}(\mu_1, \mu_2, \mu_3),$$

where $Q \in SO(3)$ and the eigenvalues μ_1, μ_2, μ_3 of I are related to those of K by: $\mu_1 = \lambda_2 + \lambda_3$, $\mu_2 = \lambda_1 + \lambda_3$, $\mu_3 = \lambda_1 + \lambda_2$. Notice that the eigenvalues of

I for a three-dimensional configuration need not only to be positive definite (as it is the case for those of K) but also satisfy the relations: $\mu_2 + \mu_3 > \mu_1 > 0$, $\mu_1 + \mu_3 > \mu_2 > 0$ and $\mu_1 + \mu_2 > \mu_3 > 0$. Hence the space of moment of inertia tensors is only equivalent to a subset of $\mathbb{R}^{3\times3}_{sym,>0}$ (while $\mathcal{K} = \mathbb{R}^{3\times3}_{sym,>0}$). Working with the moment of inertia tensors, as opposed to the coefficient of inertia tensors, would have the disadvantage of having to constantly enforce these relations between eigenvalues.

The coefficient of inertia tensor of a configuration can also be interpreted as the scaled second moment (covariance) of the spatial distribution of mass with respect to the center of mass. Given a collective configuration with respect to the center of mass $\mathbf{c} = [\mathbf{c_1} \dots \mathbf{c_n}]$, the corresponding spatial distribution of mass with respect to the center of mass is $dm(\mathbf{r}) \triangleq \sum_{i=1}^{n} \frac{m_i}{M} \delta(\mathbf{c_i} - \mathbf{r})$, $\forall \mathbf{r} \in \mathbb{R}^3$, with δ being the Dirac delta function. Then the first moment (mean) of this distribution is always zero: $\overline{\mathbf{r}}_{dm} \triangleq \int_{\mathbb{R}^3} \mathbf{r}\, dm(\mathbf{r}) = \sum_{i=1}^{n} \frac{m_i}{M} \mathbf{c_i} = \mathbf{0}$, while its second moment (covariance) is actually given by the coefficient of inertia tensor divided by the total mass: $Cov_{dm} \triangleq \int_{\mathbb{R}^3} (\mathbf{r} - \overline{\mathbf{r}}_{dm})(\mathbf{r} - \overline{\mathbf{r}}_{dm})^T dm(\mathbf{r}) = \sum_{i=1}^{n} \frac{m_i}{M} \mathbf{c_i} \mathbf{c_i}^T = K(\mathbf{c})/M$.

Taking this interpretation a step further, one can construct a continuous spatial distribution of mass that coarsely approximates the actual (discrete) one, by taking a Gaussian distribution with zero mean and covariance matrix equal to $K(\mathbf{c})/M$; the surfaces of equal mass density corresponding to this Gaussian distribution are ellipsoids, with directions and relative lengths of the semi-axis given by the eigenvectors and eigenvalues of K. If all the masses are equal,

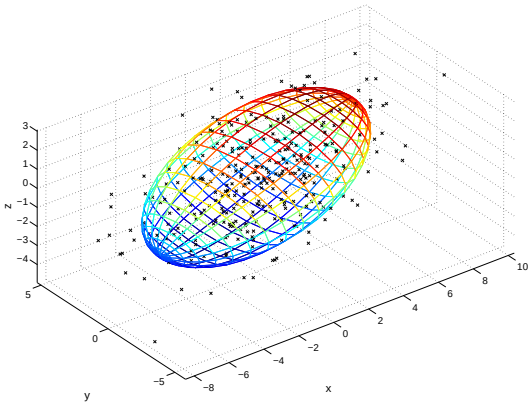

Figure 3.1: Ellipsoid obtained from the coefficient of inertia tensor as a visual approximation of the configuration of the collective.

then the spatial distribution of mass is the same as the spatial distribution of particles, and the ellipsoid constructed from eigendecomposition of K provides a coarse visual approximation of the configuration of the collective. The visual approximation can be quite effective if the particles are mostly distributed in symmetric fashion with respect to the center of mass, as shown in figure 3.1; notice that the positions of the 300 simulated particles in the figure were drawn from a Gaussian distribution. This ellipsoid is also strictly related to the ellipsoid of inertia of the collective, which is obtained from the eigendecomposition of the moment of inertia tensor: the semi-axis of the two ellipsoids have same directions (since the corresponding matrices have same eigenvectors) but different relative lengths.

To complete the discussion on the coefficient of inertia tensors, we remark that $\sqrt{\mathrm{tr}(K)} = \sqrt{\sum_{i=1}^{n} m_i(\mathbf{c_i}^T\mathbf{c_i})} = \sqrt{\sum_{i=1}^{n} m_i|\mathbf{c_i}|^2}$ gives a useful measure of the

"size" of the collective (sometimes referred to as the "hyperradius" of the n-body system).

We now concentrate on the fibers of the bundle $(\mathcal{C}^{3d}, \pi, \mathcal{K}, \mathcal{V}_{n-1,3})$, which are diffeomorphic to the Stiefel manifold $\mathcal{V}_{n-1,3}$. For any given $K \in \mathcal{K}$, the fiber over K is composed of all the configurations having K as their coefficient of inertia tensor, given by (using (3.29)):

$$\pi^{-1}(K) = \{Q^T \Lambda^{\frac{1}{2}} V^T W^T \mathbb{M}^{-\frac{1}{2}} : \ V \in \mathcal{V}_{n-1,3}\}. \tag{3.34}$$

What are the configuration changes that leave K invariant? Assume we have a reference configuration: $\tilde{\mathbf{c}} = Q^T \Lambda^{\frac{1}{2}} \tilde{V}^T W^T \mathbb{M}^{-\frac{1}{2}} \in \pi^{-1}(K)$, for some $\tilde{V} \in \mathcal{V}_{n-1,3}$. Since $\mathcal{V}_{n-1,3} \equiv O(n-1)/O(n-4)$ (see section 2.3), $\tilde{V}$ can be mapped to any other element of the Stiefel manifold by premultiplication by orthogonal matrices in $O(n-1)$: $\tilde{V} \mapsto Q_{\tilde{V}} \tilde{V}, \forall Q_{\tilde{V}} \in O(n-1)$; this allows to map $\tilde{\mathbf{c}}$ into any other $\mathbf{c} \in \pi^{-1}(K)$ as follows: $\tilde{\mathbf{c}} \mapsto Q^T \Lambda^{\frac{1}{2}} \tilde{V}^T Q_{\tilde{V}}^T W^T \mathbb{M}^{-\frac{1}{2}} = \tilde{\mathbf{c}}(\mathbb{M}^{\frac{1}{2}} W Q_{\tilde{V}}^T W^T \mathbb{M}^{-\frac{1}{2}}), \forall Q_{\tilde{V}} \in O(n-1)$. Hence given any $\tilde{\mathbf{c}} \in \pi^{-1}(K)$, we have the following alternative expression for $\pi^{-1}(K)$:

$$\pi^{-1}(K) = \mathcal{O}_{\mathcal{D}}(\tilde{\mathbf{c}}) \triangleq \{\tilde{\mathbf{c}} D \ s.t. \ D \in \mathcal{D}\}, \tag{3.35}$$

where:

$$\mathcal{D} = \{D = \mathbb{M}^{\frac{1}{2}} W Q_{\tilde{V}}^T W^T \mathbb{M}^{-\frac{1}{2}} \ s.t. \ Q_{\tilde{V}} \in O(n-1)\}. \tag{3.36}$$

It is trivial to prove that (3.36) is a group. We refer to $\mathcal{D}$ as the *democracy group*, because it is the analogue to the democracy group in the context of Jacobi vectors (briefly described in remark 3.2.2). Just like the classical democracy group, (3.36)

acts through right multiplication, is diffeomorphic to $O(n-1)$, commutes with the left action of $SO(3)$, and is a symmetry group for the metric induced by the kinetic energy, as shown in the following.

Proposition 3.3.6. *The Riemannian metric* (3.8) *is invariant to the democracy group action:* $\langle \mathbf{v_c}D, \mathbf{w_c}D\rangle_{\mathbf{c}D} = \langle \mathbf{v_c}, \mathbf{w_c}\rangle_{\mathbf{c}}\ \forall D \in \mathcal{D}$.

Proof.

$$\begin{aligned}\langle \mathbf{v_c}D, \mathbf{w_c}D\rangle_{\mathbf{c}D} =& \mathrm{tr}(\mathbf{v_c}D\mathbb{M}D^T{\mathbf{w_c}}^T) = \\ =& \mathrm{tr}(\mathbf{v_c}\mathbb{M}^{\frac{1}{2}}WQ_{\tilde{V}}^TW^T\mathbb{M}^{-\frac{1}{2}}\mathbb{M}\mathbb{M}^{-\frac{1}{2}}WQ_{\tilde{V}}W^T\mathbb{M}^{\frac{1}{2}}{\mathbf{w_c}}^T) = \\ =& \mathrm{tr}(\mathbf{v_c}\mathbb{M}^{\frac{1}{2}}WW^T\mathbb{M}^{\frac{1}{2}}{\mathbf{w_c}}^T) = \\ =& \mathrm{tr}(\mathbf{v_c}\mathbb{M}{\mathbf{w_c}}^T) \ = \ \langle \mathbf{v_c}, \mathbf{w_c}\rangle_{\mathbf{c}}.\end{aligned}$$

Notice that we used the following useful property, arising from the definition of $\tilde{Q}_W$ given in the proof of theorem 3.3.3:

$$\begin{aligned}&\mathbb{1} = \tilde{Q}_W^T\tilde{Q}_W = [\sqrt{m_1/M}\cdots\sqrt{m_n/M}]^T[\sqrt{m_1/M}\cdots\sqrt{m_n/M}] + WW^T \Rightarrow \\ &\Rightarrow WW^T = \mathbb{1} - [\sqrt{m_1/M}\cdots\sqrt{m_n/M}]^T[\sqrt{m_1/M}\cdots\sqrt{m_n/M}], \qquad (3.37)\end{aligned}$$

and we used the fact that $\mathbf{v_c}[m_1\cdots m_n]^T = [m_1\cdots m_n]{\mathbf{w_c}}^T = \mathbf{0}\ \forall \mathbf{v_c}, \mathbf{w_c} \in T_{\mathbf{c}D}\mathcal{C}^{3d}$. □

The fibers of $(\mathcal{C}^{3d}, \pi, \mathcal{K}, \mathcal{V}_{n-1,3})$ are therefore equivalent to the orbits of the democracy group action on $\mathcal{C}^{3d}$. Of course, since the fibers are diffeomorphic to $\mathcal{V}_{n-1,3} = O(n-1)/O(n-4)$, this action is not free but has an isotropy subgroup equivalent to $O(n-4)$ at each configuration.

If all the masses are equal, the orbits of the democracy group include the discrete family of particle relabelings (or position exchanges between particles). To show this, observe that a configuration $\tilde{\mathbf{c}}'$ is obtained from $\tilde{\mathbf{c}}$ via particle relabeling if and only if $\tilde{\mathbf{c}}' = \tilde{\mathbf{c}}P$ for some permutation matrix $P \in P(n) \subset O(n)$. Now $P \in \mathcal{D}$ if and only if $\mathbb{M}^{\frac{1}{2}} W Q_{\tilde{V}}^T W^T \mathbb{M}^{-\frac{1}{2}} = P$ for some $Q_{\tilde{V}} \in O(n-1)$, i.e. if and only if $W^T \mathbb{M}^{-\frac{1}{2}} P \mathbb{M}^{\frac{1}{2}} W \in O(n-1)$. The latter is certainly true (using (3.37)) if $\mathbb{M} = m\mathbb{1}$, i.e. the masses are equal, but is not true in general if the masses are distinct.

If the masses are equal (but only in this case) there exist orbits of the democracy group that interpolate between the family of particle position exchanges; motions along these special orbits allow the particles to exchange positions (hence treating each particle "democratically") without changing the approximated configuration of the collective (described by the coefficient of inertia tensor corresponding to the given fiber).

3.3.3 Vertical spaces and relation to the Stiefel manifold

At any configuration $\mathbf{c} \in \mathcal{C}^{3d}$, the tangent vectors belonging to the vertical space $V_{\mathbf{c}} \triangleq ker(d\pi_{\mathbf{c}})$ are those that correspond to motions along the fibers, which leave unchanged the coefficient of inertia tensor. Using the derivative of the projection map, already computed in (3.26), $V_{\mathbf{c}}$ can be defined as follows:

$$V_{\mathbf{c}} = \{\mathbf{v}_{\mathbf{c}} \in T_{\mathbf{c}}\mathcal{C}^{3d} \; s.t. \; \mathrm{sym}(\mathbf{v}_{\mathbf{c}} \mathbb{M} \mathbf{c}^T) = \mathbb{0}\}. \tag{3.38}$$

Notice that the dimension of $V_{\mathbf{c}}$ is $3n-9$, since the dimension of $T_{\mathbf{c}}\mathcal{C}^{3d}$ is $3n-3$ and the skew-symmetry condition (3.38) imposes six additional constraints.

From the diffeomorphism (3.29) established between each fiber $\pi^{-1}(K)$ and the Stiefel manifold $\mathcal{V}_{n-1,3}$, it is possible to establish a useful one-to-one mapping between each vertical tangent vector and a corresponding tangent vector to the Stiefel manifold:

$$\begin{aligned} df_{K,W} : T_{\mathbf{c}}\pi^{-1}(K) = V_{\mathbf{c}} &\to T_{f_{K,W}(\mathbf{c})}\mathcal{V}_{n-1,3} \\ \mathbf{v_c} \quad &\mapsto \ \Delta = df_{K,W}(\mathbf{v_c}) = W^T\mathbb{M}^{\frac{1}{2}}{\mathbf{v_c}}^T Q^T\Lambda^{-\frac{1}{2}} \end{aligned} \tag{3.39}$$

Notice that we used the fact that on any fiber K is fixed, and so are Q and Λ. It is easy to verify that Δ defined in (3.39) indeed satisfies the condition $\mathrm{sym}(V^T\Delta) = \mathbb{O}$ for tangent vectors to the Stiefel manifold (at $V = f_{K,W}(\mathbf{c})$). The inverse mapping of (3.39) is given by:

$$\begin{aligned} df^{-1}_{K,W} : T_V\mathcal{V}_{n-1,3} &\to T_{f^{-1}_{K,W}(V)}\pi^{-1}(K) = V_{f^{-1}_{K,W}(V)} \\ \Delta \quad &\mapsto \ \mathbf{v}_{f^{-1}_{K,W}(V)} = Q^T\Lambda^{\frac{1}{2}}\Delta^T W^T\mathbb{M}^{-\frac{1}{2}}. \end{aligned} \tag{3.40}$$

The mapping (3.40) is very useful to produce vector fields in configuration space that leave invariant the coefficient of inertia tensor (i.e. democratic motions), starting from vector fields on the Stiefel manifold. We will exploit this idea in section 4.2.1, using a gradient vector field on $\mathcal{V}_{n-1,3}$ to produce a democratic motion maximizing a certain cost function.

3.3.4 Horizontal spaces and a splitting of kinetic energy

While the vertical space $V_{\mathbf{c}}$, $\forall \mathbf{c} \in \mathcal{C}^{3d}$, follows directly from the projection map π, there are many possible choices for the horizontal space $H_{\mathbf{c}}$ s.t. $H_{\mathbf{c}} \oplus V_{\mathbf{c}} = T_{\mathbf{c}}\mathcal{C}^{3d}$. Since $\mathcal{C}^{3d}$ is already equipped with the Riemannian metric (3.8), which is invariant along the fibers, it is sensible to choose $H_{\mathbf{c}}$ as the orthogonal complement of $V_{\mathbf{c}}$. The horizontal space defined in this way can be characterized as follows.

Proposition 3.3.7. *For each* $\mathbf{c} \in \mathcal{C}^{3d}$*, the* horizontal space $H_{\mathbf{c}}$ *orthogonal to* $V_{\mathbf{c}}$*, with respect to metric* (3.8)*, is given by:*

$$H_{\mathbf{c}} = \{\mathbf{v_c} \in T_{\mathbf{c}}\mathcal{C}^{3d} \; s.t. \; \mathbf{v_c} = S\mathbf{c}, \; S \in \mathbb{R}^{3\times 3}_{sym}\}. \tag{3.41}$$

Proof. Every tangent vector $\mathbf{v_c} = S\mathbf{c}$, $S \in \mathbb{R}^{3\times 3}_{sym}$, is orthogonal to the vertical space $V_{\mathbf{c}}$:

$$\langle \mathbf{v_c}, \mathbf{w_c} \rangle_{\mathbf{c}} = \mathrm{tr}(\mathbf{v_c}\mathbb{M}\mathbf{w_c}^T) = \mathrm{tr}(S\mathbf{c}\mathbb{M}\mathbf{w_c}^T) = 0, \; \forall \mathbf{w_c} \in V_{\mathbf{c}},$$

by the fact that $\mathbf{c}\mathbb{M}\mathbf{w_c}^T$ is skew-symmetric if $\mathbf{w_c} \in V_{\mathbf{c}}$, and the trace of the product of any symmetric matrix and any skew-symmetric one is zero. Therefore the set on the right hand side in (3.41) is a linear subspace of $T_{\mathbf{c}}\mathcal{C}^{3d}$ included in $H_{\mathbf{c}}$ (which by definition is itself a linear subspace of $T_{\mathbf{c}}\mathcal{C}^{3d}$). The dimension of such subspace is six, because $\mathbb{R}^{3\times 3}_{sym} \cong \mathbb{R}^6$. Since $H_{\mathbf{c}} \oplus V_{\mathbf{c}} = T_{\mathbf{c}}\mathcal{C}^{3d}$, the dimension of $H_{\mathbf{c}}$ must also be equal to $\dim(T_{\mathbf{c}}\mathcal{C}^{3d}) - \dim(V_{\mathbf{c}}) = (3n-3) - (3n-9) = 6$. Hence, by a simple dimensional argument, the set on the right hand side in (3.41) is actually the whole $H_{\mathbf{c}}$. □

Since $(\mathcal{C}^{3d}, \pi, \mathcal{K}, \mathcal{V}_{n-1,3})$ is not a principal bundle, we cannot use the mechanical connection machinery to obtain the orthogonal splitting of a generic tangent vector (say $\mathbf{v_c}$) into its vertical and horizontal components. Instead, we need to compute the Ehresmann connection by using the definition of orthogonal projection of a tangent vector (recall (2.1)).

Proposition 3.3.8 (**Ehresmann connection**). *For the smooth fiber bundle* $(\mathcal{C}^{3d}, \pi, \mathcal{K}, \mathcal{V}_{n-1,3})$*, the Ehresmann connection associated to the metric* (3.8) *(i.e. the one giving the orthogonal projection of each vector* $\mathbf{v_c}$ *with respect to this metric) is given by:*

$$A_{\mathbf{c}}(\mathbf{v_c}) = \mathbf{v_c} - S(\mathbf{c}, \mathbf{v_c})\mathbf{c}, \tag{3.42}$$

where $S(\mathbf{c}, \mathbf{v_c})$ *is the solution of the Lyapunov equation:*

$$S(\mathbf{c}, \mathbf{v_c})K(\mathbf{c}) + K(\mathbf{c})S(\mathbf{c}, \mathbf{v_c}) = F(\mathbf{c}, \mathbf{v_c}), \tag{3.43}$$

with $F(\mathbf{c}, \mathbf{v_c}) \triangleq \mathbf{v_c}\mathbb{M}\mathbf{c}^T + \mathbf{c}\mathbb{M}\mathbf{v_c}^T = 2\,\mathrm{sym}(\mathbf{v_c}\mathbb{M}\mathbf{c}^T)$.

Proof. From the knowledge of the vertical space (3.38) and the horizontal space (3.41), the Ehresmann connection must satisfy the following conditions, for each $\mathbf{v_c} \in T_{\mathbf{c}}\mathcal{C}^{3d}$: (i) $A_{\mathbf{c}}(\mathbf{v_c}) = \mathbf{v_c} - S\mathbf{c}$, with $S = S^T$, and (ii) $\mathrm{sym}(A_{\mathbf{c}}(\mathbf{v_c})\mathbb{M}\mathbf{c}^T) = \mathbb{O} \Rightarrow A_{\mathbf{c}}(\mathbf{v_c})\mathbb{M}\mathbf{c}^T + \mathbf{c}\mathbb{M}A_{\mathbf{c}}(\mathbf{v_c})^T = \mathbb{O}$. The combination of these constraints yields: $(\mathbf{v_c} - S\mathbf{c})\mathbb{M}\mathbf{c}^T = -\mathbf{c}\mathbb{M}(\mathbf{v_c} - S\mathbf{c})^T \Rightarrow SK + KS = \mathbf{v_c}\mathbb{M}\mathbf{c}^T + \mathbf{c}\mathbb{M}\mathbf{v_c}^T$, which is the Lyapunov equation (3.43). □

Since $K(\mathbf{c})$ is symmetric and positive definite, the existence and uniqueness of a symmetric solution $S(\mathbf{c}, \mathbf{v_c})$ to the Lyapunov equation (3.43) is always guar-

anteed (this is a well-known result that could be proved studying the equation in its vector form); one way of expressing explicitly such solution is the following:

$$S(\mathbf{c}, \mathbf{v_c}) = \int_0^\infty e^{-K(\mathbf{c})t} F(\mathbf{c}, \mathbf{v_c}) e^{-K(\mathbf{c})t} dt, \tag{3.44}$$

which highlights the symmetry of $S(\mathbf{c}, \mathbf{v_c})$ and its smoothness in the arguments (but it is not very useful in actual computations).

Alternatively, given an eigendecomposition $K = Q^T \Lambda Q$ of the coefficient of inertia tensor, with $\Lambda = \mathrm{diag}(\lambda_1, \lambda_2, \lambda_3)$, $S(\mathbf{c}, \mathbf{v_c})$ can be expressed as:

$$S(\mathbf{c}, \mathbf{v_c}) = Q^T(\mathbf{c}) F_\Lambda(\mathbf{c}, \mathbf{v_c}) Q(\mathbf{c}),\ F_\Lambda = \begin{bmatrix} \frac{\tilde{F}_{11}}{2\lambda_1} & \frac{\tilde{F}_{12}}{\lambda_1+\lambda_2} & \frac{\tilde{F}_{13}}{\lambda_1+\lambda_3} \\ \frac{\tilde{F}_{12}}{\lambda_1+\lambda_2} & \frac{\tilde{F}_{22}}{2\lambda_2} & \frac{\tilde{F}_{23}}{\lambda_2+\lambda_3} \\ \frac{\tilde{F}_{13}}{\lambda_1+\lambda_3} & \frac{\tilde{F}_{23}}{\lambda_2+\lambda_3} & \frac{\tilde{F}_{33}}{2\lambda_3} \end{bmatrix}, \tag{3.45}$$

$$\text{with } \tilde{\mathrm{F}} = \begin{bmatrix} \tilde{F}_{11} & \tilde{F}_{12} & \tilde{F}_{13} \\ \tilde{F}_{12} & \tilde{F}_{22} & \tilde{F}_{23} \\ \tilde{F}_{13} & \tilde{F}_{23} & \tilde{F}_{33} \end{bmatrix} = \mathrm{Q}\,\mathrm{F}(\mathbf{c}, \mathbf{v_c})\,\mathrm{Q}^{\mathrm{T}}. \tag{3.46}$$

As it will be shown later, the explicit expression (3.45) is more convenient than the implicit one (3.43) when discussing certain types of elementary tangent vectors. For this reason we will derive the mathematical tools associated to the connection (horizontal lift, splitting of kinetic energy) using both expressions. One issue with (3.45) is that it fails to be smooth at configurations corresponding to coefficient of inertia tensors with repeated eigenvalues.

The horizontal projection of any tangent vector $\mathbf{v_c} \in T_{\mathbf{c}}\mathcal{C}^{3d}$ is clearly given by $\mathrm{hor}(\mathbf{v_c}) = S(\mathbf{c}, \mathbf{v_c})\mathbf{c} = Q^T F_\Lambda(\mathbf{c}, \mathbf{v_c}) Q\mathbf{c}$. Notice that if $\mathbf{v_c}$ is vertical, then

$F(\mathbf{c}, \mathbf{v_c}) = \tilde{F}(\mathbf{c}, \mathbf{v_c}) = F_\Lambda(\mathbf{c}, \mathbf{v_c}) = \mathbb{O}$, hence $A_\mathbf{c}(\mathbf{v_c}) = \mathbf{v_c}$, in accordance with the projection property of Ehresmann connections.

Using the connection (3.42), it is now possible to obtain a breakdown of the kinetic energy that is alternative to the classical one presented in section 3.2 (summarized by (3.21)). We can in fact divide the relative (to the center of mass) component of kinetic energy E_{rel}, defined in (3.9), into a vertical part due to motion along an orbit of the democracy group, and a horizontal part due to change in the coefficient of inertia tensor:

$$E_{rel}(\mathbf{c}, \mathbf{v_c}) = \frac{1}{2}\langle \mathbf{v_c}, \mathbf{v_c}\rangle_\mathbf{c} = \frac{1}{2}\langle A_\mathbf{c}(\mathbf{v_c}), A_\mathbf{c}(\mathbf{v_c})\rangle_\mathbf{c} + \frac{1}{2}\langle \mathrm{hor}(\mathbf{v_c}), \mathrm{hor}(\mathbf{v_c})\rangle_\mathbf{c}$$
$$\triangleq \quad E_{dem}(\mathbf{c}, \mathbf{v_c}) \quad + \quad E_K(\mathbf{c}, \mathbf{v_c}). \tag{3.47}$$

The "horizontal" component E_K can be computed as:

$$E_K(\mathbf{c}, \mathbf{v_c}) = \frac{1}{2}\mathrm{tr}(S(\mathbf{c}, \mathbf{v_c})\mathbf{c}\mathbb{M}\mathbf{c}^T S(\mathbf{c}, \mathbf{v_c})) = \frac{1}{2}\mathrm{tr}(S(\mathbf{c}, \mathbf{v_c})KS(\mathbf{c}, \mathbf{v_c})), \tag{3.48}$$

or alternatively, using (3.45) and the invariance of the trace operator to similarity transformations, as:

$$E_K(\mathbf{c}, \mathbf{v_c}) = \frac{1}{2}\mathrm{tr}(Q^T F_\Lambda(\mathbf{c}, \mathbf{v_c})QKQ^T F_\Lambda^T(\mathbf{c}, \mathbf{v_c})Q) = \frac{1}{2}\mathrm{tr}(F_\Lambda(\mathbf{c}, \mathbf{v_c})\Lambda F_\Lambda(\mathbf{c}, \mathbf{v_c})). \tag{3.49}$$

From (3.9), (3.47) and (3.48) or (3.49), we have therefore the detailed splitting of kinetic energy:

$$E(\mathbf{r}, \mathbf{v_r}) = E_{com} + E_K + E_{dem} =$$
$$= \frac{1}{2}M|\mathbf{v_{com}}|^2 + \frac{1}{2}\mathrm{tr}(S(\mathbf{c}, \mathbf{v_c})K(\mathbf{c})S(\mathbf{c}, \mathbf{v_c})) + E_{dem} \tag{3.50}$$
$$= \frac{1}{2}M|\mathbf{v_{com}}|^2 + \frac{1}{2}\mathrm{tr}(F_\Lambda(\mathbf{c}, \mathbf{v_c})\Lambda(\mathbf{c})F_\Lambda(\mathbf{c}, \mathbf{v_c})) + E_{dem}. \tag{3.51}$$

Given the horizontal component of a tangent vector $\mathbf{v_c} \in T_{\mathbf{c}}\mathcal{C}^{3d}$ (i.e. $\text{hor}(\mathbf{v_c}) = S(\mathbf{c}, \mathbf{v_c})\mathbf{c} = Q^T F_\Lambda(\mathbf{c}, \mathbf{v_c})Q\mathbf{c}$), it is possible to use the push-forward of the projection (3.26) to obtain the corresponding tangent vector in $\mathcal{K}$:

$$d\pi_{\mathbf{c}}(S(\mathbf{c}, \mathbf{v_c})\mathbf{c}) = \mathbf{c}\mathbb{M}\mathbf{c}^T S(\mathbf{c}, \mathbf{v_c}) + S(\mathbf{c}, \mathbf{v_c})\mathbf{c}\mathbb{M}\mathbf{c}^T = F(\mathbf{c}, \mathbf{v_c}), \tag{3.52}$$

or alternatively (in terms of the eigendecomposition of K):

$$d\pi_{\mathbf{c}}(Q^T F_\Lambda(\mathbf{c}, \mathbf{v_c})Q\mathbf{c}) = Q^T(F_\Lambda(\mathbf{c}, \mathbf{v_c})\Lambda + \Lambda F_\Lambda(\mathbf{c}, \mathbf{v_c}))Q. \tag{3.53}$$

Conversely, given any tangent vector $S_K \in T_K\mathcal{K} = \mathbb{R}^{3\times 3}_{sym}$ and a configuration $\mathbf{c} \in \pi^{-1}(K)$, it is obvious from (3.52) that the horizontal lift of S_K at $\mathbf{c}$, i.e. the unique horizontal vector in $T_{\mathbf{c}}\mathcal{C}^{3d}$ that is projected to S_K by $d\pi_{\mathbf{c}}$, is:

$$\text{lift}_{\mathbf{c}} S_K = S(\mathbf{c}, \mathbf{v_c})\mathbf{c}, \tag{3.54}$$

where $S(\mathbf{c}, \mathbf{v_c})$ solves the Lyapunov equation:

$$S(\mathbf{c}, \mathbf{v_c})K(\mathbf{c}) + K(\mathbf{c})S(\mathbf{c}, \mathbf{v_c}) = S_K. \tag{3.55}$$

Notice that, because K is a positive definite matrix, the mapping between S_K and the corresponding $S(\mathbf{c}, \mathbf{v_c})$ is a bijection. It is also easy to verify the following alternative expression using (3.53):

$$\text{lift}_{\mathbf{c}} S_K = Q^T G_\Lambda Q\mathbf{c}, \quad G_\Lambda = \begin{bmatrix} \frac{\tilde{G}_{11}}{2\lambda_1} & \frac{\tilde{G}_{12}}{\lambda_1+\lambda_2} & \frac{\tilde{G}_{13}}{\lambda_1+\lambda_3} \\ \frac{\tilde{G}_{12}}{\lambda_1+\lambda_2} & \frac{\tilde{G}_{22}}{2\lambda_2} & \frac{\tilde{G}_{23}}{\lambda_2+\lambda_3} \\ \frac{\tilde{G}_{13}}{\lambda_1+\lambda_3} & \frac{\tilde{G}_{23}}{\lambda_2+\lambda_3} & \frac{\tilde{G}_{33}}{2\lambda_3} \end{bmatrix}, \tag{3.56}$$

$$\text{where } \tilde{\mathrm{G}} = [\tilde{\mathrm{G}}_{\mathrm{ij}}] = \mathrm{Q}\mathrm{S}_{\mathrm{K}}\mathrm{Q}^{\mathrm{T}}. \tag{3.57}$$

Since the metric (3.8) is invariant to actions of the democracy group (hence invariant along the fibers), the induced Riemannian metric on base space $\mathcal{K}$ is well defined, taking any $\mathbf{c} \in \pi^{-1}(K)$:

$$\langle S_K, T_K \rangle_K \triangleq \langle \text{lift}_{\mathbf{c}} S_K, \text{lift}_{\mathbf{c}} T_K \rangle = \text{tr}\left(S(\mathbf{c}, \mathbf{v_c}) K(\mathbf{c}) T(\mathbf{c}, \mathbf{v_c})\right), \tag{3.58}$$

where $S(\mathbf{c}, \mathbf{v_c})$ and $T(\mathbf{c}, \mathbf{v_c})$ are solutions of the Lyapunov equations:

$$S(\mathbf{c}, \mathbf{v_c}) K(\mathbf{c}) + K(\mathbf{c}) S(\mathbf{c}, \mathbf{v_c}) = S_K \tag{3.59}$$

$$T(\mathbf{c}, \mathbf{v_c}) K(\mathbf{c}) + K(\mathbf{c}) T(\mathbf{c}, \mathbf{v_c}) = T_K. \tag{3.60}$$

Alternatively, using (3.56)-(3.57):

$$\langle S_K, T_K \rangle_K = \langle \text{lift}_{\mathbf{c}} S_K, \text{lift}_{\mathbf{c}} T_K \rangle = \text{tr}\left(G_\Lambda \Lambda H_\Lambda\right), \tag{3.61}$$

where $H_\Lambda = \begin{bmatrix} \frac{\tilde{H}_{11}}{2\lambda_1} & \frac{\tilde{H}_{12}}{\lambda_1+\lambda_2} & \frac{\tilde{H}_{13}}{\lambda_1+\lambda_3} \\ \frac{\tilde{H}_{12}}{\lambda_1+\lambda_2} & \frac{\tilde{H}_{22}}{2\lambda_2} & \frac{\tilde{H}_{23}}{\lambda_2+\lambda_3} \\ \frac{\tilde{H}_{13}}{\lambda_1+\lambda_3} & \frac{\tilde{H}_{23}}{\lambda_2+\lambda_3} & \frac{\tilde{H}_{33}}{2\lambda_3} \end{bmatrix}$, $\tilde{H} = Q T_K Q^T$ and G_Λ, $\tilde{G}$ as before.

Notice that (3.58) and (3.61) are different from the canonical metric on the space of symmetric positive definite matrices, which is $\langle S_K, T_K \rangle_K = \text{tr}(K^{-1} S_K K^{-1} T_K)$ (see for example [42]).

3.3.5 Comparison with the classical fibering

We complete this section with a few diagrams that display the alternative fiber bundle side by side with the classical fiber bundle of section 3.2.

The notation $x \in X \overset{y \in Y}{\rightarrow} z \in Z$ used in diagrams 1 and 2 means that X is locally equivalent to $Y \times Z$, i.e. any $x \in X$ can be locally parametrized by a pair (y, z) where $y \in Y$, $z \in Z$. In diagrams 3 and 4, the tree structure stands for the decomposition into additive components.

We denote as $\mathcal{R}^{2^+d}$ and $\mathcal{R}^{3d}$ the subsets of the collective configuration space ($\mathcal{R} \cong \mathbb{R}^{3\times n}$) obtained removing the configurations that do not satisfy the appropriate conditions on the coefficient of inertia tensor with respect to the center of mass: $\mathbf{c} = \pi(\mathbf{r}) \in \mathcal{C}^{2^+d}\ \forall \mathbf{r} \in \mathcal{R}^{2^+d}$, $\mathbf{c} = \pi(\mathbf{r}) \in \mathcal{C}^{3d}\ \forall \mathbf{r} \in \mathcal{R}^{3d}$.

In diagram 3a, the vertical component of the tangent vector could also be expressed in the form $A(\mathbf{c}, \mathbf{v_c})\mathbf{c}$, with $A(\mathbf{c}, \mathbf{v_c}) \in \mathbb{R}^{3\times 3}$ being the skew-symmetric matrix associated to the vector $I_{\mathbf{c}}^{-1}\mathbf{J}(\mathbf{c}, \mathbf{v_c})$. This highlights a remarkable "duality" in the two alternative fiberings: whereas in the classical fibering the *vertical* component of $\mathbf{v_c}$ is simply equal to $\mathbf{c}$ premultiplied by a *skew-symmetric* matrix ($A(\mathbf{c}, \mathbf{v_c})\mathbf{c}$), in the alternative fibering the *horizontal* component of $\mathbf{v_c}$ is simply given by $\mathbf{c}$ premultiplied by a *symmetric* matrix ($S(\mathbf{c}, \mathbf{v_c})\mathbf{c}$).

$$\begin{array}{c} \mathbf{r} \in \mathcal{R}^{2^+d} \\ \Big\downarrow {\scriptstyle \mathbf{r_{com}} \in \mathbb{R}^3} \\ \mathbf{c} \in \mathcal{C}^{2^+d} \\ \Big\downarrow {\scriptstyle Q \in SO(3)} \\ \mathbf{s} \in \mathcal{S} \end{array} \qquad \begin{array}{c} \mathbf{r} \in \mathcal{R}^{3d} \\ \Big\downarrow {\scriptstyle \mathbf{r_{com}} \in \mathbb{R}^3} \\ \mathbf{c} \in \mathcal{C}^{3d} \\ \Big\downarrow {\scriptstyle V = f_{K,W}(\mathbf{c}) \in \mathcal{V}_{n-1,3}} \\ K = \pi(\mathbf{c}) \in \mathcal{K} \end{array}$$

$1a)$ $\qquad$ $1b)$

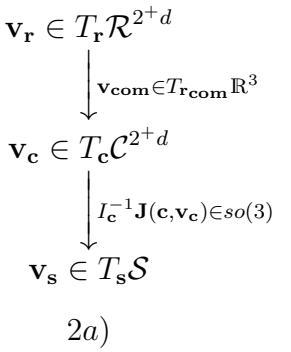

$2a)$

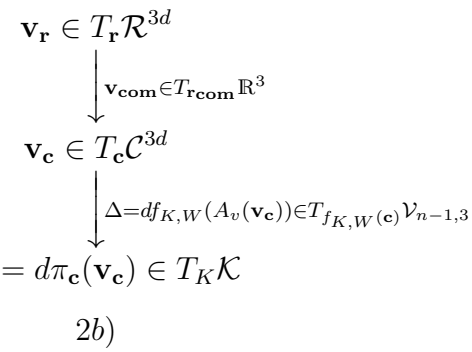

$2b)$

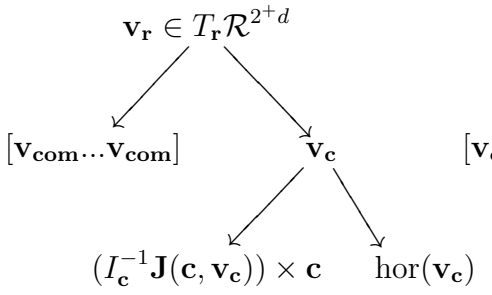

$3a)$

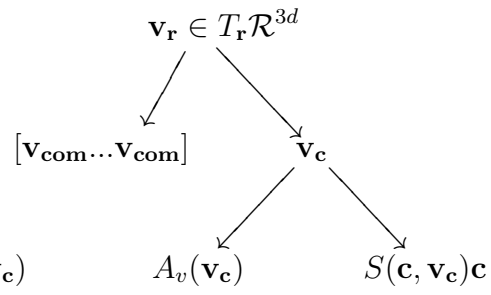

$3b)$

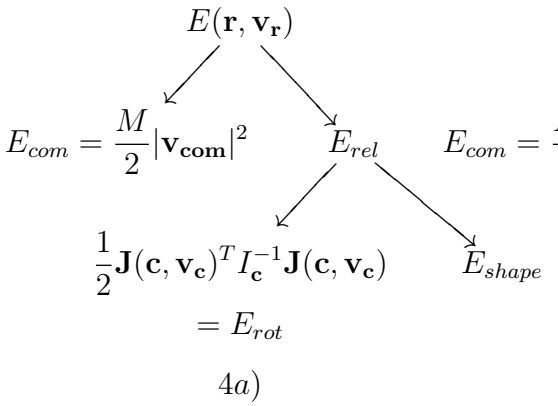

$4a)$

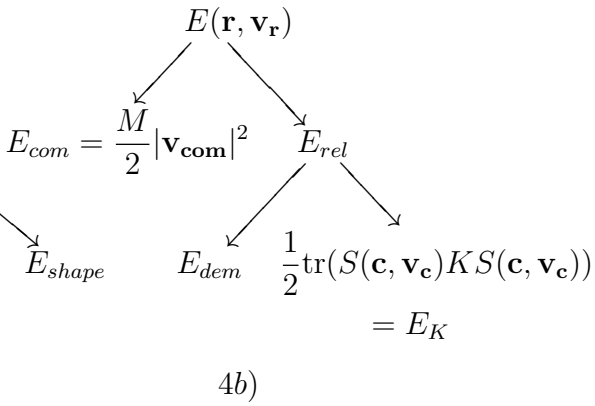

$4b)$

Comparison Diagrams. Diagrams comparing the classical fiber bundle of section 3.2 (denoted by 'a') and the alternative fiber bundle described in this section (denoted by 'b').

3.4 Decomposition of collective motions

The fiber bundle described in the previous section leads to a new decomposition of tangent vectors (instantaneous motions), and by extension of vector fields (global motions), for the n-body problem. Any tangent vector $\mathbf{v_r} \in T_{\mathbf{r}}\mathcal{R}^{3d}$ can be decomposed into three "elementary" components, as in diagram 3b, or alternatively expressed as a triple $\mathbf{v_r} \equiv (\mathbf{v_{com}}, \Delta, S_K)$ as schematically shown in diagram 2b. Vectors corresponding to triples $(\mathbf{v_{com}}, \mathbb{O}, \mathbb{O})$ (i.e. for which $E_{com} > 0, E_{dem} = E_K = 0$) correspond to rigid translations of the collective, while triples $(\mathbf{0}, \Delta, \mathbb{O})$ (i.e. $E_{dem} > 0, E_{com} = E_K = 0$) and $(\mathbf{0}, \mathbb{O}, S_K)$ (i.e. $E_K > 0, E_{com} = E_{dem} = 0$) are "vertical" and "horizontal" vectors respectively (with no rigid translation). Here vertical tangent vectors are those which preserve (instantaneously) the coefficient of inertia tensor of the collective, whereas horizontal tangent vectors induce no instantaneous motion along the fibers (no particle reshuffling) while changing the coefficient of inertia tensor. Of course a generic tangent vector will be given by a combination of these elementary tangent vectors.

This classification of elementary tangent vectors becomes even more interesting when combined with the one given by the classical fibering (see diagrams 1a-4a), for which "vertical" tangent vectors correspond to instantaneous rigid rotations of the collective about the center of mass. The two classifications are not independent, but coupled from the fact that $E_{rot} + E_{shape} = E_{rel} = E_{dem} + E_K$. The combined set of elementary types of tangent vectors, which can be thought of

as the set of elementary instantaneous motions of the collective, is listed in table 3.1. Except in very special cases, elementary motions in one of the classifications do not correspond to elementary motions in the other; this will be evident from the following discussion on some of the elementary motion types.

Elementary motion type	E_{com}	E_{rot}	E_{shape}	E_{dem}	E_K
Rigid translation	> 0	$= 0$	$= 0$	$= 0$	$= 0$
Rigid rotation	$= 0$	> 0	$= 0$	> 0	> 0
Shape transformation	$= 0$	$= 0$	> 0	> 0	> 0
Democratic motion	$= 0$	> 0	> 0	> 0	$= 0$
Inertia tensor transformation	$= 0$	> 0	> 0	$= 0$	> 0
Special case: compression/expansion	$= 0$	$= 0$	> 0	$= 0$	> 0

Table 3.1: Characterization of elementary types of tangent vectors in $T\mathcal{R}^{3d}$ (instantaneous motions of three-dimensional collectives)

Rigid rotations with respect to the center of mass. A tangent vector $\mathbf{v_r} \in T_{\mathbf{r}}\mathcal{R}^{3d}$ is a (instantaneous) *rigid rotation with respect to the center of mass* if it satisfies $\mathbf{v_r} = \mathbf{v_c} = \mathbf{a} \times \mathbf{c}$, where $\mathbf{a} = I_{\mathbf{c}}^{-1}\mathbf{J}(\mathbf{c}, \mathbf{v_c})$, and hence, in terms of energies, $E(\mathbf{r}, \mathbf{v_r}) = E_{rot} = \frac{1}{2}\mathbf{J}(\mathbf{c}, \mathbf{v_c}))^T I_{\mathbf{c}}^{-1}\mathbf{J}(\mathbf{c}, \mathbf{v_c})$. Alternatively, $\mathbf{v_r} = \mathbf{v_c} = A\mathbf{c}$ for some $A \in so(3)$, the skew-symmetric matrix associated to $\mathbf{a}$. It is interesting to decompose tangent vectors of this type (elementary for the classical fiber bundle of diagram 3a) with respect to the alternative fiber bundle (diagram 3b). From the definition of horizontal space (3.41), the first obvious result is that there is always

a vertical component (a motion along the democracy group orbit) associated to each rigid rotation: if the motion was purely horizontal, it would have to be $\mathbf{v_c} = S\mathbf{c}$ for some $S \in \mathbb{R}^{3\times 3}$ symmetric, which is clearly impossible.

The horizontal component of a rigid rotation $\mathbf{v_c} = A\mathbf{c}$ can be computed using (3.42)-(3.45), where in this case $\tilde{F} = Q(A\mathbf{c}\mathbb{M}\mathbf{c}^T + \mathbf{c}\mathbb{M}\mathbf{c}^T A^T)Q^T = Q(AK - KA)Q^T = QAQ^T\Lambda - \Lambda QAQ^T$, yielding:

$$\mathrm{hor}(A\mathbf{c}) = Q^T \begin{bmatrix} 0 & \frac{\tilde{a}_{12}(\lambda_2-\lambda_1)}{\lambda_1+\lambda_2} & \frac{\tilde{a}_{13}(\lambda_3-\lambda_1)}{\lambda_1+\lambda_3} \\ \frac{\tilde{a}_{12}(\lambda_2-\lambda_1)}{\lambda_1+\lambda_2} & 0 & \frac{\tilde{a}_{23}(\lambda_3-\lambda_2)}{\lambda_2+\lambda_3} \\ \frac{\tilde{a}_{13}(\lambda_3-\lambda_1)}{\lambda_1+\lambda_3} & \frac{\tilde{a}_{23}(\lambda_3-\lambda_2)}{\lambda_2+\lambda_3} & 0 \end{bmatrix} Q\,\mathbf{c}, \tag{3.62}$$

where $\tilde{A} = \begin{bmatrix} 0 & \tilde{a}_{12} & \tilde{a}_{13} \\ -\tilde{a}_{12} & 0 & \tilde{a}_{23} \\ -\tilde{a}_{13} & -\tilde{a}_{23} & 0 \end{bmatrix} \triangleq QAQ^T.$

The horizontal component therefore does not vanish unless at least two eigenvalues are identical and $\tilde{a}_{ij} = 0\ \forall i,j\ s.t.\ \lambda_i \neq \lambda_j$. These cases correspond to rotations about an axis orthogonal to the eigenspace of a repeated eigenvalue, i.e. to rotations about a symmetry axis of the ellipsoid of inertia tensor. Aside from these special cases, every rigid rotation of the collective induces a transformation of the coefficient of inertia tensor given by (using (3.53) and $\tilde{A}$ defined as above):

$$S_K = Q^T \begin{bmatrix} 0 & \tilde{a}_{12}(\lambda_2-\lambda_1) & \tilde{a}_{13}(\lambda_3-\lambda_1) \\ \tilde{a}_{12}(\lambda_2-\lambda_1) & 0 & \tilde{a}_{23}(\lambda_3-\lambda_2) \\ \tilde{a}_{13}(\lambda_3-\lambda_1) & \tilde{a}_{23}(\lambda_3-\lambda_2) & 0 \end{bmatrix} Q. \tag{3.63}$$

As will be shown in the following, (3.63) is a transformation that leaves invariant the eigenvalues of K, and only rotates its eigenvectors; we can think of it as a rigid rotation of the ellipsoid associated to K (in the sense of section 3.3.2) or equivalently a rigid rotation of the ellipsoid of inertia tensor.

As for the non-vanishing vertical component of a rigid rotation $\mathbf{v_c} = A\mathbf{c}$, it can be computed as:

$$A\mathbf{c} - \mathrm{hor}(A\mathbf{c}) = 2\,Q^T \begin{bmatrix} 0 & \frac{\lambda_1}{\lambda_1+\lambda_2}\tilde{a}_{12} & \frac{\lambda_1}{\lambda_1+\lambda_3}\tilde{a}_{13} \\ -\frac{\lambda_2}{\lambda_1+\lambda_2}\tilde{a}_{12} & 0 & \frac{\lambda_2}{\lambda_2+\lambda_3}\tilde{a}_{23} \\ -\frac{\lambda_3}{\lambda_1+\lambda_3}\tilde{a}_{13} & -\frac{\lambda_3}{\lambda_2+\lambda_3}\tilde{a}_{23} & 0 \end{bmatrix} Q\,\mathbf{c}, \tag{3.64}$$

or in terms of a tangent vector to the Stiefel manifold diffeomorphic to the fiber passing through $\mathbf{c}$ (obtained using (3.39)):

$$\Delta = df_{K,W}(A\mathbf{c} - \mathrm{hor}(A\mathbf{c})) = 2\,V \begin{bmatrix} 0 & \frac{-\sqrt{\lambda_1}\sqrt{\lambda_2}}{\lambda_1+\lambda_2}\tilde{a}_{12} & \frac{-\sqrt{\lambda_1}\sqrt{\lambda_3}}{\lambda_1+\lambda_3}\tilde{a}_{13} \\ \frac{\sqrt{\lambda_1}\sqrt{\lambda_2}}{\lambda_1+\lambda_2}\tilde{a}_{12} & 0 & \frac{-\sqrt{\lambda_2}\sqrt{\lambda_3}}{\lambda_2+\lambda_3}\tilde{a}_{23} \\ \frac{\sqrt{\lambda_1}\sqrt{\lambda_3}}{\lambda_1+\lambda_3}\tilde{a}_{13} & \frac{\sqrt{\lambda_2}\sqrt{\lambda_3}}{\lambda_2+\lambda_3}\tilde{a}_{23} & 0 \end{bmatrix}, \tag{3.65}$$

where $V = f_{K,W}(\mathbf{c}) \in \mathcal{V}_{n-1,3}$.

Inertia tensor transformations. We define a tangent vector $\mathbf{v_r} \in T_{\mathbf{r}}\mathcal{R}^{3d}$ an *inertia tensor transformation* if it modifies the coefficient of inertia tensor (and thus the corresponding ellipsoid) while inducing no instantaneous motion along the democracy group orbit. In terms of energies, an inertia tensor transformation must satisfy $E(\mathbf{r}, \mathbf{v_r}) = E_K = \frac{1}{2}\mathrm{tr}(S(\mathbf{c}, \mathbf{v_c})KS(\mathbf{c}, \mathbf{v_c})) = \frac{1}{2}\mathrm{tr}(F_\Lambda(\mathbf{v_c})\Lambda F_\Lambda(\mathbf{v_c}))$.

As discussed in section 3.3, vectors with these characteristics are obtained

by horizontally lifting tangent vectors $S_K \in T_K\mathcal{K}$ using (3.54)-(3.57). Every $K \in \mathcal{K}$ can be expressed as $K = Q^T \Lambda Q$, where $\Lambda = \text{diag}(\lambda_1, \lambda_2, \lambda_3)$ is the matrix of eigenvalues of K and $Q \in SO(3)$ is the corresponding matrix of eigenvectors. Hence there are two special types of vectors $S_K \in T_K\mathcal{K}$: those that (instantaneously) change the eigenvectors of K but not its eigenvalues and those that change the eigenvalues but not its eigenvectors. On the ellipsoid associated to K, and equivalently on the ellipsoid of inertia, the first vectors have the effect of a rotation, while the others have the effect of a deformation. For this reason, we call the inertia tensor transformations obtained by horizontal lift of these special types of vectors as **inertia tensor rotations** and **inertia tensor deformations** respectively.

The curves in $\mathcal{K}$ corresponding to inertia tensor rotations have the form $K(t) = Q^T(t)\Lambda Q(t)$, and hence tangent vectors of this type are given by: $S_K = A^T Q^T \Lambda Q + Q^T \Lambda Q A$, for some $A \in so(3)$ (in fact $T_Q SO(3) = \{QA,\ A \in so(3)\}$). Comparing with (3.62)-(3.63) confirms that the transformations of the coefficient of inertia tensor induced by rigid rotations of the collective are indeed rotations of the ellipsoid of inertia. Moreover, since it is impossible to have rigid rotations of the collective with no democratic motion, it cannot be $E = E_{rot} = E_K$ and therefore it is also impossible to have rigid rotations of the ellipsoid of inertia without shape transformation. Hence in general rotations of the ellipsoid of inertia are characterized by $E_{dem} = 0, E_K > 0, E_{rot} > 0, E_{shape} > 0$.

The curves in $\mathcal{K}$ corresponding to inertia tensor deformations are instead

given by: $K(t) = Q^T\Lambda(t)Q$, with tangent vectors of the type: $S_K = Q^T V_\Lambda Q$, for some $V_\Lambda = \text{diag}(v_{\lambda_1}, v_{\lambda_2}, v_{\lambda_3})$. Horizontal lift to $T_{\mathbf{r}}\mathcal{R}^{3d}$ (using (3.56)-(3.57)) yields:

$$\mathbf{v_r} = \mathbf{v_c} = \frac{1}{2}Q^T \begin{bmatrix} \frac{v_{\lambda_1}}{\lambda_1} & 0 & 0 \\ 0 & \frac{v_{\lambda_2}}{\lambda_2} & 0 \\ 0 & 0 & \frac{v_{\lambda_3}}{\lambda_3} \end{bmatrix} Q\mathbf{c}. \tag{3.66}$$

The angular momentum associated to tangent vectors like (3.66) is:

$$\mathbf{J}(\mathbf{c}, \mathbf{v_c}) = \sum_{i=1}^{n} m_i \left(\mathbf{c_i} \times Q^T \begin{bmatrix} \frac{v_{\lambda_1}}{\lambda_1} & 0 & 0 \\ 0 & \frac{v_{\lambda_2}}{\lambda_2} & 0 \\ 0 & 0 & \frac{v_{\lambda_3}}{\lambda_3} \end{bmatrix} Q\mathbf{c_i} \right), \tag{3.67}$$

hence in general $\mathbf{J}(\mathbf{c}, \mathbf{v_c}) \neq \mathbf{0}$ and $E_{rot} > 0$ for deformations of the ellipsoid of inertia. Nevertheless there is a special set of deformations, those which satisfy $v_{\lambda_1} = \alpha\lambda_1, v_{\lambda_2} = \alpha\lambda_2, v_{\lambda_3} = \alpha\lambda_3$ for some $\alpha \in \mathbb{R}$, which have zero angular momentum. Notice that these tangent vectors reduce to the simple form: $\mathbf{v_r} = \mathbf{v_c} = \alpha\mathbf{c} \Rightarrow \mathbf{v_{ri}} = \alpha(\mathbf{r_i} - \mathbf{r_{com}})\ \forall i = 1, ..., n$ for some $\alpha \in \mathbb{R}$, and hence they really correspond to instantaneous **pure compressions** (if $\alpha < 0$) or **pure expansions** (if $\alpha > 0$) of the collective, with respect to the center of mass. Compressions and expansions are rare examples of motions that are elementary with respect to both classifications; in particular they are "horizontal" motions with respect to both fiber bundle formulations.

In general, any ellipsoid of inertia transformation $\mathbf{v_c} = S(\mathbf{c}, \mathbf{v_c})\mathbf{c}$ can be decomposed into a compression (or expansion) and another component, orthogonal

to the compression (expansion):

$$S(\mathbf{c}, \mathbf{v_c})\mathbf{c} = \alpha(\mathbf{c}, \mathbf{v_c})\mathbf{c} + \tilde{S}(\mathbf{c}, \mathbf{v_c})\mathbf{c}, \tag{3.68}$$

$$\langle \alpha(\mathbf{c}, \mathbf{v_c})\mathbf{c}, \tilde{S}(\mathbf{c}, \mathbf{v_c})\mathbf{c} \rangle_{\mathbf{c}} = 0. \tag{3.69}$$

It is easy to verify that the only value of $\alpha(\mathbf{c}, \mathbf{v_c})$ that satisfies (3.68)-(3.69) (with the usual metric (3.8)) is:

$$\alpha(\mathbf{c}, \mathbf{v_c}) = \frac{\mathrm{tr}(K(\mathbf{c})S(\mathbf{c}, \mathbf{v_c}))}{\mathrm{tr}(K(\mathbf{c}))} = \frac{\mathrm{tr}(\mathbf{v_c}\mathbb{M}\mathbf{c}^T)}{\mathrm{tr}(K(\mathbf{c}))}, \tag{3.70}$$

where in the last step we have used (3.43). Hence the component of relative kinetic energy of a collective motion that is associated to its expansion (or compression) can be computed as follows:

$$E_{size}(\mathbf{c}, \mathbf{v_c}) = \langle \alpha(\mathbf{c}, \mathbf{v_c})\mathbf{c}, \alpha(\mathbf{c}, \mathbf{v_c})\mathbf{c} \rangle_{\mathbf{c}} = \alpha^2(\mathbf{c}, \mathbf{v_c})\mathrm{tr}(\mathbf{c}\mathbb{M}\mathbf{c}^T) = \frac{\mathrm{tr}^2(\mathbf{v_c}\mathbb{M}\mathbf{c}^T)}{\mathrm{tr}(K(\mathbf{c}))}. \tag{3.71}$$

The same result could have been obtained by orthogonal decomposition of shape transformations ($\mathbf{v_c} - I_{\mathbf{c}}^{-1}\mathbf{J}(\mathbf{c}, \mathbf{v_c}) \times \mathbf{c}$), which also have pure compressions or expansions as components.

Other elementary motions. The other elementary (instantaneous) motions that can be identified are rigid translations, shape transformations and democratic motions. The **rigid translations** are the simplest collective motions, characterized by all the individual particles moving in the same direction: $\mathbf{v_r} = [\mathbf{v_{com}} \ldots \mathbf{v_{com}}]$ for some $\mathbf{v_{com}} \in \mathbb{R}^3$, and $E = E_{com} = \frac{M}{2}|\mathbf{v_{com}}|^2$. The rigid motions (rigid translations and rigid rotations) correspond to *relative equilibria*

in the language of the classical fiber bundle (motions that project to equilibria in shape space). Conversely, **shape transformations** are defined as those with zero angular momentum with respect to the center of mass, i.e. those that instantaneously produce no rigid motion of the collective. They are characterized by $\mathbf{v_r} = \mathbf{v_c}$ s.t. $\mathbf{J}(\mathbf{c}, \mathbf{v_c}) = \mathbf{0}$ and therefore $E_{rot} = 0$, but in general $E_{dem} > 0$ and $E_K > 0$. Finally we call **democratic motions** the tangent vectors $\mathbf{v_r} = \mathbf{v_c}\,\text{s.t.}\,\text{sym}(\mathbf{v_c}\mathbb{M}\mathbf{c}^{\mathrm{T}}) = \mathbb{O}$ and hence, in terms of energies, $E_K = 0$. Democratic motions are interesting because they correspond to particle motions that leave invariant the coefficient of inertia tensor, which in the sense explained before coarsely approximates the overall configuration of the collective. Tangent vectors that are democratic motions can be associated to tangent vectors on a Stiefel manifold, as detailed in section 3.3.3.

Classification of elementary vector fields. This classification of elementary tangent vectors (instantaneous motions) can be extended to a classification of elementary *vector fields* in the obvious way: an elementary vector field can be defined as one composed only of tangent vectors of a certain elementary type. For example a vector field $X \in \mathcal{X}(\mathcal{R}^{3d})$ is a "rigid rotation with respect to the center of mass" if $X_{\mathbf{r}} = \mathbf{a}(\mathbf{r}) \times (\mathbf{r} - \mathbf{r_{com}})\ \forall \mathbf{r} \in \mathcal{R}^{3d}$ (and hence $E_{rot}(\mathbf{r}, X_{\mathbf{r}}) > 0, E_{com}(\mathbf{r}, X_{\mathbf{r}}) = E_{shape}(\mathbf{r}, X_{\mathbf{r}}) = 0 \quad \forall \mathbf{r} \in \mathcal{R}^{3d}$). Here one has to be careful in giving the right interpretation to the elementary vector fields that are composed of purely horizontal tangent vectors. If in fact the curvature of the connection is non-trivial, i.e. it does not vanish everywhere, even vector

fields composed of horizontal tangent vectors can produce displacements along the fiber, or "vertical motions". For example it is a well-known fact that the mechanical connection for the principal bundle of section 3.2 is non-trivial (see for example [35]), and as a result a "shape transformation" typically produces some rigid rotation while changing the shape of the collective. In particular, horizontal lifts of closed loops in shape space generate rigid rotations of the collective, known as geometric phases, which have been studied extensively (e.g. [1], [35]). As will be shown later, the Ehresmann connection (3.42) for the alternative fiber bundle of section 3.3 has also non-trivial curvature, and certain vector fields of the type "inertia tensor transformation" may also induce a particular class of democratic motions. Hence horizontal elementary vector fields such as shape transformations and inertia tensor transformations should not be thought of as motions that exclusively modify the quantities of interest (shape, coefficient of inertia tensor) but rather as motions for which the kinetic energy is solely allocated to the modification of such quantities, and the generation of other types of motion, though not excluded, comes at "no kinetic energy cost". In this sense shape transformations are the optimal choice for modifying the shape of the collective, and inertia tensor transformations are the optimal choice for modifying the coefficient of inertia tensor.

3.5 Curvature computation for the alternative fibering

Given vector fields $X, Y \in \mathcal{X}(\mathcal{C}^{3d})$, the curvature form for an Ehresmann connection A can be computed from (2.2):

$$B_{\mathbf{c}}(X(\mathbf{c}), Y(\mathbf{c})) = -A_{\mathbf{c}}([\text{hor}(X), \text{hor}(Y)](\mathbf{c})) \; \forall \mathbf{c} \in \mathcal{C}^{3d}, \tag{3.72}$$

where $\text{hor}(X)$, $\text{hor}(Y)$ are the horizontal projections of the vector fields X and Y, and $[\text{hor}(X), \text{hor}(Y)](\mathbf{c})$ is their Jacobi-Lie bracket (also a vector field on $\mathcal{C}^{3d}$) at $\mathbf{c}$. For Ehresmann connection (3.42), $\text{hor}(X)$ and $\text{hor}(Y)$ are defined by $\text{hor}(X)(\mathbf{c}) = S_X(\mathbf{c})\mathbf{c}$ and $\text{hor}(Y)(\mathbf{c}) = S_Y(\mathbf{c})\mathbf{c}$, with $S_X(\mathbf{c})$, $S_Y(\mathbf{c})$ given implicitly as the solutions to Lyapunov equations $S_X(\mathbf{c})K(\mathbf{c}) + K(\mathbf{c})S_X(\mathbf{c}) = F(\mathbf{c}, X(\mathbf{c}))$ and $S_Y(\mathbf{c})K(\mathbf{c}) + K(\mathbf{c})S_Y(\mathbf{c}) = F(\mathbf{c}, Y(\mathbf{c}))$ respectively. Alternatively, except at configurations for which K has repeated eigenvalues, one could use the explicit formulae $S_X(\mathbf{c}) = Q^T(\mathbf{c})F_\Lambda(\mathbf{c}, X(\mathbf{c}))Q(\mathbf{c})$, $S_Y(\mathbf{c}) = Q^T(\mathbf{c})F_\Lambda(\mathbf{c}, Y(\mathbf{c}))Q(\mathbf{c}) \in \mathbb{R}^{3\times 3}_{sym}$ from (3.45)-(3.46).

Proposition 3.5.1. *The Jacobi-Lie bracket of two horizontal vector fields $S_X(\mathbf{c})\mathbf{c}$, $S_Y(\mathbf{c})\mathbf{c}$ is given by:*

$$[S_X(\mathbf{c})\mathbf{c}, S_Y(\mathbf{c})\mathbf{c}](\mathbf{c}) = M_{XY}(\mathbf{c})\mathbf{c}, \tag{3.73}$$

where $M_{XY}(\mathbf{c}) \triangleq M_{XY,sym}(\mathbf{c}) + M_{XY,skew}(\mathbf{c}) \in \mathbb{R}^{3\times 3}$ has the following symmetric and skew-symmetric components:

$$M_{XY,sym}(\mathbf{c}) = \left.\frac{d}{dt}\right|_{t=0} S_Y(\mathbf{c} + tS_X(\mathbf{c})\mathbf{c}) - \left.\frac{d}{dt}\right|_{t=0} S_X(\mathbf{c} + tS_Y(\mathbf{c})\mathbf{c}) \tag{3.74}$$

$$M_{XY,skew}(\mathbf{c}) = S_Y(\mathbf{c})S_X(\mathbf{c}) - S_X(\mathbf{c})S_Y(\mathbf{c}). \tag{3.75}$$

Proof. Given vector fields $X, Y \in \mathcal{X}(\mathcal{C}^{3d})$, their Jacobi-Lie bracket can be computed in the ambient space $\mathbb{R}^{3\times n}$ (of which $\mathcal{C}^{3d}$ is a subset) as follows:

$$\begin{aligned}
[X,Y](\mathbf{c}) =& (DY)_{\mathbf{c}}X(\mathbf{c}) - (DX)_{\mathbf{c}}Y(\mathbf{c}) = \\
&= \frac{d}{dt}\bigg|_{t=0} Y(\mathrm{Fl}_t^X \mathbf{c}) - \frac{d}{dt}\bigg|_{t=0} X(\mathrm{Fl}_t^Y \mathbf{c}) \\
&= \frac{d}{dt}\bigg|_{t=0} Y(\mathbf{c} + tX(\mathbf{c})) - \frac{d}{dt}\bigg|_{t=0} X(\mathbf{c} + tY(\mathbf{c})).
\end{aligned} \tag{3.76}$$

Applying this to the special case $X(\mathbf{c}) = S_X(\mathbf{c})\mathbf{c}$, $Y(\mathbf{c}) = S_Y(\mathbf{c})\mathbf{c}$:

$$\begin{aligned}
[S_X(\mathbf{c})\mathbf{c}, S_Y(\mathbf{c})\mathbf{c}](\mathbf{c}) =& \frac{d}{dt}\bigg|_{t=0} S_Y(\mathbf{c} + tS_X(\mathbf{c})\mathbf{c})(\mathbf{c} + tS_X(\mathbf{c})\mathbf{c}) \\
&- \frac{d}{dt}\bigg|_{t=0} S_X(\mathbf{c} + tS_Y(\mathbf{c})\mathbf{c})(\mathbf{c} + tS_Y(\mathbf{c})\mathbf{c}) \\
=& \left(\frac{d}{dt}\bigg|_{t=0} S_Y(\mathbf{c} + tS_X(\mathbf{c})\mathbf{c})\right)\mathbf{c} + S_Y(\mathbf{c})S_X(\mathbf{c})\,\mathbf{c} \\
&- \left(\frac{d}{dt}\bigg|_{t=0} S_X(\mathbf{c} + tS_Y(\mathbf{c})\mathbf{c})\right)\mathbf{c} - S_Y(\mathbf{c})S_X(\mathbf{c})\,\mathbf{c} \\
=& M_{XY}(\mathbf{c})\mathbf{c}.
\end{aligned} \tag{3.77}$$

Since $S_X(\mathbf{c}+tS_Y(\mathbf{c})\mathbf{c})$, $S_Y(\mathbf{c}+tS_X(\mathbf{c})\mathbf{c}) \in \mathbb{R}^{3\times 3}_{sym}$ $\forall t$, their derivatives with respect to t are also symmetric; on the other hand, the matrix commutation of two symmetric matrices, and in particular of $S_X(\mathbf{c}), S_Y(\mathbf{c})$, is always skew-symmetric.

□

Proposition 3.5.2. *The curvature form of Ehresmann connection* (3.42) *is:*

$$B_{\mathbf{c}}(X(\mathbf{c}),Y(\mathbf{c})) = A_{\mathbf{c}}(-M_{XY,skew}(\mathbf{c})\mathbf{c}) \tag{3.78}$$

$$= 2\,Q^T \begin{bmatrix} 0 & \frac{\lambda_1}{\lambda_1+\lambda_2}\tilde{m}_{12} & \frac{\lambda_1}{\lambda_1+\lambda_3}\tilde{m}_{13} \\ -\frac{\lambda_2}{\lambda_1+\lambda_2}\tilde{m}_{12} & 0 & \frac{\lambda_2}{\lambda_2+\lambda_3}\tilde{m}_{23} \\ -\frac{\lambda_3}{\lambda_1+\lambda_3}\tilde{m}_{13} & -\frac{\lambda_3}{\lambda_2+\lambda_3}\tilde{m}_{23} & 0 \end{bmatrix} Q\,\mathbf{c}, \tag{3.79}$$

$$\text{where } \tilde{M}_{XY} = \begin{bmatrix} 0 & \tilde{m}_{12} & \tilde{m}_{13} \\ -\tilde{m}_{12} & 0 & \tilde{m}_{23} \\ -\tilde{m}_{13} & -\tilde{m}_{23} & 0 \end{bmatrix} \triangleq -Q\,M_{XY,skew}\,Q^T,$$

and $M_{XY,skew}(\mathbf{c}) = S_Y(\mathbf{c})S_X(\mathbf{c}) - S_X(\mathbf{c})S_Y(\mathbf{c})$.

Proof. From (3.72) and (3.73): $B_{\mathbf{c}}(X(\mathbf{c}),Y(\mathbf{c})) = -A_{\mathbf{c}}(M_{XY}(\mathbf{c})\mathbf{c})$. Since clearly $M_{XY,sym}(\mathbf{c})\mathbf{c}$ is in the horizontal subspace of vectors orthogonal to the fiber (recall Proposition 3.3.7), $A_{\mathbf{c}}(M_{XY,sym}(\mathbf{c})\mathbf{c}) = \mathbb{O}$ and (3.78) follows. The expression (3.79) then follows observing that $-M_{XY,skew}(\mathbf{c})\mathbf{c}$ is an instantaneous rigid rotation of the collective with respect to the center of mass, whose vertical component can be computed using (3.64). □

Remark 3.5.3 Proposition 3.5.2 shows that the infinitesimal vertical (democratic) motion obtained from an infinitesimal loop constructed using horizontal vector fields $\mathrm{hor}(X)(\mathbf{c}) = S_X(\mathbf{c})\mathbf{c}$ and $\mathrm{hor}(Y)(\mathbf{c}) = S_Y(\mathbf{c})\mathbf{c}$ (which is how the Jacobi-Lie bracket $[\mathrm{hor}(X),\mathrm{hor}(Y)](\mathbf{c})$ can be interpreted), is the same that would be obtained from an infinitesimal rigid rotation of the collective about the

axis corresponding to the skew-symmetric matrix $-M_{XY,skew}(\mathbf{c}) = S_X(\mathbf{c})S_Y(\mathbf{c}) - S_Y(\mathbf{c})S_X(\mathbf{c})$.

It is very easy to find examples of vector fields for which $M_{XY,skew}(\mathbf{c})$ does not vanish, and hence the curvature $B(X,Y)$ is nonzero; for example consider constant vector fields $X(\mathbf{c}) = S_X\,\mathbf{c}$, $Y(\mathbf{c}) = S_Y\,\mathbf{c}$ with $S_X, S_Y \in \mathbb{R}^{3\times 3}_{sym}$ constant and non-commuting. Hence the Ehresmann connection for the alternative fiber bundle of section 3.3 is indeed non-trivial. On the other hand, there are choices of vector fields for which the curvature vanishes; this is the case, for example, if both X and Y are inertia tensor deformations, since the corresponding symmetric matrices $S_X(\mathbf{c})$ and $S_Y(\mathbf{c})$ always commute (recall (3.66)).

3.6 Application to the analysis of a starling flock

The decomposition of collective motions presented in section 3.4 could be useful in the analysis and interpretation of collective behaviors in nature. Given a set of individual trajectories (positions and velocity vectors) recorded during natural events, decomposing the kinetic energy or the velocity vectors themselves as in sections 3.2 and 3.3 (classical and alternative fibering), could yield important information on what are the predominant components of motion. For example, questions regarding the "rigidness" of the collective motion and the relevance of "reshufflings" (exchange of positions between the individuals) could be quantitatively answered by evaluating the rigid rotation, shape transformation and

democratic motion components of kinetic energy.

In this section, we present an example of such analysis applied to experimental data collected from a starling flock. The time-sampled trajectories of individual starlings, obtained from high-resolution stereo photography of a flocking event in Rome, Italy, were kindly provided by Dr. A. Cavagna and collaborators (Consiglio Nazionale delle Ricerche and Università di Roma "La Sapienza"). Notice that extracting this information requires reconstruction, at each time-sample, of the three-dimensional positions of the birds via stereoscopic matching of the photographs, followed by temporal matching between different time-samples to identify which is the data belonging to a same bird. The sophisticated techniques used by the group of Dr. Cavagna are described in [14] and in the supporting information of [13]. The starling velocities were obtained by smoothing of the time-sampled trajectories, using the regularized optimization method described in [46], and further improved upon by Biswadip Dey (private communication). This method searches for the optimal trajectory, among those with piecewise constant curvatures and speeds, that minimizes the sum of a fit-error cost (evaluating how well the reconstructed trajectory fits the samples) and a smoothing cost (penalizing sharp curvature changes between subsequent samples).

The flocking event analyzed had duration 4.5 seconds, with bird positions originally sampled at 10 Hertz; upsampling to 40 Hertz was performed as part of the trajectory smoothing, yielding 180 time-samples of reconstructed individual positions and velocities of the birds. The flock had roughly 120 birds, which is a

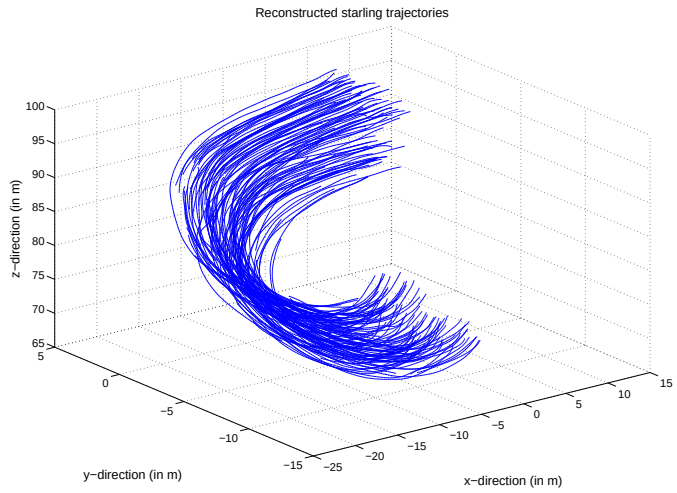

Figure 3.2: Reconstructed starling trajectories in the flocking event analyzed.

relatively small number in the context of starlings. From the reconstructed trajectories, showed in figure 3.2, it is quite easy to assess qualitatively the flocking event as a sharp turn performed by the flock in a strikingly coordinated fashion. The decomposition of kinetic energy, performed using the mathematical tools described in section 3.4 (considering unit masses for all the birds), allows to attach some quantitative evaluation to this qualitative assessment.

We concentrate on four energy ratios that, once computed at a particular instant of time, capture all the information on the instantaneous kinetic energy distribution at that time:

(a) E_{com}/E_{tot} captures the percentage of energy that goes into the rigid translation component of motion; it is a measure of how much the birds are moving in the same direction, versus how much they are accomplishing other types of motion.

(b) E_{dem}/E_{rel} captures the percentage of relative kinetic energy (after the rigid translation component has been removed) that goes into the democratic motion of the flock; it is a measure of how much the birds are reshuffling their positions while maintaining constant coefficient of inertia tensor of the flock, versus how much they are changing the coefficient of inertia tensor.

(c) E_{rot}/E_{rel} captures the percentage of relative kinetic energy that goes into the rigid rotation of the flock with respect to its center of mass; it measures how much the flock is rotating as a rigid body, versus how much it is changing in shape.

(d) E_{size}/E_{rel} captures the percentage of relative kinetic energy that goes into expansion (or compression) of the flock; it measures how much the flock is changing its volume, versus how much it is performing volume-preserving motions. Notice that E_{size}/E_{rel} will always be less or equal than both $1 - E_{rot}/E_{rel}$ and $1 - E_{dem}/E_{rel}$.

Figures 3.3-3.6 show how these energy ratios evolve in time and their statistical distributions over the whole flocking event.

Figure 3.3 shows that the rigid translation of the flock is by far the dominant component of motion; the percentage of kinetic energy that goes into rigid translation is in fact always above 95%, except for a few time samples (around time-sample 70) when it reaches a minimum value of 92%. This gives a strong quantitative support to the qualitative assessment of this flocking event as a striking example of efficient coordination of the motion of starlings during high-speed,

sharp turns. The relatively abrupt decrease from 98% to 92% around time-sample 70 corresponds to the sharpest part of the turn.

Among the other modes of collective motion, figure 3.4 shows that the percentage of relative kinetic energy associated to democratic motion is almost always greater than 50%; this means that there is more energy spent in reshufflings of positions that preserve the coefficient of inertia tensor, rather than in coefficient of inertia transformations. The energy percentage associated to democratic motion reduces almost linearly, from 90% to 30%, at the end of the flock turn (after time-sample 160). A complementary effect is observed in the energy component associated to expansion or compression of the flock (figure 3.6) which increases almost linearly from 0% to 35% during the same time period. Since the volume of the flock increases, this seems to imply that after the turn the flock undergoes some significant expansion.

Figure 3.5 shows instead that the rigid rotation of the flock with respect to the center of mass accounts for always less than 50% (and often less than 25%) of the relative kinetic energy. Even if qualitatively it has been observed that starling flocks perform some sort of rigid banking during turns [4], quantitative analysis for this event does not support rigid rotation of the flock as one of the main components of motion. For this event, shape transformation is almost always more significant that rigid rotation.

Finally, figure 3.6 shows that the percentage of relative kinetic energy that goes into expansion (or compression) of the flock is very low (less than 0.05%)

for most of the event. This means that the flock maintains its volume almost constant during the turn. Only in the first and last few samples, the pure expansion (compression) accounts for more than 20% of the kinetic energy; as already observed, after time-sample 160 there is an almost linear growth of this energy component, corresponding to expansion of the flock after the turn.

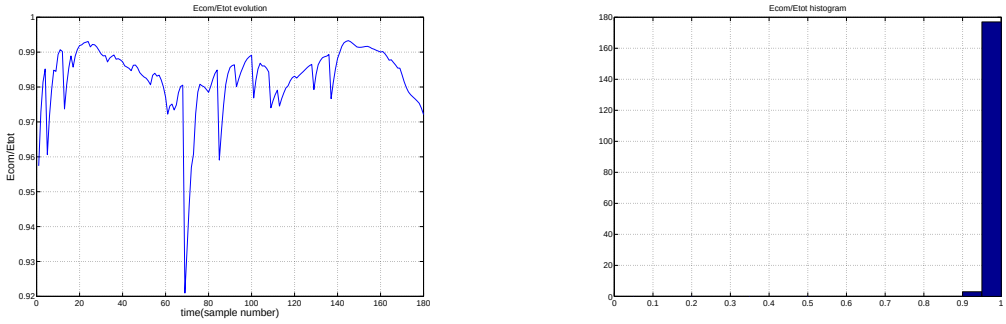

(a) (b)

Figure 3.3: Ratio between rigid translation energy (E_{com}) and total kinetic energy (E_{tot}) during starling flock event: (a) time evolution; (b) histogram.

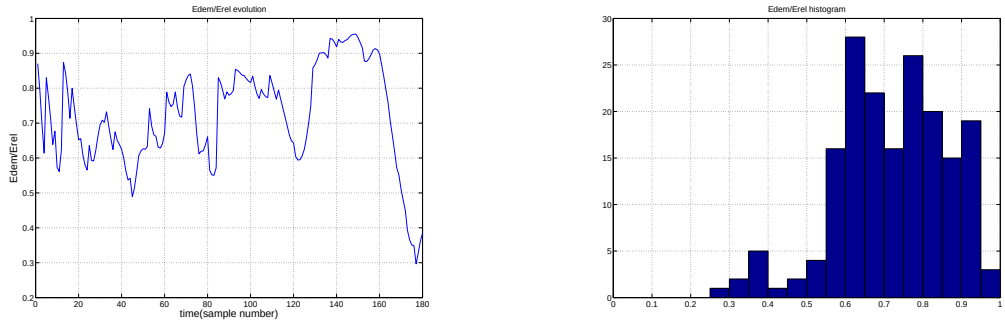

(a) (b)

Figure 3.4: Ratio between democratic motion energy (E_{dem}) and kinetic energy relative to the center of mass (E_{rel}) during starling flock event: (a) time evolution; (b) histogram.

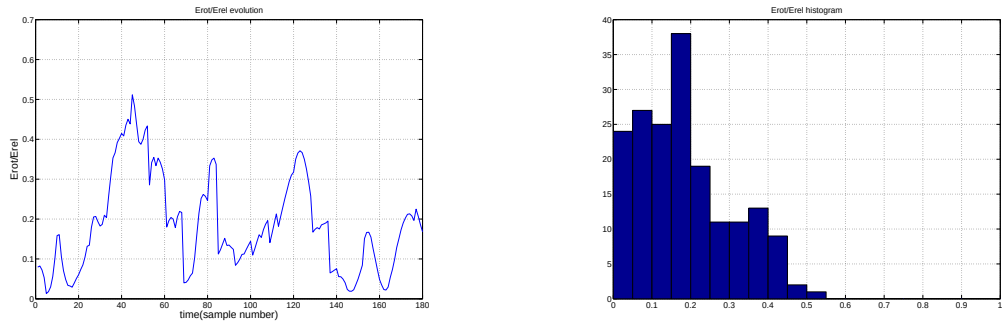

(a) (b)

Figure 3.5: Ratio between rigid rotation energy with respect to the center of mass (E_{rot}) and kinetic energy relative to the center of mass (E_{rel}) during starling flock event: (a) time evolution; (b) histogram.

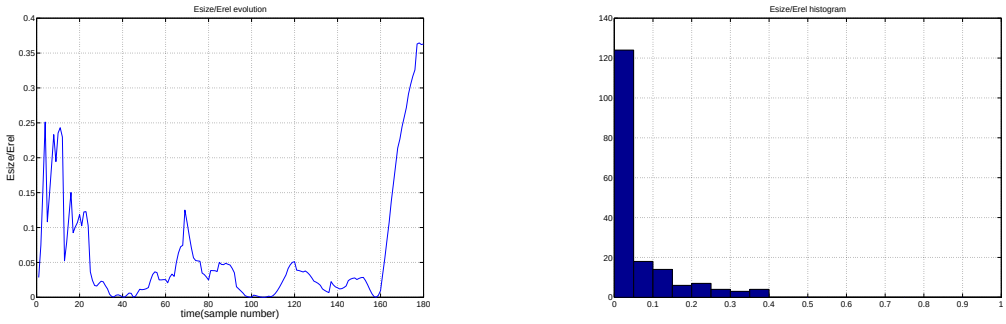

(a) (b)

Figure 3.6: Ratio between expansion (or compression) energy with respect to the center of mass (E_{size}) and kinetic energy relative to the center of mass (E_{rel}) during starling flock event: (a) time evolution; (b) histogram.

Chapter 4

Synthesis of elementary collective motions

The decomposition of collective motions described in the previous chapter can be useful not only for the analysis of observed collective behaviors (e.g. in nature) but also for the synthesis of new behaviors for multi-agent engineered systems (e.g. teams of robots). If the agents are modeled as point particles, the artificial collective can be modeled as in chapter 3, and the choice of a vector field on configuration space can be thought of as a design step, having the objective of enforcing a certain behavior to the collective. In this context, elementary vector fields (in the sense of section 3.4) can be used to produce certain simple behaviors, which could then be combined to generate complex ones. For example, to obtain a "rigid" behavior characterized by constant relative positions between the agents, the vector field must be a combination of rigid translations and rotations. Inertia tensor transformations are suitable instead for changing the coefficient of inertia tensor (corresponding to the covariance of the distribution of agents, if the masses are equal) with minimal agent reshufflings. Conversely, democratic motions are useful if it is desired to have reshuffling of the positions of the agents while the

coefficient of inertia tensor is maintained constant.

In this chapter, we present the synthesis of some interesting elementary vector fields that could be applicable, for example, to the motion planning of a team of robots engaged in a collective task such as distributed sensing.

We first concentrate on vector fields that modify the coefficient of inertia tensor of the collective. In section 4.1.1, we prove that the most energy-efficient method of modifying the coefficient of inertia tensor is by designing appropriate inertia tensor transformations (the horizontal vector fields for the alternative fibering, introduced in section 3.4). In particular, we derive a locally optimal choice for regulating the coefficient of inertia to a desired one in fixed time. When certain sensing and communication constraints are satisfied, inertia tensor transformations can be implemented in distributed fashion; in section 4.1.2 we present several distributed algorithms that can be used under different scenarios.

We then discuss vector fields that preserve the coefficient of inertia tensor of the collective (the democratic motions of section 3.4), while achieving other goals. In particular, in section 4.2.1 we introduce a democratic motion which maximizes a reward function quantifying the separation between "neighboring" agents, defined in accordance with some interaction graph. The result is a reshuffling of the agent positions towards certain fixed configurations, that depend on the choice of the graph. Certain choices produce very interesting and potentially useful results, such as distributing the agents along some sort of three-dimensional chain, or splitting the agents into two groups symmetrically distributed with respect to

the center of mass.

Finally, in section 4.3 we suggest an application of the motions synthesized in this chapter to the task of sensing a physical spatial variable with a team of robots.

4.1 Motions that modify the coefficient of inertia tensor

4.1.1 Optimal regulation of the coefficient of inertia tensor

In this section, we study the problem of designing the individual motion of each agent (modeled as a point particle) with respect to the center of mass, so that the coefficient of inertia tensor of the collective reaches a desired value $K_1 \in \mathcal{K}$ in fixed time (say $T = 1$) while minimizing the path-energy (with respect to the center of mass). The problem can be formalized as follows.

Problem 4.1.1 (**Coefficient of inertia regulation)** Given initial configuration $\mathbf{c_0} \in \mathcal{C}^{3d}$ with coefficient of inertia tensor $K(\mathbf{c_0}) \triangleq K_0 \in \mathcal{K}$, and a desired coefficient of inertia $K_1 \in \mathcal{K}$, find (if it exists) a differentiable curve in $\mathcal{C}^{3d}$, $\mathbf{\Gamma} : [0, 1] \mapsto \mathcal{C}^{3d}$, such that $\mathbf{\Gamma}(0) = \mathbf{c_0}$, $K(\mathbf{\Gamma}(1)) = K_1$, that minimizes the path-energy with respect to the center of mass:

$$E_{path}(\mathbf{\Gamma}) \triangleq \int_0^1 \langle \dot{\mathbf{\Gamma}}(t), \dot{\mathbf{\Gamma}}(t) \rangle_{\mathbf{\Gamma}(t)} dt = \int_0^1 \mathrm{tr}(\dot{\mathbf{\Gamma}}(t)\, \mathbb{M}\, \dot{\mathbf{\Gamma}}^T(t)) dt. \tag{4.1}$$

Using the mathematical machinery developed in section 3.3 for the alter-

native fiber bundle, it is simple to reduce the problem to the computation of path-energy minimizing geodesics on the space of coefficient of inertia tensors $\mathcal{K}$.

Theorem 4.1.2. *Assume that the coefficient of inertia regulation problem admits (at least) a solution. Then:*

(i) there exists a differentiable curve $\mathbf{\Gamma} : [0,1] \mapsto \mathcal{C}^{3d}$ *solving the coefficient of inertia regulation problem, with the property that all its tangent vectors are inertia tensor transformations, i.e. are horizontal with respect to the alternative fiber bundle:*

$$\dot{\mathbf{\Gamma}}(t) = S(t, \mathbf{\Gamma}(t))\mathbf{\Gamma}(t), \;\; S(t, \mathbf{\Gamma}(t)) \in \mathbb{R}^{3\times 3}_{sym}, \; \forall t \in [0,1] \tag{4.2}$$

(ii) such curve $\mathbf{\Gamma}$ *is the horizontal lift, computed using* (3.54)-(3.57)*, of a path-energy minimizing geodesic curve on* $\mathcal{K}$*, with respect to the induced Riemannian metric* (3.58)*:*

$$\dot{\mathbf{\Gamma}}(t) = \mathrm{lift}_{\mathbf{\Gamma}(t)}\dot{K}(t) \; \forall t \in [0,1], \tag{4.3}$$

where $K : [0,1] \mapsto \mathcal{K}$ *satisfies* $K(0) = K_0$*,* $K(1) = K_1$ *and minimizes the path-energy functional:*

$$E(K) \triangleq \int_0^1 \langle \dot{K}(t), \dot{K}(t) \rangle_{K(t)} dt = \int_0^1 \mathrm{tr}(S(K(t), \dot{K}(t)) \, K(t) \, S(K(t), \dot{K}(t))) dt. \tag{4.4}$$

Here $S(K(t), \dot{K}(t))$ *is the solution to the Lyapunov equation:*

$$S(K(t), \dot{K}(t)) \, K(t) + K(t) \, S(K(t), \dot{K}(t)) = \dot{K}(t), \; \forall t \in [0,1]. \tag{4.5}$$

If $\mathbf{\Gamma}(t)$ *is the horizontal lift of a curve in* $\mathcal{K}$*, i.e.* $\mathbf{\Gamma}(t) = \mathrm{lift}K(t)$*, then* $E_{path}(\mathbf{\Gamma}) = E(K)$*; hence the existence of a path-energy minimizing geodesic (a curve mini-*

mizing (4.4)*) follows from the existence, guaranteed by (i), of a solution of the type* (4.2) *minimizing* (4.1)*.*

Conversely:

(iii) if $K : [0,1] \mapsto \mathcal{K}$*,* $K(0) = K_0$*,* $K(1) = K_1$ *is a path-energy minimizing geodesic in* $\mathcal{K}$ *with respect to the induced Riemannian metric* (3.58)*, then its horizontal lift is a solution of the coefficient of inertia regulation problem.*

Proof. (i) Let $\mathbf{\Gamma_s} : [0,1] \mapsto \mathcal{C}^{3d}$ be any solution of the coefficient of inertia regulation problem and $E_{path}(\mathbf{\Gamma_s})$ its corresponding path energy. Then we can define another curve $\mathbf{\Gamma} : [0,1] \mapsto \mathcal{C}^{3d}$ which satisfies $\mathbf{\Gamma}(0) = \mathbf{c_0}$, $K(\mathbf{\Gamma}(1)) = K_1$ and (4.2), by taking: $\mathbf{\Gamma}(0) = \mathbf{\Gamma_s}(0)$, $\dot{\mathbf{\Gamma}}(t) = \mathrm{hor}(\dot{\mathbf{\Gamma}}_\mathbf{s}(t))\, \forall t \in [0,1]$, with the horizontal projection computed as in section 3.3.4. Now observe that:

$$E_{path}(\mathbf{\Gamma_s}) = \int_0^1 \langle \dot{\mathbf{\Gamma}}_\mathbf{s}(t), \dot{\mathbf{\Gamma}}_\mathbf{s}(t) \rangle_{\mathbf{\Gamma_s}(t)} dt = \int_0^1 \langle \mathrm{hor}(\dot{\mathbf{\Gamma}}_\mathbf{s}(t)), \mathrm{hor}(\dot{\mathbf{\Gamma}}_\mathbf{s}(t)) \rangle_{\mathbf{\Gamma_s}(t)} dt +$$
$$\int_0^1 \langle A_{\mathbf{\Gamma_s}(t)}(\dot{\mathbf{\Gamma}}_\mathbf{s}(t)), A_{\mathbf{\Gamma_s}(t)}(\dot{\mathbf{\Gamma}}_\mathbf{s}(t)) \rangle_{\mathbf{\Gamma_s}(t)} dt \;\geq \int_0^1 \langle \dot{\mathbf{\Gamma}}(t), \dot{\mathbf{\Gamma}}(t) \rangle_{\mathbf{\Gamma_s}(t)} dt = E_{path}(\mathbf{\Gamma}),$$

where in the last step we have used the invariance of the Riemannian metric along the fibers: $\langle \dot{\mathbf{\Gamma}}(t), \dot{\mathbf{\Gamma}}(t) \rangle_{\mathbf{\Gamma_s}(t)} = \langle \dot{\mathbf{\Gamma}}(t), \dot{\mathbf{\Gamma}}(t) \rangle_{\mathbf{\Gamma}(t)}\, \forall t$, since $\pi(\mathbf{\Gamma_s}(t)) = \pi(\mathbf{\Gamma}(t))\, \forall t$. Hence $\mathbf{\Gamma}$ must also be solution of the coefficient of inertia regulation problem.

(ii) The curve $\mathbf{\Gamma}$ from (i) is certainly the horizontal lift of some curve K in $\mathcal{K}$:

$\mathbf{\Gamma}(t) = \text{lift}K(t),\ t \in [0,1]$. Hence:

$$\begin{aligned} E_{path}(\mathbf{\Gamma}) &= \int_0^1 \text{tr}(\dot{\mathbf{\Gamma}}(t)\,\mathbb{M}\,\dot{\mathbf{\Gamma}}^T(t))dt \\ &= \int_0^1 \text{tr}(S(K(\mathbf{\Gamma}(t)), \dot{K}(t))\mathbf{\Gamma}(t)\,\mathbb{M}\,\mathbf{\Gamma}^T(t)S(K(\mathbf{\Gamma}(t), \dot{K}(t)))dt \\ &= \int_0^1 \langle \dot{K}(t), \dot{K}(t) \rangle_{K(t)} dt \\ &= E(K), \end{aligned}$$

since $S(K(\mathbf{\Gamma}(t)), \dot{K}(t))$ is indeed the solution of (4.5) (by the definition of horizontal lift). The fact that $\mathbf{\Gamma}$ minimizes $E_{path}(\mathbf{\Gamma})$ implies that the corresponding K minimizes, among all curves with $K(0) = K_0$ and $K(1) = K_1$, the path-energy functional $E(K)$. Hence $\mathbf{\Gamma}$ is the horizontal lift of a path-energy minimizing geodesic on $\mathcal{K}$, with respect to the induced Riemannian metric (3.58).

(iii) If K is a path-energy minimizing geodesic, then it minimizes $E(K)$ among all the curves in $\mathcal{K}$, hence its horizontal lift is a minimizer for $E_{path}(\mathbf{\Gamma})$ among all horizontal lifts of curves in $\mathcal{K}$ connecting K_0 and K_1. By (i), this horizontal lift is indeed a minimizer among all possible curves $\mathbf{\Gamma} : [0,1] \mapsto \mathcal{C}^{3d}$, such that $\mathbf{\Gamma}(0) = \mathbf{c_0}$, $K(\mathbf{\Gamma}(1)) = K_1$. □

Theorem 4.1.2 proves that a solution of the coefficient of inertia regulation problem, if it exists, can be computed by finding a path-energy minimizing geodesic on $\mathcal{K}$ with respect to the Riemannian metric (3.58), with end points $K(0) = K_0$, $K(1) = K_1$, and then lifting it horizontally to $\mathcal{C}^{3d}$ using (3.54)-(3.57). The problem of finding path-energy minimizing geodesics in $\mathcal{K}$ can be formalized as a calculus of variations problem.

Problem 4.1.3 (**Computation of a path-energy minimizing geodesic**) Given fixed end points $K_0 \in \mathcal{K}$ and $K_1 \in \mathcal{K}$, find (if it exists) a differentiable curve in $\mathcal{K}$, $K : [0,1] \mapsto \mathcal{K}$, with $K(0) = K_0$, $K(1) = K_1$, that minimizes the path-energy functional:

$$E(K) = \int_0^1 L(K(t), \dot{K}(t))dt, \tag{4.6}$$

with Lagrangian:

$$L(K(t), \dot{K}(t)) \triangleq \langle \dot{K}(t), \dot{K}(t) \rangle_{K(t)} = \mathrm{tr}(S(K(t), \dot{K}(t))\, K(t)\, S(K(t), \dot{K}(t))), \tag{4.7}$$

where $S(K(t), \dot{K}(t))$ is the solution to the Lyapunov equation (4.5).

By the classical variational argument in the calculus of variations, a curve $K : [0,1] \mapsto \mathcal{K}$ is a path-energy minimizing geodesic only if it satisfies, $\forall t \in [0,1]$:

$$\frac{d}{dt} D_2 L(K(t), \dot{K}(t)) \cdot I - D_1 L(K(t), \dot{K}(t)) \cdot I = 0 \;\; \forall I \in \mathbb{R}^{3\times 3}_{sym} = T_K\mathcal{K}, \tag{4.8}$$

which leads to the Euler-Lagrange equations:

$$\frac{d}{dt} D_2 L(K(t)\dot{K}(t)) - D_1 L(K(t), \dot{K}(t)) = 0. \tag{4.9}$$

Here D_i denotes the Frechet derivative with respect to the i-th argument.

Remark 4.1.4 Solutions to the Euler-Lagrange equations (4.9), when the Lagrangian is given by the instantaneous energy $\langle \dot{K}(t), \dot{K}(t) \rangle_{K(t)}$ or equivalently by $\sqrt{\langle \dot{K}(t), \dot{K}(t) \rangle_{K(t)}}$ (whose integral is the length of the curve), are typically referred to as *geodesics*, but should not to be confused with the *path-energy minimizing* geodesics defined above.

All geodesics are *locally* path-energy minimizing, in the following sense: given any initial K_0, there exists a sufficiently small $\epsilon(K_0) > 0$ such that every geodesic satisfying $K(0) = K_0$, $\dot{K}(0) = \dot{K}_0$ with $\langle \dot{K}_0, \dot{K}_0 \rangle_{K_0} < \epsilon(K_0)$ is a path-energy minimizing curve between K_0 and some other point. Note that geodesics have constant speed, i.e. $\langle \dot{K}(t), \dot{K}(t) \rangle_{K(t)} = \langle \dot{K}(0), \dot{K}(0) \rangle_{K(0)} \, \forall t$; this follows from the fact that the Hamiltonian $H(K(t), \dot{K}(t)) \triangleq D_2 L(K(t), \dot{K}(t)) \cdot \dot{K}(t) - L(K(t), \dot{K}(t))$, which is a conserved quantity along solutions of the Euler-Lagrange equations whenever the Lagrangian is time-invariant, is equal to the Lagrangian itself in this problem. Hence geodesics are guaranteed to be path-energy minimizing between points that are "close enough".

A path-energy minimizing geodesic that solves problem 4.1.3 is instead a curve (if it exists) that *globally* minimizes the path-energy between given points K_0 and K_1. Since K_0, K_1 might not be close to each other, the local property of geodesics described above does not guarantee that every geodesic connecting K_0 and K_1, if it exists, minimizes the path-energy. On the other hand, the Euler-Lagrange equations are necessary conditions for any path-energy minimizing geodesic, hence it is among the geodesics that potential candidate solutions for problem 4.1.3 can be found.

The example of the sphere, equipped with the canonical Riemannian metric, helps clarifying these concepts. On the sphere, the geodesics (solutions to the Euler-Lagrange equations) are the segments of great circles; hence for any given pair of points there are two geodesics connecting them: the shorter and the

longer segment of the great circle passing through the two points. Only one of these geodesics (the shorter segment) minimizes the path-energy between the two points.

In the case of the sphere, for any pair of points there exists a path-energy minimizing geodesic connecting them (the shorter segment of the great circle passing through the points). This is a property of all Riemannian manifolds that are *geodesically complete*, i.e. for which every geodesic is maximally definable on the whole of $\mathbb{R}$, as proved by the Hopf-Rinow theorem (see for example [37]). Hence for geodesically complete manifolds, such as the sphere, the path-energy minimizing geodesic between two given points (guaranteed to exist) is given by the geodesic with lowest path-energy (among those connecting the given points).

For manifolds that are not geodesically complete, there could be pairs of points for which a path-energy minimizing geodesic does not exist, i.e. there might not be a curve with path-energy lower than or equal to that of any other differentiable curve. For example, consider the sphere removed of a single point; this manifold is not geodesically complete, since geodesics starting on the great circle passing through the removed point cannot be extended indefinitely in time. For two points lying on the same great circle of the removed point, and close to this point but on opposite sides, there is no path-energy minimizing geodesic; one can in fact define a sequence of curves connecting these points and having monotonically decreasing path-energy, which has as a limit the shorter segment of the great circle connecting these points, which does not live on the manifold.

In this case, the unique geodesic that connects the two points, given by the long segment of the great circle, is not path-energy minimizing. Nevertheless, for pairs of points for which a path-energy minimizing geodesic exists, the latter is indeed given by the geodesic with lowest path-energy; this is true even for manifolds that are not geodesically complete.

We therefore concentrate on finding the geodesics for the Lagrangian (4.7).

Proposition 4.1.5. *The geodesic curves in $\mathcal{K}$ (for Lagrangian (4.7)) are the solutions to the following Euler-Lagrange equations:*

$$\ddot{K}(t) = 2\, S(K(t), \dot{K}(t))K(t)S(K(t), \dot{K}(t)), \tag{4.10}$$

where $\forall t\ S(K(t), \dot{K}(t))$ is the unique solution to Lyapunov equation (4.5).

Proof. Let $I \in \mathbb{R}^{3\times 3}_{sym} = T_K\mathcal{K}$. Then, at each $t \in [0,1]$ (which we drop for convenience of notation):

$$\begin{aligned} D_2L(K,\dot{K})\cdot I &= \left.\frac{d}{d\epsilon}\right|_{\epsilon=0} L(K, \dot{K}+\epsilon I) \\ &= \left.\frac{d}{d\epsilon}\right|_{\epsilon=0} \mathrm{tr}(\hat{S}(K,\dot{K}+\epsilon I)\, K\, \hat{S}(K,\dot{K}+\epsilon I)), \end{aligned}$$

where $\hat{S}(K, \dot{K}+\epsilon I)$ is the solution to the Lyapunov equation $\hat{S}K + K\hat{S} = \dot{K} + \epsilon I$. The latter is given by $\hat{S}(K,\dot{K}+\epsilon I) = S(K,\dot{K}) + \epsilon T(K,I)$, where $T(K,I)$ is the solution to another Lyapunov equation $TK + KT = I$; therefore:

$$\begin{aligned} D_2L(K,\dot{K})\cdot I &= \left.\frac{d}{d\epsilon}\right|_{\epsilon=0} \mathrm{tr}((S(K,\dot{K}) + \epsilon T(K,I))K(S(K,\dot{K}) + \epsilon T(K,I))) \\ &= \mathrm{tr}(S(K,\dot{K})\, K\, T(K,I) + T(K,I)\, K\, S(K,\dot{K})) \\ &= \mathrm{tr}(2\, S(K,\dot{K})\, K\, T(K,I)). \end{aligned}$$

Derivation with respect to time yields:

$$\frac{d}{dt}D_2L(K,\dot{K})\cdot I = 2\,\mathrm{tr}\left[\frac{d}{dt}S(K,\dot{K})\,K\,T(K,I)\right]$$
$$= 2\,\mathrm{tr}[\dot{S}(K,\dot{K})\,K\,T(K,I) + S(K,\dot{K})(\dot{K}\,T(K,I) + K\,\dot{T}(K,I))].$$

Taking time derivatives of both sides of the Lyapunov equation $SK + KS = \dot{K}$, we obtain that $\dot{S}K + K\dot{S} = 2\,\mathrm{sym}(\dot{S}K) = \ddot{K} - S\dot{K} - \dot{K}S$ and hence $\mathrm{tr}(\dot{S}\,K\,T) = \mathrm{tr}(\mathrm{sym}(\dot{S}K)\,T) + \mathrm{tr}(\mathrm{skew}(\dot{S}K)\,T) = \frac{1}{2}\,\mathrm{tr}[(\ddot{K} - S\dot{K} - \dot{K}S)T]$, since the trace of the product of a symmetric matrix and a skew-symmetric one is always zero. Similarly, by time derivation of both sides of the Lyapunov equation $TK + KT = I$, we obtain that $\dot{K}T + K\dot{T} = -T\dot{K} - \dot{T}K$ is skew-symmetric, and hence $\mathrm{tr}(S(\dot{K}\,T + K\,\dot{T})) = 0$. We conclude that:

$$\frac{d}{dt}D_2L(K,\dot{K})\cdot I = \mathrm{tr}\left[(\ddot{K} - S(K,\dot{K})\dot{K} - \dot{K}S(K,\dot{K}))\,T(K,I)\right], \tag{4.11}$$

where: $S(K,\dot{K})K + KS(K,\dot{K}) = \dot{K}$ and $T(K,I)K + KT(K,I) = I$.

Furthermore, at each $t \in [0,1]$:

$$\begin{aligned} D_1L(K,\dot{K})\cdot I &= \left.\frac{d}{d\epsilon}\right|_{\epsilon=0} L(K+\epsilon I,\dot{K}) \\ &= \left.\frac{d}{d\epsilon}\right|_{\epsilon=0} \mathrm{tr}\left[\tilde{S}(K+\epsilon I,\dot{K})\,(K+\epsilon I)\,\tilde{S}(K+\epsilon I,\dot{K})\right] \\ &= \mathrm{tr}\left[S(K,\dot{K})\,I\,S(K,\dot{K}) + 2\,S(K,\dot{K})K\left.\frac{d}{d\epsilon}\right|_{\epsilon=0}\tilde{S}(K+\epsilon I,\dot{K})\right], \end{aligned}$$

where $\tilde{S}(K+\epsilon I,\dot{K})$ is the solution to the Lyapunov equation $\tilde{S}(K+\epsilon I,\dot{K})\,(K+\epsilon I) + (K+\epsilon I)\,\tilde{S}(K+\epsilon I,\dot{K}) = \dot{K}$, which is symmetric (and so is its derivative with respect to ϵ) and corresponds to $S(K,\dot{K})$ when $\epsilon = 0$. Now taking derivatives

with respect to ϵ of both sides of the Lyapunov equation, and setting $\epsilon = 0$, yields:

$$\frac{d}{d\epsilon}\bigg|_{\epsilon=0} \tilde{S}(K+\epsilon I, \dot{K})\, K + K\, \frac{d}{d\epsilon}\bigg|_{\epsilon=0} \tilde{S}(K+\epsilon I, \dot{K}) = -S(K,\dot{K})\, I - I\, S(K,\dot{K}),$$

and therefore:

$$\begin{aligned} D_1 L(K,\dot{K}) \cdot I &= \mathrm{tr}\left[S(K,\dot{K})\, \mathrm{sym}\left(I\, S(K,\dot{K}) + 2\, K\, \frac{d}{d\epsilon}\bigg|_{\epsilon=0} \tilde{S}(K+\epsilon I, \dot{K}) \right) \right] \\ &= \mathrm{tr}[-S(K,\dot{K})\, \mathrm{sym}(I\, S(K,\dot{K}))] \\ &= -\frac{1}{2}\mathrm{tr}[S(K,\dot{K})\, I\, S(K,\dot{K}) + S^2(K,\dot{K})\, I] = -\mathrm{tr}[S^2(K,\dot{K})\, I] \\ &= -\mathrm{tr}[S^2(K,\dot{K})\, T(K,I)\, K + S^2(K,\dot{K})\, K\, T(K,I)] \\ &= -\mathrm{tr}[K\, S^2(K,\dot{K})\, T(K,I) + S^2(K,\dot{K})\, K\, T(K,I)], \end{aligned} \tag{4.12}$$

where again: $S(K,\dot{K})K + KS(K,\dot{K}) = \dot{K}$ and $T(K,I)K + KT(K,I) = I$.

The necessary condition (4.8) of the calculus of variations therefore requires that, $\forall\, I \in \mathbb{R}^{3\times 3}_{sym}$:

$$\mathrm{tr}[(\ddot{K} - S(K,\dot{K})\dot{K} - \dot{K}S(K,\dot{K}) + K\, S^2(K,\dot{K}) + S^2(K,\dot{K})\, K)\, T(K,I)] = 0,$$

which yields the following Euler-Lagrange equations (in fact $\forall\, I \in \mathbb{R}^{3\times 3}_{sym}$ there is a different $T(K,I) \in \mathbb{R}^{3\times 3}_{sym}$ such that $T(K,I)\, K + K\, T(K,I) = I$):

$$\ddot{K} - S(K,\dot{K})\dot{K} - \dot{K}S(K,\dot{K}) + K\, S^2(K,\dot{K}) + S^2(K,\dot{K})\, K = \mathbb{O}. \tag{4.13}$$

The form (4.10) of the Euler-Lagrange equations follows from substituting (4.5) into (4.13). □

The Euler-Lagrange equations (4.10) are given in implicit form, a natural consequence of the fact that the Lagrangian itself is given as an implicit function of $K(t)$, $\dot{K}(t)$. A quite simple (but still somewhat implicit) expression for the solutions to these equations can be obtained through further manipulation of (4.10) and (4.5).

Proposition 4.1.6. *The geodesic curve in $\mathcal{K}$ (for Lagrangian (4.7)) starting at K_0 and with initial tangent vector $\dot{K}_0 \in \mathbb{R}^{3\times 3}_{sym}$ is given by:*

$$K(t) = (\mathbb{1} + tS_0(K_0, \dot{K}_0))\, K_0\, (\mathbb{1} + tS_0(K_0, \dot{K}_0)), \tag{4.14}$$

where $S_0(K_0, \dot{K}_0)$ is the unique solution to the Lyapunov equation:

$$S_0(K_0, \dot{K}_0)\, K_0 + K_0\, S_0(K_0, \dot{K}_0) = \dot{K}_0. \tag{4.15}$$

Proof. Taking time derivatives of both sides of (4.5), and comparing with (4.10), we obtain that:

$$\dot{S}(K,\dot{K})K + S(K,\dot{K})\dot{K} + \dot{K}S(K,\dot{K}) + K\dot{S}(K,\dot{K}) = 2\, S(K,\dot{K})\, K\, S(K,\dot{K})$$

$$\Rightarrow \dot{S}(K,\dot{K})K + K\dot{S}(K,\dot{K}) = -S^2(K,\dot{K})K - KS^2(K,\dot{K}).$$

Hence $\dot{S}(K,\dot{K})$ must satisfy: $\dot{S}(K,\dot{K}) = -S^2(K,\dot{K}) + U(K)$, with $U(K)$ any matrix such that $U(K)\, K + K\, U(K) = \mathbb{O}$. Since $S(K,\dot{K})$ is symmetric, so is $\dot{S}(K,\dot{K})$, thus $U(K)$ must be symmetric and $U(K)\, K$ must be skew-symmetric. By contradiction, we can show that indeed $U(K) = \mathbb{O}$. Assume $U(K) \neq \mathbb{O}$ and $U(K)\, K = A$, skew-symmetric (and $\neq 0$); then $U(K) = AK^{-1}$ is the product of a skew-symmetric matrix and a symmetric one, which is always skew-symmetric.

This contradicts the fact that $U(K)$ is a non-zero symmetric matrix. Therefore the following system of equations is equivalent to the Euler-Lagrange equations of proposition 4.1.5:

$$\dot{S} = -S^2 \tag{4.16}$$

$$\dot{K} = SK + KS. \tag{4.17}$$

Let $K(0) = K_0 \in \mathcal{K}$ be the initial coefficient of inertia tensor for a geodesic, and $\dot{K}(0) = \dot{K}_0 \in \mathbb{R}^{3\times3}_{sym}$ the initial tangent vector. Then there is a unique $S_0(K_0, \dot{K}_0)$ that solves the Lyapunov equation (4.15), and the solution to (4.16) is given by:

$$S(t) = (t\mathbb{1} + S_0^{-1})^{-1} = (\mathbb{1} + tS_0)^{-1}S_0 = S_0(\mathbb{1} + tS_0)^{-1}. \tag{4.18}$$

Notice that while we were expecting $S(t)$ to depend on both $K(t)$ and $\dot{K}(t)$ $\forall t$ (see proposition 4.1.5), it actually depends only on $K(0)$ and $\dot{K}(0)$ (which uniquely define S_0). Substituting (4.18) into (4.17), we conclude that the geodesic $K(t)$ starting from K_0 with initial tangent vector $\dot{K}_0$, must satisfy $\forall t$:

$$\dot{K}(t) = S_0(\mathbb{1} + tS_0)^{-1}K(t) + K(t)(\mathbb{1} + tS_0)^{-1}S_0, \tag{4.19}$$

where $S_0 = S_0(K_0, \dot{K}_0)$ is the unique solution to the Lyapunov equation (4.15). It is easy to verify that the solution to (4.19) is given by (4.14). □

Remark 4.1.7 Manifold $\mathcal{K}$ is not geodesically complete (with respect to the Riemannian metric induced by kinetic energy). Consider in fact for example any geodesic with $\dot{K}_0 = -2K_0$; from (4.15) it is clear that in this case $S_0 = -\mathbb{1}$, and the corresponding geodesic (computed using (4.14)) is not well-defined at

$t = 1$. In general, geodesics are not well-defined at times t at which the matrix $\mathbb{1} + tS_0(K_0, \dot{K}_0)$ loses full rank, because then $K(t) \notin \mathcal{K}$.

A consequence of the lack of completeness is that the Hopf-Rinow theorem does not hold (recall the discussion in remark 4.1.4), and therefore the existence of path-energy minimizing geodesics connecting any pair of coefficient of inertia tensors is not guaranteed. In general, given two arbitrary $K_0, K_1 \in \mathcal{K}$, we do not know if a path-energy minimizing geodesic connecting them exists, unless K_1 is "close enough" to K_0 in the sense of remark 4.1.4. On the other hand, if the path-energy minimizing geodesic exists, it has to be one of the geodesics (4.14), so in the following we derive the set of geodesics connecting K_0 and K_1 as the set of candidate solutions to problem 4.1.3.

The existence of a geodesic curve $K : [0, 1] \mapsto \mathcal{K}$ with $K(0) = K_0$ and $K(1) = K_1$ is subordinated to the existence of an initial tangent vector $\dot{K}_0 \in \mathbb{R}^{3\times3}_{sym} = T_{K_0}\mathcal{K}$ and a corresponding $S_0(K_0, \dot{K}_0) \in \mathbb{R}^{3\times3}_{sym}$ that solves the following Algebraic Riccati Equation:

$$S_0K_0 + K_0S_0 + S_0K_0S_0 = K_1 - K_0. \tag{4.20}$$

It is therefore useful to recall the following classical result on Algebraic Riccati Equations.

Corollary 4.1.8 (J. E. Potter [45]). *Consider the matrix quadratic equation:*

$$A + BX + XB^* - XCX = \mathbb{O}, \tag{4.21}$$

where $A, B, C, X \in \mathbb{C}^{n\times n}$. *Assume that the following* $2n \times 2n$ *matrix:*

$$M = \begin{bmatrix} B & A \\ C & -B^* \end{bmatrix}, \tag{4.22}$$

has a diagonal Jordan canonical form, i.e. there exist $2n$ *eigenpairs* $(\lambda_i, \mathbf{a_i})$ *with all the eigenvectors* $\mathbf{a_i}$, *for* $i = 1, ..., 2n$, *linearly independent.*

Then every solution of (4.21) *has the form:*

$$X = [\mathbf{b_1 b_2 ... b_n}][\mathbf{c_1 c_2 ... c_n}]^{-1}, \tag{4.23}$$

where the column vectors $\mathbf{b_i} \in \mathbb{C}^n$ *and* $\mathbf{c_i} \in \mathbb{C}^n$ *are the upper and lower halves of an eigenvector* $\mathbf{a_i} \in \mathbb{C}^{2n}$ *of* M. *Conversely, if* $\mathbf{a_i} = [\mathbf{b_i}^T \mathbf{c_i}^T]^T$, $i = 1, ..., n$, *are eigenvectors of* M *and* $[\mathbf{c_1 c_2 ... c_n}]$ *is nonsingular, then* $X = [\mathbf{b_1 b_2 ... b_n}][\mathbf{c_1 c_2 ... c_n}]^{-1}$ *satisfies* (4.21). *Moreover, if* A *and* C *are hermitian,* $\mathbf{a_i} = [\mathbf{b_i}^T \mathbf{c_i}^T]^T$, $i = 1, ..., n$, *are eigenvectors of* M *corresponding to eigenvalues* $\lambda_1, ..., \lambda_n$ *such that* $\lambda_i \neq -\lambda_j^*$ *for* $1 \leq i, j \leq n$, *and* $[\mathbf{c_1 c_2 ... c_n}]$ *is nonsingular, then the solution* (4.23) *is hermitian.*

The Algebraic Riccati Equation (4.20) is indeed a special case of (4.21), with $X = S_0$, $A = K_0 - K_1 \in \mathbb{R}^{3\times3}_{sym}$ and $B = B^* = -C = K_0 \in \mathbb{R}^{3\times3}_{sym,>0}$. The matrix (4.22) associated to (4.20) has the particularly simple form:

$$M = \begin{bmatrix} K_0 & K_0 - K_1 \\ -K_0 & -K_0 \end{bmatrix}, \tag{4.24}$$

with eigenvectors that can be directly derived from those of the matrix $K_1 K_0 \in \mathbb{R}^{3\times3}$. To see that this is the case, observe first of all that M is similar to the

following matrix:

$$M' = \begin{bmatrix} \mathbb{0} & -K_1 \\ -K_0 & \mathbb{0} \end{bmatrix} = \begin{bmatrix} \mathbb{1} & \mathbb{1} \\ \mathbb{0} & \mathbb{1} \end{bmatrix} \begin{bmatrix} K_0 & K_0 - K_1 \\ -K_0 & -K_0 \end{bmatrix} \begin{bmatrix} \mathbb{1} & -\mathbb{1} \\ \mathbb{0} & \mathbb{1} \end{bmatrix} \triangleq P^{-1}MP. \tag{4.25}$$

Hence the eigenpairs $(\lambda_i, \mathbf{a_i})$ for M can be found searching for the corresponding eigenpairs $(\lambda_i, P^{-1}\mathbf{a_i})$ for M'. Any eigenpair $(\lambda_i, [\mathbf{u_i}^T \mathbf{v_i}^T]^T)$ for M' must in turns satisfy:

$$\begin{bmatrix} \mathbb{0} & -K_1 \\ -K_0 & \mathbb{0} \end{bmatrix} \begin{bmatrix} \mathbf{u_i} \\ \mathbf{v_i} \end{bmatrix} = \lambda_i \begin{bmatrix} \mathbf{u_i} \\ \mathbf{v_i} \end{bmatrix} \Rightarrow \begin{matrix} -K_1\mathbf{v_i} = \lambda_i\mathbf{u_i} \\ -K_0\mathbf{u_i} = \lambda_i\mathbf{v_i} \end{matrix} \Rightarrow \begin{matrix} -K_1\mathbf{v_i} = \lambda_i\mathbf{u_i} \\ K_1K_0\mathbf{u_i} = \lambda_i^2\mathbf{u_i} \end{matrix},$$

hence $\mathbf{u_i}$ must be eigenvector of K_1K_0 associated to some eigenvalue $\lambda_i^2 > 0$, and $\mathbf{v_i} = -K_1^{-1}\lambda_i\mathbf{u_i}$. Let $K_0^{1/2}$ be the principal square root (symmetric and positive-definite) of K_0, and $K_0^{-1/2}$ its inverse; if $K_0 = Q_0^T\Lambda_0 Q_0$ is an eigendecomposition of K_0, then $K_0^{1/2} \triangleq Q_0^T\Lambda_0^{1/2}Q_0$ and $K_0^{-1/2} \triangleq Q_0^T\Lambda_0^{-1/2}Q_0$. Since $K_1K_0 = K_0^{-1/2}K_0^{1/2}K_1K_0^{1/2}K_0^{1/2}$ is similar to the symmetric positive definite matrix $K_0^{1/2}K_1K_0^{1/2}$, K_1K_0 is diagonalizable and has strictly positive eigenvalues; i.e. K_1K_0 admits linearly independent eigenvectors $\mathbf{u_1}, \mathbf{u_2}, \mathbf{u_3}$ associated to strictly positive (possibly repeated) eigenvalues μ_1, μ_2, μ_3.

Let $(\mu_i, \mathbf{u_i})$ be one of these eigenpairs for K_1K_0; then there are two corresponding eigenpairs for M' given by: $(\sqrt{\mu_i}, [\mathbf{u_i}^T \ -K_1^{-1}\sqrt{\mu_i}\mathbf{u_i}^T]^T)$ and $(-\sqrt{\mu_i}, [\mathbf{u_i}^T \ K_1^{-1}\sqrt{\mu_i}\mathbf{u_i}^T])$, and more importantly two corresponding eigenpairs for $M =$

$PM'P^{-1}$ given by:

$$\left(\sqrt{\mu_i}, \begin{bmatrix} \mathbf{u_i} + K_1^{-1}\sqrt{\mu_i}\mathbf{u_i} \\ -K_1^{-1}\sqrt{\mu_i}\mathbf{u_i} \end{bmatrix}\right), \left(-\sqrt{\mu_i}, \begin{bmatrix} \mathbf{u_i} - K_1^{-1}\sqrt{\mu_i}\mathbf{u_i} \\ +K_1^{-1}\sqrt{\mu_i}\mathbf{u_i} \end{bmatrix}\right). \tag{4.26}$$

Since the eigenvectors $\mathbf{u_1}, \mathbf{u_2}, \mathbf{u_3}$ of K_1K_0 are linearly independent, so are the six eigenvectors in the eigenpairs of type (4.26), and therefore the matrix M in (4.24) is itself diagonalizable.

The algebraic Riccati equation (4.20) satisfies therefore the conditions of corollary 4.1.8. In particular, since the matrices $A = K_0 - K_1$ and $C = -K_0$ are symmetric, and the matrices $[\mp K_1^{-1}\sqrt{\mu_1}\mathbf{u_1} \mp K_1^{-1}\sqrt{\mu_2}\mathbf{u_2} \mp K_1^{-1}\sqrt{\mu_3}\mathbf{u_3}]$ constructed using the (linearly independent) eigenvectors of K_1K_0 are certainly invertible, there exist multiple symmetric solutions to (4.20) given by:

$$\begin{aligned} S_0 &= [\mathbf{u_1} \pm K_1^{-1}\sqrt{\mu_1}\mathbf{u_1} .. \mathbf{u_3} \pm K_1^{-1}\sqrt{\mu_3}\mathbf{u_3}][\mp K_1^{-1}\sqrt{\mu_1}\mathbf{u_1} .. \mp K_1^{-1}\sqrt{\mu_3}\mathbf{u_3}]^{-1} \\ &= [\mathbf{u_1}\,\mathbf{u_2}\,\mathbf{u_3}][\mp\sqrt{\mu_1}\mathbf{u_1} \mp \sqrt{\mu_2}\mathbf{u_2} \mp \sqrt{\mu_3}\mathbf{u_3}]^{-1}K_1 - \mathbb{1} \\ &= [\mathbf{u_1}\,\mathbf{u_2}\,\mathbf{u_3}] \begin{bmatrix} \mp\frac{1}{\sqrt{\mu_1}} & & \\ & \mp\frac{1}{\sqrt{\mu_2}} & \\ & & \mp\frac{1}{\sqrt{\mu_3}} \end{bmatrix} [\mathbf{u_1}\,\mathbf{u_2}\,\mathbf{u_3}]^{-1}K_1 - \mathbb{1}. \end{aligned} \tag{4.27}$$

For each of the matrices S_0 identified in (4.27), there is a curve of the type (4.19) that satisfies the necessary conditions for a geodesic as well as the boundary conditions $K(0) = K_0$, $K(1) = K_1$. To identify which of these curves is truly a candidate for being a path-energy minimizing geodesic, we need to evaluate the

corresponding path-energy functionals (4.6):

$$E(K) = \int_0^1 \mathrm{tr}(S(K(t), \dot{K}(t))\, K(t)\, S(K(t), \dot{K}(t)))dt = \int_0^1 \mathrm{tr}(S_0 K_0 S_0)dt$$

$$= \mathrm{tr}(K_1 - K_0) - \mathrm{tr}(S_0 K_0) - \mathrm{tr}(K_0 S_0) = \mathrm{tr}(K_1 - K_0) - 2\,\mathrm{tr}(S_0 K_0)$$

$$= \mathrm{tr}(K_1 + K_0) - 2\,\mathrm{tr}\left([\mathbf{u_1}\ \mathbf{u_2}\ \mathbf{u_3}] \begin{bmatrix} \mp\frac{1}{\sqrt{\mu_1}} & & \\ & \mp\frac{1}{\sqrt{\mu_2}} & \\ & & \mp\frac{1}{\sqrt{\mu_3}} \end{bmatrix} [\mathbf{u_1}\ \mathbf{u_2}\ \mathbf{u_3}]^{-1} K_1 K_0 \right). \tag{4.28}$$

The path-energy is minimal when the trace on the right hand side of (4.28) is maximal. Since $(\mu_1, \mathbf{u_1})$, $(\mu_2, \mathbf{u_2})$, $(\mu_3, \mathbf{u_3})$ are eigenpairs for $K_1 K_0$, we have that:

$$[\mathbf{u_1}\ \mathbf{u_2}\ \mathbf{u_3}] = (K_1 K_0)^{-1} [\mathbf{u_1}\ \mathbf{u_2}\ \mathbf{u_3}] \begin{bmatrix} \mu_1 & & \\ & \mu_2 & \\ & & \mu_3 \end{bmatrix} \Rightarrow$$

$$\mathrm{tr}\left([\mathbf{u_1}\ \mathbf{u_2}\ \mathbf{u_3}] \begin{bmatrix} \mp\frac{1}{\sqrt{\mu_1}} & & \\ & \mp\frac{1}{\sqrt{\mu_2}} & \\ & & \mp\frac{1}{\sqrt{\mu_3}} \end{bmatrix} [\mathbf{u_1}\ \mathbf{u_2}\ \mathbf{u_3}]^{-1} K_1 K_0 \right) = \mp\sqrt{\mu_1} \mp \sqrt{\mu_2} \mp \sqrt{\mu_3}.$$

Therefore the choice of S_0 in (4.27) that guarantees minimization of the path-energy (among the geodesics connecting K_0 and K_1) is the one with all positive signs:

$$S_0 = [\mathbf{u_1}\ \mathbf{u_2}\ \mathbf{u_3}] \begin{bmatrix} \frac{1}{\sqrt{\mu_1}} & & \\ & \frac{1}{\sqrt{\mu_2}} & \\ & & \frac{1}{\sqrt{\mu_3}} \end{bmatrix} [\mathbf{u_1}\ \mathbf{u_2}\ \mathbf{u_3}]^{-1} K_1 - \mathbb{1} \triangleq (K_1 K_0)^{-\frac{1}{2}} K_1 - \mathbb{1}, \tag{4.29}$$

where we have indicated with $(K_1K_0)^{-\frac{1}{2}}$ the inverse of the principal square root of the matrix K_1K_0 (i.e. the inverse of the unique matrix $(K_1K_0)^{\frac{1}{2}}$ with all positive eigenvalues such that $(K_1K_0)^{\frac{1}{2}}(K_1K_0)^{\frac{1}{2}} = K_1K_0$). The computation of $(K_1K_0)^{-\frac{1}{2}}$ is independent of the order in which the eigenpairs $(\mu_i, \mathbf{u_i})$ appear, hence the matrix S_0 defined by (4.29) is unique.

We have therefore derived the unique candidate solution to the problem of finding a path-energy minimizing geodesic connecting K_0 and K_1, which of course is the solution if the problem admits one; the following theorem summarizes this result.

Theorem 4.1.9 (**Path-energy minimizing geodesic**). *Let $K_0 \in \mathcal{K}$ and $K_1 \in \mathcal{K}$ be symmetric positive definite matrices. Then the unique path-energy minimizing geodesic (with respect to the metric (3.58)) $K : [0,1] \mapsto \mathcal{K}$, $K(0) = K_0$, $K(1) = K_1$, if it exists, is given by:*

$$K(t) = ((1-t)\mathbb{1} + t(K_1K_0)^{-\frac{1}{2}}K_1)K_0((1-t)\mathbb{1} + t(K_1K_0)^{-\frac{1}{2}}K_1), \tag{4.30}$$

where $(K_1K_0)^{-\frac{1}{2}}$ can be computed from the eigenpairs $(\mu_1, \mathbf{u_1})$, $(\mu_2, \mathbf{u_2})$, $(\mu_3, \mathbf{u_3})$ of K_1K_0 (taken in any order, as long as the eigenvectors $\mathbf{u_i}$ are linearly independent) as follows:

$$(K_1K_0)^{-\frac{1}{2}} = [\mathbf{u_1}\ \mathbf{u_2}\ \mathbf{u_3}] \begin{bmatrix} \frac{1}{\sqrt{\mu_1}} & & \\ & \frac{1}{\sqrt{\mu_2}} & \\ & & \frac{1}{\sqrt{\mu_3}} \end{bmatrix} [\mathbf{u_1}\ \mathbf{u_2}\ \mathbf{u_3}]^{-1}. \tag{4.31}$$

The value of path-energy associated to the geodesic K is:

$$E(K) = \int_0^1 \langle \dot{K}(t), \dot{K}(t) \rangle_{K(t)} dt = \mathrm{tr}(K_0) + \mathrm{tr}(K_1) - 2(\sqrt{\mu_1} + \sqrt{\mu_2} + \sqrt{\mu_3}). \quad (4.32)$$

Direct application of theorem 4.1.2 leads to the following solution to the coefficient of inertia regulation problem 4.1.1.

Theorem 4.1.10 (**Optimal coefficient of inertia regulation).** *Let $\mathbf{c_0} \in \mathcal{C}^{3d}$ be an initial configuration for the collective, with coefficient of inertia tensor $K(\mathbf{c_0}) \triangleq K_0 \in \mathcal{K}$, and let $K_1 \in \mathcal{K}$ be a desired coefficient of inertia. Then the unique differentiable curve in $\mathcal{C}^{3d}$, $\mathbf{\Gamma} : [0,1] \mapsto \mathcal{C}^{3d}$, $\mathbf{\Gamma}(0) = \mathbf{c_0}$, $K(\mathbf{\Gamma}(1)) = K_1$, that minimizes the path-energy* (4.1)*, if it exists, is given by the solution to the following ordinary differential equation, $\forall t \in [0,1]$:*

$$\dot{\mathbf{\Gamma}}(t) = ((K_1 K_0)^{-\frac{1}{2}} K_1 - \mathbb{1})((1-t)\mathbb{1} + t(K_1 K_0)^{-\frac{1}{2}} K_1)^{-1} \mathbf{\Gamma}(t), \quad (4.33)$$

$$\mathbf{\Gamma}(0) = \mathbf{c_0}.$$

The corresponding path-energy is:

$$E_{path}(\mathbf{\Gamma}) = \int_0^1 \langle \dot{\mathbf{\Gamma}}(t), \dot{\mathbf{\Gamma}}(t) \rangle_{\mathbf{\Gamma}(t)} dt = \mathrm{tr}(K_0) + \mathrm{tr}(K_1) - 2(\sqrt{\mu_1} + \sqrt{\mu_2} + \sqrt{\mu_3}). \quad (4.34)$$

Remark 4.1.11 If K_0 and K_1 differ only in their eigenvalues (i.e. $K_0 = Q^T \Lambda_0 Q$, $K_1 = Q^T \Lambda_1 Q$, for $Q \in SO(3)$, $\Lambda_0 = \mathrm{diag}(\lambda_{1,0}, \lambda_{2,0}, \lambda_{3,0})$ and $\Lambda_1 = \mathrm{diag}(\lambda_{1,1}, \lambda_{2,1}, \lambda_{3,1})$), then the optimal coefficient of inertia regulation, if it exists, is given by an *inertia tensor deformation*, i.e. the horizontal lift of a curve $K(t) = Q^T \Lambda(t) Q$ (see section 3.4). In fact in this case $K_1 K_0 = Q^T \Lambda_1 Q Q^T \Lambda_0 Q = Q^T \Lambda_1 \Lambda_0 Q$,

$(K_1K_0)^{-\frac{1}{2}} = Q^T\Lambda_1^{-\frac{1}{2}}\Lambda_0^{-\frac{1}{2}}Q$, and the candidate path-energy minimizing geodesic connecting $K(0) = K_0$ and $K(1) = K_1$ is:

$$\begin{aligned}
K(t) &= ((1-t)\mathbb{1} + t(Q^T\Lambda_1^{\frac{1}{2}}\Lambda_0^{-\frac{1}{2}}Q))Q^T\Lambda_0Q((1-t)\mathbb{1} + t(Q^T\Lambda_1^{\frac{1}{2}}\Lambda_0^{-\frac{1}{2}}Q)) \\
&= Q^T((1-t)^2\Lambda_0 + 2t(1-t)\Lambda_1^{\frac{1}{2}}\Lambda_0^{\frac{1}{2}} + t^2\Lambda_1)Q \\
&= Q^T\begin{bmatrix} (\sqrt{\lambda_{1,0}} - t(\sqrt{\lambda_{1,0}} - \sqrt{\lambda_{1,1}}))^2 & & \\ & (\sqrt{\lambda_{2,0}} - t(\sqrt{\lambda_{2,0}} - \sqrt{\lambda_{2,1}}))^2 & \\ & & (\sqrt{\lambda_{3,0}} - t(\sqrt{\lambda_{3,0}} - \sqrt{\lambda_{3,1}}))^2 \end{bmatrix}Q.
\end{aligned}$$

The horizontal lift of this curve, given by (4.33), has the simple form:

$$\begin{aligned}
\dot{\mathbf{\Gamma}}(t) &= ((Q^T\Lambda_1^{\frac{1}{2}}\Lambda_0^{-\frac{1}{2}}Q - \mathbb{1})(((1-t)\mathbb{1} + tQ^T\Lambda_1^{\frac{1}{2}}\Lambda_0^{-\frac{1}{2}}Q)^{-1}\,\mathbf{\Gamma}(t) \\
&= Q^T((\Lambda_1^{\frac{1}{2}}\Lambda_0^{-\frac{1}{2}} - \mathbb{1})((1-t)\mathbb{1} + t\Lambda_1^{\frac{1}{2}}\Lambda_0^{-\frac{1}{2}})^{-1})Q\,\mathbf{\Gamma}(t) \\
&= Q^T\begin{bmatrix} \frac{\sqrt{\lambda_{1,1}}-\sqrt{\lambda_{1,0}}}{\sqrt{\lambda_{1,0}}+t\,(\sqrt{\lambda_{1,1}}-\sqrt{\lambda_{1,0}})} & & \\ & \frac{\sqrt{\lambda_{2,1}}-\sqrt{\lambda_{2,0}}}{\sqrt{\lambda_{2,0}}+t\,(\sqrt{\lambda_{2,1}}-\sqrt{\lambda_{2,0}})} & \\ & & \frac{\sqrt{\lambda_{3,1}}-\sqrt{\lambda_{3,0}}}{\sqrt{\lambda_{3,0}}+t\,(\sqrt{\lambda_{3,1}}-\sqrt{\lambda_{3,0}})} \end{bmatrix}Q\,\mathbf{\Gamma}(t),
\end{aligned}$$

with corresponding path-energy:

$$\begin{aligned}
E_{path}(\mathbf{\Gamma}) &= \mathrm{tr}(Q^T\Lambda_0Q) + \mathrm{tr}(Q^T\Lambda_1Q) - 2(\sqrt{\lambda_{1,0}\lambda_{1,1}} + \sqrt{\lambda_{2,0}\lambda_{2,1}} + \sqrt{\lambda_{3,0}\lambda_{3,1}}) \\
&= (\sqrt{\lambda_{1,1}} - \sqrt{\lambda_{1,0}})^2 + (\sqrt{\lambda_{2,1}} - \sqrt{\lambda_{2,0}})^2 + (\sqrt{\lambda_{3,1}} - \sqrt{\lambda_{3,0}})^2.
\end{aligned}$$

Conversely, if K_0 and K_1 have the same eigenvalues but differ in their eigenvectors (i.e. $K_0 = Q_0^T\Lambda Q_0$, $K_1 = Q_1^T\Lambda Q_1$ for some $Q_0, Q_1 \in SO(3)$ and $\Lambda = \mathrm{diag}(\lambda_1, \lambda_2, \lambda_3)$), the optimal coefficient of inertia regulation, if it exists, is *not* given by an *inertia tensor rotation*, i.e. the horizontal lift of a curve

$K(t) = Q(t)^T \Lambda Q(t)$. From the expression (4.30) for the candidate path-energy minimizing geodesic connecting K_0 and K_1, and the fact that $K_0 = Q_0^T \Lambda Q_0$, the geodesic cannot in fact be in the form $K(t) = Q(t)^T \Lambda Q(t)$ unless the matrix $((1-t)\mathbb{1} + t(K_1 K_0)^{-\frac{1}{2}} K_1)$ is symmetric and orthogonal (hence a permutation matrix) $\forall t \in [0,1]$, which is not the case. Therefore the optimal coefficient of inertia regulation, if it exists, involves temporarily changing the eigenvalues of the coefficient of inertia tensor, despite the fact that the initial and final coefficient of inertia tensors have the same eigenvalues.

Corollary 4.1.12. *If the desired coefficient of inertia tensor K_1 has to be reached in an arbitrary fixed time T (instead of exactly one second, i.e. $T = 1$), the optimal coefficient of inertia regulation is given by (cfg.* (4.33)*):*

$$\begin{aligned} \dot{\mathbf{\Gamma}}(t) &= ((K_1 K_0)^{-\frac{1}{2}} K_1 - \mathbb{1})((T-t)\mathbb{1} + t(K_1 K_0)^{-\frac{1}{2}} K_1)^{-1} \mathbf{\Gamma}(t), \\ \mathbf{\Gamma}(0) &= \mathbf{c_0}. \end{aligned} \tag{4.35}$$

Proof. The path-energy minimizing geodesic in $\mathcal{K}$ starting at K_0 must still satisfy (4.14), but now $S_0(K_0, \dot{K}_0) \in \mathbb{R}^{3\times 3}_{sym}$ must solve the following Algebraic Riccati Equation (instead of (4.20)):

$$T(S_0 K_0 + K_0 S_0) + T^2 (S_0 K_0 S_0) = K_1 - K_0. \tag{4.36}$$

If S_0 is the solution to (4.20) (given by (4.29)), then the solution to (4.36) is given by S_0/T. Hence $S(t)$ must be given by (instead of (4.18)):

$$S(t) = \frac{1}{T} S_0 \left(\mathbb{1} + \frac{t}{T} S_0 \right)^{-1} = S_0 \left(T\mathbb{1} + t S_0 \right)^{-1}, \tag{4.37}$$

which yields exactly (4.35). □

4.1.2 Distributed implementations

The implementation of an inertia tensor transformation $\dot{\mathbf{c}}(t) = S(t)\mathbf{c}(t)$, with $S(t) \in \mathbb{R}^{3\times3}_{sym}\, \forall t$, requires each member of the collective to move with respect to the center of mass according to:

$$\dot{\mathbf{c}}_\mathbf{i}(t) = S(t)\mathbf{c}_\mathbf{i}(t) \quad \forall i = 1, ..., n, \quad \forall t. \tag{4.38}$$

Even when the prescribed evolution of $S(t)$ is known to every agent (it could be for example the one given by (4.33), that modifies the coefficient of inertia tensor from K_0 to K_1), in general each agent needs to know its relative position and velocity with respect to the center of mass ($\mathbf{c}_\mathbf{i}(t)$, $\dot{\mathbf{c}}_\mathbf{i}(t)$), and control the latter in accordance to (4.38). Since the center of mass depends on the position of all the agents (recall (3.3)), condition (4.38) might appear to exclude a distributed implementation of vector fields of this type, which is needed when each agent is able to sense only a limited number of other agents. On the contrary, we prove in this section that under certain conditions on the "sensing network" between the agents, it is possible to indirectly guarantee (4.38) through alternative constraints on the individual agent motions that are compatible with distributed implementation.

There are two types of alternative constraints, one prescribing the relative motion of each agent with respect to one other agent (among those it can sense), the other prescribing its relative motion with respect to the center of mass of a

subset of the agents it can sense. Note that the same results could be applied to the distributed implementation of rigid rotations of the collective (vector fields of the type $\dot{\mathbf{c}}(t) = A(t)\mathbf{c}(t)$, with $A(t)$ skew-symmetric $\forall t$).

Some terminology and results from graph theory are needed before introducing the conditions for distributed implementation. The "neighbors" of an agent are the other agents that it actively senses, in particular with respect to which relative positions and velocities are known and used by the agent in the control of its own motion. Notice that agent sensing could, but does not have to, rely on exchange of information between neighbors via communication lines; even in cases where sensing does depend on communication, the sensing network does not have to be equal to the underlying communication network, but it could be a subset of it. Agents that are outside the sensing (or, if needed, communication) range of a particular agent cannot be part of its "neighborhood", but the latter does not have to include all the agents within the range, since the agent might use only some of the available information in controlling its motion.

We define the *sensing network*, that describes the neighborhood associated to each agent, as a simple directed weighted graph $\mathcal{G}$ with n vertices (one for each agent) and edges (i, j), directed from vertex i to vertex j, whenever agent j is a neighbor of agent i. The number of edges starting from a vertex is called its *out-degree*, and corresponds to the number of neighbors of that particular agent. The number of edges ending at a particular vertex is instead called its *in-degree*. The *degree* of a vertex in a directed graph is the sum of its in-degree and its

out-degree.

To the graph $\mathcal{G}$, we associate a *weighted adjacency matrix* $A_{\mathcal{G}}$ and a corresponding *weighted Laplacian matrix* $L_{\mathcal{G}}$. The weighted adjacency matrix is defined as: $A_{\mathcal{G}} = [a_{ij}]$, where $a_{ij} \neq 0 \in \mathbb{R}$ if $\mathcal{G}$ has an edge (i, j), and $a_{ij} = 0$ otherwise; the weighted Laplacian matrix is defined as $L_{\mathcal{G}} = D_{\mathcal{G}} - A_{\mathcal{G}}$, where $D_{\mathcal{G}}$ is the diagonal matrix defined so that all the rows of $L_{\mathcal{G}}$ add up to zero (i.e. $d_{ii} = \sum_{j \neq i} a_{ij}$, and $d_{ij} = 0 \, \forall i \neq j$).

The simplest choice for the weights associated to the edges is to take $a_{ij} \in \{0, 1\} \, \forall i, j$ (1 if there is an edge (i, j), 0 otherwise); in that case $D_{\mathcal{G}}$ is the diagonal matrix of out-degrees of the vertices. For the proof of one of the theorems below, it is instead more convenient to choose the edge weights equal to the masses, as follows: $a_{ij} = m_j$ if (i, j) is an edge of $\mathcal{G}$, and $a_{ij} = 0$ otherwise.

Let (i, j) be an edge of $\mathcal{G}$; we refer to (i, j) as a *bidirectional* edge if (j, i) is also an edge, and as a *unidirectional* edge otherwise. The *undirected graph associated to* $\mathcal{G}$ is the graph obtained from $\mathcal{G}$ by substituting every unidirectional edge with a bidirectional edge (i.e. adding an edge (j, i) with weight $a_{j,i} = a_{i,j}$ whenever (i, j) is a unidirectional edge of $\mathcal{G}$). The graph $\mathcal{G}$ is *strongly connected* if there exists a path (a sequence of edges $(i, j), (j, k), (k, l), ...$) that connects every pair of vertices, and *weakly connected* if the undirected graph associated to $\mathcal{G}$ is strongly connected (clearly strong connectivity implies weak connectivity).

A *spanning tree of* $\mathcal{G}$ *directed into vertex* i, if it exists, is a subgraph of $\mathcal{G}$ containing all of its vertices, and such that: (i) each vertex has out-degree 1

except i, which has out-degree 0, and (ii) there exists a path between every vertex and i. The *weight of a spanning tree* is the product of all the weights of the edges in the spanning tree. Notice that a spanning tree has always exactly $n-1$ edges; moreover an undirected graph is connected if and only if it has a spanning tree.

A *Hamiltonian path* of $\mathcal{G}$, if it exists, is a path that touches all the nodes exactly once. A Hamiltonian path that is also a cycle (i.e. closed loop) is called *Hamiltonian cycle*. Clearly a Hamiltonian path that is not a cycle is a special type of *spanning tree*. A graph that has a Hamiltonian path is called *traceable*, and one that also has a Hamiltonian cycle is called *Hamiltonian graph*.

The (weighted) Laplacian of a graph $\mathcal{G}$ has several important properties:
(i) Since all the rows add up to zero, $L_{\mathcal{G}}$ is singular (has always a zero eigenvalue).
(ii) The minor of $L_{\mathcal{G}}$ obtained by removing its i-th row and i-th column is equal to the sum of the weights of all spanning trees directed into vertex i (this is referred to as the *matrix-tree theorem* [52]).
(iii) If all the weights associated to the edges are non-negative (which is the case with the choice $a_{ij} = m_j$), then all the nonzero eigenvalues of $L_{\mathcal{G}}$ are in the right half plane (this follows from the Gershgorin disk theorem, see for example [26]). Moreover, for non-negative weights, the multiplicity of the zero eigenvalue of $L_{\mathcal{G}}$ is one (the rank of $L_{\mathcal{G}}$ is $n-1$) if and only if there exists a spanning tree directed into one of the vertices of $\mathcal{G}$ (this follows from (ii)).
(iv) For an undirected graph with non-negative edge weights, the multiplicity of the zero eigenvalue of $L_{\mathcal{G}}$ is one if and only if the graph is connected (this directly

follows from (iii)), and is in general equal to the number of connected components in the graph (see for example [43]).

We are now ready to state several sufficient conditions for the distributed implementation of inertia tensor transformations. We start by considering the case in which each agent controls its motion with respect to one other agent or, alternatively, moves independently of all the others (we allow for "terminal vertices" in the graph). Therefore we initially restrict our attention to sensing graphs in which each vertex has at most out-degree one.

Theorem 4.1.13. *Assume that the sensing network $\mathcal{G}$ has the following properties: (i) it is weakly connected, (ii) each of its vertices has at most out-degree one, i.e. the neighborhood of each agent is composed of at most one other agent. For each agent i, let j_i denote its neighbor (if any), and $\mathbf{r_{i,j_i}} \triangleq \mathbf{r_i} - \mathbf{r_{j_i}}$, $\dot{\mathbf{r}}_{\mathbf{i,j_i}} \triangleq \dot{\mathbf{r}}_{\mathbf{i}} - \dot{\mathbf{r}}_{\mathbf{j_i}}$ the corresponding relative position and velocity. Then a sufficient condition for the collective to implement the inertia tensor transformation* (4.38) *is that the relative motion of each agent with respect to its neighbor, if any, satisfies:*

$$\dot{\mathbf{r}}_{\mathbf{i,j_i}}(t) = S(t)\mathbf{r_{i,j_i}}(t) \quad \forall i = 1, ..., n, \quad \forall t. \tag{4.39}$$

Proof. For each agent i, the relative position and velocity with respect to the center of mass can be expressed as:

$$\mathbf{c_i} = \mathbf{r_i} - \mathbf{r_{com}} = \mathbf{r_i} - \sum_{j=1}^{n} \frac{m_j}{M}\mathbf{r_j} = \sum_{j=1}^{n} \frac{m_j}{M}\mathbf{r_i} - \sum_{j=1}^{n} \frac{m_j}{M}\mathbf{r_j} = \sum_{j=1}^{n} \frac{m_j}{M}\mathbf{r_{i,j}}, \tag{4.40}$$

$$\dot{\mathbf{c}}_\mathbf{i} = \sum_{j=1}^{n} \frac{m_j}{M}\dot{\mathbf{r}}_{\mathbf{i,j}}, \tag{4.41}$$

where $M = \sum_{i=1}^{n} m_i$ and $\mathbf{r_{i,j}} = \mathbf{r_i} - \mathbf{r_j}$. Hence a sufficient condition for (4.38) to be satisfied is that $\dot{\mathbf{r}}_{\mathbf{i,j}}(t) = S(t)\mathbf{r_{i,j}}(t)\,\forall i, j, \forall t$. For all pairs of neighbors (i, j_i) this is guaranteed by (4.39); we want to prove that the condition is also satisfied for non-neighboring pairs of agents. By the hypothesis that the graph $\mathcal{G}$ is weakly connected, $\forall i, j$ there exists a path in the undirected graph associated to $\mathcal{G}$ that connects vertices i and j. Denote as $k_l, l = 1, ..., n_{ij}$ the n_{ij} intermediate vertices in such path ($n_{ij} \leq n-2$, can vary with the pair i, j). Then: $\mathbf{r_{i,j}} = \mathbf{r_{i,k_1}} + \mathbf{r_{k_1,k_2}} + ... + \mathbf{r_{k_{n_{ij}},j}}$ and $\dot{\mathbf{r}}_{\mathbf{i,j}} = \dot{\mathbf{r}}_{\mathbf{i,k_1}} + \dot{\mathbf{r}}_{\mathbf{k_1,k_2}} + ... + \dot{\mathbf{r}}_{\mathbf{k_{n_{ij}},j}}$. Since vertex i is connected with vertex k_1 in the undirected graph associated to $\mathcal{G}$, in the original graph $\mathcal{G}$ either k_1 is the neighbor of i, or i is the neighbor of k_1; in the first case, hypothesis (4.39) directly guarantees that $\dot{\mathbf{r}}_{\mathbf{i,k_1}}(t) = S(t)\mathbf{r_{i,k_1}}(t)\,\forall t$, while in the other case it guarantees that $\dot{\mathbf{r}}_{\mathbf{k_1,i}}(t) = S(t)\mathbf{r_{k_1,i}}(t)\,\forall t$. In either case, $\dot{\mathbf{r}}_{\mathbf{i,k_1}}(t) = S(t)\mathbf{r_{i,k_1}}(t)\,\forall t$; the same argument could be used to prove that $\dot{\mathbf{r}}_{\mathbf{k_l,k_{l+1}}}(t) = S(t)\mathbf{r_{k_l,k_{l+1}}}(t)\,\forall l = 1, ..., n_{ij}-1$, $\forall t$, and $\dot{\mathbf{r}}_{\mathbf{k_{n_{ij}},j}}(t) = S(t)\mathbf{r_{k_{n_{ij}},j}}(t)\,\forall t$. Therefore $\dot{\mathbf{r}}_{\mathbf{i,j}}(t) = (\dot{\mathbf{r}}_{\mathbf{i,k_1}} + \dot{\mathbf{r}}_{\mathbf{k_1,k_2}} + ... + \dot{\mathbf{r}}_{\mathbf{k_{n_{ij}},j}})(t) = S(t)(\mathbf{r_{i,k_1}} + \mathbf{r_{k_1,k_2}} + ... + \mathbf{r_{k_{n_{ij}},j}})(t) = S(t)\mathbf{r_{i,j}}(t)\,\forall i, j, \forall t$. □

Remark 4.1.14 By definition, $\mathcal{G}$ is weakly connected if and only if the undirected graph associated to $\mathcal{G}$ is (strongly) connected, and hence it admits a spanning tree (with $n-1$ undirected edges); hence $\mathcal{G}$ must have at least $n-1$ edges, and at most one vertex can be a "terminal vertex" (with out-degree zero).

Sensing networks in which each agent relies only on the information ob-

tained from one other agent, to which theorem 4.1.13 applies, are appealing for they require the minimum amount of individual sensing (or communication). On the other hand, it might sometimes be preferable (e.g. for robustness) to have each agent rely on cumulative information obtained from multiple neighbors (rather than a single one). For this reason, we present two alternative examples of decentralized implementations of inertia tensor transformations, in which each agent controls its relative motion with respect to the center of mass of its neighborhood, which can be composed of multiple agents. Let $N_i \triangleq \{j_i^1, j_i^2, ..., j_i^{n_i}\}$ be the set of n_i neighbors of agent i ($n_i \leq n-1$, can vary with the agent i); the center of mass of the neighborhood of agent i, or the *local center of mass* of agent i, is given by:

$$\mathbf{r_{com,i}} \triangleq \sum_{j \in N_i} \frac{m_j}{M_i} \mathbf{r_j} = \sum_{l=1}^{n_i} \frac{m_{j_i^l}}{M_i} \mathbf{r_{j_i^l}}, \tag{4.42}$$

where $M_i \triangleq \sum_{j \in N_i} m_j = \sum_{l=1}^{n_i} m_{j_i^l}$.

Theorem 4.1.15. *Assume that the sensing network $\mathcal{G}$ has the following properties: (i) it is weakly connected, (ii) the sum of the number of unidirectional edges (n_{ue}) and bidirectional edges (n_{be}) is less than or equal to the number of vertices with at least one outgoing edge (given by $n - n_{ter}$, where n_{ter} is the number of terminal vertices):*

$$n_{ue} + n_{be} \leq n - n_{ter}. \tag{4.43}$$

Then a sufficient condition for the collective to implement the inertia tensor transformation (4.38) *is that the relative motion of each agent with respect to its local*

center of mass satisfies:

$$\dot{\mathbf{r}}_{\mathbf{i},\mathbf{com_i}}(t) = S(t)\mathbf{r}_{\mathbf{i},\mathbf{com_i}}(t) \quad \forall i = 1, ..., n, \quad \forall t. \tag{4.44}$$

Proof. We first show that the hypothesis of the theorem are sufficient to guarantee that for each pair of neighboring vertices (i, j_i^l), $i = 1, ..., n$, $l = 1, ..., n_i$:

$$\dot{\mathbf{r}}_{\mathbf{i},\mathbf{j_i^l}}(t) = S(t)\mathbf{r}_{\mathbf{i},\mathbf{j_i^l}}(t) \quad \forall i = 1, ..., n, \quad \forall l = 1, ..., n_i, \quad \forall t. \tag{4.45}$$

To prove this, observe that for each agent i that has at least one neighbor (its corresponding vertex in the sensing graph is not a terminal vertex), condition (4.44) yields an equation of the type:

$$\sum_{l=1}^{n_i} \frac{m_{j_i^l}}{M_i} \dot{\mathbf{r}}_{\mathbf{i},\mathbf{j_i^l}}(t) = \sum_{l=1}^{n_i} \frac{m_{j_i^l}}{M_i} S(t)\mathbf{r}_{\mathbf{i},\mathbf{j_i^l}}(t). \tag{4.46}$$

The overall system of $n - n_{ter}$ such equations, for a fixed time t, can be thought of as a linear system in the unknowns $\dot{\mathbf{r}}_{\mathbf{i},\mathbf{j_i^l}}(t)$, $\forall i = 1, ..., n$, $\forall l = 1, ..., n_i$ (whereas $S(t)$ and the relative agent positions at time t are known quantities). A feasible solution to this system of equations is given by (4.45). Not all the unknowns $\dot{\mathbf{r}}_{\mathbf{i},\mathbf{j_i^l}}(t)$ are in general linearly independent; for example if there is a pair of vertices (a, b) connected by a bidirectional edge, then $\dot{\mathbf{r}}_{\mathbf{a},\mathbf{b}}(t) = -\dot{\mathbf{r}}_{\mathbf{b},\mathbf{a}}(t)$. The number of independent unknowns is therefore $\leq n_{ue} + n_{be}$, with equality achieved if there is exactly one path connecting each pair of vertices in the undirected graph associated to $\mathcal{G}$ (i.e. if the latter is a spanning tree). When (4.43) holds, the number of unknowns is less than or equal to the number of constraints, hence the only solution is (4.45).

Finally, since the graph $\mathcal{G}$ is weakly connected, (4.45) allows to use the same steps of the proof of theorem 4.1.13 to show that $\dot{\mathbf{r}}_{\mathbf{i,j}}(t) = S(t)\mathbf{r}_{\mathbf{i,j}}(t)$, $\forall i, j, \forall t$, which in turns guarantees (4.38). □

Remark 4.1.16 The number of edges of the undirected graph associated to $\mathcal{G}$ is exactly $n_{ue} + n_{be}$; since $\mathcal{G}$ is weakly connected, it must be $n_{ue} + n_{be} \geq n - 1$ (see remark 4.1.14). Hence $n - 1 \leq n - n_{ter} \Rightarrow n_{ter} \leq 1$. Note also that if a graph satisfies the conditions of theorem 4.1.13, then it has either $n - 1$ unidirectional edges (if there is a terminal node) or it has $n - 2$ unidirectional edges and 1 bidirectional node; in both cases, the conditions of theorem 4.1.15 are satisfied. Hence theorem 4.1.13 can be thought of as a special case of theorem 4.1.15.

Condition (4.43) is quite limiting in terms of number of edges in the sensing graph (and hence in terms of number of neighbors that each agent considers); for example if all the edges are bidirectional, then their number has to be lower than or equal to n (note that there cannot be terminal nodes, or the graph would not be connected). The next theorem does not impose limitations on the maximum number of edges; on the contrary, a sufficient condition to satisfy its conditions on the topology of the sensing graph (existence of a spanning tree) is for the graph to have a large enough number of edges.

Theorem 4.1.17. *Assume that the sensing network $\mathcal{G}$ admits a spanning tree directed into one of its vertices. Then a sufficient condition for the collective to implement the inertia tensor transformation* (4.38) *is that the relative motion of*

each agent with respect to its local center of mass satisfies:

$$\dot{\mathbf{r}}_{\mathbf{i},\mathbf{com_i}}(t) = S(t)\mathbf{r}_{\mathbf{i},\mathbf{com_i}}(t) \quad \forall i = 1, ..., n, \quad \forall t. \tag{4.47}$$

Proof. As shown by (4.40)-(4.41), the inertia tensor transformation (4.38) is implemented if and only if, for each agent i, $\sum_{j=1}^{n} m_j \dot{\mathbf{r}}_{\mathbf{i},\mathbf{j}}(t) = S(t) \sum_{j=1}^{n} m_j \mathbf{r}_{\mathbf{i},\mathbf{j}}(t)$, $\forall t$. For each agent i, the other agents ($j \in \{1, 2, ..., n\}, j \neq i$) can be partitioned into the set of neighbors N_i and the set of non-neighbors, which we denote as $\tilde{N}_i$; defining $\mathbf{R}_{\mathbf{i},\mathbf{N_i}} \triangleq \sum_{j \in N_i} m_j \mathbf{r}_{\mathbf{i},\mathbf{j}}$ and $\mathbf{R}_{\mathbf{i},\tilde{\mathbf{N}}_\mathbf{i}} \triangleq \sum_{j \in \tilde{N}_i} m_j \mathbf{r}_{\mathbf{i},\mathbf{j}}$, the condition above can be conveniently expressed as:

$$\dot{\mathbf{R}}_{\mathbf{i},\mathbf{N_i}}(t) + \dot{\mathbf{R}}_{\mathbf{i},\tilde{\mathbf{N}}_\mathbf{i}}(t) = S(t)\mathbf{R}_{\mathbf{i},\mathbf{N_i}}(t) + S(t)\mathbf{R}_{\mathbf{i},\tilde{\mathbf{N}}_\mathbf{i}}(t), \ \forall t. \tag{4.48}$$

In the proof of theorem 4.1.15, we showed that hypothesis (4.47) guarantees that, for each agent i, (4.46) holds, or equivalently (multiplying both sides by M_i):

$$\dot{\mathbf{R}}_{\mathbf{i},\mathbf{N_i}}(t) = S(t)\mathbf{R}_{\mathbf{i},\mathbf{N_i}}(t), \ \forall t. \tag{4.49}$$

Hence what remains to be proved is that, under the hypothesis of the theorem:

$$\dot{\mathbf{R}}_{\mathbf{i},\tilde{\mathbf{N}}_\mathbf{i}}(t) = S(t)\mathbf{R}_{\mathbf{i},\tilde{\mathbf{N}}_\mathbf{i}}(t), \quad \forall i = 1, ..., n, \quad \forall t. \tag{4.50}$$

In theorems 4.1.13 and 4.1.15, (4.50) was guaranteed by the stronger conditions (4.39) and (4.45) respectively. The hypothesis of this theorem are not sufficient for (4.45) to hold, but we will show that they are sufficient for each $\mathbf{R}_{\mathbf{i},\tilde{\mathbf{N}}_\mathbf{i}}$ to be a linear combination of the $\mathbf{R}_{\mathbf{j},\mathbf{N_j}}, j = 1, ..., n$, which in turns guarantees (4.50) when (4.49) is satisfied.

Without loss of generality, let the spanning tree in $\mathcal{G}$ be directed into vertex n. Each $\mathbf{r_{i,j}}$, $\forall i, j$, and hence each $\mathbf{R_{i,N_i}}$, $\mathbf{R_{i,\tilde{N}_i}}$, $\forall i$, can be expressed as linear combinations of the relative positions: $\mathbf{r_{1,2}}$, $\mathbf{r_{2,3}}$, ..., $\mathbf{r_{n-1,n}}$; in particular, for each i, there exist coefficients $\alpha^i_{l,l+1}$ and $\beta^i_{l,l+1}$, $l = 1, ..., n-1$ such that: $\mathbf{R_{i,N_i}} = \sum_{l=1}^{n-1} \alpha^i_{l,l+1}\mathbf{r_{l,l+1}}$ and $\mathbf{R_{i,\tilde{N}_i}} = \sum_{l=1}^{n-1} \beta^i_{l,l+1}\mathbf{r_{l,l+1}}$.

$\mathbf{R_{i,\tilde{N}_i}}$ is a linear combination of $\mathbf{R_{j,N_j}}, j = 1, ..., n$, if and only if there exist n coefficients γ^i_1, γ^i_2, ..., γ^i_n such that:

$$\mathbf{R_{i,\tilde{N}_i}} = \sum_{j=1}^{n} \gamma^i_j \mathbf{R_{j,N_j}} \Rightarrow \sum_{l=1}^{n-1} \beta^i_{l,l+1}\mathbf{r_{l,l+1}} = \sum_{j=1}^{n} \gamma^i_j \sum_{k=1}^{n-1} \alpha^j_{k,k+1}\mathbf{r_{k,k+1}}, \tag{4.51}$$

or, alternatively, if there exists a vector $\mathbf{Vec^i_\gamma} \triangleq [\gamma^i_1\, \gamma^i_2 \ldots \gamma^i_n]^T \in \mathbb{R}^n$ that solves the matrix equation:

$$\underbrace{\begin{bmatrix} \alpha^1_{1,2} & \alpha^2_{1,2} & \cdots & \alpha^n_{1,2} \\ \alpha^1_{2,3} & \alpha^2_{2,3} & \cdots & \alpha^n_{2,3} \\ \vdots & \vdots & \ddots & \vdots \\ \alpha^1_{n-1,n} & \alpha^2_{n-1,n} & \cdots & \alpha^n_{n-1,n} \end{bmatrix}}_{Mat_\alpha} \underbrace{\begin{bmatrix} \gamma^i_1 \\ \gamma^i_2 \\ \vdots \\ \gamma^i_n \end{bmatrix}}_{\mathbf{Vec^i_\gamma}} = \underbrace{\begin{bmatrix} \beta^i_{1,2} \\ \beta^i_{2,3} \\ \vdots \\ \beta^i_{n-1,n} \end{bmatrix}}_{\mathbf{Vec^i_\beta}}. \tag{4.52}$$

A sufficient condition for all the matrix equations of the form (4.52) (for $i = 1, ..., n$) to admit a solution, is that the matrix $Mat_\alpha \in \mathbb{R}^{(n-1)\times n}$ is full rank. Then the solutions can be computed using the pseudo-inverse of Mat_α: $\mathbf{Vec^i_\gamma} = Mat^T_\alpha (Mat_\alpha Mat^T_\alpha)^{-1} \mathbf{Vec^i_\beta}$, $\forall i = 1, ..., n$. We can show that the existence of the spanning tree in $\mathcal{G}$ directed into vertex n guarantees that Mat_α is full rank. Since each relative position between two agents can be expressed as $\mathbf{r_{i,j}} = \sum_{k=i}^{j-1} \mathbf{r_{k,k+1}}$

if $i < j$, or $\mathbf{r_{i,j}} = -\mathbf{r_{j,i}} = -\sum_{k=j}^{i-1} \mathbf{r_{k,k+1}}$ if $i > j$, $\mathbf{R_{i,N_i}}$ is given for each i by:

$$\begin{aligned}\mathbf{R_{i,N_i}} &= \sum_{j\in N_i} m_j \mathbf{r_{i,j}} = \sum_{j=1}^{n} a_{ij}\mathbf{r_{i,j}} = \sum_{j>i} a_{ij}\mathbf{r_{i,j}} + \sum_{j<i} a_{ij}\mathbf{r_{i,j}} \\ &= \sum_{j=i+1}^{n} a_{ij} \sum_{k=i}^{j-1} \mathbf{r_{k,k+1}} - \sum_{j=1}^{i-1} a_{ij} \sum_{k=j}^{i-1} \mathbf{r_{k,k+1}},\end{aligned}$$

where a_{ij} is the (i,j)-th component of the weighted adjacency matrix $A_{\mathcal{G}}$ ($a_{ij} = m_j$ if j is a neighbor of i, $a_{ij} = 0$ otherwise). Hence the coefficients $\alpha^i_{l,l+1}$, $l = 1, ..., n-1$ such that $\mathbf{R_{i,N_i}} = \sum_{l=1}^{n-1} \alpha^i_{l,l+1}\mathbf{r_{l,l+1}}$, are given by: $\alpha^i_{l,l+1} = -\sum_{k=1}^{l} a_{ik}$ if $l < i$ and $\alpha^i_{l,l+1} = \sum_{k=l+1}^{n} a_{ik}$ if $l \geq i$; therefore the columns of the matrix $Mat_\alpha = [\mathbf{Vec^1_\alpha}\, \mathbf{Vec^2_\alpha} \ldots \mathbf{Vec^{n-1}_\alpha}\, \mathbf{Vec^n_\alpha}]$ have components:

$$\mathbf{Vec^1_\alpha} = \begin{bmatrix} a_{12} + a_{13} + ... + a_{1n} \\ a_{13} + ... + a_{1n} \\ \vdots \\ a_{1n} \end{bmatrix}, \ \mathbf{Vec^2_\alpha} = \begin{bmatrix} -a_{21} \\ a_{23} + ... + a_{2n} \\ \vdots \\ a_{2n} \end{bmatrix},$$

$$\mathbf{Vec^3_\alpha} = \begin{bmatrix} -a_{31} \\ -a_{31} - a_{32} \\ \vdots \\ a_{3n} \end{bmatrix}, \ \ldots, \ \mathbf{Vec^{n-1}_\alpha} = \begin{bmatrix} -a_{(n-1)1} \\ -a_{(n-1)1} - a_{(n-1)2} \\ \vdots \\ a_{(n-1)n} \end{bmatrix},$$

$$\mathbf{Vec^n_\alpha} = \begin{bmatrix} -a_{n1} \\ -a_{n1} - a_{n2} \\ \vdots \\ -a_{n1} - a_{n2} - ... - a_{n(n-1)} \end{bmatrix}. \tag{4.53}$$

We prove that Mat_α is full rank, by showing that the first $n-1$ columns $\mathbf{Vec}_\alpha^{\mathbf{i}}$, $i = 1, ..., n-1$, are linearly independent; to do that, we investigate the determinant of the square matrix $\widehat{Mat}_\alpha = [\mathbf{Vec}_\alpha^{\mathbf{1}}\, \mathbf{Vec}_\alpha^{\mathbf{2}} \ldots \mathbf{Vec}_\alpha^{\mathbf{n-1}}] \in \mathbb{R}^{(n-1)\times(n-1)}$. Exploiting some basic property of the determinant operator, we obtain the following useful expression (where the matrix on the right hand side is obtained by subtracting to each row of $\widehat{Mat}_\alpha$, except the first one, its preceding row):

$$\det(\widehat{Mat}_\alpha) = \det \begin{bmatrix} \sum_{j\neq 1} a_{1j} & -a_{21} & \cdots & -a_{(n-1)1} \\ -a_{12} & \sum_{j\neq 2} a_{2j} & \cdots & -a_{(n-1)2} \\ \vdots & \vdots & \ddots & \vdots \\ -a_{1(n-1)} & -a_{2(n-1)} & \cdots & \sum_{j\neq n-1} a_{(n-1)j} \end{bmatrix}. \tag{4.54}$$

Consider now the matrix $L_{\mathcal{G}}^T \in \mathbb{R}^{n\times n}$, the transpose of the Laplacian of $\mathcal{G}$:

$$L_{\mathcal{G}}^T = \begin{bmatrix} \sum_{j\neq 1} a_{1j} & -a_{21} & \cdots & -a_{(n-1)1} & -a_{n1} \\ -a_{12} & \sum_{j\neq 2} a_{2j} & \cdots & -a_{(n-1)2} & -a_{n2} \\ \vdots & \vdots & \ddots & \vdots & \vdots \\ -a_{1(n-1)} & -a_{2(n-1)} & \cdots & \sum_{j\neq n-1} a_{(n-1)j} & -a_{n(n-1)} \\ -a_{1n} & -a_{2n} & \cdots & -a_{(n-1)n} & \sum_{j\neq n} a_{nj} \end{bmatrix}. \tag{4.55}$$

The matrix in (4.54) is equal to the submatrix of $L_{\mathcal{G}}^T$ obtained by removing its n-th row and n-th column. By one of the properties of the Laplacian listed earlier, the determinant of this submatrix is equal to the sum of the weights of all spanning trees directed into vertex n; since by hypothesis there is at least one such spanning tree, and the weights of spanning trees can only be non-negative (having chosen non-negative weights for the edges), this guarantees that $\det(\widehat{Mat}_\alpha) \neq 0$.

Therefore Mat_α is full rank, which completes the proof. □

Several sufficient conditions for a directed graph to be Hamiltonian (hence traceable, and hence admitting a spanning tree directed into one of its vertices) can be found in the literature of graph theory; here we report a few classical results based on the graph being strongly connected and having "enough edges".

Corollary 4.1.18 (see for example [5] and references therein). *The following conditions are sufficient for a directed graph $\mathcal{G}$ with n vertices to be Hamiltonian (and hence to admit a spanning tree directed into one of its vertices):*
(i) $\mathcal{G}$ is strongly connected and for all non-adjacent vertices a and b (for which neither (a,b) nor (b,a) are edges): $\text{degree}(a)+\text{degree}(b)\geq 2n-1$
(ii) $\mathcal{G}$ is strongly connected and for all pairs of vertices a, b with no edge (a,b): $\text{out-degree}(a) + \text{in-degree}(b) \geq n$
(iii) $\mathcal{G}$ is strongly connected and for each vertex $a \in \mathcal{G}$: $\text{degree}(a)\geq n$.

Figure 4.1 shows examples of sensing networks with five agents that satisfy the conditions of one or more of the theorems presented in this section. The graphs that satisfy the conditions for theorem 4.1.13 are the leftmost ones. All the graphs except the rightmost ones satisfy the conditions of theorem 4.1.15. Finally, all the graphs satisfy the conditions of theorem 4.1.17. Notice that in the upper three graphs, the neighborhoods of each agent are defined by a common rule (e.g. agent i has neighbors $(i+1)$ and $(i-1)$ or $(i+2)$, all modulo n) while in the lower three graphs there is either one agent or a pair of agents playing

the role of "leaders" (they affect the motion of all the others, but they are not affected by any of them).

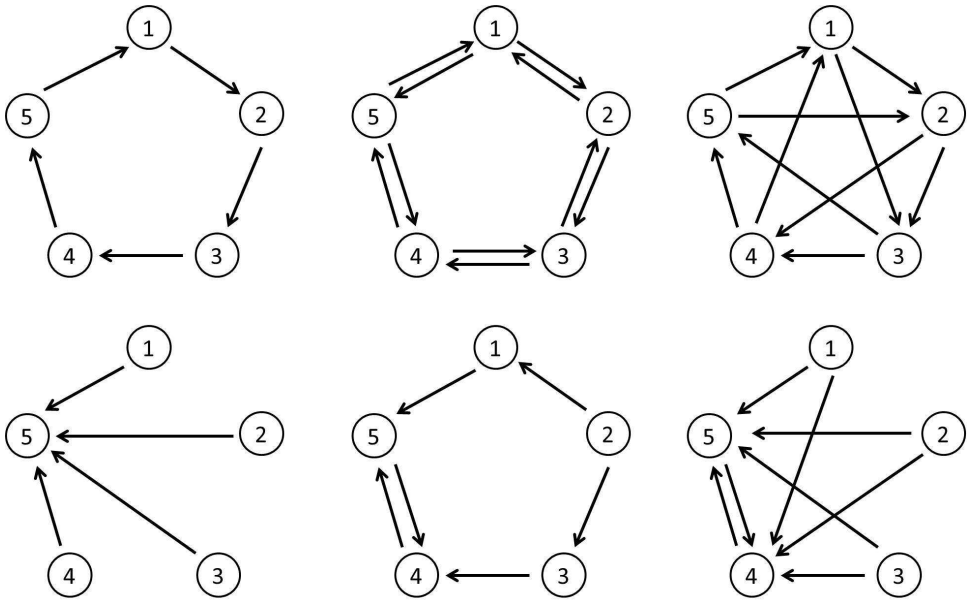

Figure 4.1: Examples of five-agent network graphs that satisfy the hypothesis of theorem 4.1.13 (graphs on the left), theorem 4.1.15 (on the left and center) or theorem 4.1.17 (all the graphs)

4.2 Motions that preserve the coefficient of inertia tensor

4.2.1 Maximization of separation between neighbors

The collective motions that allow to reshuffle the particles (agents) while preserving the coefficient of inertia tensor of the collective, are the democratic motions introduced in section 3.4. As there are many configurations corresponding to a same coefficient of inertia tensor, it can be useful to design democratic

motions that steer the collective towards certain preferred configurations, or at least away from undesirable ones. To each coefficient of inertia tensor, for example, correspond certain configurations in which two or more particles share the same position (thus colliding), the extreme case being given by (3.25) and other similar configurations having $(n-4)$ collisions at the center of mass. Inspired by the consideration that physical artificial collectives (e.g. teams of robots) need to operate away from these configurations, we introduce a democratic motion that maximizes a measure of cumulative distance between neighboring particles, with the objective of spreading the particles apart. We frame the problem as follows.

Problem 4.2.1 (**Maximization of cumulative distance between neighbors)** Given an initial configuration $\mathbf{c_0} \in \mathcal{C}^{3d}$ with coefficient of inertia tensor $K = K(\mathbf{c_0}) \in \mathcal{K}$, design a vector field that preserves K (hence is a democratic motion) and converges to a configuration maximizing the following "reward" function, which is a weighted sum of squares of the distances between neighboring particles (a measure of cumulative distance between neighbors):

$$R(\mathbf{r}) \triangleq \frac{1}{2}\sum_{i=1}^{n}\sum_{j=1}^{n} w_{ij}|\mathbf{r_i} - \mathbf{r_j}|^2 = \frac{1}{2}\sum_{i=1}^{n}\sum_{j=1}^{n} w_{ij}|\mathbf{c_i} - \mathbf{c_j}|^2. \tag{4.56}$$

The fixed weights are chosen to satisfy $w_{ij} \geq 0$, $w_{ii} = 0$, $\forall\, i,j = 1,...,n$. A compact way of expressing (4.56) is:

$$R(\mathbf{c}) = \frac{1}{2}\sum_{i=1}^{n}\sum_{j=1}^{n}(w_{ij}+w_{ji})|\mathbf{c_i}|^2 - \sum_{i=1}^{n}\sum_{j=1}^{n} w_{ij}\mathbf{c_i}^T\mathbf{c_j} = \mathrm{tr}(\mathbf{c}\mathbb{W}\mathbf{c}^T), \tag{4.57}$$

where we have introduced for convenience the "weight matrix" $\mathbb{W}$ (the bolder

script is just to distinguish it from the matrix W introduced before):

$$\mathbb{W} \triangleq \begin{bmatrix} \frac{1}{2}\sum_{j=1}^{n}(w_{1j}+w_{j1}) & -w_{12} & \cdots & -w_{1n} \\ -w_{21} & \frac{1}{2}\sum_{j=1}^{n}(w_{2j}+w_{j2}) & \cdots & -w_{2n} \\ \vdots & \vdots & \ddots & \vdots \\ -w_{n1} & -w_{n2} & \cdots & \frac{1}{2}\sum_{j=1}^{n}(w_{nj}+w_{jn}) \end{bmatrix}. \tag{4.58}$$

In the reward function (4.56), only the weights w_{ij} corresponding to pairs of neighboring particles should be chosen to be nonzero, with the concept of neighborhood defined by some underlying weighted graph $\mathcal{G}_{\mathcal{W}}$ (not necessarily equal to the sensing graph $\mathcal{G}$ introduced before). We will only consider the case of symmetric weights $w_{ij} = w_{ji}\,\forall i, j$, so that the weighted graph $\mathcal{G}_{\mathcal{W}}$ is undirected (while $\mathcal{G}$ is typically directed) and $\mathbb{W}$ is the weighted *Laplacian* of this graph (see definitions in section 4.1.2). Neighbors of an agent could be chosen among those that are physically closest to it *at the initial time*, but, since the weights are not dynamically updated, it is possible that at some later time one or more of the non-neighbors could be closer to an agent than some of its neighbors. Alternatively, one could choose a fixed number of neighbors for each particle, for example defining that particle i has neighbors $i \pm 1$, $i \pm 2$, ... , $i \pm k$, all modulo n, for some $k \leq (n-1)/2$. The nonzero weights w_{ij} could be chosen to be all identical, or proportional to the masses, for example. In general, the matrix $\mathbb{W}$ should be fairly sparse, since we want the democratic motion to take care of the "local" interactions (reshufflings) between particles rather than the "global"

configuration of the collective, which is approximately fixed by K. Note that in the special case of a fully connected graph with weights $w_{ij} = m_i m_j$, then the reward function becomes $R = M \operatorname{tr}(K)$, which is invariant to democratic motions; this highlights that not all the choices of $\mathbb{W}$ are useful, as will also become clear later.

To solve the problem of maximizing the cumulative distance between neighbors, we use the diffeomorphisms (3.29)-(3.30) to design a gradient vector field for R on the Stiefel manifold $\mathcal{V}_{n-1,3}$ diffeomorphic to the fiber $\pi^{-1}(K)$, and then map it to the corresponding vector field on $\pi^{-1}(K)$.

Since each $\mathbf{c} \in \pi^{-1}(K)$ can be expressed as $\mathbf{c} = Q^T \Lambda^{\frac{1}{2}} V^T W^T \mathbb{M}^{-\frac{1}{2}}$ for some $V \in \mathcal{V}_{n-1,3}$ (recall (3.30)), the reward function R restricted to the Stiefel manifold diffeomorphic to $\pi^{-1}(K)$ is:

$$\begin{aligned} R(V) =& \operatorname{tr}(Q^T \Lambda^{\frac{1}{2}} V^T W^T \mathbb{M}^{-\frac{1}{2}} \mathbb{W} \mathbb{M}^{-\frac{1}{2}} W V \Lambda^{\frac{1}{2}} Q) = \operatorname{tr}(\Lambda^{\frac{1}{2}} V^T \mathbb{A} V \Lambda^{\frac{1}{2}}) \\ =& \operatorname{tr}(\Lambda V^T \mathbb{A} V), \end{aligned} \tag{4.59}$$

where $\mathbb{A} \triangleq W^T \mathbb{M}^{-\frac{1}{2}} \mathbb{W} \mathbb{M}^{-\frac{1}{2}} W \in \mathbb{R}^{(n-1)\times(n-1)}$ is symmetric under the assumption that the graph is undirected (so that $\mathbb{W}$ is symmetric). As usual, $K = Q^T \Lambda Q$ is an eigendecomposition of the (constant) coefficient of inertia tensor.

For a given Riemannian metric $\langle ., . \rangle$ on $\mathcal{V}_{n-1,3}$, the gradient of R is defined as the vector field ∇R that satisfies, $\forall V \in \mathcal{V}_{n-1,3},\ \forall \Delta \in T_V \mathcal{V}_{n-1,3}$:

$$\langle \nabla R(V), \Delta \rangle_V = \operatorname{tr}(R_V^T(V)\Delta) = 2 \operatorname{tr}(\Lambda V^T \mathbb{A} \Delta). \tag{4.60}$$

The fact that $R_V(V) = 2\,\mathbb{A}^T V\Lambda$ is shown by the following calculation:

$$(R_V(V))(\Delta) = \left.\frac{d}{dt}\right|_{t=0} R(V + t\Delta) = \left.\frac{d}{dt}\right|_{t=0} \operatorname{tr}(\Lambda(V^T + t\Delta^T)\mathbb{A}(V + t\Delta)) =$$

$$= \operatorname{tr}(\Lambda\Delta^T\mathbb{A}V + \Lambda V^T\mathbb{A}\Delta) = 2\operatorname{tr}(\Lambda V^T\mathbb{A}\Delta) =$$

$$= 2\operatorname{tr}((\mathbb{A}^T V\Lambda)^T\Delta) \quad \forall\Delta \in T_V\mathcal{V}_{n-1,3}.$$

Let us first consider the metric induced on the Stiefel manifold diffeomorphic to $\pi^{-1}(K)$ by the Riemannian metric (3.8) on $\mathcal{C}^{3d}$:

$$\langle\Delta_1, \Delta_2\rangle_V \triangleq \langle df^{-1}_{K,W}(\Delta_1), df^{-1}_{K,W}(\Delta_2)\rangle_{f^{-1}_{K,W}(V)} = \operatorname{tr}(df^{-1}_{K,W}(\Delta_1)\,\mathbb{M}\,df^{-1}_{K,W}(\Delta_2)^T)$$

$$= \operatorname{tr}(Q^T\Lambda^{\frac{1}{2}}\Delta_1^T W^T\mathbb{M}^{-\frac{1}{2}}\mathbb{M}\mathbb{M}^{-\frac{1}{2}}W\Delta_2\Lambda^{\frac{1}{2}}Q) = \operatorname{tr}(\Lambda^{\frac{1}{2}}\Delta_1^T\Delta_2\Lambda^{\frac{1}{2}})$$

$$= \operatorname{tr}(\Lambda\Delta_1^T\Delta_2). \tag{4.61}$$

The gradient vector field with respect to this metric is given by:

$$\nabla R(V) = 2\mathbb{A}^T V - 2V \begin{bmatrix} \tilde{v}_{11} & \frac{2\lambda_1}{\lambda_1+\lambda_2}\tilde{v}_{12} & \frac{2\lambda_1}{\lambda_1+\lambda_3}\tilde{v}_{13} \\ \frac{2\lambda_2}{\lambda_1+\lambda_2}\tilde{v}_{12} & \tilde{v}_{22} & \frac{2\lambda_2}{\lambda_2+\lambda_3}\tilde{v}_{23} \\ \frac{2\lambda_3}{\lambda_1+\lambda_3}\tilde{v}_{13} & \frac{2\lambda_3}{\lambda_2+\lambda_3}\tilde{v}_{23} & \tilde{v}_{33} \end{bmatrix}, \tag{4.62}$$

$$\text{with } \tilde{\mathrm{V}} = \begin{bmatrix} \tilde{v}_{11} & \tilde{v}_{12} & \tilde{v}_{13} \\ \tilde{v}_{12} & \tilde{v}_{22} & \tilde{v}_{23} \\ \tilde{v}_{13} & \tilde{v}_{23} & \tilde{v}_{33} \end{bmatrix} \triangleq \mathrm{V}^{\mathrm{T}}\mathbb{A}\mathrm{V}. \tag{4.63}$$

It is in fact a simple exercise to verify that (4.62) satisfies (4.60) and the condition for being a tangent vector to the Stiefel manifold: $\nabla R(V)^T V = -V^T\nabla R(V)\,\forall V$.

An alternative approach is to consider the canonical metric on the Stiefel manifold, defined in section 2.3, instead of the induced metric (4.61). The corresponding gradient vector field, computed using (2.13), is:

$$\nabla R(V) = R_V(V) - V R_V^T(V) V = 2(\mathbb{A}^T V \Lambda - V \Lambda V^T \mathbb{A} V). \tag{4.64}$$

One advantage of this approach is that, since $\mathbb{A}$ is symmetric and positive semidefinite, (4.64) is equivalent to a vector field used to perform principal component analysis of the covariance matrix of an input process (or any other symmetric positive semidefinite matrix) using neural networks, which was introduced in [55] and further discussed in [15]. In the special case that $V \in SO(3)$, which occurs when there are exactly four particles, (4.64) is also an instance of the *Brockett flow* [12]. Using some of the relevant results, it is possible to prove that, under certain conditions on the weight matrix $\mathbb{W}$, almost all integral curves of (4.64) converge to one of the global maxima of (4.59).

Theorem 4.2.2 (adapted from theorems 5-6 in [55]). *Let the matrix* $\mathbb{A}$ *in the gradient vector field* (4.64) *be symmetric positive definite with eigenpairs* $(a_i, \mathbf{a_i})$, $i = 1, ..., n-1$. *Then the following holds true.*

(i) The equilibria (corresponding to critical points of the gradient) are:

$$V_{eq,p} = [\pm \mathbf{a_{p(1)}} \pm \mathbf{a_{p(2)}} \pm \mathbf{a_{p(3)}}], \tag{4.65}$$

where p *is any permutation of the index set* $\{1, ..., n\}$ *to* $\{p(1), ..., p(n)\}$.

If all the eigenvalues of $\mathbb{A}$ *are distinct, there are* $\frac{n!}{3!(n-3)!}2^3$ *such equilibria.*

(ii) The global maximizers for the reward function are:

$$V_{eq,\tilde{p}} = [\pm \mathbf{a}_{\tilde{\mathbf{p}}(\mathbf{1})} \pm \mathbf{a}_{\tilde{\mathbf{p}}(\mathbf{2})} \pm \mathbf{a}_{\tilde{\mathbf{p}}(\mathbf{3})}], \tag{4.66}$$

where $\tilde{p}$ is any permutation that maximizes the sum $a_{\tilde{p}(1)}\lambda_1 + a_{\tilde{p}(2)}\lambda_2 + a_{\tilde{p}(3)}\lambda_3$. Hence the global maximizers have columns that are eigenvectors associated to the three largest eigenvalues of $\mathbb{A}$, ordered like the elements of Λ (i.e. $\lambda_1, \lambda_2, \lambda_3$, which are the eigenvalues of K) when the latter are organized in a decreasing sequence (e.g. if $\lambda_1 \geq \lambda_3 \geq \lambda_2$, then it must be $a_{\tilde{p}(1)} \geq a_{\tilde{p}(3)} \geq a_{\tilde{p}(2)}$). If all the eigenvalues of $\mathbb{A}$ are distinct and all the eigenvalues of K are distinct, there are only 2^3 such global maxima.

(iii) The reward function has no local maximizers. The only stable equilibria are those corresponding to the global maximizers $V_{eq,\tilde{p}}$.

(iv) All the integral curves of (4.64), excluding those starting in the stable manifold of one of the saddle point equilibria, converge to one of the maximizers $V_{eq,\tilde{p}}$.

Sketch of the proof. (i) Let Q_A be a matrix whose columns are eigenvectors of $\mathbb{A}$, and let Λ_A be the corresponding diagonal matrix of eigenvalues, so that $\mathbb{A} = Q_A \Lambda_A Q_A^T$. Let the singular value decomposition of a generic $V \in \mathcal{V}_{n-1,3}$ be: $V = \Psi D R^T$, where $\Psi \in O(n-1)$, $R \in O(3)$ and $D = [D_1 \,|\, \mathbb{O}]^T \in \mathbb{R}^{(n-1)\times 3}$ with $D_1 \in \mathbb{R}^{3\times 3}$ diagonal and positive definite. Let the corresponding singular value decomposition of $\mathbb{A}^{-1}V$ be: $\mathbb{A}^{-1}V = \Psi' D' R'^T$, where $\Psi' \in O(n-1)$, $R' \in O(3)$ and $D' = [D_1' \,|\, \mathbb{O}]^T \in \mathbb{R}^{(n-1)\times 3}$ with $D_1' \in \mathbb{R}^{3\times 3}$ diagonal and positive definite. Comparing the two singular value decompositions, it must be: $R = R'$, $D = P\Lambda_A P^T D'$ and $\Psi = \Psi' = Q_A P^T$ for some permutation matrix P. Therefore

every $V \in \mathcal{V}_{n-1,3}$ can be written as: $V = Q_A P^T D R^T$. Critical points of the reward function must satisfy $\nabla R(V) = 0$ and hence $\mathbb{A}V\Lambda = V\Lambda V^T \mathbb{A}V$. Plugging the decompositions $V = Q_A P^T D R^T$ and $\mathbb{A} = Q_A \Lambda_A Q_A^T$ into this equality, yields that R must be equal to the identity matrix, and the components of D_1 must be all equal ± 1. Hence the critical points are all given by: $V_{eq,p} = Q_A P^T D$, with $D = [D_1 \,|\, \mathbb{0}]^T$ satisfying $D_1^3 = \mathbb{1}$. This is just a compact way of expressing (4.65).

(ii) The value of the reward function at each equilibrium is:

$R(V_{eq,p}) = \mathrm{tr}(\Lambda V_{eq,p}^T \mathbb{A} V_{eq,p}) = \mathrm{tr}(\Lambda D P \Lambda_A P^T D) = \lambda_1 a_{p(1)} + \lambda_2 a_{p(2)} + \lambda_3 a_{p(3)}$. Hence the global maximizers are the equilibria that maximize this sum.

(iii) Let $V_{eq,p}$ be a critical point for the reward function, that is not a global maximizer. Then there exists at least one of the columns of $V_{eq,p}$, say the j-th column $\pm \mathbf{a_{p(j)}}$ ($j \in \{1,2,3\}$), that is different from $\pm \mathbf{a_{\tilde{p}(j)}}$. Consider the following perturbation about $V_{eq,p}$ and the corresponding perturbed value of the reward function:

$$V_{eq,p}^{\epsilon} = \frac{\pm \mathbf{a_{p(j)}} + \epsilon\, \mathbf{a_{\tilde{p}(j)}}}{\sqrt{1+\epsilon^2}},\; R(V_{eq,p}^{\epsilon}) = R(V_{eq,p}) + \frac{1}{1+\epsilon^2}(\lambda_j a_{\tilde{p}(j)} - \lambda_j a_{p(j)}).$$

Clearly $R(V_{eq,p}^{\epsilon}) > R(V_{eq,p})$ no matter how small we take ϵ. Hence the critical point $V_{eq,p}$ cannot be a local maximizer, but can at most be a saddle point equilibrium.

(iv) Observe that the reward function increases monotonically along solutions of

(4.64):

$$\frac{d}{dt}R(V(t)) = \frac{d}{dt}\mathrm{tr}(\Lambda V^T(t)\mathbb{A}V(t)) = 2\,\mathrm{tr}(\Lambda V^T(t)\mathbb{A}\dot{V}(t))$$
$$= 2\,\mathrm{tr}(\Lambda V^T(t)\mathbb{A}\nabla R(V(t))) = \langle \nabla R(V(t)), \nabla R(V(t))\rangle_{V(t)} \geq 0\ \forall t,$$

with $\frac{d}{dt}R(V(t)) = 0 \Leftrightarrow \nabla R(V(t)) = 0$. Hence a typical integral curve will eventually converge to one of the maximizers of the reward function, given by (4.66). The only exceptions are the integral curves starting on the stable manifold of one of the saddle point equilibria, which converge to the corresponding saddle point. □

The following theorem specializes these results to the case in which $\mathbb{A} = W^T\mathbb{M}^{-\frac{1}{2}}\mathbb{W}\mathbb{M}^{-\frac{1}{2}}W$.

Theorem 4.2.3. *If* $\mathbb{W}$ *is the Laplacian of a* **connected** *weighted undirected graph, then almost all the integral curves of the gradient vector field* (4.64) *converge to one of the global maxima of the reward function* (4.59)*, given by:*

$$V_{eq,\tilde{p}} = [\pm W^T\mathbf{e}_{\tilde{\mathbf{p}}(\mathbf{1})} \pm W^T\mathbf{e}_{\tilde{\mathbf{p}}(\mathbf{2})} \pm W^T\mathbf{e}_{\tilde{\mathbf{p}}(\mathbf{3})}], \tag{4.67}$$

where $(\mu_i, \mathbf{e_i})$*,* $i = 1, ..., n-1$*, are eigenpairs of* $\mathbb{M}^{-\frac{1}{2}}\mathbb{W}\mathbb{M}^{-\frac{1}{2}}$ *with* $\mu_i > 0$*, and* $\tilde{p}$ *is any permutation that maximizes* $\mu_{\tilde{p}(1)}\lambda_1 + \mu_{\tilde{p}(2)}\lambda_2 + \mu_{\tilde{p}(3)}\lambda_3$*.*

Proof. From the properties of Laplacians for weighted undirected graphs with non-negative weights, described in section 4.1.2, $\mathbb{W}$ is positive semidefinite; moreover, if the graph $\mathcal{G}_{\mathcal{W}}$ is connected, $\mathbb{W}$ has exactly $n-1$ eigenvalues in the open right half plane, and so does the matrix $\mathbb{M}^{-\frac{1}{2}}\mathbb{W}\mathbb{M}^{-\frac{1}{2}}$. It is easy to prove that for

each of the eigenpairs $(\mu_i, \mathbf{e_i})$ of $\mathbb{M}^{-\frac{1}{2}}\mathbb{W}\mathbb{M}^{-\frac{1}{2}}$ with $\mu_i > 0$, there is an associated eigenpair $(\mu_i, W^T\mathbf{e_i})$ for $\mathbb{A}$:

$$\begin{aligned}\mathbb{A}W^T\mathbf{e_i} =& W^T\mathbb{M}^{-\frac{1}{2}}\mathbb{W}\mathbb{M}^{-\frac{1}{2}}WW^T\mathbf{e_i} = \\ =& W^T\mathbb{M}^{-\frac{1}{2}}\mathbb{W}\mathbb{M}^{-\frac{1}{2}}(\mathbb{1} - [\sqrt{m_1}\cdots\sqrt{m_n}]^T[\sqrt{m_1}\cdots\sqrt{m_n}]/M)\mathbf{e_i} = \\ =& W^T\mathbb{M}^{-\frac{1}{2}}\mathbb{W}\mathbb{M}^{-\frac{1}{2}}\mathbf{e_i} = \mu_i W^T\mathbf{e_i}.\end{aligned}$$

Here we used (3.37) and the fact that $\mathbb{W}[1...1]^T = \mathbf{0}$. Notice that the other eigenpair $(0, \mathbb{M}^{\frac{1}{2}}[1...1]^T/\sqrt{M})$ of $\mathbb{M}^{-\frac{1}{2}}\mathbb{W}\mathbb{M}^{-\frac{1}{2}}$ does not yield a corresponding eigenpair of $\mathbb{A}$ because $W^T\mathbb{M}^{\frac{1}{2}}[1...1]^T/\sqrt{M} = \mathbf{0}$ (by construction of W). The fact that $|W^T\mathbf{e_i}| = |\mathbf{e_i}| = 1\ \forall i$ follows from the properties of W. Hence the hypothesis of the theorem are sufficient for the matrix $\mathbb{A}$ to be symmetric positive definite with eigenpairs $(a_i, \mathbf{a_i}) = (\mu_i, W^T\mathbf{e_i})$, $i = 1, ..., n-1$. The result then follows from theorem 4.2.2. □

When the conditions of theorem 4.2.3 are satisfied, the gradient vector field on the Stiefel manifold (4.64) accomplishes the objective of maximizing the reward function R. Under the same conditions, the vertical vector field on $\mathcal{C}^{3d}$ obtained by the mapping $df^{-1}_{K,W}$ (3.40) applied to (4.64), maximizes R while

preserving K:

$$\begin{aligned}
\mathbf{X_c} =& df_{K,W}^{-1}(\nabla R(V)) = Q^T\Lambda^{\frac{1}{2}}(\nabla R(V))^T W^T\mathbb{M}^{-\frac{1}{2}} = \\
=& 2Q^T\Lambda^{\frac{1}{2}}(\mathbb{A}^T V\Lambda - V\Lambda V^T\mathbb{A}V)^T W^T\mathbb{M}^{-\frac{1}{2}} = \\
=& 2Q^T(\Lambda Q\mathbf{c}\mathbb{M}^{\frac{1}{2}}W\mathbb{A} - Q\mathbf{c}\mathbb{M}^{\frac{1}{2}}W\mathbb{A}W^T\mathbb{M}^{\frac{1}{2}}\mathbf{c}^T\mathbf{c}\mathbb{M}^{\frac{1}{2}}W)W^T\mathbb{M}^{-\frac{1}{2}} = \\
=& 2K\mathbf{c}\mathbb{W}\mathbb{M}^{-\frac{1}{2}}WW^T\mathbb{M}^{-\frac{1}{2}} - 2\mathbf{c}\mathbb{W}\mathbf{c}^T\mathbf{c} = \\
=& 2K\mathbf{c}\mathbb{W}\mathbb{M}\mathbb{M}^{-1} - 2\mathbf{c}\mathbb{W}\mathbf{c}^T\mathbf{c} \quad \forall \mathbf{c} \in \mathcal{C}^{3d}.
\end{aligned} \tag{4.68}$$

The vector field (4.68) converges to one of the configurations corresponding to $\mathbf{c_{eq,\tilde{p}}} \triangleq f_{K,W}^{-1}(V_{eq,\tilde{p}})$, given by:

$$\mathbf{c_{eq,\tilde{p}}} = Q^T\Lambda^{\frac{1}{2}} \begin{bmatrix} \pm\mathbf{e_{\tilde{p}(1)}}^T \\ \pm\mathbf{e_{\tilde{p}(2)}}^T \\ \pm\mathbf{e_{\tilde{p}(3)}}^T \end{bmatrix} \left(\mathbb{M}^{-\frac{1}{2}} - \frac{1}{M} \begin{bmatrix} \sqrt{m_1} & \cdots & \sqrt{m_1} \\ \vdots & \cdots & \vdots \\ \sqrt{m_n} & \cdots & \sqrt{m_n} \end{bmatrix} \right). \tag{4.69}$$

Notice that in the derivation of (4.68) and (4.69), we have used the fact that $WW^T\mathbb{M}^{-\frac{1}{2}} = \mathbb{M}^{-\frac{1}{2}} - [\sqrt{m_1}...\sqrt{m_n}]^T[1...1]/M$ (cfg. (3.37)) and therefore $\mathbf{c}\mathbb{M}^{\frac{1}{2}}WW^T\mathbb{M}^{-\frac{1}{2}} = \mathbf{c}$, $\mathbb{W}\mathbb{M}^{-\frac{1}{2}}WW^T\mathbb{M}^{-\frac{1}{2}} = \mathbb{W}\mathbb{M}^{-1}$.

Remark 4.2.4 Maximization of the reward function (4.56) does not guarantee collision avoidance between every pair of particles. On the other hand, for any choice of the weight matrix $\mathbb{W}$, it is possible to use (4.69) to verify if the resulting particle distributions are collision-free. Different choices of $\mathbb{W}$ produce different results, sometimes surprising. For example, consider a unit-weighted graph $\mathcal{G}_{\mathcal{W}}$ in which each particle i has neighbors $i \pm 1$, $i \pm 2$, ... , $i \pm (n/2 - 1)$, all modulo n. If the number of particles (n) is even, this corresponds to maximizing the

cumulative distance of each particle i from all other particles except one (particle $i + n/2$, modulo n). Simulations show that in this case, if all the masses are equal, the resulting configurations $\mathbf{c}_{\mathbf{eq},\tilde{\mathbf{p}}}$ have exactly n collisions: $\forall i = 1, ..., n$, particles i and $i + n/2$ (modulo n) end up sharing the same position. Conversely, if the number of particles is odd, the same graph corresponds to maximizing the cumulative distance of each particle i from all other particles except two (particles $i + (n \pm 1)/2$, modulo n) and the resulting configurations are not only collision-free but also produce a nice chain-like distribution of particles. Hence this choice of $\mathbb{W}$ can produce positive or negative results (for collision-avoidance considerations) depending on the number of particles. A choice of unit-weighted graph that produces collision-free and interesting distributions of particles, is the Hamiltonian cycle obtained by choosing the neighbors of each particle i to be given by particles $i+1$ and $i-1$, modulo n. If there is an odd number of particles, and the masses are equal, this choice produces a nice chain-like distribution of particles. Conversely, if n is even, the particles split into two groups, each having $n/2$ particles distributed along circles of same radii and symmetrically located with respect to the center of mass. Figure 4.2 shows examples of these interesting particle distributions.

Remark 4.2.5 It is interesting to compare (4.68) with the gradient vector field of the reward function R on $\mathcal{C}^{3d}$ that would have been obtained if the requirement

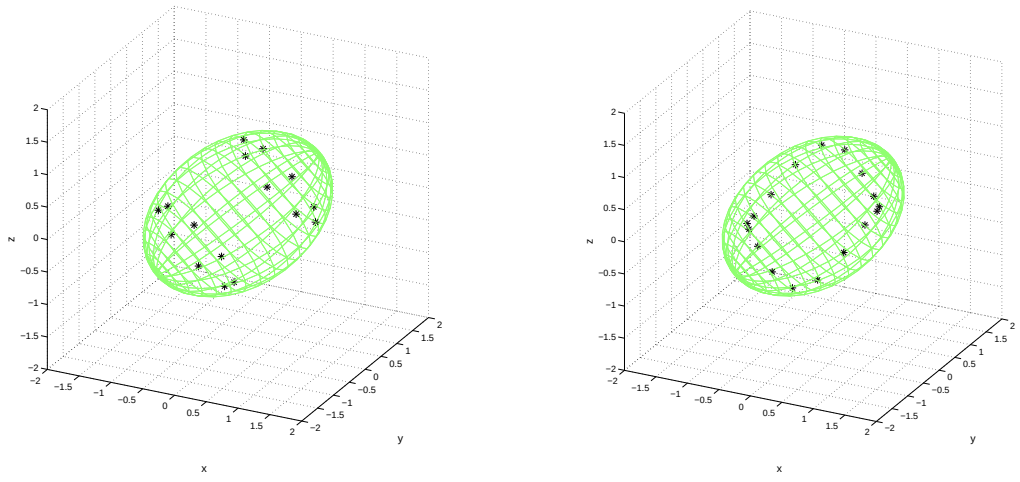

(a) (b)

Figure 4.2: Examples of particle distributions obtained with an Hamiltonian cycle: (a) n=16 particles; (b) n=17 particles.

of preserving K was not enforced. To compute the latter, observe that:

$$(\nabla R(\mathbf{c}))(\mathbf{v_c}) = \frac{d}{dt} R(\mathbf{c} + t\mathbf{v_c})\Big|_{t=0} = \frac{d}{dt} \mathrm{tr}((\mathbf{c} + t\mathbf{v_c})\mathbb{W}(\mathbf{c} + t\mathbf{v_c})^T)\Big|_{t=0} =$$

$$= \mathrm{tr}(\mathbf{v_c}\mathbb{W}\mathbf{c}^T + \mathbf{c}\mathbb{W}\mathbf{v_c}^T) \quad \forall \mathbf{v_c} \in T_{\mathbf{c}}\mathcal{C}^{3d}.$$

When $\mathbb{W}$ is symmetric, then $(\nabla R(\mathbf{c}))(\mathbf{v_c}) = \mathrm{tr}(2\mathbf{c}\mathbb{W}\mathbf{v_c}^T)$ $\forall \mathbf{v_c} \in T_{\mathbf{c}}\mathcal{C}^{3d}$ and therefore the gradient vector field is $\nabla R(\mathbf{c}) = 2\mathbf{c}\mathbb{W}$, similar to the first component of (4.68). An important difference between the two vector fields is that $\nabla R(\mathbf{c})$ has a decentralized nature, since the tangent vectors associated to each particle are in the form $\mathbf{v_{ci}} = \nabla R_{\mathbf{i}}(\mathbf{c}) = 2\sum_{j=1}^{n} w_{ij}(\mathbf{c_i} - \mathbf{c_j})$, which depend only on the relative position of the particle from its neighbors. Conversely in (4.68) each tangent vector $\mathbf{v_{ci}}$ depends on the configuration of all the other particles, making nontrivial the distributed implementation of these democratic motions.

4.3 Application to distributed sensing

A potential application for these ideas is in the context of distributed sensing of spatial physical variables. Assume we have autonomous robotic agents that have access to noisy measurements of a spatial physical variable of interest, such as the position of a landmark (e.g. a point source of sound, light or chemical pollutant). By merging their measurements, the agents can obtain a joint estimate of the landmark position that is better than that obtainable by each agent alone.

After the estimate is computed, it might be useful for the agents to distribute in space in such a way that their center of mass corresponds to the estimated position of the landmark, and their coefficient of inertia tensor with respect to the center of mass corresponds to the covariance matrix of the estimate. One motivation for the robotic agents to distribute in this way could be to smartly reposition themselves before taking further measurements. Another motivation could be to "communicate" the sensed information on the landmark position (its estimate and the covariance of such estimate) to an external "supervisor", located away from the landmark, without the need of an actual communication line. If in fact the supervisor could track the positions of the robotic agents (e.g. visually), then it would just need to compute the corresponding center of mass and coefficient of inertia tensor to reconstruct the estimated position of the landmark, and the covariance of such estimate (useful to evaluate the confidence in the estimate).

In addition to being robust to unavailability or unreliability of a communi-

cation line between the robotic agents and the supervisor, this approach has the advantage that the robotic agents can save the battery power (typically one of the operational bottlenecks for autonomous robots) that would otherwise be needed for establishing and maintaining a communication line with the supervisor. In a typical scenario, the robotic agents would still need to maintain a communication network to exchange information among themselves (to estimate the spatial variable, for example by jointly implementing a maximum likelihood estimator, and to coordinate their motion), but these short-range communications would be less power-demanding than any long-range communication with a supervisor.

After completing the estimate, the robots would need to collectively move to the correct positions, so that their center of mass matches the estimated landmark position, and their coefficient of inertia tensor matches the covariance of the estimate. The required collective motion is a composition of rigid translation and inertia tensor transformation; the results of section 4.1.1 provide a recipe for accomplishing the latter task in the most energy-efficient way.

Once the robots are in the correct position, then the vector field described in section 4.2 would provide a method for taking care of another potentially important task, such as spreading the robots apart, while still achieving the main task of relaying the landmark position information to the supervisor.

The following algorithm suggests a concrete implementation of these ideas when the agents can locally exchange information with some of their neighbors, defined by an underlying *communication network graph* $\mathcal{G}_{\mathcal{C}}$; the latter should not

be confused with the sensing network $\mathcal{G}$ defined in section 4.1.2 for distributed implementation of inertia tensor transformations.

Algorithm 4.1

1. Each agent computes a "global" estimate $\hat{\mathbf{p}} \in \mathbb{R}^3$ for the landmark position $\mathbf{p} \in \mathbb{R}^3$, and the corresponding estimate covariance $W_{\hat{p}} \in \mathbb{R}^{3\times 3}_{sym,>0}$, based on all of the agents measurements; this must be accomplished by each agent using only local exchange of information with its neighbors (as defined by the communication network $\mathcal{G}_{\mathcal{C}}$).

2. Using only local exchange of information, each agent computes the current relative position of the center of mass of the collective with respect to the estimated landmark position (i.e. $\hat{\mathbf{p}} - \mathbf{r_{com}}(0)$)), and the current coefficient of inertia tensor of the collective ($K(0)$).

3. The agents jointly implement in decentralized fashion the following collective motion, which yields $\mathbf{r_{com}}(T) = \hat{\mathbf{p}}$ and $K(T) = W_{\hat{p}}$ at a suitable fixed time T:

$$\dot{\mathbf{r}}(t) = [\dot{\mathbf{r}}_{\mathbf{1}}(t) \ ... \ \dot{\mathbf{r}}_{\mathbf{n}}(t)] = [\dot{\mathbf{r}}_{\mathbf{com}}(t) \ ... \ \dot{\mathbf{r}}_{\mathbf{com}}(t)] + S(t)[\mathbf{c}_{\mathbf{1}}(t) \ ... \ \mathbf{c}_{\mathbf{n}}(t)]; \quad (4.70)$$

where $\dot{\mathbf{r}}_{\mathbf{com}}(t) = \frac{1}{T}(\hat{\mathbf{p}} - \mathbf{r_{com}}(0))\, \forall t \in [0, T]$ produces the desired rigid translation of the collective, and $S(t) = ((W_{\hat{p}}K(0))^{-\frac{1}{2}}W_{\hat{p}} - \mathbb{1})((T-t)\mathbb{1} + t(W_{\hat{p}}K(0))^{-\frac{1}{2}}W_{\hat{p}})^{-1}\, \forall t \in [0, T]$ produces the optimal inertia tensor transformation, as prescribed by (4.35), when $K_0 = K(0)$ and $K_1 = W_{\hat{p}}$. Assume it is feasible to establish a sensing network $\mathcal{G}$ that, possibly (but not

necessarily) relying on the underlying communication network $\mathcal{G}_{\mathcal{C}}$, satisfies the conditions for one of the theorems of section 4.1.1, for example theorem 4.1.17. Then (4.70) can be implemented in distributed fashion by each agent controlling its relative motion with respect to the center of mass of its "sensing" neighborhood according to $\dot{\mathbf{r}}_{\mathbf{i},\mathbf{com_i}}(t) = S(t)\mathbf{r}_{\mathbf{i},\mathbf{com_i}}(t)$, while at the same time adding to its velocity a constant "drift" given by $\frac{1}{T}(\hat{\mathbf{p}} - \mathbf{r}_{\mathbf{com}}(0))$. Notice that this drift is common to each agent, hence it does not affect the relative motion between agents.

4. (Optional) The agents jointly implement some useful democratic motion, for example (4.68) with appropriate choice of $\mathbb{W}$, to spread themselves apart without affecting the center of mass and coefficient of inertia tensor of the formation.

5. Repeat from 1.

The first step of the algorithm requires the agents to combine their local measurements of the physical spatial variable $\mathbf{p}$, to jointly compute an estimate $\hat{\mathbf{p}}$ (for example the maximum likelihood estimate given all the individual measurements) and the corresponding covariance $W_{\hat{p}}$. Similarly, the second step requires the agents to share some of their locally sensed data, e.g. their relative positions with respect to the neighbors and to the estimated landmark position, to jointly compute some global quantity of the collective, such as the relative position of the center of mass with respect to the landmark and the coefficient of inertia tensor

with respect to the center of mass. These are "data-fusion" problems that can be solved, for example, using variants of the so-called *consensus dynamics*. In the remainder of this section, we recall some results on consensus dynamics in continuous time that are simply based on the properties of the Laplacian matrix of a weighted directed graph, already introduced in section 4.1.2. These simple results, along with discrete-time versions of consensus dynamics and more complex results that include dynamically changing graphs and asynchronous peer-to-peer communication, can be found in the literature (see for example [6], [29] and [36]). We will then describe how to use consensus dynamics to solve the data-fusion problems in algorithm 4.1.

Let us first consider scalar consensus dynamics. For each agent i, let $x_i(t)$ be a scalar variable of interest, that is initialized at a value $x_i(0)$ and then updated in time according to the following dynamical rules:

$$\dot{x}_i(t) = -\sum_{j=1}^{n} a_{ij}(x_i(t) - x_j(t)), \tag{4.71}$$

where $a_{ij} > 0$ if $j \in N_i$ (j is a neighbor of i in the communication graph $\mathcal{G}_\mathcal{C}$), and $a_{ij} = 0$ otherwise. The values $x_j(t)$, $\forall j \in N_i$, are assumed to be known to agent i via local communication with its neighbors.

All the equations of the type (4.71), $\forall i = 1, ..., n$, are coupled to each other in such a way that if we define a vector $\mathbf{x} \triangleq [x_1\, x_2 \,...\, x_n]^T \in \mathbb{R}^n$, then its evolution satisfies:

$$\dot{\mathbf{x}}(t) = -L_{\mathcal{G}_\mathcal{C}}\mathbf{x}(t), \tag{4.72}$$

where $L_{\mathcal{G}_\mathcal{C}}$ is the Laplacian of the communication graph.

Since the weights a_{ij}, corresponding to the elements of the weighted adjacency matrix, are non-negative, $L_{\mathcal{G}_\mathcal{C}}$ has all eigenvalues on the right half plane, with the zero eigenvalue being unique if and only if there is a spanning tree directed into one of the vertices of $\mathcal{G}_\mathcal{C}$. If such a spanning tree exists, the eigenspace associated to the zero eigenvalue is given by $\alpha[1\,1\,...\,1]^T$, $\alpha \in \mathbb{R}$, and corresponds to an attracting equilibrium subspace for the dynamics (4.72). This means that the individual variables $x_i(t)$, $\forall i$, will converge asymptotically to a common "consensus" value, in general depending on the initial values $x_i(0)$, $i = 1, ..., n$. For this reason, the coupled dynamics (4.72) induced by local update rules (4.71), are referred to as "consensus dynamics".

If there is a vertex (say k) that has out-degree zero in the communication graph (i.e. it does not communicate with anybody else), then $x_k(t) = x_k(0)\,\forall t$, and the consensus value achieved by all agents must be $x_k(0)$.

If the communication graph $\mathcal{G}_\mathcal{C}$ is undirected and connected, with unit weights ($a_{ij} = 1\,\forall j \in N_i$), then the consensus value is equal to the average of the initial conditions: $\frac{1}{n}\sum_{i=1}^{n} x_i(0)$. To see this, observe that under these conditions the sum $\sum_{i=1}^{n} x_i(t)$ is a conserved quantity of the system:

$$\frac{d}{dt}\left(\sum_{i=1}^{n} x_i(t)\right) = \frac{d}{dt}\left([1\,1\,...\,1]\mathbf{x}(t)\right) = -[1\,1\,...\,1]L_{\mathcal{G}_\mathcal{C}}\mathbf{x}(t) = 0.$$

In this case, we refer to the coupled dynamics (4.72) as "average consensus dynamics".

Similar results apply to vector consensus dynamics, which arise when each

agent i has a vector of interest $\mathbf{x_i}(t) \in \mathbb{R}^m$ which is updated according to a rule equivalent to (4.71):

$$\dot{\mathbf{x}}_\mathbf{i}(t) = -\sum_{j=1}^{n} a_{ij}(\mathbf{x_i}(t) - \mathbf{x_j}(t)). \tag{4.73}$$

If we define a long vector $\mathbf{x} \triangleq [\mathbf{x_1}^T \mathbf{x_2}^T ... \mathbf{x_n}^T]^T \in \mathbb{R}^{nm}$, then its evolution satisfies:

$$\dot{\mathbf{x}}(t) = (-L_{\mathcal{G}_\mathcal{C}} \otimes \mathbb{1})\mathbf{x}(t), \tag{4.74}$$

where $\otimes$ is the Kronecker product, and $\mathbb{1}$ is the m-dimensional identity matrix. As in the scalar case, consensus is achieved asymptotically if the communication graph admits a spanning tree directed towards one of its vertices; average consensus is achieved if the graph is undirected, connected and has unit weights.

Finally, matrix consensus dynamics, which arise when each agent updates a matrix of interest $M_i(t) \in \mathbb{R}^{m \times n}$ according to:

$$\dot{M}_i(t) = -\sum_{j=1}^{n} a_{ij}(M_i(t) - M_j(t)), \tag{4.75}$$

can be thought of as n vector consensus dynamics of the type (4.73)-(4.74) by considering each column of the matrix separately.

We can show that, under certain assumptions, all the data-fusion problems in algorithm 4.1 can be solved using some kind of consensus dynamics.

Problem 4.3.1 (**Distributed estimation of a physical spatial variable** $\mathbf{p} \in \mathbb{R}^3$**)** Assume that each agent i has access to a noisy measurement $\mathbf{z_i}$ of the physical variable $\mathbf{p}$, with additive noise having multivariate Gaussian distribution with zero mean and covariance W_i, i.e. $\mathbf{z_i} \sim \mathcal{N}(\mathbf{p}, W_i)$. Also assume that

the noises affecting the agents are statistically independent of each other and of $\mathbf{p}$. Then the maximum likelihood estimate of $\mathbf{p}$ given a set of measurements $\mathbf{z_1}, \mathbf{z_2}, ..., \mathbf{z_n}$ is:

$$\hat{\mathbf{p}}(\mathbf{z_1}, \mathbf{z_2}, ..., \mathbf{z_n}) = \left(\sum_{i=1}^{n} W_i^{-1} \right)^{-1} \left(\sum_{i=1}^{n} W_i^{-1} \mathbf{z_i} \right). \tag{4.76}$$

Under the given assumptions, (4.76) is also the least square estimate of $\mathbf{p}$, i.e. $\hat{\mathbf{p}}(\mathbf{z_1}, \mathbf{z_2}, ..., \mathbf{z_n})$ minimizes $\mathbb{E}_{\mathbf{p}|\mathbf{z_1},\mathbf{z_2},...,\mathbf{z_n}}(\hat{\mathbf{p}}(\mathbf{z_1}, \mathbf{z_2}, ..., \mathbf{z_n}) - \mathbf{p})^2$. The estimate (4.76) is unbiased, in the sense that if $\mathbf{p}$ is the actual value of the variable, then $\mathbb{E}_{\mathbf{z_1},\mathbf{z_2},...,\mathbf{z_n}|\mathbf{p}} \hat{\mathbf{p}}(\mathbf{z_1}, \mathbf{z_2}, ..., \mathbf{z_n}) = \mathbf{p}$; the covariance of the estimate, defined as $W_{\hat{p}} \triangleq \mathbb{E}_{\mathbf{z_1},\mathbf{z_2},...,\mathbf{z_n}|\mathbf{p}}[(\hat{\mathbf{p}}(\mathbf{z_1}, \mathbf{z_2}, ..., \mathbf{z_n}) - \mathbf{p})(\hat{\mathbf{p}}(\mathbf{z_1}, \mathbf{z_2}, ..., \mathbf{z_n}) - \mathbf{p})^T]$, is instead given by:

$$W_{\hat{p}} = \left(\sum_{i=1}^{n} W_i^{-1} \right)^{-1}. \tag{4.77}$$

Notice that the maximum likelihood estimate of $\mathbf{p}$ that an agent could compute using only its own measurement, would be $\hat{\mathbf{p}}_\mathbf{i}(\mathbf{z_i}) = \mathbf{z_i}$ and would have covariance equal to W_i; clearly the "global" estimator (4.76) performs better than any of the individual estimators.

If the communication graph is undirected, connected and has unit weights, the following vector consensus dynamics introduced in [49] allow each agent i to obtain asymptotically the estimate (4.76) by exchanging information only with its neighbors:

$$\dot{\mathbf{x}}_\mathbf{i}(t) = -W_i \sum_{j \in N_i} (\mathbf{x_i}(t) - \mathbf{x_j}(t)) \tag{4.78}$$

$$\mathbf{x_i}(0) = \mathbf{z_i}. \tag{4.79}$$

The only difference between (4.78) and the update rule (4.73) for the standard vector consensus dynamics is the presence of the positive definite matrix W_i; it is easy to see that this does not affect the asymptotic achievement of consensus, but only the value at which consensus is achieved, which is now:

$$\lim_{t\to\infty} \mathbf{x_i}(t) = \left(\sum_{i=1}^{n} W_i^{-1}\right)^{-1} \left(\sum_{i=1}^{n} W_i^{-1}\mathbf{x_i}(0)\right) = \hat{\mathbf{p}}(\mathbf{z_1}, \mathbf{z_2}, ..., \mathbf{z_n}) \ \ \forall i. \tag{4.80}$$

This follows from the fact that $\sum_{i=1}^{n} W_i^{-1}\mathbf{x_i}(t)$ is a conserved quantity of the coupled dynamics given by (4.78), for $i = 1, ..., n$.

Under the same hypothesis on the communication graph, the covariance of the estimator (4.77) can be asymptotically computed using the following matrix average consensus dynamics (adapted from [49]):

$$\dot{M}_i(t) = -\sum_{j\in N_i} (M_i(t) - M_j(t)) \tag{4.81}$$

$$M_i(0) = nW_i^{-1}, \tag{4.82}$$

which converge asymptotically to the inverse of the desired $W_{\hat{p}}$:

$$\lim_{t\to\infty} M_i(t) = \frac{1}{n}\sum_{i=1}^{n} M_i(0) = \sum_{i=1}^{n} W_i^{-1} = W_{\hat{p}}^{-1} \ \ \forall i. \tag{4.83}$$

Problem 4.3.2 (Distributed computation of $\hat{\mathbf{p}} - \mathbf{r_{com}}$) In the implementation of algorithm 4.1, each agent needs to know the relative position of the center of mass of the collective with respect to the estimated position $\hat{\mathbf{p}}$ of the landmark. Since the center of mass depends on the positions of all the agents, individual agents might not have direct access to this variable; instead, they might only have access to their own relative position $\mathbf{r_i} - \hat{\mathbf{p}}$. Assuming that the positions of

the center of mass and of the landmark are constant, each agent could asymptotically compute the required $\mathbf{r_{com}} - \hat{\mathbf{p}}$ through the following average consensus dynamics:

$$\dot{\mathbf{x}}_\mathbf{i}(t) = -\sum_{j \in N_i} (\mathbf{x_i}(t) - \mathbf{x_j}(t)) \tag{4.84}$$

$$\mathbf{x_i}(0) = n\frac{m_i}{M}(\mathbf{r_i} - \hat{\mathbf{p}}), \tag{4.85}$$

where $M = \sum_{i=1}^{n} m_i$. Under the usual assumptions on the communication graph (undirectedness, connectedness and unit weights), the dynamics induced by (4.84) converge asymptotically to the desired vector $\mathbf{r_{com}} - \hat{\mathbf{p}}$:

$$\lim_{t\to\infty} \mathbf{x_i}(t) = \frac{1}{n}\sum_{i=1}^{n} n\frac{m_i}{M}(\mathbf{r_i} - \hat{\mathbf{p}}) = \frac{1}{M}\left(\sum_{i=1}^{n} m_i \mathbf{r_i} - M\hat{\mathbf{p}}\right) = \mathbf{r_{com}} - \hat{\mathbf{p}} \;\; \forall i.$$

Problem 4.3.3 (Distributed computation of the coefficient of inertia tensor K) The coefficient of inertia tensor K, like the center of mass, depends on all of the agent positions, hence might not be directly available to the agents. Nevertheless it can be expressed in terms of quantities known locally to individual agents, such as those introduced in the proof of theorem (4.1.17):

$$\begin{aligned} K &= \sum_{i=1}^{n} m_i(\mathbf{r_i} - \mathbf{r_{com}})(\mathbf{r_i} - \mathbf{r_{com}})^T = \frac{1}{M^2}\sum_{i=1}^{n} m_i \left(\sum_{j=1}^{n} m_j \mathbf{r_{i,j}}\right)\left(\sum_{j=1}^{n} m_j \mathbf{r_{i,j}}^T\right) \\ &= \frac{1}{M^2}\sum_{i=1}^{n} m_i \left(\mathbf{R_{i,N_i}} + \mathbf{R_{i,\tilde{N}_i}}\right)\left(\mathbf{R_{i,N_i}} + \mathbf{R_{i,\tilde{N}_i}}\right)^T \\ &= \frac{1}{M^2}\sum_{i=1}^{n} m_i \left(\mathbf{R_{i,N_i}} + \sum_{j=1}^{n}\gamma_j^i \mathbf{R_{j,N_j}}\right)\left(\mathbf{R_{i,N_i}} + \sum_{j=1}^{n}\gamma_j^i \mathbf{R_{j,N_j}}\right)^T. \end{aligned} \tag{4.86}$$

For each agent i, N_i and $\tilde{N}_i$ are its sets of neighbors and non-neighbors in the sensing network $\mathcal{G}$ (that might be different from the communication network

$\mathcal{G}_{\mathcal{C}}$); $\mathbf{R_{i,N_i}} \triangleq \sum_{j\in N_i} m_j \mathbf{r_{i,j}}$ is known to agent i via local sensing, while $\mathbf{R_{i,\tilde{N}_i}} \triangleq \sum_{j\in \tilde{N}_i} m_j \mathbf{r_{i,j}}$ is not known to agent i, but we assume there exist coefficients γ_j^i, $j = 1, ..., n$, such that $\mathbf{R_{i,\tilde{N}_i}} = \sum_{j=1}^{n} \gamma_j^i \mathbf{R_{j,N_j}}$. Recalling the results obtained in the proof of theorem (4.1.17), if the sensing graph $\mathcal{G}$ has a spanning tree directed into one of its vertices, the coefficients γ_j^i certainly exist and can be computed explicitly from the formulae $\mathbf{Vec_\gamma^i} = Mat_\alpha^T (Mat_\alpha Mat_\alpha^T)^{-1} \mathbf{Vec_\beta^i}$, $\forall i = 1, ..., n$. Provided that every agent knows the masses of the others and knows the sensing graph $\mathcal{G}$, and the latter does admit a spanning tree, every agent can compute the coefficients γ_j^i and then use (4.86) to compute the coefficient of inertia tensor from all the local quantities $\mathbf{R_{1,N_1}}$, $\mathbf{R_{2,N_2}}$, ... , $\mathbf{R_{n,N_n}}$. Under these assumptions, the agents only need to communicate to each other these locally sensed quantities. If the communication network $\mathcal{G}_{\mathcal{C}}$ is undirected and connected, and includes $\mathcal{G}$ as a subgraph, each agent can asymptotically obtain the vector $[\mathbf{R_{1,N_1}}^T \mathbf{R_{2,N_2}}^T ... \mathbf{R_{n,N_n}}^T]^T$ containing all these quantities, through the following average consensus dynamics:

$$\dot{\mathbf{x}}_\mathbf{i}(t) = -\sum_{j\in N_i} (\mathbf{x_i}(t) - \mathbf{x_j}(t)) \tag{4.87}$$

$$\mathbf{x_i}(0) = n \left[\mathbf{0}^T \cdots \mathbf{0}^T \mathbf{R_{i,N_i}}^T \mathbf{0}^T \cdots \mathbf{0}^T\right]^T \in \mathbb{R}^{3n}, \tag{4.88}$$

which in fact converge to:

$$\lim_{t\to\infty} \mathbf{x_i}(t) = \frac{1}{n} \sum_{i=1}^{n} \mathbf{x_i}(0) = [\mathbf{R_{1,N_1}}^T \mathbf{R_{2,N_2}}^T ... \mathbf{R_{n,N_n}}^T]^T \ \ \forall i.$$

Remark 4.3.4 If instead of having access only to locally sensed information (such as the vector $\mathbf{R_{i,N_i}}$), each agent i has also access to its relative position

with respect to the center of mass ($\mathbf{c_i} = \mathbf{r_i} - \mathbf{r_{com}}$), then the following matrix average consensus dynamics (dimensionally more convenient than (4.87)-(4.88)) can alternatively be used to obtain K:

$$\dot{M}_i(t) = -\sum_{j \in N_i} (M_i(t) - M_j(t)) \tag{4.89}$$

$$M_i(0) = n m_i \mathbf{c_i} \mathbf{c_i}^T. \tag{4.90}$$

It is easy to verify, in fact, that:

$$\lim_{t \to \infty} M_i(t) = \frac{1}{n} \sum_{i=1}^{n} M_i(0) = \sum_{i=1}^{n} m_i \mathbf{c_i} \mathbf{c_i}^T = K \ \ \forall i. \tag{4.91}$$

Chapter 5

Collective motion based on Motion Camouflage

In this chapter we pursue a biologically-inspired approach to the synthesis of collective motion, using a steering law called *motion camouflage proportional guidance*, first derived in [47] (and in [32] for a planar version), as a "building-block". As explained in section 5.2, if the pursuer is modeled as a self-steering particle, motion camouflage proportional guidance provides a biologically-plausible implementation for a pursuit strategy called *motion camouflage (with respect to infinity)*, described in section 5.1. This strategy, also referred to as *constant absolute target direction*, has been observed in experimental data of echolocating bats and dragonflies chasing insect prey, male hoverflies chasing females, and male dragonflies engaged in territorial aerial battles.

Most of section 5.3 is devoted to studying the simple but fundamental case of two individuals in mutual pursuit, which we call *mutual motion camouflage*. Before analyzing the general three-dimensional case, we study the simpler case in which both individuals are constrained on a plane (section 5.3.1). The dynamics of mutual motion camouflage on a plane are theoretically interesting because

they produce an oscillatory system somewhat similar to the Kepler problem, a comparison with which is presented in section 5.3.2. The planar dynamics are also closely related to the full dynamics of mutual motion camouflage in three dimensions, which are derived in section 5.3.3. The mutual motion camouflage dynamics can be extended to a kind of swarming motion for a n-unit collective, with the individuals moving on average in a common direction, as explained in section 5.4.

Note that while the synthesis of collective motion in chapter 4 is in the context of first-order dynamical models, with the velocities of the individuals being the controls, this chapter focuses on second-order dynamical models. The controls are expressed as curvature (steering) laws, but can also be thought of as gyroscopic forces imposed on unit-mass particles.

The notation here is independent from that of the previous chapters; unless otherwise specified, quantities represented with a certain symbol in this chapter are not related to quantities defined previously with the same symbol.

5.1 Motion Camouflage pursuit strategy

For many animal species, survival and reproduction depend on their ability to pursue potential preys and mates. Given the importance of this task, many species have highly developed pursuit skills, often tailored to effectively use their sensory and motor capabilities.

Different animal species typically accomplish pursuit tasks in different ways,

and even within the same species, different types of pursuit seem to be used in different circumstances. Nevertheless there are some common pursuit strategies, which can be identified by studying the geometry of the trajectories of pursuers and evaders, that are recurring across different species. Certain animal pursuers employ the most basic strategy of going straight towards the current position of the evader; this strategy is sometimes called *classical pursuit* or *tracking* and is geometrically described by the pursuer velocity being aligned with the baseline (or line-of-sight vector) between pursuer and evader. A somewhat similar strategy employed by other animal pursuers is to go towards the current position of the evader while keeping a fixed offset angle with the line-of-sight vector. This strategy is called *constant bearing pursuit*. Our focus is on another strategy, in which the pursuer moves so that the absolute direction of the line-of-sight vector remains constant in time, or in other words the relative velocity between pursuer and evader is always parallel to the relative position. In mathematical terms, if $\mathbf{r} = \mathbf{r_p} - \mathbf{r_e}$ is the relative position of the pursuer with respect to the evader, and $\dot{\mathbf{r}}$ is its time derivative, then this strategy holds when:

$$\Gamma(\mathbf{r}, \dot{\mathbf{r}}) \triangleq \frac{\dot{\mathbf{r}}}{|\dot{\mathbf{r}}|} \cdot \frac{\mathbf{r}}{|\mathbf{r}|} = -1. \tag{5.1}$$

This strategy is sometimes referred to as *constant absolute target direction* or as *parallel navigation*, in reference to the constraint that the relative position vector remains always parallel to itself. If perfectly executed, this strategy leads a pursuer that moves faster than the evader to always intercept the latter; for this reason, it is also sometimes called *interception* (for example in [44]).

The classical pursuit and constant absolute target direction strategies are observed for example in experimental data collected from echolocating bats. It appears that the strategy used by a single bat in hunting for prey (such as a praying mantis) can be identified with a strategy of constant absolute target direction [21]; conversely, when there are two bats competing for the same prey, the bat behind follows the first one with a classical pursuit strategy for most of the time, before changing strategy at the end to attempt (often successfully) capture of the prey [16]. An example of constant bearing pursuit can instead be found in the study of peregrine falcon stoop [51]. The peregrine falcon spots a prey from very high distance and altitude, and then starts a spiral trajectory towards the target which is driven by a constant bearing condition; the motivation for this could be that the falcon needs to maintain sideways vision due to the lateral position of the eyes, and of the deep fovea in particular, but at the same time it needs to keep the head aligned with the direction of flight to minimize aerodynamic drag.

The constant absolute target direction strategy appears not only in the study of echolocating bats but also of visual insects. In [44], it is shown that dragonflies intercept their prey by keeping the absolute angle to the prey constant. Moreover, in the context of male hoverflies chasing female ones [50] and male-male territorial air-battles between dragonflies [41], it has been observed that the pursuer moves in such a way that the direction of the line-of-sight between pursuer and evader remains always parallel to itself or always intersects a common

point. It has been postulated that the pursuer moves in this way to null the optic flow produced in the eyes of the evader, hence making it believe that the pursuer is co-located with a familiar, stationary object (such as a flower). It is well-known that insects like hoverflies and dragonflies have compound eyes that are very effective at detecting optic flow, but have poor sensitivity to looming. This strategy allows therefore the pursuer to "camouflage" its motion towards the evader, and for this reason it is called *motion camouflage*. In this context the constant absolute target direction strategy is seen as a special case, in which the stationary object of reference is placed at infinity; this motivates yet another name for this strategy: *motion camouflage with respect to infinity*. Figure 5.1 sketches the two strategies of motion camouflage with respect to a point and with respect to infinity (identical to constant absolute target direction).

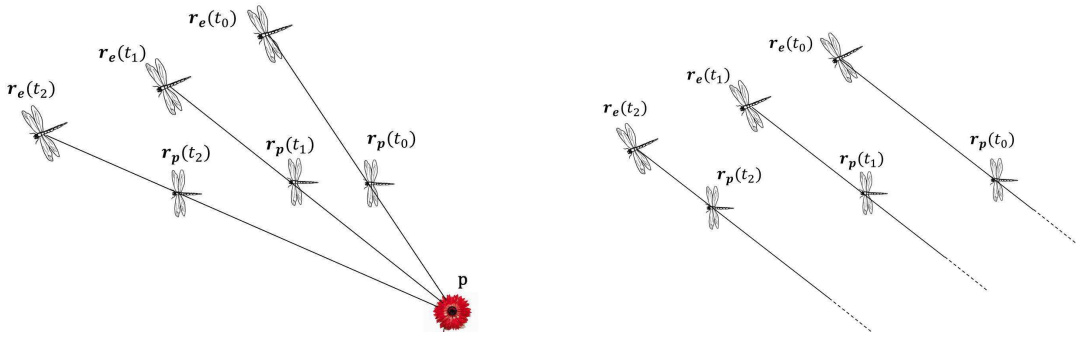

(a) (b)

Figure 5.1: Motion camouflage strategy: (a) with respect to a point **p**; (b) with respect to infinity (constant absolute target direction).

As an additional motivation for considering this pursuit strategy, a game-theoretical comparison of the three different strategies has showed that it is the

most effective in capturing randomly moving evaders [54].

Biologically-plausible steering laws that execute this strategy, for a pursuer modeled as a self-steering particle, have been introduced in [47] and [32] (for a three-dimensional and a planar setting respectively) and will be recalled in the following section. These steering laws are referred to as *motion camouflage proportional guidance (MCPG)* laws, hence for consistency we will refer to the constant absolute target direction strategy as simply *motion camouflage (MC)* strategy in the remainder of the chapter.

5.2 Motion Camouflage Proportional Guidance steering law

Let the pursuer be modeled as a unit-mass particle moving along twice-differentiable curves in $\mathbb{R}^3$, and capable of controlling its own steering (i.e. a "self-steering particle"). Then a convenient set of equations to describe the pursuer dynamics is the one based on the natural Frenet framing of curves in $\mathbb{R}^3$ (described for example in [8] and [31]):

$$\begin{aligned} \dot{\mathbf{r}}_\mathbf{p} &= \nu_p \mathbf{x}_\mathbf{p} \\ \dot{\mathbf{x}}_\mathbf{p} &= \nu_p (u_p \mathbf{y}_\mathbf{p} + v_p \mathbf{z}_\mathbf{p}) \\ \dot{\mathbf{y}}_\mathbf{p} &= -\nu_p u_p \mathbf{x}_\mathbf{p} \\ \dot{\mathbf{z}}_\mathbf{p} &= -\nu_p v_p \mathbf{x}_\mathbf{p}. \end{aligned} \tag{5.2}$$

Here $\mathbf{r_p}$ is the position of the pursuer and $\mathbf{x_p}$ is the unit vector in its direction of motion, while $\mathbf{y_p}, \mathbf{z_p}$ complete with $\mathbf{x_p}$ a right-handed orthonormal

frame for the particle trajectory. Notice that $\mathbf{y_p}, \mathbf{z_p}$ need to be chosen arbitrarily at the initial time; then their evolution in time is uniquely defined by (5.2). The natural curvatures u_p, v_p can be thought of as the steering controls, which do not affect the speed ν_p; to see this, notice that they act on $\dot{\mathbf{x}}_\mathbf{p}$ in directions $\mathbf{y_p}$ and $\mathbf{z_p}$, orthogonal to $\mathbf{x_p}$. The speed is not considered an active control, but a time function dictated by propulsive or lift mechanisms; this assumption simplifies the model and is reasonable in the context of birds and other pursuers that need to maintain a certain speed to remain aloft. Alternatively, (5.2) can be interpreted as the model for a particle subject only to a *gyroscopic* force, controllable through the scalar functions u_p and v_p, leaving unchanged the kinetic energy,.

For these pursuer dynamics, the *motion camouflage proportional guidance* steering law is defined as follows [47]:

$$\begin{aligned} u_p^{MCPG}(t) &= -\mu \left[\mathbf{z_p}(t) \cdot \left(\dot{\mathbf{r}}(t) \times \tfrac{\mathbf{r}(t)}{|\mathbf{r}(t)|} \right) \right] \\ v_p^{MCPG}(t) &= +\mu \left[\mathbf{y_p}(t) \cdot \left(\dot{\mathbf{r}}(t) \times \tfrac{\mathbf{r}(t)}{|\mathbf{r}(t)|} \right) \right], \end{aligned} \tag{5.3}$$

where $\mu > 0$ is a constant gain, and $\mathbf{r} = \mathbf{r_p} - \mathbf{r_e}$ is the line-of-sight vector between the pursuer and the evader, also modeled as a particle.

Motion camouflage proportional guidance, with high gain μ, is a biologically-plausible steering law that a pursuer interested in executing the motion camouflage strategy could successfully employ. It is in fact shown in [47] that if the initial conditions satisfy $\Gamma(\mathbf{r}(0), \dot{\mathbf{r}}(0)) \neq 1$ and $|\mathbf{r}(0)| > 0$, and the motion of the evader satisfies certain constraints (slower than the pursuer, trajectories with bounded and continuous curvatures), then (5.3) guarantees that the mo-

tion camouflage state (5.1) is "accessible in finite time": $\forall \epsilon > 0$, there exists a finite time $T > 0$ such that $\Gamma(T) \leq -1 + \epsilon$ if the gain μ is sufficiently high. This result holds independently of how the speed of the pursuer varies, provided it is bounded, has bounded and piecewise continuous derivatives, and remains higher than the evader speed. In support of the claim that this control law is a biologically-plausible implementation of the motion camouflage strategy, [46] reports high correlation between the curvatures produced by a delayed version of (5.3), which accounts for sensorimotor reaction times, and the actual curvatures extracted from experimental trajectories of single echolocating bats engaged in prey pursuit.

Remark 5.2.1 If the pursuer model (5.2) is interpreted as a particle subject to gyroscopic force, the motion camouflage proportional guidance law corresponds to the following force (and corresponding lateral acceleration) applied on the pursuer:

$$\begin{aligned} \ddot{\mathbf{r}}_{\mathbf{p},\mathbf{lat}}(t) = \mathbf{F}^{\mathbf{MCPG}}(t) &= \nu_p^2(u_p^{MCPG}(t)\mathbf{y_p}(t) + v_p^{MCPG}(t)\mathbf{z_p}(t)) \\ &= \mu\nu_p|\mathbf{r}(t)|(\boldsymbol{\Omega}_\mathbf{l}(t) \times \dot{\mathbf{r}}_\mathbf{p}(t)), \end{aligned} \tag{5.4}$$

where $\boldsymbol{\Omega}_\mathbf{l} \triangleq \left(\frac{\mathbf{r}(t)}{|\mathbf{r}(t)|^2} \times \dot{\mathbf{r}}(t)\right)$ is the angular velocity of the baseline vector $\mathbf{r}$, considered instantaneously as a rigid rod.

5.2.1 The planar case

It is also useful to introduce a planar version of the motion camouflage proportional guidance law, which executes the motion camouflage strategy when both pursuer and evader are constrained on a common plane.

In this case the pursuer is modeled as a unit-mass self-steering particle moving along twice-differentiable curves in $\mathbb{R}^2$, its dynamics described by the planar natural Frenet frame equations:

$$\begin{aligned} \dot{\mathbf{r}}_\mathbf{p} &= \nu_p \mathbf{x}_\mathbf{p} \\ \dot{\mathbf{x}}_\mathbf{p} &= \nu_p u_p \mathbf{y}_\mathbf{p} \\ \dot{\mathbf{y}}_\mathbf{p} &= -\nu_p u_p \mathbf{x}_\mathbf{p}. \end{aligned} \tag{5.5}$$

Here $\mathbf{r}_\mathbf{p} \in \mathbb{R}^2$ is the position of the pursuer on the plane, $\mathbf{x}_\mathbf{p} \in \mathbb{R}^2$ is the tangent vector to the pursuer trajectory and $\mathbf{y}_\mathbf{p} = \mathbf{x}_\mathbf{p}{}^\perp$ is its counterclockwise rotation by $\pi/2$ radians, which completes with $\mathbf{x}_\mathbf{p}$ an orthonormal frame. The curvature u_p is the steering control, which affects the direction of motion of the pursuer but not its speed ν_p, assumed to be an independently defined time function.

The planar motion camouflage proportional guidance law, first introduced in [32], is given by:

$$u_p^{MCPG}(t) = -\mu \left(\frac{\mathbf{r}(t)}{|\mathbf{r}(t)|} \cdot \dot{\mathbf{r}}^\perp(t) \right), \tag{5.6}$$

where $\mu > 0$ is a constant gain, and $\mathbf{r} = \mathbf{r}_\mathbf{p} - \mathbf{r}_\mathbf{e} \in \mathbb{R}^2$ is the line-of-sight vector between the pursuer and the evader.

Just as in the three-dimensional case, if $\Gamma(\mathbf{r}(0), \dot{\mathbf{r}}(0)) \neq 1$ and $|\mathbf{r}(0)| > 0$,

and the motion of the evader satisfies certain constraints (its trajectories have bounded and continuous curvatures and its speed is always lower than that of the pursuer), then (5.6) guarantees that the motion camouflage state (5.1) is accessible in finite time.

Remark 5.2.2 The planar motion camouflage proportional guidance steering law can alternatively be expressed as follows:

$$u_p^{MCPG}(t) = \mu|\mathbf{r}(t)|\omega_{\mathbf{r}}(t), \tag{5.7}$$

where $\omega_{\mathbf{r}}$ is the angular rate of the baseline vector $\mathbf{r}$ with respect to an absolute reference frame (given $\mathbf{r} = (|\mathbf{r}|, \alpha_{\mathbf{r}})$ in polar coordinates, $\omega_{\mathbf{r}} \triangleq \dot{\alpha}_{\mathbf{r}}$). This alternative expression highlights the simplicity of the control law and the variables required for its implementation, namely the distance and the angular rate, which can be easily sensed without the need of inertial frame information.

5.3 Mutual Motion Camouflage

In this section we study the coupled system composed of two individuals engaged in a *mutual* (reciprocal) pursuit, with each individual executing the motion camouflage proportional guidance steering law with the other one as the "target". We refer to this system as *Mutual Motion Camouflage (MMC)*. We first study the dynamics of mutual motion camouflage in the planar case, which are interesting in their own right and as a stepping stone in the analysis of the general three-dimensional case. Parts of sections 5.3.1 and 5.3.2 are adapted

from [39], and part of the analysis in section 5.3.3 can also be found in [40], together with modifications of the system that are tailored towards spatial coverage applications.

5.3.1 Planar Mutual Motion Camouflage

We define as **planar Mutual Motion Camouflage** the system composed of two individuals, each subject to dynamics (5.5) and *moving at constant speeds* (not necessarily equal) that are in mutual pursuit with the motion camouflage proportional guidance law (5.6), *with gains inversely proportional to the speeds*:

$$u_i(t) = -\mu_i \left(\frac{\mathbf{r}(t)}{|\mathbf{r}(t)|} \cdot \dot{\mathbf{r}}^{\perp}(t) \right), \quad \mu_i = \frac{\mu}{\nu_i}, \quad i = 1, 2. \tag{5.8}$$

Here $\mathbf{r} \triangleq \mathbf{r_1} - \mathbf{r_2}$ is the relative position of particle 1 with respect to particle 2, and $\mu > 0$ is a constant gain. The individual gains μ_1, μ_2 are chosen to be inversely proportional to the speeds to preserve a certain symmetry in the system even when the individual (constant) speeds are different; this allows the mutual motion camouflage system to produce coordinated motion of the particles, as will be proved in the following. For the purpose of obtaining coordinated motion patterns, it is not important that μ is a high-gain (as it would be if, instead, each individual wanted to intercept the other); we will therefore consider it as a free positive parameter, that can be chosen to affect certain characteristics of the resulting coordinated motion.

In studying the planar mutual motion camouflage system, we separate the

relative motion between the two self-steering particles from the evolution of the pair with respect to the absolute reference frame, described by the motion of the center of mass. For the relative motion analysis, in addition to the relative position $\mathbf{r} = \mathbf{r_1} - \mathbf{r_2}$ we define the relative velocity $\mathbf{g} \triangleq \nu_1 \mathbf{x_1} - \nu_2 \mathbf{x_2}$ and the vector $\mathbf{h} \triangleq \nu_1 \mathbf{y_1} - \nu_2 \mathbf{y_2}$, which satisfies $\mathbf{h} = \mathbf{g}^{\perp} = \dot{\mathbf{r}}^{\perp}$ by the linearity of vector rotation. For the center of mass, we introduce the scaled position $\mathbf{z} \triangleq \mathbf{r_1} + \mathbf{r_2}$ and velocity $\mathbf{k} \triangleq \nu_1 \mathbf{x_1} + \nu_2 \mathbf{x_2}$; we also introduce $\mathbf{w} \triangleq \nu_1 \mathbf{y_1} + \nu_2 \mathbf{y_2} = \mathbf{k}^{\perp}$. The equations of the coupled system, when the particles are controlled according to (5.8), are:

$$\begin{aligned} \dot{\mathbf{r}} &= \mathbf{g} \\ \dot{\mathbf{g}} &= -\mu \left(\tfrac{\mathbf{r}}{|\mathbf{r}|} \cdot \mathbf{h} \right) \mathbf{h} \\ \dot{\mathbf{h}} &= +\mu \left(\tfrac{\mathbf{r}}{|\mathbf{r}|} \cdot \mathbf{h} \right) \mathbf{g} \end{aligned} \tag{5.9}$$

$$\begin{aligned} \dot{\mathbf{z}} &= \mathbf{k} \\ \dot{\mathbf{k}} &= -\mu \left(\tfrac{\mathbf{r}}{|\mathbf{r}|} \cdot \mathbf{h} \right) \mathbf{w} \\ \dot{\mathbf{w}} &= +\mu \left(\tfrac{\mathbf{r}}{|\mathbf{r}|} \cdot \mathbf{h} \right) \mathbf{k}. \end{aligned} \tag{5.10}$$

It is possible to apply a reduction to equations (5.9)-(5.10), by introducing the scalar variables $\rho \triangleq |\mathbf{r}| = (\mathbf{r} \cdot \mathbf{r})^{1/2}$, $\gamma \triangleq \dot{\rho} = (\mathbf{r} \cdot \mathbf{g}) / |\mathbf{r}|$ and $\lambda = (\mathbf{r} \cdot \mathbf{h}) / |\mathbf{r}|$ for the relative motion, and similarly $\zeta = |\mathbf{z}| = (\mathbf{z} \cdot \mathbf{z})^{1/2}$, $\xi = \dot{\zeta} = (\mathbf{z} \cdot \mathbf{k}) / |\mathbf{z}|$ and $\eta = (\mathbf{z} \cdot \mathbf{w}) / |\mathbf{z}|$ for the center of mass. The following propositions are used in deriving the reduced equations; notice that the important property in proposition 5.3.1 holds not only for mutual motion camouflage but for all cases of mutual interaction in which the steering controls satisfy $u_1 \nu_1 = u_2 \nu_2$.

Proposition 5.3.1. *The relative velocity vector* $\mathbf{g}$ *and the (scaled) center of mass velocity vector* $\mathbf{k}$ *have constant magnitude in mutual motion camouflage.*

Proof.

$$\frac{d(\mathbf{g}\cdot\mathbf{g})}{dt} = \frac{d(|\mathbf{g}|^2)}{dt} = 2\,(\mathbf{g}\cdot\dot{\mathbf{g}}) = -2\,\mu\left(\frac{\mathbf{r}}{|\mathbf{r}|}\cdot\mathbf{h}\right)\,(\mathbf{g}\cdot\mathbf{h}) = 0.$$

An analogous proof shows that $|\mathbf{k}|$ is constant. □

We indicate these magnitudes as $|\mathbf{g}| = |\mathbf{h}| \triangleq \delta$ and $|\mathbf{k}| = |\mathbf{w}| \triangleq \theta$; notice that $|\nu_1 - \nu_2| \leq \delta, \theta \leq \nu_1 + \nu_2$.

Proposition 5.3.2. *The variables* γ *and* λ*, and similarly* ξ *and* η*, are related as follows:*

$$\delta^2 = \gamma^2 + \lambda^2 \tag{5.11}$$

$$\theta^2 = \xi^2 + \eta^2. \tag{5.12}$$

Proof. From the orthogonality of $\mathbf{g}$ and $\mathbf{h}$:

$$\begin{aligned}
\frac{\mathbf{r}}{|\mathbf{r}|} &= \left(\frac{\mathbf{r}}{|\mathbf{r}|}\cdot\frac{\mathbf{g}}{|\mathbf{g}|}\right)\frac{\mathbf{g}}{|\mathbf{g}|} + \left(\frac{\mathbf{r}}{|\mathbf{r}|}\cdot\frac{\mathbf{h}}{|\mathbf{h}|}\right)\frac{\mathbf{h}}{|\mathbf{h}|} \quad \Rightarrow \\
1 &= \frac{1}{\delta^2}\left(\frac{\mathbf{r}}{|\mathbf{r}|}\cdot\mathbf{g}\right)^2 + \frac{1}{\delta^2}\left(\frac{\mathbf{r}}{|\mathbf{r}|}\cdot\mathbf{h}\right)^2 \quad \Rightarrow \\
\delta^2 &= \gamma^2 + \lambda^2.
\end{aligned}$$

A similar calculation yields (5.12). □

Using these results, the equations (5.9)-(5.10) can be reduced to:

$$\begin{aligned}
\dot{\rho} &= \gamma \\
\dot{\gamma} &= \left(\tfrac{1}{\rho} - \mu\right)\,(\delta^2 - \gamma^2) \\
\dot{\lambda} &= \left(\mu - \tfrac{1}{\rho}\right)\,\lambda\,\gamma
\end{aligned} \tag{5.13}$$

$$\begin{aligned} \dot{\zeta} &= \xi \\ \dot{\xi} &= \tfrac{1}{\zeta}\,(\theta^2 - \xi^2) - \mu\,\lambda\,\eta \\ \dot{\eta} &= -\tfrac{1}{\zeta}\,\xi\,\eta + \mu\,\lambda\,\xi. \end{aligned} \tag{5.14}$$

The process of reducing the full configuration of the system $(\mathbf{r_1}, \mathbf{r_2})$ to the relative position $\mathbf{r}$ is equivalent (on the plane) to the reduction of the translational degree of freedom described in section 3.1. Further reduction of $\mathbf{r}$ to the relative distance ρ is similar to the reduction to shape space described in section 3.2, in the sense that the reduced configuration (here just ρ) is invariant to the group $SO(2)$ of rotations of the absolute reference frame. For this reason we will sometimes refer to ρ as the "shape" of the system, and to (5.13) as the "shape dynamics", even if technically this does not fit the definition of shape given in 3.2 (where the collinear configurations were excluded and the space was $\mathbb{R}^3$). Notice that the shape dynamics (5.13) are self-contained because the motion camouflage proportional guidance law is invariant to rotations and translations of the absolute reference frame; in fact it can completely be expressed in terms of the shape variable λ: $u^{MCPG}(t) = -\mu\lambda(t)$. The reduced center of mass dynamics (5.14) are driven by the shape dynamics through the coupling in λ.

Remark 5.3.3 For a system of n particles described by model (5.5), an alternative definition of "shape space" is presented in [30], where the shape space is $(SE(2) \times SE(2) \times ... \times SE(2))/SE(2)$, obtained by quotienting the original configuration space (equivalent to n copies of the special Euclidean group $SE(2)$)

by the symmetry group $SE(2)$ corresponding to rigid motions of the absolute reference frame. Since the variables ρ, γ, λ are invariant to this $SE(2)$ action, they are "shape variables", and (5.13) can be interpreted as "shape dynamics", even in this alternative context.

We derive the motion patterns generated by planar mutual motion camouflage by studying (5.13)-(5.14) and then reconstructing the complete trajectories of the particles from those in the reduced variables. We first concentrate on the relative motion equations (5.13), and then show that the dynamics of the center of mass can be derived from those of the relative motion in a very direct way, thanks to a special property of the system.

Relative motion: a conservative system

The analysis of the relative motion in planar MMC reduces to the solution of the first two scalar differential equations in (5.13):

$$\begin{aligned} \dot{\rho} &= \gamma \\ \dot{\gamma} &= \left(\tfrac{1}{\rho} - \mu\right)\,(\delta^2 - \gamma^2)\,, \end{aligned} \tag{5.15}$$

defined on the manifold $M = \{(\rho, \gamma) : \rho > 0, -\delta \leq \gamma \leq \delta\}$. The time evolution of λ, appearing in the center of mass equations (5.14), can then be derived from that of ρ and γ by solving the third differential equation in (5.13).

The system (5.15) has a unique equilibrium $(\rho_{eq}, \gamma_{eq}) = (1/\mu, 0)$ and two obvious invariant manifolds $\{\gamma = +\delta\}$ and $\{\gamma = -\delta\}$, with restricted dynamics $(\dot{\rho} = \delta, \dot{\gamma} = 0)$ and $(\dot{\rho} = -\delta, \dot{\gamma} = 0)$ respectively. On these manifolds, $\lambda =$

$0 \Rightarrow \mathbf{r} \perp \dot{\mathbf{r}}^{\perp} \Rightarrow \Gamma(\mathbf{r}, \dot{\mathbf{r}}) = \pm 1$. The case $\gamma = -\delta$ corresponds to the motion camouflage pursuit strategy being perfectly executed, and on this manifold the baseline between the particles keeps shortening till the particles eventually collide; conversely in the case that $\gamma = \delta$ the baseline keeps lengthening and the particle positions diverge. The remaining part of the state space of (5.15) is also filled with invariant manifolds, each a periodic orbit. To prove this, we use a certain symmetry property in the vector field of (5.15), namely its *F-reversibility*, and the following theorem due to Birkhoff.

Definition 5.3.4 (**Involution**) A diffeomorphism $F : M \to M$ from a manifold M to itself is said to be an *involution* if $F \neq id_M$, the identity diffeomorphism, and $F^2 = id_M$, i.e. $F(F(m)) = m, \forall m \in M$.

Definition 5.3.5 (**F-reversibility**) A vector field X defined over a manifold M is said to be *F-reversible*, if there exists an involution F such that: $F_*(X) = -X$; i.e. F maps orbits of X to orbits of X, reversing the time parametrization. Here $(F_*(X))(m) = (DF)_{F^{-1}(m)} X(F^{-1}(m)) \forall m \in M$ is the push-forward of F. We call F the *reverser* of X.

Theorem 5.3.6 (**G.D. Birkhoff [7]**). *Let X be a F-reversible vector field on M and Σ_F the fixed-point set of the reverser F. If an orbit of X through a point of Σ_F intersects Σ_F in another point, then it is periodic.*

Proof. Let $t \mapsto x(t)$ be an integral curve of X and let $t_0 < t_1 \in \mathbb{R}$ be such that $x(t_0) \in \Sigma_F, x(t_1) \in \Sigma_F$ and $x(t) \notin \Sigma_F \ \forall t_0 < t < t_1$. Since $F_*(X) = -X$ and

$F^{-1} = F$ (because F is an involution), then $y(t) = F(x(2t_1 - t))$ is also an orbit of X (i.e. it solves $\dot{y} = X(y)$). But $y(t_1) = F(x(2\,t_1 - t_1)) = F(x(t_1)) = x(t_1)$, since $x(t_1) \in \Sigma_F$. By uniqueness of solutions, $y(t) = x(t)$. Hence: $x(t_0 + 2\,(t_1 - t_0)) = y(t_0 + 2(t_1 - t_0)) = F(x(2t_1 - t_0 - 2(t_1 - t_0))) = F(x(t_0)) = x(t_0)$, since $x(t_0) \in \Sigma_F$. Thus $x(t)$ is periodic with period $2\,(t_1 - t_0)$. Also $x(t) = F(x(2\,t_1 - t))$. □

Remark 5.3.7 This version of the proof of Birkhoff's theorem follows the thesis of J. Hermans (under J.J. Duistermaat) [25].

Theorem 5.3.6 can be applied to (5.15) to prove that all orbits in M, outside of the motion camouflage invariant manifolds, are periodic. We also prove that each of these periodic orbits is associated to a conserved quantity.

Proposition 5.3.8. *The vector field defined by* (5.15) *is F-reversible, with reverser* $F(\rho, \gamma) = (\rho, -\gamma)$.

Proof. Consider the involution $F(\rho, \gamma) = (\rho, -\gamma)$. Its push-forward maps the vector field X defined by (5.15) to the vector field:

$$\begin{aligned}(F_*(X))(\rho,\gamma) &= \begin{bmatrix} 1 & 0 \\ 0 & -1 \end{bmatrix} \begin{bmatrix} -\gamma \\ (1/\rho - \mu)(\delta^2 - \gamma^2) \end{bmatrix} \\ &= -X(\rho,\gamma).\end{aligned}$$

Hence X is F-reversible. □

Lemma 5.3.9. *Every orbit of* (5.15) *which intersects the* ρ*-axis twice is periodic.*

Proof. From proposition 5.3.8, $F(\rho, \gamma) = (\rho, -\gamma)$ is a reverser for the vector field

of (5.15). The fixed-point set of F is $\Sigma_F = \{(\rho, 0) : \rho > 0\}$, the ρ-axis. The result then directly follows from theorem 5.3.6. □

Theorem 5.3.10. *Every orbit of* (5.15) *with initial conditions* $(\rho_0, \gamma_0) \neq (\rho_{eq}, \gamma_{eq})$ *and such that* $\rho_0 > 0$, $-\delta < \gamma_0 < \delta$ *(i.e. not at the equilibrium point or on the motion camouflage manifolds):*

(a) has a conserved quantity

$$E(\rho, \gamma) = \rho^2 \left(\delta^2 - \gamma^2\right) e^{-2\mu\rho} \tag{5.16}$$

(b) is periodic.

Proof. (a) Orbits not on the motion camouflage manifolds ($\gamma = \pm\delta$) satisfy $\gamma^2 < \delta^2$ and, from (5.15):

$$\begin{aligned}
\frac{d\gamma}{d\rho} = \frac{d\gamma}{dt}\,\frac{dt}{d\rho} = \left(\frac{1}{\rho} - \mu\right)\left(\delta^2 - \gamma^2\right)\frac{1}{\gamma} \quad &\Rightarrow \\
\left(\frac{\gamma}{\delta^2 - \gamma^2}\right) d\gamma = \left(\frac{1}{\rho} - \mu\right) d\rho \quad &\Rightarrow \\
\int_{\gamma_0}^{\gamma} \left(\frac{\gamma}{\delta^2 - \gamma^2}\right) d\gamma = \int_{\rho_0}^{\rho} \left(\frac{1}{\rho} - \mu\right) d\rho \quad &\Rightarrow \\
-\frac{1}{2}\, ln\left(\frac{\delta^2 - \gamma^2}{\delta^2 - \gamma_0^2}\right) = ln\left(\frac{\rho}{\rho_0}\right) - \mu\left(\rho - \rho_0\right) \quad &\Rightarrow \\
\gamma^2(\rho) = \delta^2 - (1/\rho^2)\, E(\rho_0, \gamma_0)\, e^{2\mu\rho}. \quad &(5.17)
\end{aligned}$$

Hence, for an orbit starting at (ρ_0, γ_0), $E(\rho, \gamma) = E(\rho_0, \gamma_0)\ \forall(\rho, \gamma)$.

(b) From (5.17), the intersections of each orbit with the ρ-axis occur when $E(\rho, 0) = \rho^2\, \delta^2\, e^{-2\mu\rho} = E(\rho_0, \gamma_0)$. The function $E(\rho, 0)$ has limit values $E(0, 0) = E(\infty, 0) = 0$ and a unique critical point at $\rho = 1/\mu$ corresponding to its maximum

value $\delta^2\, e^{-2}/\mu^2$. Hence if the initial conditions satisfy $0 < E(\rho_0, \gamma_0) < \delta^2\, e^{-2}/\mu^2$, the corresponding orbit has two intersections with the ρ-axis and, by lemma 5.3.9, is periodic. Since the maximum value of energy $E(\rho_0, \gamma_0) = \delta^2\, e^{-2}/\mu^2$ is only achieved at the equilibrium $(\rho_{eq}, \gamma_{eq}) = (1/\mu, 0)$, all the orbits of interest (not at the equilibrium point or on the motion camouflage manifolds) are indeed periodic. □

Corollary 5.3.11. *The periodic orbits described in theorem 5.3.10 have period:*

$$T = 2 \int_{\rho_{min}}^{\rho_{max}} d\rho / \sqrt{\delta^2 - E(\rho_0, \gamma_0)\, e^{2\mu\rho}/\rho^2}, \tag{5.18}$$

where ρ_{min} and ρ_{max} are the positive solutions to equation:

$$\rho^2\, \delta^2\, e^{-2\mu\rho} = E(\rho_0, \gamma_0). \tag{5.19}$$

Proof. From the proof of Birkhoff's theorem, the period T of a periodic orbit of (5.15) is twice the elapsed time between the two intersections of the orbit with the ρ-axis. The latter can be computed, using (5.17) and considering without loss of generality the half-orbit where $\gamma > 0$, in the following way:

$$\begin{aligned}
d\rho/dt = \gamma = \sqrt{\delta^2 - E(\rho_0, \gamma_0)\, e^{2\mu\rho}/\rho^2} \quad &\Rightarrow \\
dt = d\rho / \sqrt{\delta^2 - E(\rho_0, \gamma_0)\, e^{2\mu\rho}/\rho^2} \quad &\Rightarrow \\
\int_0^{T/2} dt = \int_{\rho_{min}}^{\rho_{max}} d\rho / \sqrt{\delta^2 - E(\rho_0, \gamma_0)\, e^{2\mu\rho}/\rho^2} \quad &\Rightarrow \\
T/2 = \int_{\rho_{min}}^{\rho_{max}} d\rho / \sqrt{\delta^2 - E(\rho_0, \gamma_0)\, e^{2\mu\rho}/\rho^2}. &
\end{aligned}$$

As discussed in part (b) of the proof of theorem 5.3.10, the values of ρ_{min} and

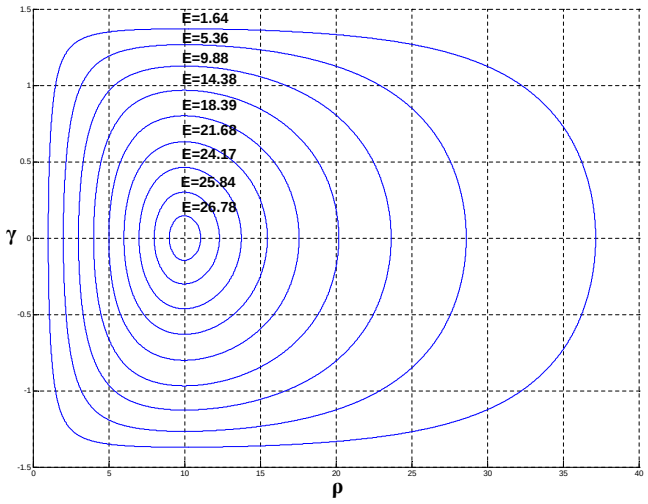

Figure 5.2: Phase portrait of system (5.15) when $\mu = 0.1, \delta = \sqrt{2}$

ρ_{max} are those where the orbit intersects the ρ-axis, given by the positive roots of (5.19). □

The periodic orbits of (5.15) are the level-sets of the "energy function" E, whose shape depends on the choice of the control law gain μ and on the magnitude δ of the initial relative velocity. Figure 5.2 shows a representative phase portrait of (5.15); the nine orbits in the plot are those corresponding to $\rho_{min} = n\mu/10, n = 1, 2, .., 9$, when $\mu = 0.1, \delta = \sqrt{2}$.

A very important feature of planar MMC is that the distance between the particles never goes below a certain minimum value ρ_{min} or above a maximum value ρ_{max}. By choosing the initial conditions and the gain appropriately, or with the simple modifications of the control law presented in [38], it is possible to make the orbits compatible with collision avoidance and wireless connectivity criteria which need to be met in practical multi-vehicle applications.

The relative motion of the particles in mutual motion camouflage displays some similarities with that of the Kepler problem (modeling the gravitational interaction of two bodies): both are conservative systems which produce periodic orbits that are collision-free (the orbits in the Kepler problem are elliptic). The theoretical analogies and differences between the two problems will be discussed in section 5.3.2.

To conclude the discussion of the relative motion, we derive the evolution of the remaining shape variable $\lambda(t)$, important for the reconstruction of the particle trajectories.

Proposition 5.3.12. *The evolution of $\lambda(t)$ is given by:*

$$\lambda(t) = \frac{\lambda_0 \, \rho_0 \, e^{\mu(\rho(t)-\rho_0)}}{\rho(t)}, \tag{5.20}$$

where λ_0, ρ_0 are initial conditions.

Proof. From the third differential equation in (5.13):

$$\begin{aligned} \frac{\dot{\lambda}}{\lambda} = \left(\mu - \frac{1}{\rho}\right) \gamma = \left(\mu - \frac{1}{\rho}\right) \dot{\rho} \quad &\Rightarrow \\ ln\left(\frac{\lambda}{\lambda_0}\right) = \mu\,(\rho - \rho_0) - ln\left(\frac{\rho}{\rho_0}\right) \quad &\Rightarrow \\ \lambda = \lambda_0 \, e^{\mu(\rho-\rho_0)} \rho_0 \, / \rho. & \end{aligned}$$

□

Notice that the sign of $\lambda(t)$ is constant, as opposed to $\gamma(t)$ which assumes both positive and negative values along every orbit.

Motion of the center of mass

We study the motion of the center of mass of the system by analyzing the evolution of the relevant reduced variables ζ, ξ and η; this requires solving the six-dimensional system (5.13)-(5.14). We accomplish this using the invariance of this system of equations to translations of the absolute reference frame, and the existence of a choice of translation that makes the dynamics of the center of mass a (scaled) copy of the relative motion dynamics.

Proposition 5.3.13. *The mutual motion camouflage dynamics* (5.13)-(5.14) *are invariant to translations of the absolute reference frame.*

Proof. Let $\mathbf{z_0}/2 \in \mathbb{R}^2$ be an arbitrary translation of the absolute reference frame. Denote the center of mass and relative motion variables with respect to the translated frame as: $\tilde{\mathbf{z}} = \mathbf{r_1} - \mathbf{z_0}/2 + \mathbf{r_2} - \mathbf{z_0}/2 = \mathbf{z} - \mathbf{z_0}$, $\tilde{\mathbf{r}} = \mathbf{r_1} - \mathbf{z_0}/2 - \mathbf{r_2} + \mathbf{z_0}/2 = \mathbf{r}$, $\tilde{\zeta} = |\tilde{\mathbf{z}}|$, $\tilde{\xi} = (\tilde{\mathbf{z}} \cdot \mathbf{k})/|\tilde{\mathbf{z}}|$, $\tilde{\eta} = (\tilde{\mathbf{z}} \cdot \mathbf{w})/|\tilde{\mathbf{z}}|$, $\tilde{\rho} = \rho$, $\tilde{\gamma} = \gamma$ and $\tilde{\lambda} = \lambda$. Consider now the differential equations to which the 'tilde' variables are subject. The relative motion equations will of course be identical to (5.13), since $\tilde{\rho} = \rho$, $\tilde{\gamma} = \gamma$ and $\tilde{\lambda} = \lambda$. Also unchanged is $\theta = |\mathbf{k}|$, whose computation does not involve the position of the particles. Moreover it is easy to verify that (5.10), (5.12) and hence (5.14) still hold for the 'tilde' variables (since λ and θ are unchanged). □

Lemma 5.3.14. *The following is a 3-dimensional invariant manifold for* (5.13)-(5.14)*:*

$$M_\sigma = \{(\rho, \gamma, \lambda, \zeta, \xi, \eta) : \zeta = \sigma\, \rho, \xi = \sigma\, \gamma, \eta = \sigma\, \lambda\}, \tag{5.21}$$

where $\sigma = \theta/\delta$.

Proof. The invariance of (5.21) can be proved as follows:

$$\begin{aligned}
\dot{\zeta} - \sigma\,\dot{\rho} &= \xi - \sigma\,\gamma \\
\dot{\xi} - \sigma\,\dot{\gamma} &= \eta^2/\zeta - \sigma\,\lambda^2/\rho - \mu\,\lambda\,(\eta - \sigma\,\lambda) \\
\dot{\eta} - \sigma\,\dot{\lambda} &= -\xi\,\eta/\zeta + \sigma\,\lambda\,\gamma/\rho + \mu\,\lambda\,(\xi - \sigma\,\gamma)
\end{aligned}$$

hence $\dot{\zeta} - \sigma\,\dot{\rho} = 0$, $\dot{\xi} - \sigma\,\dot{\gamma} = 0$ and $\dot{\eta} - \sigma\,\dot{\lambda} = 0$ when $\zeta = \sigma\,\rho, \xi = \sigma\,\gamma, \eta = \sigma\,\lambda$. The scaling factor $\sigma = \theta/\delta$ arises from the definition of the manifold: because $\xi^2 + \eta^2 = \theta^2$ and $\gamma^2 + \lambda^2 = \delta^2$, the choice $\sigma = \theta/\delta$ is the only one that satisfies $\xi = \sigma\,\gamma$ and $\eta = \sigma\,\lambda$. □

If the initial conditions of the system fall within the invariant manifold (5.21), the behavior of the center of mass reduced variables (ζ, ξ, η) is just a scaled version (with scaling factor $\sigma = \theta/\delta$) of the behavior of the relative motion variables (ρ, γ, λ). For a fixed absolute reference frame, only a restricted set of initial conditions will be within (5.21); nevertheless one can try to force any given arbitrary initial conditions on M_σ by choosing an appropriate translation of the absolute frame. It is a remarkable property of the planar MMC system that a frame translation which makes the initial conditions fall on (5.21) exists (almost) always.

Lemma 5.3.15. *Let* $\mathbf{r_1}(0)$, $\mathbf{r_2}(0)$, $\mathbf{x_1}(0)$ *and* $\mathbf{x_2}(0)$ *be arbitrary initial positions and orientations for the particles, defined with respect to an arbitrary absolute reference frame. Assume that* $\mathbf{r_1}(0) \neq \mathbf{r_2}(0)$ *and* $\nu_1\,\mathbf{x_1}(0) \neq \pm\nu_2\,\mathbf{x_2}(0)$, *i.e. the*

particles are not initially in the same position and their initial velocity vectors are neither identical nor opposite. Then there exists a (unique) translation $\mathbf{z_0}/2$ *of the reference frame such that, for* $\sigma = \theta/\delta$*:*

$$\begin{aligned} \zeta_0 &= \sigma\, \rho_0 \\ \xi_0 &= \sigma\, \gamma_0 \\ \eta_0 &= \sigma\, \lambda_0. \end{aligned} \tag{5.22}$$

The translation vector $\mathbf{z_0}$ *is given by:*

$$\mathbf{z_0} = \mathbf{z}(0) - \frac{1}{\delta^2} \begin{bmatrix} \mathbf{r}(0)\cdot\mathbf{g}(0) & -\mathbf{r}(0)\cdot\mathbf{h}(0) \\ \mathbf{r}(0)\cdot\mathbf{h}(0) & \mathbf{r}(0)\cdot\mathbf{g}(0) \end{bmatrix} \mathbf{k}(0). \tag{5.23}$$

Proof. Finding the desired translation vector $\mathbf{z_0}$ is equivalent to finding $\tilde{\mathbf{z}}(0) = \mathbf{z}(0) - \mathbf{z_0}$ that satisfies (5.22), i.e.:

$$|\tilde{\mathbf{z}}(0)| = \sigma\ |\mathbf{r}(0)| \tag{5.24}$$

$$(\tilde{\mathbf{z}}(0)\cdot\mathbf{k}(0))/\,|\tilde{\mathbf{z}}(0)| = \sigma\,(\mathbf{r}(0)\cdot\mathbf{g}(0))/\,|\mathbf{r}(0)| \tag{5.25}$$

$$(\tilde{\mathbf{z}}(0)\cdot\mathbf{w}(0))/\,|\tilde{\mathbf{z}}(0)| = \sigma\,(\mathbf{r}(0)\cdot\mathbf{h}(0))/\,|\mathbf{r}(0)|\,. \tag{5.26}$$

Using (5.24) and the fact that $\sigma \neq 0$ and $|\mathbf{r}(0)| \neq 0$ from the assumptions on the initial conditions, then (5.25) and (5.26) become:

$$\begin{aligned} \tilde{\mathbf{z}}(0)\cdot\mathbf{k}(0) &= \sigma^2\,(\mathbf{r}(0)\cdot\mathbf{g}(0)) \\ \tilde{\mathbf{z}}(0)\cdot\mathbf{w}(0) &= \sigma^2\,(\mathbf{r}(0)\cdot\mathbf{h}(0)), \end{aligned}$$

which in matrix form can also be expressed as:

$$\begin{bmatrix} \mathbf{k}^T(0) \\ \mathbf{w}^T(0) \end{bmatrix} \tilde{\mathbf{z}}(0) = \sigma^2 \begin{bmatrix} \mathbf{r}(0)\cdot\mathbf{g}(0) \\ \mathbf{r}(0)\cdot\mathbf{h}(0) \end{bmatrix}.$$

Since $\mathbf{w}(0) = \mathbf{k}^{\perp}(0)$ and both vectors are non-zero because of the assumptions on the initial conditions, the matrix on the left hand side is invertible (it is a scalar times an orthogonal matrix) and $\tilde{\mathbf{z}}(0)$ can be obtained from:

$$\begin{aligned}\tilde{\mathbf{z}}(0) &= \sigma^2 \begin{bmatrix} \mathbf{k}^T(0) \\ \mathbf{w}^T(0) \end{bmatrix}^{-1} \begin{bmatrix} \mathbf{r}(0)\cdot\mathbf{g}(0) \\ \mathbf{r}(0)\cdot\mathbf{h}(0) \end{bmatrix} = \frac{1}{\delta^2}\,[\mathbf{k}(0)\ \mathbf{w}(0)] \begin{bmatrix} \mathbf{r}(0)\cdot\mathbf{g}(0) \\ \mathbf{r}(0)\cdot\mathbf{h}(0) \end{bmatrix} \\ &= \frac{1}{\delta^2}[(\mathbf{r}(0)\cdot\mathbf{g}(0))\mathbf{k}(0) + (\mathbf{r}(0)\cdot\mathbf{h}(0))\mathbf{k}^{\perp}(0)] \\ &= \frac{1}{\delta^2} \begin{bmatrix} \mathbf{r}(0)\cdot\mathbf{g}(0) & -\mathbf{r}(0)\cdot\mathbf{h}(0) \\ \mathbf{r}(0)\cdot\mathbf{h}(0) & \mathbf{r}(0)\cdot\mathbf{g}(0) \end{bmatrix} \mathbf{k}(0).\end{aligned}$$

So the desired $\mathbf{z_0}$ exists and is given by (5.23) (by the definition of $\tilde{\mathbf{z}}$). □

The following theorem is a direct consequence of lemma 5.3.14 and lemma 5.3.15 and summarizes the "recipe" for finding the center of mass dynamics.

Theorem 5.3.16. *Let* $\mathbf{z_0}$ *be the vector given by* (5.23)*, which always exists provided* $\mathbf{r_1}(0) \neq \mathbf{r_2}(0)$ *and* $\nu_1\ \mathbf{x_1}(0) \neq \pm\nu_2\ \mathbf{x_2}(0)$*. Translate the initial absolute reference frame by* $\mathbf{z_0}/2$*. Then the evolution in time of* (ζ, ξ, η)*, describing the center of mass dynamics with respect to the translated reference frame, can simply be obtained scaling the evolution of the relative motion variables* (ρ, γ, λ) *by a factor* $\sigma = \theta/\delta$*.*

Proof. By lemma 5.3.15, if we define $\zeta = |\tilde{\mathbf{z}}|$, $\xi = (\tilde{\mathbf{z}}\cdot\mathbf{k})/|\tilde{\mathbf{z}}|$ and $\eta = (\tilde{\mathbf{z}}\cdot\mathbf{w})/|\tilde{\mathbf{z}}|$, where $\tilde{\mathbf{z}} = \mathbf{z} - \mathbf{z_0}$, then the initial conditions satisfy (5.22) and are therefore on the manifold (5.21). Proposition 5.3.13 shows that the state variables (ζ, ξ, η) are subject to the differential equations (5.13)-(5.14) and therefore the manifold

(5.21) is invariant as proved in lemma 5.3.14. Therefore the solution of the system will be confined within the invariant manifold (5.21) for all positive times, and $\zeta(t) = \sigma\,\rho(t), \xi(t) = \sigma\,\gamma(t), \eta(t) = \sigma\,\lambda(t), \forall t \geq 0$. □

As a consequence, the center of mass reduced dynamics (5.14), computed with respect to the translated absolute reference frame, is also a conservative system. The trajectories of the center of mass are centered at $\mathbf{z_0}/2$ and oscillate between a minimum distance $\zeta_{min} = \sigma\,\rho_{min}/2$ and a maximum distance $\zeta_{max} = \sigma\,\rho_{max}/2$.

Reconstruction of the individual trajectories

To complete the analysis of the planar MMC dynamics, we need to reconstruct the trajectories of the particles ($\mathbf{r_i}(t)$, $\mathbf{x_i}(t)$, $\mathbf{y_i}(t)$, $i = 1, 2$, $\forall t \geq 0$) from their initial conditions $\mathbf{r_i}(0)$, $\mathbf{x_i}(0)$, $\mathbf{y_i}(0)$ and the reduced relative motion trajectories $\rho(t), \gamma(t)$, which we have already derived qualitatively (for a quantitative derivation one can numerically integrate (5.15) over one period). We first reconstruct the trajectories of the relative motion ($\mathbf{r}(t)$, $\mathbf{g}(t)$, $\mathbf{h}(t)$) and center of mass motion ($\mathbf{z}(t)$, $\mathbf{k}(t)$, $\mathbf{w}(t)$) and then combine them to reconstruct the individual trajectories of the particles.

(i) Reconstruction of $\mathbf{r}(t)$, $\mathbf{g}(t)$, $\mathbf{h}(t)$, $\mathbf{z}(t)$, $\mathbf{k}(t)$, $\mathbf{w}(t)$

First of all, from the trajectories of $\rho(t), \gamma(t)$ it is immediate to derive those of $\lambda(t)$ using proposition 5.3.12. Moreover if we translate the absolute reference

frame (the one with respect to which the initial conditions are given) by $\mathbf{z_0}/2$, where $\mathbf{z_0}$ is computed from (5.23), we know that $\zeta(t) = \sigma\,\rho(t)$, $\xi(t) = \sigma\,\gamma(t)$, $\eta(t) = \sigma\,\lambda(t)$. Here $\zeta = |\tilde{\mathbf{z}}|$, $\xi = (1/\,|\tilde{\mathbf{z}}|)\,(\tilde{\mathbf{z}} \cdot \mathbf{k})$ and $\eta = (1/\,|\tilde{\mathbf{z}}|)\,(\tilde{\mathbf{z}} \cdot \mathbf{w})$, with $\tilde{\mathbf{z}} = \mathbf{z} - \mathbf{z_0}$.

Let the notation $(|\mathbf{v}|\,, \alpha_{\mathbf{v}})$ describe the polar coordinates of a vector $\mathbf{v} \in \mathbb{R}^2$ with respect to the absolute reference frame. Since $|\mathbf{g}| = |\mathbf{h}| = \delta$ and $\cos(\alpha_{\mathbf{h}} - \alpha_{\mathbf{r}}) = -\sin(\alpha_{\mathbf{g}} - \alpha_{\mathbf{r}})$ from the fact that $\mathbf{h} = \mathbf{g}^{\perp}$, we observe that:

$$\gamma = \left(\frac{\mathbf{r}}{|\mathbf{r}|} \cdot \mathbf{g}\right) = \delta \cos(\alpha_{\mathbf{g}} - \alpha_{\mathbf{r}}) \tag{5.27}$$

$$\lambda = \left(\frac{\mathbf{r}}{|\mathbf{r}|} \cdot \mathbf{h}\right) = -\delta \sin(\alpha_{\mathbf{g}} - \alpha_{\mathbf{r}}). \tag{5.28}$$

Hence:

$$\alpha_{\mathbf{g}} - \alpha_{\mathbf{r}} = \tan^{-1}(-\lambda/\gamma). \tag{5.29}$$

If we express $\dot{\mathbf{r}}$ in terms of the polar coordinates of $\mathbf{r}$:

$$\dot{\mathbf{r}} = \frac{d}{dt}\begin{bmatrix} \rho\cos\alpha_{\mathbf{r}} \\ \\ \rho\sin\alpha_{\mathbf{r}} \end{bmatrix} = \begin{bmatrix} \gamma\cos\alpha_{\mathbf{r}} - \rho\sin\alpha_{\mathbf{r}}\,\dot{\alpha_{\mathbf{r}}} \\ \\ \gamma\sin\alpha_{\mathbf{r}} + \rho\cos\alpha_{\mathbf{r}}\,\dot{\alpha_{\mathbf{r}}} \end{bmatrix}$$

and we also express $\mathbf{g}$ in polar coordinates:

$$\begin{aligned} \mathbf{g} &= \begin{bmatrix} \delta\cos\alpha_{\mathbf{g}} \\ \\ \delta\sin\alpha_{\mathbf{g}} \end{bmatrix} = \begin{bmatrix} \delta\cos(\alpha_{\mathbf{r}} + (\alpha_{\mathbf{g}} - \alpha_{\mathbf{r}})) \\ \\ \delta\sin(\alpha_{\mathbf{r}} + (\alpha_{\mathbf{g}} - \alpha_{\mathbf{r}})) \end{bmatrix} = \\ &= \begin{bmatrix} \delta\,(\cos\alpha_{\mathbf{r}}\cos(\alpha_{\mathbf{g}} - \alpha_{\mathbf{r}}) - \sin\alpha_{\mathbf{r}}\sin(\alpha_{\mathbf{g}} - \alpha_{\mathbf{r}})) \\ \\ \delta\,(\cos\alpha_{\mathbf{r}}\sin(\alpha_{\mathbf{g}} - \alpha_{\mathbf{r}}) + \sin\alpha_{\mathbf{r}}\cos(\alpha_{\mathbf{g}} - \alpha_{\mathbf{r}})) \end{bmatrix} = \\ &= \begin{bmatrix} \gamma\cos\alpha_{\mathbf{r}} + \lambda\sin\alpha_{\mathbf{r}} \\ \\ -\lambda\cos\alpha_{\mathbf{r}} + \gamma\sin\alpha_{\mathbf{r}} \end{bmatrix}, \end{aligned}$$

then $\dot{\mathbf{r}} = \mathbf{g}$ clearly implies that:

$$\dot{\alpha_{\mathbf{r}}} = -\lambda/\rho = -\lambda_0\, \rho_0\, e^{\mu(\rho-\rho_0)}/\rho^2, \tag{5.30}$$

where we have also used (5.20). Solving (5.30) by quadratures yields the time evolution of the polar angle $\alpha_{\mathbf{r}}(t)$:

$$\alpha_{\mathbf{r}}(t) = \alpha_{\mathbf{r}}(0) - \lambda_0\, \rho_0\, e^{-\mu\rho_0} \int_0^t e^{\mu\rho(s)}/\rho^2(s)ds, \tag{5.31}$$

which completes the reconstruction of $\mathbf{r}(t)$ in polar coordinates since we already know $\rho(t)$.

Remark 5.3.17 Even if the evolution of its magnitude $\rho(t)$ is periodic with period T, the evolution of $\mathbf{r}(t)$ is not. We have in fact:

$$\alpha_{\mathbf{r}}(t+T) - \alpha_{\mathbf{r}}(t) = -\lambda_0\, \rho_0\, e^{-\mu\rho_0}\, (e^{\mu\rho}/\rho^2)_{int}, \tag{5.32}$$

which is non-zero since $(e^{\mu\rho}/\rho^2)_{int} \triangleq \int_t^{t+T} e^{\mu\rho(s)}/\rho^2(s)ds$ is the integral over one period of a positive function, and hence is positive, and $\lambda_0, \rho_0 \neq 0$ for all the initial conditions of theorem 5.3.10. Hence $\mathbf{r}(t)$ is aperiodic (for any period), unless in the special case that the right hand side of (5.32) gives a rational multiple of 2π. In all the other cases (hence almost for random initial conditions) $\alpha_{\mathbf{r}}$(t) spans over time the whole range $[-\pi, \pi)$ and $\mathbf{r}$(t) spans the whole annular region with inner radius ρ_{min} and outer radius ρ_{max}.

The reconstruction of $\mathbf{g}(t)$ in polar coordinates can be completed from that of $\mathbf{r}(t)$ using (5.29) and the fact that its magnitude is constant to the value δ. We can then also derive $\mathbf{h}(t)$ as $\mathbf{g}^{\perp}(t)$.

An analogous procedure can be followed to reconstruct $\tilde{\mathbf{z}}(t)$, $\mathbf{k}(t)$ and $\mathbf{w}(t)$ in polar coordinates, yielding:

$$\alpha_{\mathbf{k}} - \alpha_{\tilde{\mathbf{z}}} = \tan^{-1}(-\eta/\xi) = \tan^{-1}(-\lambda/\gamma) = \alpha_{\mathbf{g}} - \alpha_{\mathbf{r}} \tag{5.33}$$

$$\dot{\alpha}_{\tilde{\mathbf{z}}} = -\xi/\zeta = -\lambda/\rho = \dot{\alpha}_{\mathbf{r}}. \tag{5.34}$$

Hence $\alpha_{\tilde{\mathbf{z}}}(t) = \alpha_{\mathbf{r}}(t) + \alpha_{\tilde{\mathbf{z}}}(0) - \alpha_{\mathbf{r}}(0)$, which allows to complete the reconstruction of $\tilde{\mathbf{z}}$ in polar coordinates. Just like $\mathbf{r}$, $\tilde{\mathbf{z}}$ is generally aperiodic even if its magnitude $\zeta(t)$ has period T. Finally $\mathbf{k}$ can be reconstructed from $\tilde{\mathbf{z}}$ using (5.33), and $\mathbf{w} = \mathbf{k}^{\perp}$. The reconstructed trajectories (in polar coordinates) of $\mathbf{r}(t)$, $\mathbf{g}(t)$, $\mathbf{h}(t)$, $\tilde{\mathbf{z}}(t)$, $\mathbf{k}(t)$ and $\mathbf{l}(t)$ must be converted to cartesian coordinates for the reconstruction of the individual trajectories. In cartesian coordinates, we can compute $\mathbf{z} = \tilde{\mathbf{z}} + \mathbf{z_0}$ to have the scaled center of mass trajectory with respect to the original absolute reference frame.

(ii) Reconstruction of $\mathbf{r}_i(t)$, $\mathbf{x}_i(t)$, $\mathbf{y}_i(t)$

The individual particle trajectories can be reconstructed from $\mathbf{r}(t)$, $\mathbf{g}(t)$, $\mathbf{z}(t)$ and $\mathbf{k}(t)$ as follows (all vectors in cartesian coordinates):

$$\mathbf{r_1} = (\mathbf{r_1} + \mathbf{r_2} + \mathbf{r_1} - \mathbf{r_2})/2 = (\mathbf{z} + \mathbf{r})/2 \tag{5.35}$$

$$\mathbf{r_2} = (\mathbf{r_1} + \mathbf{r_2} - \mathbf{r_1} + \mathbf{r_2})/2 = (\mathbf{z} - \mathbf{r})/2 \tag{5.36}$$

$$\mathbf{x_1} = (\nu_1\mathbf{x_1} + \nu_2\mathbf{x_2} + \nu_1\mathbf{x_1} - \nu_2\mathbf{x_2})/(2\nu_1) = (\mathbf{k} + \mathbf{g})/(2\nu_1) \tag{5.37}$$

$$\mathbf{x_2} = (\nu_1\mathbf{x_1} + \nu_2\mathbf{x_2} - \nu_1\mathbf{x_1} + \nu_2\mathbf{x_2})/(2\nu_2) = (\mathbf{k} - \mathbf{g})/(2\nu_2). \tag{5.38}$$

To have a qualitative understanding of the reconstructed particle trajectories, it is more convenient to express them with respect to the translated (by $\mathbf{z_0}/2$) absolute reference frame. Introducing $\tilde{\mathbf{r}}_\mathbf{1} = \mathbf{r_1} - \mathbf{z_0}/2$ and $\tilde{\mathbf{r}}_\mathbf{2} = \mathbf{r_2} - \mathbf{z_0}/2$ we have (similarly to (5.35) and (5.36)): $\tilde{\mathbf{r}}_\mathbf{1} = (\tilde{\mathbf{z}}+\mathbf{r})/2$ and $\tilde{\mathbf{r}}_2 = (\tilde{\mathbf{z}}-\mathbf{r})/2$. The advantage is that now we can use (5.33), (5.34) and the fact that the reduced variables live in the manifold (5.21), to obtain the evolution in polar coordinates:

$$\begin{aligned}
|\tilde{\mathbf{r}}_\mathbf{1}| &= \frac{1}{2}\left|\begin{bmatrix} \zeta\,\cos\alpha_{\tilde{\mathbf{z}}} \\ \zeta\,\sin\alpha_{\tilde{\mathbf{z}}} \end{bmatrix} + \begin{bmatrix} \rho\,\cos\alpha_{\mathbf{r}} \\ \rho\,\sin\alpha_{\mathbf{r}} \end{bmatrix}\right| = \frac{1}{2}\sqrt{\zeta^2+\rho^2+2\rho\zeta\cos(\alpha_{\tilde{\mathbf{z}}}-\alpha_{\mathbf{r}})} \\
&= \frac{\rho}{2}\sqrt{\sigma^2+1+2\sigma\cos(\alpha_{\mathbf{k}}-\alpha_{\mathbf{g}})} = \frac{\rho}{2}\sqrt{\sigma^2+1+2\sigma\frac{\mathbf{k}}{\theta}\cdot\frac{\mathbf{g}}{\delta}} = \frac{\rho}{2\delta}|\mathbf{k}+\mathbf{g}| \\
&= \rho\,\frac{\nu_1}{\delta} \qquad (5.39)
\end{aligned}$$

$$\begin{aligned}
|\tilde{\mathbf{r}}_\mathbf{2}| &= \frac{1}{2}\left|\begin{bmatrix} \zeta\,\cos\alpha_{\tilde{\mathbf{z}}} \\ \zeta\,\sin\alpha_{\tilde{\mathbf{z}}} \end{bmatrix} - \begin{bmatrix} \rho\,\cos\alpha_{\mathbf{r}} \\ \rho\,\sin\alpha_{\mathbf{r}} \end{bmatrix}\right| = \frac{1}{2}\sqrt{\zeta^2+\rho^2-2\rho\zeta\cos(\alpha_{\tilde{\mathbf{z}}}-\alpha_{\mathbf{r}})} \\
&= \frac{\rho}{2}\sqrt{\sigma^2+1-2\sigma\cos(\alpha_{\mathbf{k}}-\alpha_{\mathbf{g}})} = \frac{\rho}{2}\sqrt{\sigma^2+1-2\sigma\frac{\mathbf{k}}{\theta}\cdot\frac{\mathbf{g}}{\delta}} = \frac{\rho}{2\delta}|\mathbf{k}-\mathbf{g}| \\
&= \rho\,\frac{\nu_2}{\delta} \qquad (5.40)
\end{aligned}$$

$$\alpha_{\tilde{\mathbf{r}}_\mathbf{1}} = \tan^{-1}\left(\frac{\zeta\,\sin\alpha_{\tilde{\mathbf{z}}}+\rho\,\sin\alpha_{\mathbf{r}}}{\zeta\,\cos\alpha_{\tilde{\mathbf{z}}}+\rho\,\cos\alpha_{\mathbf{r}}}\right) = \tan^{-1}\left(\frac{(a+1)\,\sin\alpha_{\mathbf{r}}+b\cos\alpha_{\mathbf{r}}}{(a+1)\,\cos\alpha_{\mathbf{r}}-b\sin\alpha_{\mathbf{r}}}\right)$$

$$\alpha_{\tilde{\mathbf{r}}_\mathbf{2}} = \tan^{-1}\left(\frac{\zeta\,\sin\alpha_{\tilde{\mathbf{z}}}-\rho\,\sin\alpha_{\mathbf{r}}}{\zeta\,\cos\alpha_{\tilde{\mathbf{z}}}-\rho\,\cos\alpha_{\mathbf{r}}}\right) = \tan^{-1}\left(\frac{(a-1)\,\sin\alpha_{\mathbf{r}}+b\sin\alpha_{\mathbf{r}}}{(a-1)\,\cos\alpha_{\mathbf{r}}-b\sin\alpha_{\mathbf{r}}}\right)$$

where:

$a \triangleq \sigma\cos(\alpha_{\tilde{\mathbf{z}}}(0)-\alpha_{\mathbf{r}}(0)) = \sigma\cos(\alpha_{\mathbf{k}}(0)-\alpha_{\mathbf{g}}(0)) = \sigma\frac{\mathbf{k}(0)}{\theta}\cdot\frac{\mathbf{g}(0)}{\delta} = \frac{\nu_1^2-\nu_2^2}{\delta^2}$,

$b \triangleq \sigma\sin(-\alpha_{\tilde{\mathbf{z}}}(0)+\alpha_{\mathbf{r}}(0)) = -\sigma\sin(\alpha_{\mathbf{k}}(0)-\alpha_{\mathbf{g}}(0))$.

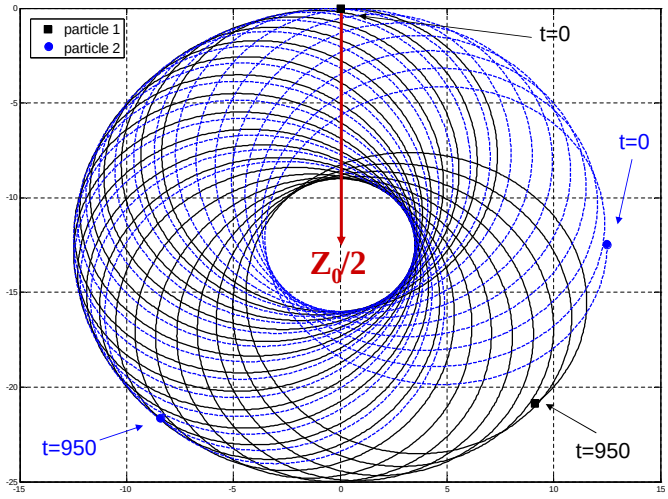

Figure 5.3: Particle trajectories generated by planar mutual motion camouflage when $\mu = 0.1$, $\delta = \theta = \sqrt{2}$, $\nu_1 = \nu_2 = 1$, $\mathbf{r_1}(0) = [0; 0]$, $\mathbf{r_2}(0) = [12.5; -12.5]$.

It derives that, as $\mathbf{r}(t)$ spans in time the whole annular region with inner radius ρ_{min} and outer radius ρ_{max}, the particles have the following individual behavior:

- particle 1 spans the annular region centered in $\mathbf{z_0}/2$ and having inner radius $\rho_{min}\,\nu_1/\delta$ and outer radius $\rho_{max}\,\nu_1/\delta$

- particle 2 spans the annular region centered in $\mathbf{z_0}/2$ and having inner radius $\rho_{min}\,\nu_2/\delta$ and outer radius $\rho_{max}\,\nu_2/\delta$.

Figure 5.3 shows an example of trajectories generated by planar mutual motion camouflage; in this particular case the speeds of the two individuals are identical, hence they cover the same annular region.

The planar dynamics of mutual motion camouflage produce therefore tra-

jectories with interesting region-filling properties. In [38], we have introduced simple modifications to the motion camouflage proportional guidance law (and hence to the coupled dynamics resulting from mutual pursuit) to exploit these properties for the solution of certain coverage path-planning problems on a plane.

5.3.2 Comparison with the Kepler problem

The Kepler problem is the study of the trajectories of two bodies resulting from their mutual gravitational interaction, and has been one of the most extensively studied problems since the seventeenth century. Here we just recall some results from classical mechanics [22] and the theory of reduction of *simple mechanical systems with symmetry* [48] which are useful to carry forward the analogy with mutual motion camouflage.

The well-known equations of motion for the Kepler problem, for unit-mass particles, are:

$$\ddot{\mathbf{r}}_1 = -\ddot{\mathbf{r}}_2 = g\,\frac{\mathbf{r}_2 - \mathbf{r}_1}{|\mathbf{r}_2 - \mathbf{r}_1|^3}, \tag{5.41}$$

and are the Euler-Lagrange equations for the classical Lagrangian:

$$L(\mathbf{r}_1, \mathbf{r}_2, \dot{\mathbf{r}}_1, \dot{\mathbf{r}}_2) = K(\dot{\mathbf{r}}_1, \dot{\mathbf{r}}_2) - V(\mathbf{r}_1, \mathbf{r}_2) = \frac{|\dot{\mathbf{r}}_1|^2 + |\dot{\mathbf{r}}_2|^2}{2} + \frac{g}{|\mathbf{r}_2 - \mathbf{r}_1|}. \tag{5.42}$$

Here $K(\dot{\mathbf{r}}_1, \dot{\mathbf{r}}_2) = (|\dot{\mathbf{r}}_1|^2 + |\dot{\mathbf{r}}_2|^2)/2$ and $V(\mathbf{r}_1, \mathbf{r}_2) = -g/|\mathbf{r}_2 - \mathbf{r}_1|$ are the kinetic and potential energies. Reduction by the symmetry group of absolute reference frame translations (where the momentum map is given by linear momentum)

yields the reduced equations:

$$\ddot{\mathbf{r}} = -2\,g\,\frac{\mathbf{r}}{|\mathbf{r}|^3}, \tag{5.43}$$

associated to the Lagrangian:

$$L'(\mathbf{r},\dot{\mathbf{r}}) = K'(\dot{\mathbf{r}}) - V'(\mathbf{r}) = \frac{|\dot{\mathbf{r}}|^2}{4} + \frac{g}{|\mathbf{r}|}. \tag{5.44}$$

A further symmetry reduction, with respect to the group of absolute frame rotations, is associated to the conservation of the angular-momentum-like vector $\mathbf{l} = \mathbf{r} \times \dot{\mathbf{r}}$; notice that the conservation of $\mathbf{l}$ implies that the relative motion of the bodies in the Kepler problem is constrained to the fixed plane orthogonal to $\mathbf{l}$. The resulting "shape" dynamics are:

$$\ddot{\rho} = -2\frac{g}{\rho^2} + 4\frac{l^2}{\rho^3}, \tag{5.45}$$

where $\rho = |\mathbf{r}| = |\mathbf{r_1} - \mathbf{r_2}|$ and $l = |\mathbf{l}|$ is the (constant) magnitude of $\mathbf{l}$. (5.45) is the Euler-Lagrange equation for a reduced Lagrangian:

$$L_l(\rho,\dot{\rho}) = K_l(\dot{\rho}) - V_l(\rho) = \frac{\dot{\rho}^2}{4} + \frac{g}{\rho} + \frac{l^2}{\rho^2}, \tag{5.46}$$

where $K_l(\dot{\rho}) = \dot{\rho}^2/4$ is the reduced kinetic energy and $V_l(\rho) = -g/\rho + l^2/\rho^2$ is the *amended potential*. Using the Legendre transformation to define the conjugate momentum $p = \partial L_l/\partial\dot{\rho} = \dot{\rho}/2$, we can also find the corresponding Hamiltonian $H_l(\rho,p) = 2p^2 - L_l(\rho,p)$, conserved along orbits of the reduced system. In terms of $\rho,\dot{\rho}$, this is the total energy $E(\rho,\dot{\rho}) = H_l(\rho,\dot{\rho}) = K_l(\dot{\rho}) + V_l(\rho)$.

The qualitative behavior of the orbits in shape space is determined by the values of l and H_l, as explained for example in [48]. In particular if $V_{l,min} \leq$

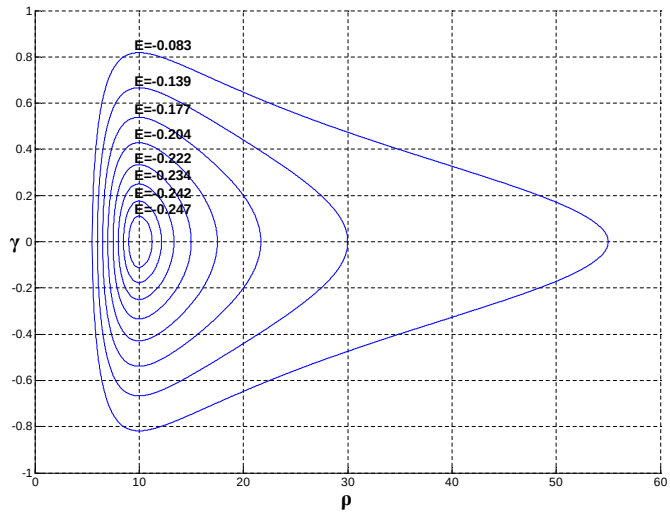

Figure 5.4: Phase portrait for Kepler problem when $l = g = 5$

$H_l < 0$, where $V_{l,min} = -g^2/(4l^2)$, then the orbits are periodic, with the distance $\rho(t)$ oscillating between extrema ρ_{min} and ρ_{max} given by the solutions to $\rho^2\, H_l + g\,\rho - l^2 = 0$. As it is well known from classical mechanics [22], these orbits are periodic because they are the projections of relative position orbits ($\mathbf{r}(t)\,\forall t \geq 0$) that are themselves periodic (typically elliptical, and circular in the special case $H_l = V_{l,min}$).

Figure 5.4 shows a representative phase portrait for the Kepler problem in the reduced variables ρ and $\gamma = \dot{\rho}$, for comparison with the MMC problem (cf. Figure 5.2); the eight orbits plotted are those corresponding to $\rho_{min} = 5.5, 6, 6.5, ..., 9$, when $l = g = 5$.

Lagrangian and Hamiltonian aspects of planar MMC

The periodic orbits in the reduced (ρ, γ)-space of the Kepler problem (shown

in Figure 5.4) are level sets for the canonical Hamiltonian H_l; the latter corresponds to the total energy (kinetic plus amended potential) and is associated to a Lagrangian (L_l) of the classical form "kinetic energy - potential energy". We show that a similar structure exists for the reduced relative motion equations (5.15) of mutual motion camouflage, which are equivalent to the following second order scalar system:

$$\ddot{\rho} = \left(\frac{1}{\rho} - \mu\right) (\delta^2 - \dot{\rho}^2). \tag{5.47}$$

Theorem 5.3.18. *The following Lagrangian function (in the form "kinetic energy - potential energy") has* (5.47) *as its Euler-Lagrange equation:*

$$\begin{aligned} L_{mmc}(\rho, \dot{\rho}) &= K_{mmc}(\rho, \dot{\rho}) - V_{mmc}(\rho) = \tfrac{1}{2} M(\rho)\dot{\rho}^2 - V_{mmc}(\rho) \\ &= \tfrac{1}{2}\rho^2 e^{-2\mu\rho}\dot{\rho}^2 + \tfrac{1}{2}\delta^2\rho^2 e^{-2\mu\rho}. \end{aligned} \tag{5.48}$$

Proof. All smooth scalar second order differential equations admit a Lagrangian formulation [11], and so does (5.47). Assume that the Lagrangian has the desired form $L_{mmc} = M(\rho)\dot{\rho}^2/2 - V_{mmc}(\rho)$ for some functions $M(\rho)$ and $V_{mmc}(\rho)$. Note that $M(\rho)$ is the "generalized mass", which we allow to depend on ρ (otherwise the Euler-Lagrange equation would have no terms in $\dot{\rho}$). For a Lagrangian in this form, the Euler-Lagrange equation is:

$$0 = \frac{d}{dt}\left(\frac{\partial L_{mmc}}{\partial \dot{\rho}}\right) - \frac{\partial L_{mmc}}{\partial \rho} = M\ddot{\rho} + \frac{1}{2}\frac{\partial M}{\partial \rho}\dot{\rho}^2 + \frac{\partial V_{mmc}}{\partial \rho}.$$

Compare term by term with the following form of (5.47), obtained multiplying both sides by ρ (which is > 0) and by an arbitrary function $F(\rho) \neq 0$:

$$0 = \rho\, F(\rho)\ddot{\rho} + (1 - \mu\rho)F(\rho)\dot{\rho}^2 - (1 - \mu\rho)F(\rho)\delta^2.$$

Hence the Lagrangian (5.48) yields (5.47) if and only if:

$$M = \rho F(\rho) \tag{5.49}$$

$$\frac{1}{2}\frac{\partial M}{\partial \rho} = (1-\mu\rho)F(\rho) \tag{5.50}$$

$$\frac{\partial V_{mmc}}{\partial \rho} = -(1-\mu\rho)F(\rho)\delta^2. \tag{5.51}$$

The two equations (5.49)-(5.50) impose a differential constraint on F of the form:

$$\rho\, F'(\rho) + F(\rho) = 2\,(1-\mu\rho)F(\rho) \;\Rightarrow\; F'(\rho) = \left(\frac{1}{\rho} - 2\mu\right) F(\rho).$$

which admits solution $F(\rho) = \rho e^{-2\mu\rho}$, corresponding to $M(\rho) = \rho^2 e^{-2\mu\rho}$. Now substituting in (5.51) we can find $V_{mmc}(\rho)$ by quadrature; we choose for convenience to integrate from $\rho = 0$ (which we can do since we can fix V_{mmc} up to an additive constant):

$$V_{mmc}(\rho) = -\int_0^\rho \delta^2(1-\mu\tilde{\rho})\tilde{\rho}\, e^{-2\mu\tilde{\rho}} d\tilde{\rho} = -\frac{1}{2}\delta^2\rho^2 e^{-2\mu\rho}.$$

This completes the construction of a Lagrangian (equal to (5.48)) which has the desired form and has (5.47) as its Euler-Lagrange equation. □

Corollary 5.3.19. *The mutual motion camouflage relative motion equations* (5.15) *correspond to the Hamiltonian vector field for the following Hamiltonian function (which can be interpreted as "total energy"):*

$$\begin{aligned} H_{mmc}(\rho,\dot{\rho}) &= K_{mmc}(\rho,\dot{\rho}) + V_{mmc}(\rho) \\ &= \tfrac{1}{2}\rho^2 e^{-2\mu\rho}\dot{\rho}^2 - \tfrac{1}{2}\delta^2\rho^2 e^{-2\mu\rho}, \end{aligned} \tag{5.52}$$

with respect to the non-canonical Poisson bracket:

$$\{f,g\}_{(\rho,\gamma)} = \nabla f^T \begin{bmatrix} 0 & \frac{e^{2\mu\rho}}{\rho^2} \\ -\frac{e^{2\mu\rho}}{\rho^2} & 0 \end{bmatrix} \nabla g,\ \forall f,g \in C^\infty(\mathbb{R}^2).$$

I.e. (5.15) *can be obtained as:*

$$\begin{aligned} \dot{\rho} &= \{\rho, H_{mmc}(\rho,\gamma)\}_{(\rho,\gamma)} \\ \dot{\gamma} &= \{\gamma, H_{mmc}(\rho,\gamma)\}_{(\rho,\gamma)}. \end{aligned} \tag{5.53}$$

Proof. Let p be the conjugate momentum associated to the Lagrangian function (5.48): $p = \partial L_{mmc}/\partial\dot{\rho} = M(\rho)\dot{\rho} = \rho^2 e^{-2\mu\rho}\dot{\rho}$. Then the canonical Hamiltonian associated to (5.48) is $H_{mmc}(\rho,p) = p\,\dot{\rho}(\rho,p) - L_{mmc}(\rho,\dot{\rho}(\rho,p)) = p^2 e^{2\mu\rho}/(2\rho^2) - \delta^2\rho^2 e^{-2\mu\rho}/2$, which in terms of $\rho,\dot{\rho}$ is exactly the total energy: $H_{mmc}(\rho,\dot{\rho}) = -\rho^2(\delta^2 - \dot{\rho}^2)e^{-2\mu\rho}/2 = K_{mmc}(\rho,\dot{\rho}) + V_{mmc}(\rho)$.

Since H_{mmc} is a conserved quantity:

$$\frac{dH_{mmc}}{dt} = \frac{\partial H_{mmc}}{\partial\rho}\dot{\rho} + \frac{\partial H_{mmc}}{\partial\gamma}\dot{\gamma} = 0,$$

and we can define a function $\beta(\rho,\gamma)$:

$$\beta(\rho,\gamma) = \frac{\dot{\rho}}{\frac{\partial H_{mmc}}{\partial\gamma}} = -\frac{\dot{\gamma}}{\frac{\partial H_{mmc}}{\partial\rho}}$$

such that the following holds:

$$\begin{aligned} \dot{\rho} &= \beta(\rho,\gamma)\,\tfrac{\partial H_{mmc}}{\partial\gamma} \\ \dot{\gamma} &= -\beta(\rho,\gamma)\,\tfrac{\partial H_{mmc}}{\partial\rho}. \end{aligned} \tag{5.54}$$

With the system in the form (5.54), it is easy to identify a choice of the Poisson bracket:

$$\{f,g\}_{(\rho,\gamma)} = \nabla f^T \begin{bmatrix} 0 & \beta(\rho,\gamma) \\ -\beta(\rho,\gamma) & 0 \end{bmatrix} \nabla g, \tag{5.55}$$

such that (5.53) holds. It is a simple exercise to verify that (5.55) satisfies all the properties for a (non-canonical) Poisson bracket. Notice that the above argument,

due to Jacobi, can be applied to any two dimensional system to find a Poisson bracket from knowledge of a conserved quantity. Finally, we complete the proof showing that $\beta(\rho,\gamma) = e^{2\mu\rho}/\rho^2$ in the case of system (5.15) with Hamiltonian (5.52):

$$\beta(\rho,\gamma) = \frac{\dot{\rho}}{\frac{\partial H_{mmc}}{\partial \gamma}} = \frac{\gamma}{\gamma\rho^2\, e^{-2\mu\rho}} = \frac{e^{2\mu\rho}}{\rho^2}.$$

□

The reduced relative motion equations of mutual motion camouflage have therefore underlying Lagrangian and Hamiltonian structures almost of the "classical" type, and similar to those of their Kepler problem counterparts. In particular the conserved quantity (5.16) is nothing else that a scaled version of the Hamiltonian H_{mmc}, which can be interpreted as the total energy of the reduced system.

The analogies between mutual motion camouflage and Kepler problem do not extend to the complete relative motion equations (those describing the evolution of the whole relative position vector $\mathbf{r}(t)$ instead of just its magnitude $\rho(t)$). One obvious difference is that in the Kepler problem the relative motion trajectories are periodic (when $V_{l,min} \leq H_l < 0$) whereas in MMC they are aperiodic. An even more fundamental difference is that the relative motion equations in the Kepler problem are associated to a Lagrangian $L'(\mathbf{r},\dot{\mathbf{r}})$ (whose reduction by symmetry is what induces the Lagrangian structure on the shape dynamics), while the relative motion equations in mutual motion camouflage have no underlying

Lagrangian structure. We dedicate the last part of this section to proving this fact, using the following result on the inverse problem of the calculus of variations for two-dimensional systems.

Theorem 5.3.20 (**J. Douglas [18]**). *Given the system composed of two scalar second order differential equations:*

$$\begin{aligned} \ddot{y} &= F(t, y, z, \dot{y}, \dot{z}) \\ \ddot{z} &= G(t, y, z, \dot{y}, \dot{z}), \end{aligned} \tag{5.56}$$

where F and G are smooth functions, then the existence (or lack thereof) of a Lagrangian function for which (5.56) *are the Euler-Lagrange equations, can be derived studying the matrix:*

$$\Delta = \begin{bmatrix} A & B & C \\ A_1 & B_1 & C_1 \\ A_2 & B_2 & C_2 \end{bmatrix}, \tag{5.57}$$

whose elements are expressions in the partial derivatives of F and G:

$$\begin{aligned} A &= dF_{\dot{z}}/dt - 2F_z - F_{\dot{z}}(F_{\dot{y}} + G_{\dot{z}})/2 \\ B &= -dF_{\dot{y}}/dt + dG_{\dot{z}}/dt + 2(F_y - G_z) \\ &\quad +(F_{\dot{y}} - G_{\dot{z}})(F_{\dot{y}} + G_{\dot{z}})/2 \\ C &= -dG_{\dot{y}}/dt + 2G_y + G_{\dot{y}}(F_{\dot{y}} + G_{\dot{z}})/2 \\ A_1 &= dA/dt - F_{\dot{y}}A - F_{\dot{z}}B/2 \\ B_1 &= dB/dt - G_{\dot{y}}A - (F_{\dot{y}} + G_{\dot{z}})B/2 - F_{\dot{z}}C \\ C_1 &= dC/dt - G_{\dot{y}}B/2 - G_{\dot{z}}C \end{aligned}$$

$$
\begin{aligned}
A_2 &= dA_1/dt - F_{\dot{y}}A_1 - F_{\dot{z}}B_1/2 \\
B_2 &= dB_1/dt - G_{\dot{y}}A_1 - (F_{\dot{y}} + G_{\dot{z}})B_1/2 - F_{\dot{z}}C_1 \\
C_2 &= dC_1/dt - G_{\dot{y}}B_1/2 - G_{\dot{z}}C_1.
\end{aligned}
$$

In particular a Lagrangian function for (5.56) *certainly exists in one of the following cases:*

(L1) rank(Δ)*=0*

(L2) rank(Δ)*=1, and the roots* λ, μ *of the quadratic equation* $A\xi^2 + B\xi + C = 0$ *are distinct and satisfy* $\lambda\lambda_{\dot{z}} - \lambda_{\dot{y}} = 0$, $\mu\mu_{\dot{z}} - \mu_{\dot{y}} = 0$.

Conversely a Lagrangian function certainly does not exist in the following cases:

(NL1) rank(Δ)*=2, and* $D = (BC_1 - B_1C)(AB_1 - A_1B) - (CA_1 - C_1A)^2 = 0$

(NL2) rank(Δ)*=3.*

In all the other cases, the existence of a Lagrangian depends on complicated algebraic conditions, involving the solutions to certain linear partial differential equations, or the exactness of certain differential forms, for which we refer the reader to [18].

Theorem 5.3.21. *The relative motion equations* (5.9) *of planar MMC are equivalent to the second order two-dimensional system:*

$$
\ddot{\mathbf{r}} = \mu \left[\left(\frac{\mathbf{r}}{|\mathbf{r}|} \cdot \dot{\mathbf{r}} \right) \dot{\mathbf{r}} - |\dot{\mathbf{r}}|^2 \, \frac{\mathbf{r}}{|\mathbf{r}|} \right], \tag{5.58}
$$

and are not the Euler-Lagrange equations for any Lagrangian function.

Proof. The unit vectors $\mathbf{g}/|\mathbf{g}|$ and $\mathbf{h}/|\mathbf{h}|$ form an orthonormal basis for $\mathbb{R}^2$ (here

$\mathbf{h} = \mathbf{g}^{\perp}$). We can therefore write $\mathbf{r}/|\mathbf{r}|$ as:

$$\frac{\mathbf{r}}{|\mathbf{r}|} = \left(\frac{\mathbf{r}}{|\mathbf{r}|} \cdot \frac{\mathbf{g}}{|\mathbf{g}|}\right) \frac{\mathbf{g}}{|\mathbf{g}|} + \left(\frac{\mathbf{r}}{|\mathbf{r}|} \cdot \frac{\mathbf{h}}{|\mathbf{h}|}\right) \frac{\mathbf{h}}{|\mathbf{h}|}.$$

Hence the system of equations (5.9) can be rewritten in second-order form as:

$$\ddot{\mathbf{r}} \;=\; -\mu \left(\frac{\mathbf{r}}{|\mathbf{r}|} \cdot \mathbf{h}\right) \mathbf{h} = \mu \left[\left(\frac{\mathbf{r}}{|\mathbf{r}|} \cdot \mathbf{g}\right) \mathbf{g} - |\mathbf{g}|^2 \, \frac{\mathbf{r}}{|\mathbf{r}|}\right],$$

or equivalently as in (5.58).

Define now as r_1 and r_2 the cartesian coordinates of $\mathbf{r}$ (not to be confused with the positions $\mathbf{r_1}$ and $\mathbf{r_2}$ of the particles). Then (5.58) is equivalent to the following system of second order scalar differential equations:

$$\begin{aligned} \ddot{r}_1 &= F(r_1, r_2, \dot{r}_1, \dot{r}_2) = \tfrac{\mu}{|\mathbf{r}|}(\dot{r}_1 \dot{r}_2 r_2 - r_1 \dot{r}_2^2) \\ \ddot{r}_2 &= G(r_1, r_2, \dot{r}_1, \dot{r}_2) = \tfrac{\mu}{|\mathbf{r}|}(\dot{r}_2 \dot{r}_1 r_1 - r_2 \dot{r}_1^2), \end{aligned} \tag{5.59}$$

where $|\mathbf{r}| = \sqrt{r_1^2 + r_2^2}$. It is then a lengthy but simple exercise to apply theorem 5.3.20 to (5.59) and show that it falls in case (NL1), hence it does not admit any Lagrangian. □

5.3.3 Mutual Motion Camouflage in three dimensions

We define as **Mutual Motion Camouflage (in 3d)** the system composed of two individuals, *moving at constant speeds in* $\mathbb{R}^3$ subject to dynamics (5.2), that are in mutual pursuit with the motion camouflage proportional guidance law (5.3), *with gains inversely proportional to the speeds*:

$$\begin{aligned} u_i(t) &= -\tfrac{\mu}{\nu_i} \left[\mathbf{z_i}(t) \cdot \left(\dot{\mathbf{r}}(t) \times \tfrac{\mathbf{r}(t)}{|\mathbf{r}(t)|}\right)\right] \\ v_i(t) &= +\tfrac{\mu}{\nu_i} \left[\mathbf{y_i}(t) \cdot \left(\dot{\mathbf{r}}(t) \times \tfrac{\mathbf{r}(t)}{|\mathbf{r}(t)|}\right)\right]. \end{aligned} \tag{5.60}$$

Here $\mu > 0$ is a constant gain, and $\mathbf{r} = \mathbf{r_1} - \mathbf{r_2}$.

Similarly to the planar case, we request the gains to be inversely proportional to the speeds to avoid the possible difference in speed from breaking the symmetry in the problem, instrumental to obtaining coordinated motion.

The study of mutual motion camouflage in three dimensions involves the analysis of the closed-loop system obtained by substituting (5.60) in the self-steering particle dynamics of the form (5.2). As in the planar case, the closed-loop system can be conveniently expressed by separating the equations of the relative motion from those of the center of mass motion. Introducing $\mathbf{r} \triangleq \mathbf{r_1} - \mathbf{r_2}$, $\mathbf{g} \triangleq \nu_1 \, \mathbf{x_1} - \nu_2 \, \mathbf{x_2}$, $\mathbf{z} \triangleq \mathbf{r_1} + \mathbf{r_2}$ and $\mathbf{k} \triangleq \nu_1 \, \mathbf{x_1} + \nu_2 \, \mathbf{x_2}$, that are some of the same variables of section 5.3.1 but here three-dimensional, the equations are:

$$\begin{aligned} \dot{\mathbf{r}} &= \mathbf{g} \\ \dot{\mathbf{g}} &= \mu \left[\mathbf{g} \times \left(\mathbf{g} \times \tfrac{\mathbf{r}}{|\mathbf{r}|} \right) \right], \end{aligned} \tag{5.61}$$

$$\begin{aligned} \dot{\mathbf{z}} &= \mathbf{k} \\ \dot{\mathbf{k}} &= \mu \left[\mathbf{k} \times \left(\mathbf{g} \times \tfrac{\mathbf{r}}{|\mathbf{r}|} \right) \right]. \end{aligned} \tag{5.62}$$

A vector quantity that plays an important role in the analysis of both the relative motion and the center of mass motion is the angular-momentum-like vector $\mathbf{l} \triangleq \mathbf{r} \times \mathbf{g}$, which evolves according to the following dynamics:

$$\dot{\mathbf{l}} = \mu \, \gamma \, \mathbf{l}, \tag{5.63}$$

where $\gamma \triangleq \mathbf{g} \cdot \mathbf{r}/|\mathbf{r}| = \dot{\rho}$, $\rho \triangleq |\mathbf{r}|$, as in section 5.3.1. Hence the direction of $\mathbf{l}$ remains constant in time (it depends only on the initial conditions). We will

denote the constant unit vector in the direction of $\mathbf{l}(t)$ as $\mathbf{e_l}$ and the time-varying magnitude $|\mathbf{l}(t)|$ as $l(t)$; the latter evolves according to:

$$l(t) = l(0)\, e^{\int_0^t \mu\gamma(s)ds} = l(0)e^{\mu(\rho(t)-\rho(0))}. \tag{5.64}$$

We will derive the three-dimensional trajectories induced by mutual motion camouflage in three steps: derivation of the relative motion between the particles, derivation of the center of mass trajectory, and finally reconstruction of the individual trajectories.

Relative motion

Using the triple vector product rule $\mathbf{a} \times (\mathbf{b} \times \mathbf{c}) = \mathbf{b}(\mathbf{a} \cdot \mathbf{c}) - \mathbf{c}(\mathbf{a} \cdot \mathbf{b})$, the system of equations (5.61) can be expressed in a form identical to (5.58):

$$\ddot{\mathbf{r}} = \dot{\mathbf{g}} = \mu \left[\left(\frac{\mathbf{r}}{|\mathbf{r}|} \cdot \dot{\mathbf{r}} \right) \dot{\mathbf{r}} - |\dot{\mathbf{r}}|^2 \frac{\mathbf{r}}{|\mathbf{r}|} \right]. \tag{5.65}$$

Of course the difference is that here $\mathbf{r} \in \mathbb{R}^3$, whereas in (5.58) $\mathbf{r} \in \mathbb{R}^2$. Nevertheless, $\mathbf{r}$ is always orthogonal to $\mathbf{e_l}$ (by the definition of $\mathbf{l}$) and, since the latter is fixed, $\mathbf{r}$ evolves on a fixed plane. Let $(\mathbf{e_x}, \mathbf{e_y}, \mathbf{e_l})$ be any orthonormal frame in $\mathbb{R}^3$ and $r_x \triangleq \mathbf{r} \cdot \mathbf{e_x}$, $r_y \triangleq \mathbf{r} \cdot \mathbf{e_y}$ and $r_l \triangleq \mathbf{r} \cdot \mathbf{e_l}$ the corresponding components of $\mathbf{r}$. Clearly r_l and $\dot{r}_l$ are always zero (the latter because $\dot{\mathbf{r}}$ is also orthogonal to $\mathbf{e_l}$), and the evolution of the projection of $\mathbf{r}$ on the plane orthogonal to $\mathbf{e_l}$, described by the two-dimensional vector $\mathbf{r_{xy}} \triangleq \begin{bmatrix} r_x \\ r_y \end{bmatrix}$, is given by:

$$\ddot{\mathbf{r}}_{\mathbf{xy}} = \mu \left[\left(\frac{\mathbf{r_{xy}}}{|\mathbf{r_{xy}}|} \cdot \dot{\mathbf{r}}_{\mathbf{xy}} \right) \dot{\mathbf{r}}_{\mathbf{xy}} - |\dot{\mathbf{r}}_{\mathbf{xy}}|^2 \frac{\mathbf{r_{xy}}}{|\mathbf{r_{xy}}|} \right]. \tag{5.66}$$

System (5.66) is truly equivalent to (5.58), and therefore the relative motion between the particles, constrained on the plane orthogonal to $\mathbf{e_l}$, has the same characteristics as in the planar MMC case: $\rho(t) = |\mathbf{r_{xy}}(t)| = |\mathbf{r}(t)|$ oscillates periodically between extrema ρ_{min} and ρ_{max} (depending on the value of the conserved quantity (5.16)) and $\mathbf{r_{xy}}(t)$ fills an annular region with radii ρ_{min} and ρ_{max}. As in the planar case, we call $\delta \triangleq |\dot{\mathbf{r}}| = |\dot{\mathbf{r}}_{\mathbf{xy}}|$ the constant relative speed between the particles.

Center of mass motion

The dynamics of the (scaled) center of mass velocity $\mathbf{k} \triangleq \dot{\mathbf{z}}$, can be expressed as a linear time-varying system: $\dot{\mathbf{k}}(t) = \mu(\mathbf{l}(t) \times \mathbf{k}(t))/\rho(t) = \mathrm{A}(t)\mathbf{k}(t)$, with $\mathrm{A}(t) \triangleq \mu(l(t)/\rho(t))\hat{\mathbf{e}}_\mathbf{l}$, $\hat{\mathbf{e}}_\mathbf{l} \in \mathrm{so}(3)$ being the skew-symmetric matrix associated to the unit vector $\mathbf{e_l}$. The solution of this system is:

$$\mathbf{k}(t) = \exp\left(\int_0^t \mathrm{A}(\sigma)d\sigma\right)\mathbf{k}(0) = \exp\left(\int_0^t \mu\frac{l(\sigma)}{\rho(\sigma)}d\sigma\,\hat{\mathbf{e}}_\mathbf{l}\right)\mathbf{k}(0).$$

From the properties of the exponential map ($\exp : \mathrm{so}(3) \to \mathrm{SO}(3)$):

$$\mathbf{k}(t) = \mathrm{Rot}\left(\mathbf{e_l}, \alpha(t)\right)\mathbf{k}(0), \tag{5.67}$$

where $\alpha(t) \triangleq \mu\int_0^t \frac{l(\sigma)}{\rho(\sigma)}d\sigma$. The notation $\mathrm{Rot}(\mathbf{e}, \alpha) \in \mathrm{SO}(3)$ denotes the matrix corresponding to counterclockwise rotation by an angle α about the axis $\mathbf{e} \in \mathbb{R}^3$.

Remark 5.3.22 Since $\rho(t) > 0\,\forall t$ and $l(t) \geq 0\,\forall t$, the "rotation angle" satisfies $\alpha(t) \geq 0\,\forall t$, $\alpha(t) = 0 \Leftrightarrow l(0) = 0$. Hence the center of mass velocity is constant in time only if either $\mathbf{r}(0)$ is parallel to $\mathbf{g}(0)$ (so that $l(0) = 0$) or $\mathbf{k}(0)$ is parallel

to $\mathbf{e_l} = \mathbf{l}(0)/l(0)$. On the other hand, the magnitude of $\mathbf{k}$, and hence the center of mass speed, is always constant in time (just as in the planar case); we call this quantity θ.

The rotation matrix in (5.67) can be expanded using Rodrigues formula, yielding the more explicit expression:

$$\mathbf{k}(t) = \cos(\alpha(t))\mathbf{k}(0) + \sin(\alpha(t))(\mathbf{e_l} \times \mathbf{k}(0)) + (1 - \cos(\alpha(t)))(\mathbf{k}(0) \cdot \mathbf{e_l})\mathbf{e_l}. \tag{5.68}$$

Equation (5.68) highlights the components of the center of mass velocity in three fixed (but in general not orthogonal) directions: $\mathbf{k}(0)$, $\mathbf{e_l}$ and $\mathbf{e_l} \times \mathbf{k}(0)$. Provided that $\mathbf{e_l} \times \mathbf{k}(0) \neq 0$ (if this is not the case, the center of mass velocity is constant as explained in remark 5.3.22), it is possible to conveniently rewrite (5.68) in terms of an orthonormal frame $(\mathbf{e_x}, \mathbf{e_y}, \mathbf{e_l})$ in $\mathbb{R}^3$, defined by $\mathbf{e_x} \triangleq \mathbf{e_l} \times \mathbf{k}(0)/|\mathbf{e_l} \times \mathbf{k}(0)|$ and $\mathbf{e_y} \triangleq \mathbf{e_l} \times \mathbf{e_x} = \mathbf{e_l} \times (\mathbf{e_l} \times \mathbf{k}(0))/|\mathbf{e_l} \times \mathbf{k}(0)| = (\mathbf{e_l}(\mathbf{k}(0) \cdot \mathbf{e_l}) - \mathbf{k}(0))/|\mathbf{e_l} \times \mathbf{k}(0)|$. It is a simple algebraic exercise to show that the resulting equation can be expressed as:

$$\mathbf{k}(t) = -|\mathbf{e_l} \times \mathbf{k}(0)|[\sin(-\alpha(t))\mathbf{e_x} + \cos(-\alpha(t))\mathbf{e_y}] + (\mathbf{k}(0) \cdot \mathbf{e_l})\mathbf{e_l}, \tag{5.69}$$

or component-wise:

$$\mathbf{k}(t) = \begin{bmatrix} k_x(t) \\ k_y(t) \\ k_l(t) \end{bmatrix} = \begin{bmatrix} -|\mathbf{e_l} \times \mathbf{k}(0)| \sin(-\alpha(t)) \\ -|\mathbf{e_l} \times \mathbf{k}(0)| \cos(-\alpha(t)) \\ \mathbf{k}(0) \cdot \mathbf{e_l} \end{bmatrix}. \tag{5.70}$$

From (5.70), it is clear that the center of mass velocity in the direction of $\mathbf{e_l}$ is constant, hence the component $z_l(t)$ of the (scaled) center of mass in

that direction grows linearly. On the other hand, it is possible to prove that the projection of $\mathbf{z}$ on the plane orthogonal to $\mathbf{e_l}$ evolves like the center of mass motion in the planar MMC case.

Theorem 5.3.23. *Let* $\mathbf{z_{xy}} \triangleq \begin{bmatrix} z_x \\ z_y \end{bmatrix} \in \mathbb{R}^2$ *be the projection of* $\mathbf{z}$ *on the plane orthogonal to* $\mathbf{e_l}$*, with components* $z_x \triangleq \mathbf{z} \cdot \mathbf{e_x}$*,* $z_y \triangleq \mathbf{z} \cdot \mathbf{e_y}$*. Then* $\mathbf{z_{xy}}$ *satisfies the following differential equations (equivalent to* (5.10)*):*

$$\ddot{\mathbf{z}}_{\mathbf{xy}}(t) = -\mu\, \lambda(t)\, \dot{\mathbf{z}}^{\perp}_{\mathbf{xy}}(t), \tag{5.71}$$

where $\lambda(t) \triangleq \mathbf{r_{xy}}(t) \cdot \dot{\mathbf{r}}^{\perp}_{\mathbf{xy}}(t)/\rho(t)$*.*

Proof. The first two components of (5.70) give $\dot{\mathbf{z}}_{\mathbf{xy}}(t)$. Hence by further differentiating with respect to time:

$$\ddot{\mathbf{z}}_{\mathbf{xy}}(t) = \dot{\alpha}(t) \begin{bmatrix} |\mathbf{e_l} \times \mathbf{k}(0)| \cos(-\alpha(t)) \\ -|\mathbf{e_l} \times \mathbf{k}(0)| \sin(-\alpha(t)) \end{bmatrix} = \dot{\alpha}(t)\, \dot{\mathbf{z}}^{\perp}_{\mathbf{xy}}(t) = \mu \frac{l(t)}{\rho(t)}\, \dot{\mathbf{z}}^{\perp}_{\mathbf{xy}}(t).$$

Now define λ as in section 5.3.1, using the vector $\mathbf{r_{xy}} \in \mathbb{R}^2$ in place of $\mathbf{r}$: $\lambda \triangleq \mathbf{r_{xy}} \cdot \dot{\mathbf{r}}^{\perp}_{\mathbf{xy}}/\rho$. Clearly it is still true (like in the planar case) that: $\gamma^2 + \lambda^2 = \delta^2$. Hence $\mathbf{r_{xy}} \cdot \dot{\mathbf{r}}^{\perp}_{\mathbf{xy}} = \mathbf{r} \cdot (\mathbf{e_l} \times \dot{\mathbf{r}}) = -(|\mathbf{r}|^2 |\dot{\mathbf{r}}|^2 - (\mathbf{r} \cdot \dot{\mathbf{r}})^2)/|\mathbf{r} \times \dot{\mathbf{r}}| = -\rho^2(\delta^2 - \gamma^2)/l = -\rho^2 \lambda^2 / l$, and therefore $\lambda = -l/\rho$. □

Recalling the results obtained in section 5.3.1 for the planar center of mass equations (5.10), it is clear that (5.71) implies that the projection of the center of mass motion on the plane orthogonal to $\mathbf{e_l}$ evolves aperiodically, filling in time an

annular region with radii proportional to ρ_{min} and ρ_{max}, and center (cfg. (5.23)):

$$\mathbf{z_{xy,0}} = \mathbf{z_{xy}}(0) - \frac{1}{\delta^2} \begin{bmatrix} \mathbf{r_{xy}}(0) \cdot \dot{\mathbf{r}}_{\mathbf{xy}}(0) & -\mathbf{r_{xy}}(0) \cdot \dot{\mathbf{r}}^{\perp}_{\mathbf{xy}}(0) \\ \mathbf{r_{xy}}(0) \cdot \dot{\mathbf{r}}^{\perp}_{\mathbf{xy}}(0) & \mathbf{r_{xy}}(0) \cdot \dot{\mathbf{r}}_{\mathbf{xy}}(0) \end{bmatrix} \dot{\mathbf{z}}_{\mathbf{xy}}(0). \tag{5.72}$$

The overall center of mass motion is therefore the vector sum of a linear motion in the direction of $\mathbf{e_l}$ (dependent on the initial conditions) and a planar MMC motion on a plane orthogonal to $\mathbf{e_l}$. The trajectory is a "modulated" helix, as shown below.

Theorem 5.3.24. *The curvature and torsion profiles of the center of mass trajectory in mutual motion camouflage (well-defined provided that* $\mathbf{k}(0)$ *is not parallel to* $\mathbf{e_l}$*) are given by:*

$$\kappa(t) = \frac{\beta(t)}{\theta^2} |\mathbf{k}(0) \times \mathbf{e_l}| \tag{5.73}$$

$$\tau(t) = \frac{\beta(t)}{\theta^2} (\mathbf{k}(0) \cdot \mathbf{e_l}), \tag{5.74}$$

and are identical to those of a "modulated" circular helix, with periodic angular frequency $\beta(t) \triangleq \dot{\alpha}(t) = \mu l(t)/\rho(t)$.

Proof. Recall that, given a thrice-differentiable curve $t \mapsto \mathbf{z}(t) \in \mathbb{R}^3$ with $|\dot{\mathbf{z}}(t)| = \theta$ (constant), the curvature and torsion profiles are defined as respectively $\kappa(t) \triangleq |\dot{\mathbf{t}}(t)|/\theta$ and $\tau(t) \triangleq (\dot{\mathbf{n}}(t) \cdot \mathbf{b}(t))/\theta$. Here $\mathbf{t}(t) \triangleq \dot{\mathbf{z}}(t)/\theta$, $\mathbf{n}(t) \triangleq \dot{\mathbf{t}}(t)/|\dot{\mathbf{t}}(t)|$ and $\mathbf{b}(t) \triangleq \mathbf{t}(t) \times \mathbf{n}(t)$ are the tangent, normal and binormal to the curve, which form its Frenet-Serret frame (see for example [8]). It is easy to verify that for a circular helix having angular frequency ω, radius $|a|/\omega$, pitch $2\pi b/\omega$ and constant speed $\sqrt{a^2 + b^2}$ (e.g. of the form $\mathbf{z}(t) = (a/\omega)\cos(\omega t)\,\mathbf{e_x} + (a/\omega)\sin(\omega t)\,\mathbf{e_y} + bt\,\mathbf{e_l}$, if

the helix axis is $\mathbf{e_l}$), the curvature and torsion profiles are constant and given by: $\kappa(t) = \frac{|a|\omega}{a^2+b^2}\,\forall t$, $\tau(t) = \frac{b\omega}{a^2+b^2}\,\forall t$.

Before computing the curvature and torsion of the center of mass trajectory, we remark the following consequences of the fact that $\dot{\mathbf{k}}(t) = -\beta(t)(\mathbf{k}(t) \times \mathbf{e_l})$:

$$\frac{d}{dt}|\mathbf{k}(t) \times \mathbf{e_l}| = \frac{(\mathbf{k}(t) \times \mathbf{e_l}) \cdot (\dot{\mathbf{k}}(t) \times \mathbf{e_l})}{|\mathbf{k}(t) \times \mathbf{e_l}|} = 0 \quad \forall t$$
$$\frac{d}{dt}(\mathbf{k}(t) \cdot \mathbf{e_l}) = \dot{\mathbf{k}}(t) \cdot \mathbf{e_l} = 0 \quad \forall t.$$

Hence, $\forall t > 0$, $|\mathbf{k}(t) \times \mathbf{e_l}| = |\mathbf{k}(0) \times \mathbf{e_l}|$ (which we assume nonzero) and $\mathbf{k}(t) \cdot \mathbf{e_l} = \mathbf{k}(0) \cdot \mathbf{e_l}$ are constant. Exploiting these facts, we can compute the relevant quantities for the center of mass trajectory as follows:

$$\mathbf{t}(t) = \frac{\mathbf{k}(t)}{\theta}, \quad \dot{\mathbf{t}}(t) = \frac{\dot{\mathbf{k}}(t)}{\theta} = \frac{-\beta(t)(\mathbf{k}(t) \times \mathbf{e_l})}{\theta},$$
$$\mathbf{n}(t) = \frac{\dot{\mathbf{t}}(t)}{|\dot{\mathbf{t}}(t)|} = \frac{-\mathbf{k}(t) \times \mathbf{e_l}}{|\mathbf{k}(0) \times \mathbf{e_l}|},$$
$$\dot{\mathbf{n}}(t) = \frac{-\dot{\mathbf{k}}(t) \times \mathbf{e_l}}{|\mathbf{k}(0) \times \mathbf{e_l}|} = \beta(t)\frac{\mathbf{e_l}(\mathbf{k}(0) \cdot \mathbf{e_l}) - \mathbf{k}(t)}{|\mathbf{k}(0) \times \mathbf{e_l}|},$$
$$\mathbf{b}(t) = \mathbf{t}(t) \times \mathbf{n}(t) = \frac{-\mathbf{k}(t)(\mathbf{k}(0) \cdot \mathbf{e_l}) + \mathbf{e_l}\theta^2}{\theta|\mathbf{k}(0) \times \mathbf{e_l}|}.$$

So the curvature and torsion of the center of mass trajectory are given by:

$$\kappa(t) = \frac{|\dot{\mathbf{t}}(t)|}{\theta} = \frac{\beta(t)}{\theta^2}|\mathbf{k}(0) \times \mathbf{e_l}|,$$
$$\tau(t) = \frac{\dot{\mathbf{n}}(t) \cdot \mathbf{b}(t)}{\theta} = \frac{\beta(t)}{\theta^2}(\mathbf{k}(0) \cdot \mathbf{e_l}).$$

If we compare with the curvature and torsion of a standard circular helix, we see that there is an exact correspondence between the center of mass trajectory and a "modulated" helix with periodic angular frequency $\beta(t)$, radius $|\mathbf{k}(0) \times \mathbf{e_l}|/\beta(t)$,

pitch $2\pi(\mathbf{k}(0)\cdot\mathbf{e_l})/\beta(t)$ and constant speed θ. It is indeed the "modulation" in the angular frequency (driven by the changes in relative distance between the particles) that makes the trajectory more complicated (and interesting) than a standard circular helix. □

Reconstruction of individual trajectories

Since $\mathbf{r_1} = (\mathbf{z}+\mathbf{r})/2$ and $\mathbf{r_2} = (\mathbf{z}-\mathbf{r})/2$, the individual dynamics are:

$$\ddot{\mathbf{r}}_\mathbf{1} = \frac{1}{2}(\ddot{\mathbf{z}}+\ddot{\mathbf{r}}) = \frac{\mu}{\rho}(\mathbf{l}\times\dot{\mathbf{r}}_\mathbf{1}) = \frac{\mu l}{\rho}\hat{\mathbf{e}}_\mathbf{l}\,\dot{\mathbf{r}}_\mathbf{1} \tag{5.75}$$

$$\ddot{\mathbf{r}}_\mathbf{2} = \frac{1}{2}(\ddot{\mathbf{z}}-\ddot{\mathbf{r}}) = \frac{\mu}{\rho}(\mathbf{l}\times\dot{\mathbf{r}}_\mathbf{2}) = \frac{\mu l}{\rho}\hat{\mathbf{e}}_\mathbf{l}\,\dot{\mathbf{r}}_\mathbf{2}, \tag{5.76}$$

and therefore $\mathbf{r_1}$ and $\mathbf{r_2}$ satisfy:

$$\dot{\mathbf{r}}_\mathbf{i}(t) = \mathrm{Rot}\,(\mathbf{e_l}, \alpha(t))\,\dot{\mathbf{r}}_\mathbf{i}(0), \quad i = 1,2, \tag{5.77}$$

with $\alpha(t) \triangleq \mu\int_0^t \frac{l(s)}{\rho(s)}ds$. The motion of the i-th agent ($i=1,2$) is rectilinear if $\dot{\mathbf{r}}_\mathbf{i}(0)$ is parallel to $\mathbf{e_l}$, or if $\mathbf{e_l} = \mathbf{0}$. In the other cases, it can be decomposed with respect to the orthonormal frame $(\mathbf{e_x}, \mathbf{e_y}, \mathbf{e_l})$ as it was done for the center of mass:

$$\dot{\mathbf{r}}_\mathbf{i}(t) = \begin{bmatrix} \dot{r}_{ix}(t) \\ \dot{r}_{iy}(t) \\ \dot{r}_{il}(t) \end{bmatrix} = \begin{bmatrix} -|\mathbf{e_l}\times\dot{\mathbf{r}}_\mathbf{i}(0)|\sin(-\alpha(t)) \\ -|\mathbf{e_l}\times\dot{\mathbf{r}}_\mathbf{i}(0)|\cos(-\alpha(t)) \\ \dot{\mathbf{r}}_\mathbf{i}(0)\cdot\mathbf{e_l} \end{bmatrix}. \tag{5.78}$$

Therefore each of the particles travels at constant speed ν_i along a "modulated" circular helix of the type described in theorem 5.3.24, with axis $\mathbf{e_l}$ and curvature

and torsion profiles:

$$\kappa_i(t) = \frac{\beta(t)}{\nu_i^2}|\dot{\mathbf{r}}_\mathbf{i}(0) \times \mathbf{e}_\mathbf{l}| \tag{5.79}$$

$$\tau_i(t) = \frac{\beta(t)}{\nu_i^2}(\dot{\mathbf{r}}_\mathbf{i}(0) \cdot \mathbf{e}_\mathbf{l}). \tag{5.80}$$

Figure 5.5 shows a typical set of trajectories obtained for two individuals engaged in mutual motion camouflage. Notice that the speeds of the two individuals are different in this example.

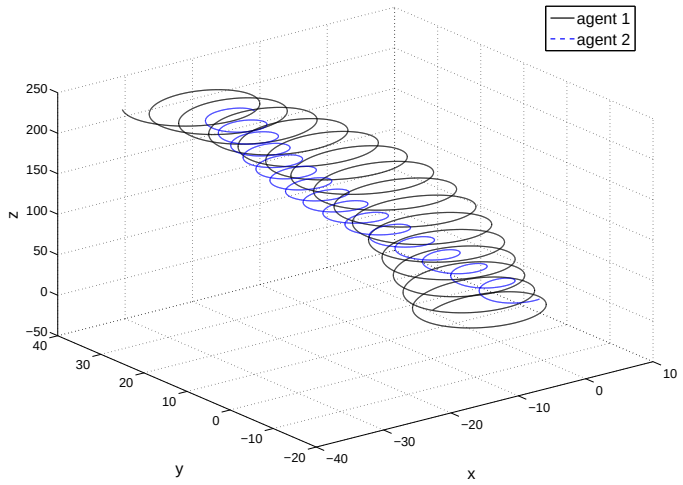

Figure 5.5: Representative trajectories obtained with mutual motion camouflage

Special trajectories

Among the trajectories that can be obtained with mutual motion camouflage, we highlight some interesting special cases and suitable choices of initial conditions to achieve them.

(i) *Rectilinear motion of both particles*

Both agents have constant velocity, and hence move in straight lines, if $\mathbf{e_l} = \mathbf{0} \Rightarrow \mathbf{r}(0) \times \dot{\mathbf{r}}(0) = \mathbf{0}$. Since we exclude collision configurations (otherwise the motion camouflage proportional guidance laws are not well-defined), this can happen only if either $\dot{\mathbf{r}}(0) = \nu_1 \mathbf{x_1} - \nu_2 \mathbf{x_2} = \mathbf{0}$ or if $\dot{\mathbf{r}}(0)$ is parallel to $\mathbf{r}(0)$. The first case is possible only if the agent speeds are equal ($\nu_1 = \nu_2$), and their initial directions of motion are identical; in this case the agents move along parallel lines. The second case corresponds to $\Gamma(\mathbf{r}(0), \dot{\mathbf{r}}(0)) = \pm 1$. Just as in planar MMC, the sets $\Gamma(\mathbf{r}, \dot{\mathbf{r}}) = \pm 1$ are (non-attracting) invariant manifolds, and therefore the particles remain in a state of motion camouflage with the distance either increasing (if $\Gamma = 1$) or reducing till collision (if $\Gamma = -1$).

(ii) *Rectilinear motion of one of the particles*

The i-th agent moves along a straight line if $\dot{\mathbf{r}}_\mathbf{i}(0) = \nu_i \mathbf{e_l}$. By the definition of $\mathbf{e_l}$, this requires $\dot{\mathbf{r}}_\mathbf{i}(0)$ to be orthogonal to $\mathbf{r}(0)$. For given initial relative position $\mathbf{r}(0)$, and desired initial velocity (and hence direction of the straight line trajectory) for one of the agents (say $\dot{\mathbf{r}}_\mathbf{1}(0) = \nu_1 \mathbf{x_1}(0) \perp \mathbf{r}(0)$), the only choice of velocity for the other agent that guarantees that $\mathbf{e_l} = \dot{\mathbf{r}}_\mathbf{1}(0)/\nu_1$ is: $\dot{\mathbf{r}}_\mathbf{2}(0) = \nu_2 \mathbf{x_2}(0) = \nu_1 \mathbf{x_1}(0) + (\mathbf{r}(0) \times \mathbf{x_1}(0))$.

(iii) *Rectilinear motion of the center of mass*

The center of mass moves along a straight line if $\mathbf{k}(0)$ is parallel to $\mathbf{e_l}$. Let $\mathbf{r}(0)$ be the initial relative position between the agents, and $\mathbf{e_l}$ a vector orthogonal to $\mathbf{r}(0)$ (the desired direction for the center of mass motion). For $\mathbf{k}(0)$ to be parallel to $\mathbf{e_l}$, the initial relative velocity $\mathbf{g}(0)$ must satisfy the condition $\mathbf{g}(0)/|\mathbf{g}(0)| =$

$\mathbf{r}(0)\times\mathbf{e_l}/|\mathbf{r}(0)\times\mathbf{e_l}|$. Since $\mathbf{k}(0)$ must be parallel to $\mathbf{l}(0)=\mathbf{r}(0)\times\mathbf{g}(0)$, it must also be orthogonal to $\mathbf{g}(0)$, and thus $2\nu_1=|\mathbf{k}(0)+\mathbf{g}(0)|=|\mathbf{k}(0)-\mathbf{g}(0)|=2\nu_2$. Hence the two agent speeds must be equal: $\nu_1=\nu_2\triangleq\nu$. The magnitudes $\delta=|\mathbf{g}(0)|$ and $\theta=|\mathbf{k}(0)|$ must be related to the common speed by the relation $\sqrt{\delta^2+\theta^2}=2\nu$ (if $\theta=0$ we have the planar mutual motion camouflage described in (v)). Provided that these conditions are satisfied, the following initial directions of motion for the agents guarantee that the center of mass will move in the direction $\mathbf{e_l}$ at speed θ: $\mathbf{x_1}(0)=\frac{\mathbf{k}(0)+\mathbf{g}(0)}{2\nu}=\frac{\delta}{2\nu}\frac{\mathbf{r}(0)\times\mathbf{e_l}}{|\mathbf{r}(0)\times\mathbf{e_l}|}+\frac{\theta}{2\nu}\mathbf{e_l}$, $\mathbf{x_2}(0)=\frac{\mathbf{k}(0)-\mathbf{g}(0)}{2\nu}=\frac{\theta}{2\nu}\mathbf{e_l}-\frac{\delta}{2\nu}\frac{\mathbf{r}(0)\times\mathbf{e_l}}{|\mathbf{r}(0)\times\mathbf{e_l}|}$.

(iv) *Motion of both particles along a double helix*

The trajectories of the particles (and of their center of mass) are true circular helices in the special case that the relative distance $\rho(t)$ remains constant in time. In that case in fact $\beta(t)=\dot{\alpha}(t)$ is constant in the curvature and torsion profiles (5.79)-(5.80). This occurs if the initial conditions fall on the equilibrium point $\rho(0)=1/\mu,\dot{\rho}(0)=0$ of the relative distance dynamics. Notice that $\dot{\rho}(0)=\gamma(0)=(\mathbf{g}(0)\cdot\mathbf{r}(0))/|\mathbf{r}(0)|=0$ requires $\mathbf{g}(0)$ to be orthogonal to $\mathbf{r}(0)$ (and of course to $\mathbf{e_l}$). Hence this special motion is achieved if initially the positions of the agents have distance $1/\mu$ and their velocities satisfy: $\frac{\mathbf{g}(0)}{|\mathbf{g}(0)|}=\frac{\nu_1\mathbf{x_1}(0)-\nu_2\mathbf{x_2}(0)}{|\nu_1\mathbf{x_1}(0)-\nu_2\mathbf{x_2}(0)|}=\frac{\mathbf{r}(0)\times\mathbf{e_l}}{\rho(0)}=\mu(\mathbf{r}(0)\times\mathbf{e_l})$.When this is the case: $\beta(t)=\dot{\alpha}(t)=\mu l(t)/\rho(t)=\mu^2|\mathbf{l}(0)|=\mu^2|\mathbf{r}(0)\times\mathbf{g}(0)|=\mu^2\delta\rho(0)=\mu\delta$, where $\delta=|\mathbf{g}(0)|=|\nu_1\mathbf{x_1}(0)-\nu_2\mathbf{x_2}(0)|$. The curvature and torsion for each agent, given by the constants $\kappa_i(t)=\mu\delta|\dot{\mathbf{r}}_\mathbf{i}(0)\times\mathbf{e_l}|/\nu_i^2$ and $\tau_i(t)=\mu\delta(\dot{\mathbf{r}}_\mathbf{i}(0)\cdot\mathbf{e_l})/\nu_i^2$, correspond to circular helices with angular frequency $\mu\delta$, pitch $2\pi(\dot{\mathbf{r}}_\mathbf{i}(0)\cdot\mathbf{e_l})/(\mu\delta)$ and radius

$|\dot{\mathbf{r}}_\mathbf{i}(0) \times \mathbf{e_l}|/(\mu\delta)$, covered at speed ν_i.

(v) *Planar mutual motion camouflage*

The last special case is the one in which $\mathbf{k}(0) = \mathbf{0}$. Then $\mathbf{k}(t) = \mathbf{0}\ \forall t \geq 0$ and thus $\dot{\mathbf{r}}_\mathbf{1}(t) = \dot{\mathbf{r}}(t)/2$, $\dot{\mathbf{r}}_\mathbf{2}(t) = -\dot{\mathbf{r}}(t)/2$. From the results found before, each agent moves on the fixed plane orthogonal to $\mathbf{e_l}$ (the direction of $\mathbf{l}(0)$), and the two agents perform a planar mutual motion camouflage on that plane. For the system to fall into this special case, with motion constrained on the plane orthogonal to a prescribed $\mathbf{e_l}$, the initial positions and velocities of the particles must satisfy the constraints $\nu_1\mathbf{x_1}(0) = -\nu_2\mathbf{x_2}(0)$ and $\frac{(\mathbf{r_1}(0)-\mathbf{r_2}(0))\times\nu_1\mathbf{x_1}(0)}{|(\mathbf{r_1}(0)-\mathbf{r_2}(0))\times\nu_1\mathbf{x_1}(0)|} = \mathbf{e_l}$. The first constraint can be satisfied only if the speeds of the particles are identical.

Figure 5.6 shows examples of the special trajectories described above (except the simple case of rectilinear motion of both agents).

Comparison with the Kepler problem

Most of the discussion presented in section 5.3.2 also holds for mutual motion camouflage in three dimensions. The relative distance between the particles still satisfies a second order system of the type (5.47) which, as proved before, is Lagrangian and has significant similarities with that of the Kepler problem. Another similarity is that the axis $\mathbf{e_l} = \mathbf{l}/|\mathbf{l}|$, with $\mathbf{l} = \mathbf{r} \times \dot{\mathbf{r}}$, is fixed in both problems, and therefore the relative position between the particles is constrained in both cases to a fixed plane (orthogonal to $\mathbf{e_l}$). Nevertheless, while in the Kepler

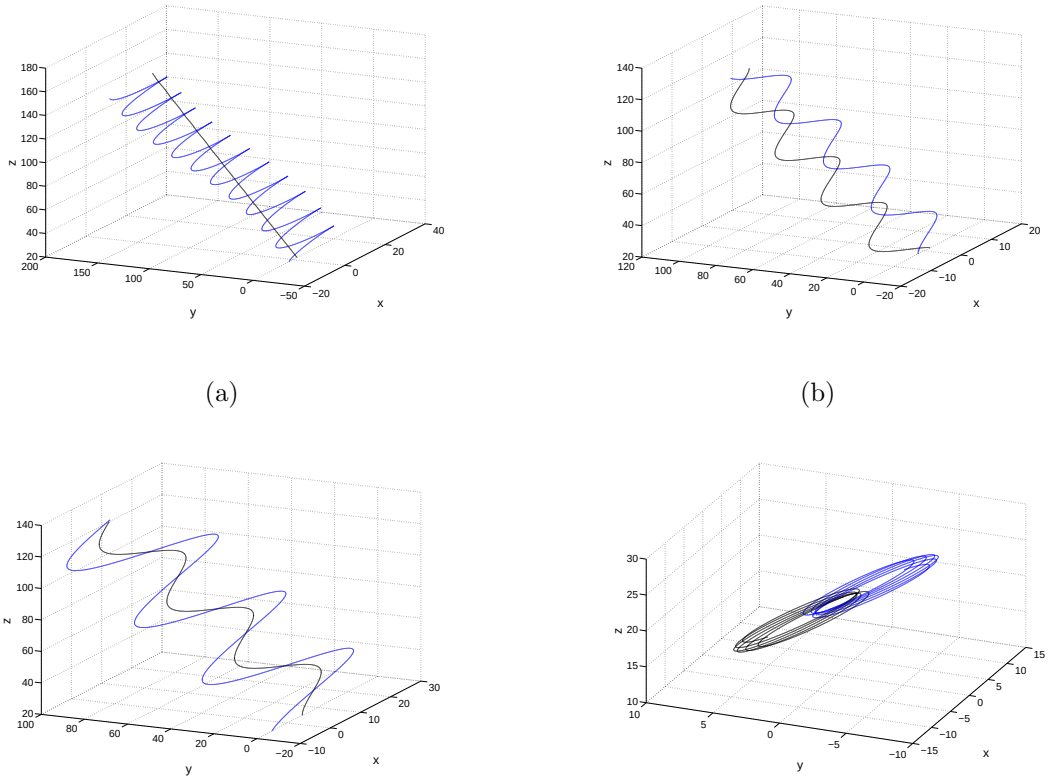

(a) (b)

(c) (d)

Figure 5.6: Examples of special trajectories obtained with MMC-3d: (a) rectilinear motion of one agent; (b) rectilinear motion of the center of mass; (c) double helix; (d) planar MMC.

	Kepler problem	**Mutual motion camouflage**
Full dynamics	$\ddot{\mathbf{r}}_\mathbf{1} = -\ddot{\mathbf{r}}_\mathbf{2} = -g\frac{\mathbf{r}}{\lvert\mathbf{r}\rvert^3}$	$\ddot{\mathbf{r}}_\mathbf{i} = \mu\left[\left(\frac{\mathbf{r}}{\lvert\mathbf{r}\rvert}\times\dot{\mathbf{r}}\right)\times\dot{\mathbf{r}}_i\right],\ i=1,2$
Conservation laws	$\dot{\mathbf{r}}_\mathbf{1}+\dot{\mathbf{r}}_\mathbf{2}$	$\lvert\dot{\mathbf{r}}_\mathbf{1}\rvert,\ \lvert\dot{\mathbf{r}}_\mathbf{2}\rvert,\ \delta\triangleq\lvert\dot{\mathbf{r}}_\mathbf{1}-\dot{\mathbf{r}}_\mathbf{2}\rvert$
Lagrangian	$L\triangleq\frac{\lvert\dot{\mathbf{r}}_\mathbf{1}\rvert^2+\lvert\dot{\mathbf{r}}_\mathbf{2}\rvert^2}{2}+\frac{g}{\lvert\mathbf{r}\rvert}$	none
Relative motion	$\ddot{\mathbf{r}} = -2g\frac{\mathbf{r}}{\lvert\mathbf{r}\rvert^3}$	$\ddot{\mathbf{r}} = \mu\left(\left(\frac{\mathbf{r}}{\lvert\mathbf{r}\rvert}\cdot\dot{\mathbf{r}}\right)\dot{\mathbf{r}}-\lvert\dot{\mathbf{r}}\rvert^2\frac{\mathbf{r}}{\lvert\mathbf{r}\rvert}\right)$
Conservation laws	$\mathbf{l}\triangleq\mathbf{r}\times\dot{\mathbf{r}}$	$\mathbf{e_l}\triangleq\frac{\mathbf{l}}{\lvert\mathbf{l}\rvert}$ (but not $l\triangleq\lvert\mathbf{l}\rvert$)
Lagrangian	$L'\triangleq\frac{\lvert\dot{\mathbf{r}}\rvert^2}{4}+\frac{g}{\lvert\mathbf{r}\rvert}$	none
Shape dynamics	$\ddot{\rho}=\frac{-2g}{\rho^2}+\frac{4l^2}{\rho^3}$	$\ddot{\rho}=\left(\frac{1}{\rho}-\mu\right)(\delta^2-\dot{\rho}^2)$
Lagrangian	$L_l\triangleq\frac{\dot{\rho}^2}{4}+\frac{g}{\rho}-\frac{l^2}{\rho^2}$	$L_{mmc}\triangleq\frac{\rho^2e^{-2\mu\rho}\dot{\rho}^2}{2}+\frac{\delta^2\rho^2e^{-2\mu\rho}}{2}$
Hamiltonian	$H_l\triangleq\frac{\dot{\rho}^2}{4}-\frac{g}{\rho}+\frac{l^2}{\rho^2}$	$H_{mmc}\triangleq\frac{\rho^2e^{-2\mu\rho}\dot{\rho}^2}{2}-\frac{\delta^2\rho^2e^{-2\mu\rho}}{2}$
Periodic orbits	if $\frac{-g^2}{4l^2}\leq H_l<0$	if $-\frac{\delta^2e^{-2}}{2\mu^2}\leq H_{mmc}<0$
Phase portrait	Figure 5.4	Figure 5.2

Table 5.1: Comparison between the Kepler problem and the dynamics of mutual motion camouflage (in 3d)

problem the magnitude of $\mathbf{l}$ is constant, in mutual motion camouflage it changes periodically. The main difference between the two problems is that while the relative motion in the Kepler problem (5.43) is Lagrangian, this is not the case for mutual motion camouflage; we observed in fact that the evolution of $\mathbf{r}(t)$ on the plane orthogonal to $\mathbf{e_l}$ is described by equation (5.66), equivalent to (5.58), that is not Lagrangian (as proved in section 5.3.2).

The comparison between the Kepler problem and mutual motion camouflage (in 3d) is summarized in table 5.1.

5.4 Swarming motion based on Mutual Motion Camouflage

The three-dimensional dynamics of mutual motion camouflage produce individual trajectories that are special types of helices with common axis $\mathbf{e_l}$ (recall (5.75)-(5.77)). Hence, a motion of the two individuals that is in average in the same absolute direction ($\mathbf{e_l}$), is achieved through a simple interaction with each other (given by the MCPG steering law). The following theorem describes a method, based on mutual motion camouflage, for obtaining this same feature in artificial collectives with an arbitrary number of individuals, hence producing a "swarming motion" in a common absolute direction through simple local interactions between the individuals. We use the term "swarming" for the resulting motion, to highlight that the individual trajectories are quite rich and sophisti-

cated, recalling more the "fluid" motion of insect swarms than the "rigid" motion of military planes in formation (or flocks of geese).

Theorem 5.4.1. *Consider a system of n individuals, e.g. robotic agents, modeled as unit-mass particles moving at constant speed with dynamics described by* (5.2)*. Let the individual steering controls be given by the following feedback laws (for* $i = 1, 2, ..., n$*):*

$$\begin{aligned} u_i(t) &= -\frac{\mu}{\nu_i}\left[\mathbf{z_i}(t)\cdot\left(\dot{\mathbf{r}}_{\mathbf{12}}(t)\times\frac{\mathbf{r_{12}}(t)}{|\mathbf{r_{12}}(t)|}\right)\right] \\ v_i(t) &= +\frac{\mu}{\nu_i}\left[\mathbf{y_i}(t)\cdot\left(\dot{\mathbf{r}}_{\mathbf{12}}(t)\times\frac{\mathbf{r_{12}}(t)}{|\mathbf{r_{12}}(t)|}\right)\right], \end{aligned} \tag{5.81}$$

where $\mu > 0$ *is a constant gain, and* $\mathbf{r_{12}} \triangleq \mathbf{r_1} - \mathbf{r_2}$*. Notice that, for* $i = 1, 2$*, steering laws* (5.81) *correspond to mutual motion camouflage.*

Then the resulting individual trajectories are the following special types of helices, with common axis $\mathbf{e_{l_{12}}} \triangleq \mathbf{r_{12}}(0)\times\dot{\mathbf{r}}_{\mathbf{12}}(0)/|\mathbf{r_{12}}(0)\times\dot{\mathbf{r}}_{\mathbf{12}}(0)|$*:*

$$\dot{\mathbf{r}}_{\mathbf{i}}(t) = \mathrm{Rot}\left(\mathbf{e_{l_{12}}}, \alpha_{12}(t)\right)\dot{\mathbf{r}}_{\mathbf{i}}(0), \quad i = 1, 2, ..., n. \tag{5.82}$$

Here the constant unit vector $\mathbf{e_{l_{12}}}$ *and the periodic scalar function* $\alpha_{12}(t)$ *arise from the mutual motion camouflage of the first two individuals, and have the same meaning and computation of the quantities* $\mathbf{e_l}$ *and* $\alpha(t)$ *introduced in section 5.3.3.*

Proof. The first two individuals ($i = 1, 2$) are in mutual motion camouflage, hence their individual trajectories are special helices of the type (5.82), as already showed in section 5.3.3. Hence we only need to prove (5.82) for $i > 2$. For that,

we use the following:

$$\dot{\mathbf{r}}_\mathbf{i} = \nu_i \mathbf{x}_\mathbf{i} \quad \Rightarrow \quad \ddot{\mathbf{r}}_\mathbf{i} = \nu_i u_i \mathbf{y}_\mathbf{i} + \nu_i v_i \mathbf{z}_\mathbf{i} = \frac{\mu}{|\mathbf{r_{12}}|}(\mathbf{l_{12}} \times \dot{\mathbf{r}}_\mathbf{i}), \tag{5.83}$$

where $\mathbf{l_{12}} \triangleq \mathbf{r_{12}} \times \dot{\mathbf{r}}_\mathbf{12}$. As discussed in the context of section 5.3.3, (5.83) has solution given by (5.82) since the direction of $\mathbf{l_{12}}$ is constant (because the first two individuals are engaged in mutual motion camouflage). □

Remark 5.4.2 Implementation of control laws (5.81) requires each individual to compute the vector $\dot{\mathbf{r}}_\mathbf{12}(t) \times \frac{\mathbf{r_{12}}(t)}{|\mathbf{r_{12}}(t)|}$. The two individuals in mutual motion camouflage need to just be able to sense their position and velocity relative to each other $(\mathbf{r_{12}}(t), \dot{\mathbf{r}}_\mathbf{12}(t))$. The other individuals can also locally compute the required quantities, provided they can sense their relative positions and velocities with respect to both individuals $i = 1, 2$. From knowledge of $\mathbf{r_{i1}}(t) \triangleq \mathbf{r_i} - \mathbf{r_1}$, $\mathbf{r_{i2}}(t) \triangleq \mathbf{r_i} - \mathbf{r_2}$ and the corresponding derivatives $\dot{\mathbf{r}}_\mathbf{i1}(t)$, $\dot{\mathbf{r}}_\mathbf{i2}(t)$, each individual can in fact compute $\mathbf{r_{12}}(t) = -\mathbf{r_{i1}}(t) + \mathbf{r_{i2}}(t)$ and $\dot{\mathbf{r}}_\mathbf{12}(t) = -\dot{\mathbf{r}}_\mathbf{i1}(t) + \dot{\mathbf{r}}_\mathbf{i2}(t)$.

Each particle subject to (5.82) moves at constant speed in the direction $\mathbf{e}_{\mathbf{l_{12}}}$ and fills an annular region on the plane orthogonal to $\mathbf{e}_{\mathbf{l_{12}}}$. As the direction of constant motion $\mathbf{e}_{\mathbf{l_{12}}}$ is common for each particle, the overall motion of the collective is a kind of "swarming motion" in that direction.

The constant speed at which the i-th particle moves along $\mathbf{e}_{\mathbf{l_{12}}}$ is given by $\dot{\mathbf{r}}_\mathbf{i}(0) \cdot \mathbf{e}_{\mathbf{l_{12}}}$. The speeds along $\mathbf{e}_{\mathbf{l_{12}}}$ of the two particles in mutual motion camouflage ($i = 1, 2$) are always the same, since $\dot{\mathbf{r}}_\mathbf{1}(0) \cdot \mathbf{e}_{\mathbf{l_{12}}} = (\dot{\mathbf{r}}_\mathbf{2}(0) + \dot{\mathbf{r}}(0)) \cdot \mathbf{e}_{\mathbf{l_{12}}} = \dot{\mathbf{r}}_\mathbf{2}(0) \cdot \mathbf{e}_{\mathbf{l_{12}}}$. For $i > 2$, instead, $\dot{\mathbf{r}}_\mathbf{i}(0) \cdot \mathbf{e}_{\mathbf{l_{12}}}$ is in general different from $\dot{\mathbf{r}}_\mathbf{1}(0)) \cdot \mathbf{e}_{\mathbf{l_{12}}}$, hence

the speeds of the other particles along $\mathbf{e_{l_{12}}}$ are in general different from those of particles 1 and 2.

On the plane orthogonal to $\mathbf{e_{l_{12}}}$, each particle fills in time an annular region which depends on its initial conditions, its speed and the value of the gain μ. Let the notation $\mathbf{v_{xy}} \in \mathbb{R}^2$ denote the projection of a vector $\mathbf{v} \in \mathbb{R}^3$ on the plane orthogonal to $\mathbf{e_{l_{12}}}$. Then the centers of the annular regions covered by each particle i, obtained following the same steps of the reconstruction of individual trajectories in section 5.3.1, are given by (here $\delta_{12} \triangleq |\dot{\mathbf{r}}_{\mathbf{12}}(0)|$):

$$\mathbf{r^0_{i,xy}} = \mathbf{r_{i,xy}}(0) - \frac{1}{\delta_{12}^2} \begin{bmatrix} \mathbf{r_{12,xy}}(0) \cdot \dot{\mathbf{r}}_{\mathbf{12,xy}}(0) & -\mathbf{r_{12,xy}}(0) \cdot \dot{\mathbf{r}}^{\perp}_{\mathbf{12,xy}}(0) \\ \mathbf{r_{12,xy}}(0) \cdot \dot{\mathbf{r}}^{\perp}_{\mathbf{12,xy}}(0) & \mathbf{r_{12,xy}}(0) \cdot \dot{\mathbf{r}}_{\mathbf{12,xy}}(0) \end{bmatrix} \dot{\mathbf{r}}_{\mathbf{i,xy}}(0). \tag{5.84}$$

A simple way of verifying (5.84) is to check that there is an invariant manifold with $|\mathbf{r_{i,xy}} - \mathbf{r^0_{i,xy}}| = (\nu_{i,xy}/\delta_{12})|\mathbf{r_{12,xy}}|$, where $\nu_{i,xy} \triangleq |\dot{\mathbf{r}}_{\mathbf{i,xy}}|$ is the constant speed of the particle i on the plane orthogonal to $\mathbf{e_{l_{12}}}$, and (5.84) implies $|\mathbf{r_{i,xy}}(0) - \mathbf{r^0_{i,xy}}| = (\nu_{i,xy}/\delta_{12})|\mathbf{r_{12,xy}}(0)|$.

The particles in mutual motion camouflage ($i = 1, 2$) cover annular regions with common center; in particular, $\mathbf{r^0_{1,xy}} = \mathbf{r^0_{2,xy}} = \mathbf{z_{xy,0}}/2$, where $\mathbf{z_{xy,0}}$ is given by (5.72) (in that equation, $\mathbf{r}$ stands for $\mathbf{r_{12}}$). The centers of the annular regions covered by the other particles ($i > 2$) are instead in general different from each other and from $\mathbf{z_{xy,0}}/2$.

Figure 5.7 shows an example of three-dimensional "swarming motion" obtained with four particles; figure 5.8 is the corresponding two-dimensional projec-

tion on the plane orthogonal to $\mathbf{e_{l_{12}}}$. Notice that in this example all the particles have identical constant speeds. As a result, the annular regions covered by the particles on the plane orthogonal to $\mathbf{e_{l_{12}}}$ have identical radii (but not centers); on the other hand, this does not guarantee equal speeds of motion along the direction $\mathbf{e_{l_{12}}}$.

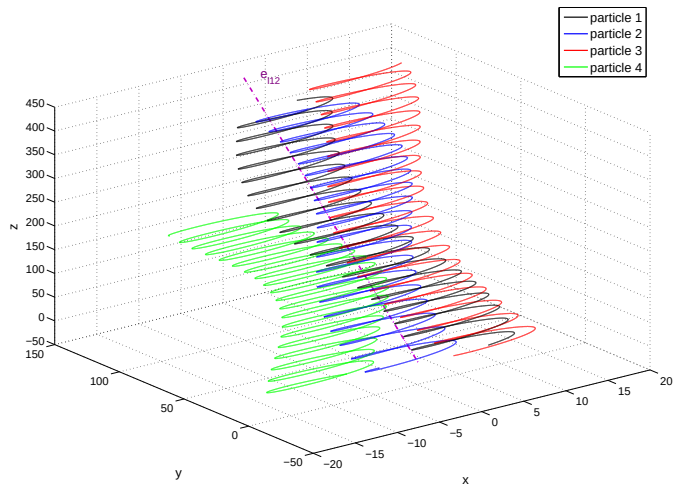

Figure 5.7: Example of representative trajectories with 4 particles.

To obtain a more coherent swarming motion, the initial conditions of the particles not in mutual motion camouflage (i.e. $i > 2$) must satisfy certain conditions, as summarized in the following proposition. These can be thought of as "merging conditions" for the other particles to coherently join the mutual motion camouflage of particles 1 and 2.

Proposition 5.4.3. *If the initial conditions of all particles $i > 2$ satisfy $\dot{\mathbf{r}}_\mathbf{i}(0) \cdot \mathbf{e_{l_{12}}} = \dot{\mathbf{r}}_\mathbf{1}(0) \cdot \mathbf{e_{l_{12}}}$ $(= \dot{\mathbf{r}}_\mathbf{2}(0) \cdot \mathbf{e_{l_{12}}})$ and $\mathbf{r^0_{i,xy}} = \mathbf{r^0_{1,xy}}$ $(= \mathbf{r^0_{2,xy}})$, all the particles move at the same speed in the direction $\mathbf{e_{l_{12}}}$ while covering annular regions with*

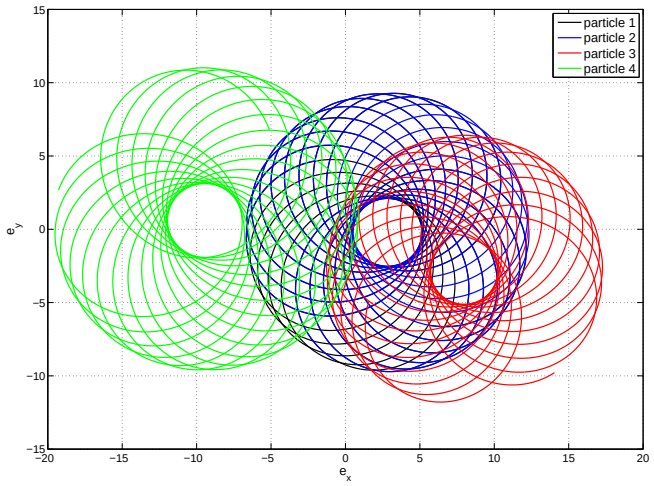

Figure 5.8: Projection on the plane orthogonal to $\mathbf{e_{l_{12}}}$ of the trajectories of figure 5.7.

common center on the plane orthogonal to $\mathbf{e_{l_{12}}}$. *The above conditions can be expressed in terms of initial relative positions and velocities of each particle* $i > 2$ *with respect to particle* 1 *(i.e.* $\mathbf{r_{i1}} \triangleq \mathbf{r_i} - \mathbf{r_1}$ *and* $\dot{\mathbf{r}}_{\mathbf{i1}}$*) as follows:*

$$\dot{\mathbf{r}}_{\mathbf{i1}}(0) \cdot \mathbf{e_{l_{12}}} = 0$$

$$\mathbf{r_{i1,xy}}(0) = \frac{1}{\delta_{12}^2} \begin{bmatrix} \mathbf{r_{12,xy}}(0) \cdot \dot{\mathbf{r}}_{\mathbf{12,xy}}(0) & -\mathbf{r_{12,xy}}(0) \cdot \dot{\mathbf{r}}^{\perp}_{\mathbf{12,xy}}(0) \\ \mathbf{r_{12,xy}}(0) \cdot \dot{\mathbf{r}}^{\perp}_{\mathbf{12,xy}}(0) & \mathbf{r_{12,xy}}(0) \cdot \dot{\mathbf{r}}_{\mathbf{12,xy}}(0) \end{bmatrix} \dot{\mathbf{r}}_{\mathbf{i1,xy}}(0).$$

Figures 5.9 and 5.10 show an example of the coherent swarming motion that can be obtained when the conditions of proposition 5.4.3 are satisfied. Even in this example all the particles have the same constant speed, hence the annular regions covered by the particles on the plane orthogonal to $\mathbf{e_{l_{12}}}$ are identical.

With appropriate choices of speed and initial conditions for the two particles in mutual motion camouflage ($i = 1, 2$), it is also possible to obtain the n-particle

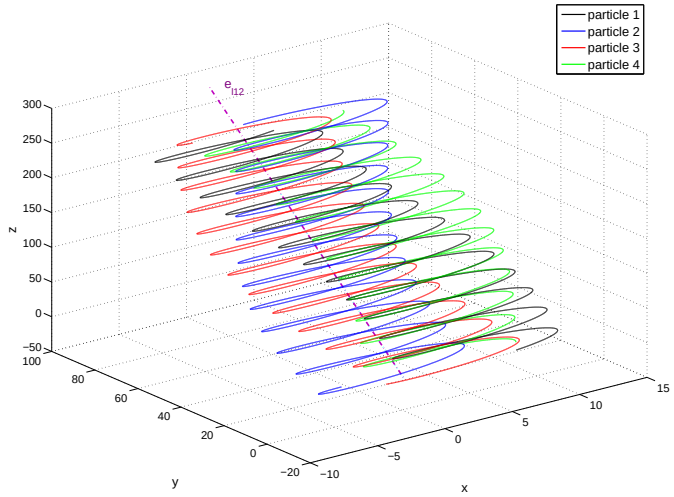

Figure 5.9: Example of trajectories with 4 particles when the conditions of proposition 5.4.3 are satisfied.

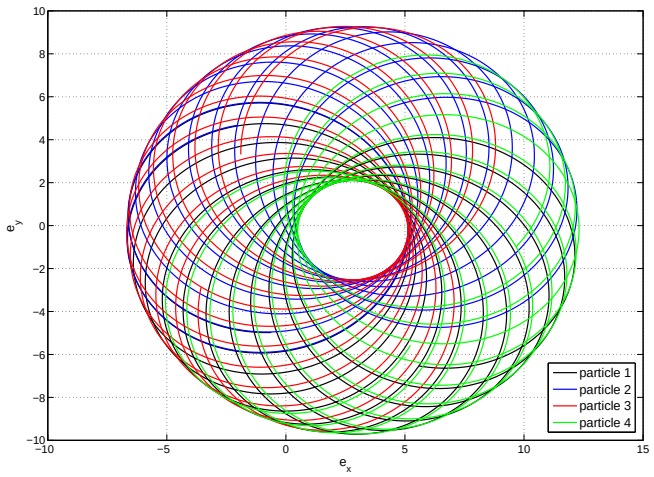

Figure 5.10: Projection on the plane orthogonal to $\mathbf{e_{l_{12}}}$ of the trajectories of figure 5.9.

extensions of the special trajectories described in section 5.3.3. Figure 5.11 shows for example the case in which the first particle moves on a straight line (while the other particles "swarm" around the first one), and the case in which the all the particle trajectories are exact circular helices; note that in both figures the individual speeds were all chosen different from each other.

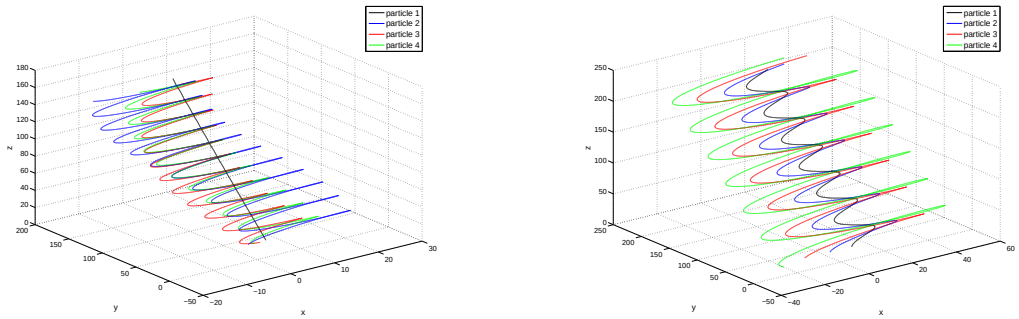

(a) (b)

Figure 5.11: Examples of special trajectories obtained with the swarming motion based on MMC: (a) rectilinear motion of one agent; (b) circular helices.

Chapter 6

Conclusions and future directions of research

In this dissertation, we have presented several mathematical tools for the analysis and synthesis of collective motion in three-dimensional space. The unifying idea is that of considering certain simple motions, that are elementary either from a geometrical point of view or from biological considerations, as potential building blocks for complex collective motions. Decomposing observed collective motions into elementary geometrical components, and studying collective motions that can arise from simple biologically-inspired individual control laws, are two approaches presented here that can help uncover the fundamental mechanisms underlying collective phenomena in nature. The implementation of elementary motions, possibly in decentralized fashion, can also be a useful step in the design of complex coordinated motions for engineered systems, such as teams of robots.

In the following, we summarize the key results and suggest possible future directions of research on the three main topics of this dissertation.

Decomposition and analysis of collective motion

We have geometrically characterized as elementary collective motions those that are either "vertical" or "horizontal" with respect to some fiber bundle structure for an n-particle system. Vertical motions are those along a fiber, i.e. that leave unchanged the projection of the system on a lower-dimensional space; horizontal motions are those orthogonal to the vertical ones, as defined for splitting the instantaneous kinetic energy associated to the motion in two components.

In chapter 3, we have first used this mathematical framework to decompose an arbitrary collective motion into the classical elementary components of rigid translation, rigid rotation and shape transformation, and then derived an alternative fiber bundle structure with associated new types of elementary motions. This fiber bundle, which is the highlight of the chapter, has the remarkable property that both the base space and the fiber are classical manifolds: the space of 3×3 symmetric positive definite matrices and the Stiefel manifold $\mathcal{V}_{n-1,3}$. The vertical motions associated to this bundle, called democratic motions, are those that preserve the coefficient of inertia tensor of the collective, which provides some coarse information on the distribution of particles in space (its second moment). The horizontal motions are instead called inertia tensor deformations, and display a remarkable "duality" with the rigid rotations of the collective, which can be appreciated from the curvature computation for the alternative fibering.

From an abstract geometrical point of view, it would be interesting to study if, and how, this fiber bundle extends to n-body systems in $\mathbb{R}^m$ (with $m > 3$) and

to continuum models in which the discrete particle positions are substituted with a continuous density function (this is relevant for collectives in which $n \to \infty$).

For the analysis of experimental data (positions and velocities) from collective phenomena in nature, we suggest to apply the two decompositions at each time sample and then observe the temporal evolution and the statistical distribution of the kinetic energy allocation to the different elementary components. This provides some quantitative information on what are the predominant components of motion in the observed phenomenon, and could possibly give insight on how the phenomenon can be approximated and modeled. At the very least, the energy decompositions are additional tools at the disposal of researchers trying to understand natural collective motions and to validate (or discard) existing mathematical models of such phenomena.

As a proof of concept, we have applied these ideas to the analysis of a starling flock performing a sharp turn; one of the results we observed is a very strong dominance of the rigid translation component of motion, suggesting a very high degree of coordination in the turn of each individual bird. Of course studying an individual event is not sufficient to draw conclusions on the natural phenomenon studied or on the utility, or lack thereof, of the two decompositions of collective motion. Hence future work should include testing the suggested techniques on multiple collective motion events, possibly across different animal species. We speculate that collective motions performed by different species could be characterized by very different energy distributions, and certain phenomena could be

associated to characteristic "energy signatures". For example we speculate that the swirling motion of certain fish schools could have a dominant component of rigid rotation with respect to the center of the school, whereas the coordinated migration of certain birds could have a strong rigid translation component. Analysis of the energy decomposition statistics might be a useful metric for comparing collective phenomena across different species.

It would also be interesting to explore whether there is any biological relevance to the elementary motions arising from the alternative fiber bundle, for example if there is any natural collective motion that has either democratic motion or inertia tensor transformation as one of its dominant components. Democratic motions could be related to the reshufflings of positions (and maybe of roles) between members of a collective, probably motivated by the individual needs of reducing risk of predation, that have been observed in starling flocks [4].

Finally, a broad direction of research extending these ideas would be to search for other fiber bundle structures, alternative to the two described in this dissertation, to find other geometrically elementary motions and derive alternative decompositions applicable to observed collective motions.

Synthesis of elementary collective motions

In chapter 4, we have exploited the geometrical structure of the alternative fiber bundle to design optimal inertia tensor transformations (minimizing the kinetic energy expenditure) and democratic motions that produce useful reshufflings of the agent positions. Attaining or maintaining a prescribed coefficient of

inertia tensor can be useful for certain applications employing many simple and inexpensive robots, where it might be impossible (or inconvenient) to design and implement motion planning at the individual level; planning the evolution of the coefficient of inertia tensor of the collective, hence controlling the second moment of the distribution of robots in space, could be a viable alternative in these cases. We have also suggested a distributed sensing application in which controlling the coefficient of inertia tensor of the collective would be useful to encode and convey information, such as the covariance of a noisy spatial measurement, to external observers.

We designed optimal inertia tensor transformations by deriving geodesic curves on the manifold of 3×3 symmetric positive definite matrices, equipped with the metric induced by kinetic energy (different from the standard metric on this manifold). One of the key results of this chapter is the analytic expression for the path-energy minimizing geodesic, whenever it exists, that connects an arbitrary initial coefficient of inertia tensor to a desired one (see theorem 4.1.10). The democratic motions were designed instead from gradient vector fields on the Stiefel manifold $\mathcal{V}_{n-1,3}$, and result in the agent positions converging to distributions of interest (e.g. chain-like distribution or symmetrical splitting of the agents in two groups) while preserving the coefficient of inertia tensor.

A significant part of chapter 4 has been devoted to deriving sufficient conditions for the implementation of inertia tensor transformations in decentralized fashion, i.e. with each agent using only local sensing of neighboring agents. The

key result is theorem 4.1.17, which shows that if the directed graph that describes the neighborhood relations admits a spanning tree, then any inertia tensor transformation can be implemented by each agent controlling appropriately its relative motion with respect to the center of mass of its neighborhood. This result can be applied in the implementation of the optimal inertia tensor transformations. Finding distributed implementations of the democratic motions presented in the dissertation appears instead more problematic, and is left to future work.

Another property regarding the practical implementability of these vector fields, is collision-avoidance; for both the optimal inertia tensor transformations and the democratic motions we have designed, simulations show that there exists a wide set of initial configurations guaranteeing collision-free motions, but this set has yet to be determined analytically.

Further directions of research that could be explored include the design of other useful democratic motions; one idea is that of designing democratic motions that produce permutations in the positions of one or more pairs of agents (e.g. agent 1 takes the place that was initially occupied by agent 2, and viceversa). These vector fields could allow to imitate in artificial collectives the role-exchanging and risk-sharing motions which are believed to occur within some animal collectives.

Collective motion based on Motion Camouflage

In chapter 5 we have explored a different approach to the synthesis of collective motion, using a biologically-inspired control law called motion camouflage

proportional guidance as a building block. This control law is a biologically-plausible model, backed by the analysis of experimental data, for how an echolocating bat controls its steering when pursuing an insect prey, such as a praying mantis. As the pursuit strategy used by these bats is geometrically equivalent to one used by dragonflies and hoverflies in their own pursuit encounters, known as motion camouflage with respect to infinity, this control law is of particular biological relevance.

Most of the chapter has been devoted to studying the case of two individuals that are mutually pursuing each other using the motion camouflage proportional guidance law. We showed that the closed-loop dynamics associated to the mutual pursuit (mutual motion camouflage), display very interesting theoretical and practical properties. From a theoretical point of view, we showed that the relative distance dynamics are Lagrangian, and evolve periodically in time along the level sets of a certain "energy" function. The oscillations in the relative distance, and the governing equations, have some similarities with those in the Kepler problem describing the gravitational interaction of two bodies. From a practical point of view, we showed that the resulting individual trajectories are special types of coordinated helices along a common and fixed axis; on the plane orthogonal to the axis, the trajectories fill annular regions with common center and radii proportional to the individual speeds.

Hence this two-unit system supports the hypothesis that complex coordinated motions, in nature as in engineered systems, may be attainable through

local pursuit between members of the collective. In separate publications, we have also exploited the properties of mutual motion camouflage to produce useful trajectories for spatial monitoring applications (see [38] and [40]).

Future directions of research on mutual motion camouflage include the analysis of robustness of the dynamics to the presence of delays and noise in the quantities sensed by the two individuals. Some of the nice properties of mutual motion camouflage, such as the conservation of the "energy function", rely on certain symmetries in the dynamics that would be broken if the two individuals were subject to unequal delays or noise. Nevertheless if the delays and noises were to be "in average" balanced between the two individuals, one might be able to recover an "average" behavior of the system similar to the one obtained in absence of delays and noise.

It would also be interesting to verify if there is any biological relevance to the mutual motion camouflage system; in this context, the territorial aerial battles between two male dragonflies would be the natural candidates for comparison with mutual motion camouflage.

Finally, we have presented an extension of the mutual motion camouflage dynamics to systems with an arbitrary number of agents. This extension is based on having the first two agents engaged in mutual motion camouflage, and each of the other agents appropriately controlling their own steering on the basis of the relative motion between the first two. The result is a kind of "swarming" motion of all the agents in a common fixed direction, uniquely determined by

the initial conditions of the two agents in mutual motion camouflage. A highly coherent swarming motion, with all the agents moving at the same speed along the common direction and covering a common annular region on the plane orthogonal to such direction, can be obtained if the initial conditions of the agents satisfy specific constraints.

Clearly this design has two agents playing a leading role, and all the others acting somewhat as "followers"; it would be interesting to obtain similar swarming behaviors with a more balanced interaction between the agents, i.e. with all the agents playing an equal role towards generating the collective motion.

Another possible direction of research is that of studying which of the geometrically elementary motions of chapter 3 can be synthesized using the motion camouflage proportional guidance law, or some modifications of the same. A preliminary result that we have found is that when n individuals are cyclically pursuing each other with the motion camouflage proportional guidance law, possibly changed in sign, the resulting collective motion is approximately a combination of rigid translation and pure compression or expansion (depending on the sign in the control law).

Bibliography

[1] S. B. Andersson. *Geometric phases in sensing and control*. PhD thesis, University of Maryland, College Park, 2003.

[2] V. Aquilanti, A. Lombardi, and M. B. Sevryuk. Phase-space invariants for aggregates of particles: hyperangular momenta and partitions of the classical kinetic energy. *J. Chem. Physics*, 121(12):5579–5589, 2004.

[3] M. Ballerini, N. Cabibbo, R. Candelier, A. Cavagna, E. Cisbani, I. Giardina, V. Lecomte, A. Orlandi, G. Parisi, A. Procaccini, M. Viale, and V. Zdravkovic. Interaction ruling animal collective behavior depends on topological rather than metric distance: Evidence from a field study. *Proc. Natl. Acad. Sci.*, 105(4):1232–1237, 2008.

[4] M. Ballerini, N. Cabibbo, R. Candelier, A. Cavagna, E. Cisbani, I. Giardina, A. Orlandi, G. Parisi, A. Procaccini, M.Viale, and V. Zdravkovic. Empirical investigation of starling flocks: a benchmark study in collective animal behaviour. *Animal Behaviour*, 76(1):201–215, 2008.

[5] K. A. Berman and X. Liu. Cycles through large degree vertices in digraphs: a generalization of Meyniel's theorem. *J. Comb. Theory, Ser. B*, 74(1):20–27, 1998.

[6] D. P. Bertsekas and J. N. Tsitsiklis. *Parallel and Distributed computation: Numerical Methods*. Prentice-Hall, Englewood Cliffs, NJ, 1989.

[7] G. D. Birkhoff. The restricted problem of three bodies. *Rendi. Circ. Mat. Palermo*, 39:265–334, 1915.

[8] R. L. Bishop. There is more than one way to frame a curve. *The American Mathematical Monthly*, 82(3):246–251, 1975.

[9] A. M. Bloch, J. Baillieul, P. E. Crouch, and J. E. Mardsen. *Nonholonomic mechanics and control*. Springer-Verlag, NY, 2003.

[10] A. M. Bloch, P. S. Krishnaprasad, J. E. Mardsen, and R. M. Murray. Nonholonomic mechanical systems with symmetry. *Arch. Rational Mech. Anal.*, 136:21–99, 1996.

[11] O. Bolza. *Lectures on the calculus of variations*. The University of Chicago press, Chicago, 1904. (see also books.google.com).

[12] R. W. Brockett. Dynamical systems that sort lists, diagonalize matrices, and solve linear programming problems. *Linear Algebra and its applications*, 146:79–91, 1991.

[13] A. Cavagna, A. Cimarelli, I. Giardina, G. Parisi, R. Santagati, F. Stefanini, and M. Viale. Scale-free correlations in starling flocks. *Proc. Natl. Acad. Sci.*, 107(26):11865–11870, 2010.

[14] A. Cavagna, I. Giardina, A. Orlandi, G. Parisi, A. Procaccini, M. Viale, and V. Zdravkovic. The starflag handbook on collective animal behaviour: 1. empirical methods. *Animal behaviour*, 76:237–248, 2008.

[15] T. Chen, S. I. Amari, and Q. Lin. A unified algorithm for principal and minor components extraction. *Neural networks*, 11:385–390, 1998.

[16] C. Chiu. *Adaptive echolocation and flight behaviors in free-flying bats, Eptesicus Fuscus*. PhD thesis, University of Maryland, College Park, 2008.

[17] T. S. Deisboeck and I. D. Couzin. Collective behavior in cancer cell populations. *BioEssays*, 31(2):190–197, 2009.

[18] J. Douglas. Solution of the inverse problem of the calculus of variations. *Trans. Am. Math. Soc.*, 50:71–128, 1941.

[19] A. Edelman, T. A. Arias, and S. T. Smith. The geometry of algorithms with orthogonality constraints. *J. Matrix Anal. Appl.*, 20(2):303–353, 1998.

[20] K. S. Galloway, E. W. Justh, and P. S. Krishnaprasad. Geometry of cyclic pursuit. *Proc. 48th IEEE Conf. Decision and Control*, pages 7485–7490, 2009.

[21] K. Ghose, T. Horiuchi, P. S. Krishnaprasad, and C. Moss. Echolocating bats use a nearly time-optimal strategy to intercept prey. *PLoS Biology*, 4(5):865–873, e108, 2006.

[22] H. Goldstein. *Classical mechanics*. Addison-Wesley, Reading, MA, 1950.

[23] V. Guillemin and A. Pollack. *Differential topology*. Prentice-Hall, Englewood Cliffs, NJ, 1974.

[24] E. Hensor, I. D. Couzin, R. James, and J. Krause. Modelling density-dependent fish shoal distributions in the laboratory and field. *Oikos*, 110(2):344–352, 2005.

[25] J. Hermans. *Rolling rigid bodies with and without symmetries*. PhD thesis, University of Utrecht, 1995.

[26] R. A. Horn and C. R. Johnson. *Matrix analysis*. Cambridge Univ. Press, Cambridge, U.K., 1985.

[27] D. Husemoller. *Fibre bundles*. McGraw-Hill, NY, 1966.

[28] Y. Inada and K. Kawachi. Order and flexibility in the motion of fish schools. *J. Theor. Biol.*, 214:371–387, 2002.

[29] A. Jadbabaie, J. Lin, and A. S. Morse. Coordination of groups of mobile autonomous agents using nearest neighbor rules. *IEEE Trans. Automat. Control*, 48(6):988–1001, 2003.

[30] E. W. Justh and P. S. Krishnaprasad. Equilibria and steering laws for planar formations. *Systems & Control Letters*, 52:25–38, 2004.

[31] E. W. Justh and P. S. Krishnaprasad. Natural frames and interacting particles in three dimensions. *Proc. 44th IEEE Conf. Decision and Control*, pages 2841–2846, 2005.

[32] E. W. Justh and P. S. Krishnaprasad. Steering laws for motion camouflage. *Proc. R. Soc. A*, 462:3629–3643, 2006.

[33] R. G. Littlejohn, K. A. Mitchell, V. Aquilanti, and S. Cavalli. Body frames and frame singularities for three-atom systems. *Physical Review A*, 58(5):3705–3717, 1998.

[34] R. G. Littlejohn, K. A. Mitchell, M. Reinsch, V. Aquilanti, and S. Cavalli. Internal spaces, kinematic rotations, and body frames for four-atom systems. *Physical Review A*, 58(5):3718–3738, 1998.

[35] R. G. Littlejohn and M. Reinsch. Gauge fields in the separation of rotations and internal motions in the n-body problem. *Reviews of Modern Physics*, 69(1):213–275, 1997.

[36] M. Mehyar, D. P. Spanos, J. Pongsajapan, S. H. Low, and R. M. Murray. Asynchronous distributed averaging on communication networks. *IEEE/ACM Trans. Networking*, 15(3):512–520, 2007.

[37] P. W. Michor. *Topics in differential geometry*. American Mathematical Society, Providence, 2008.

[38] M. Mischiati and P. S. Krishnaprasad. Motion camouflage for coverage. *Proc. American Control Conference*, pages 6429–6435, 2010.

[39] M. Mischiati and P. S. Krishnaprasad. The dynamics of mutual motion camouflage. *Submitted for publication*, 2011.

[40] M. Mischiati and P. S. Krishnaprasad. Mutual motion camouflage in 3D. *Proc. 18th IFAC World Congress*, pages 4483–4488, 2011. (see also extended version at http://www.isr.umd.edu/Labs/ISL/PURSUIT).

[41] A. K. Mizutani, J. Chahl, and M. V. Srinivasan. Motion camouflage in dragonflies. *Nature*, 423:604, 2003.

[42] M. Moakher. A differential geometric approach to the geometric mean of symmetric positive-definite matrices. *J. Matrix Anal. Appl.*, 26(3):735–747, 2005.

[43] B. Mohar. The laplacian spectrum of graphs. In Y. Alavi, G. Chartrand, O. R. Oellermann, and A. J. Schwenk, editors, *Graph theory, combinatorics, and applications*, pages 871–898. Wiley, 1991.

[44] R. M. Olberg, A. H. Worthington, and K. R. Venator. Prey pursuit and interception in dragonfies. *J. Comp. Physiol. A*, 186:155–162, 2000.

[45] J. E. Potter. Matrix quadratic solutions. *SIAM J. Appl. Math.*, 14(3):496–501, 1966.

[46] P. V. Reddy. Steering laws for pursuit. Master's thesis, University of Maryland, College Park, 2007.

[47] P. V. Reddy, E. W. Justh, and P. S. Krishnaprasad. Motion camouflage in three dimensions. *Proc. 45th IEEE Conf. Decision and Control*, pages 3327–3332, 2006. (see also arXiv:math.OC/0603176).

[48] S. Smale. Topology and mechanics. I. *Inventiones math.*, 10:305–331, 1970.

[49] D. P. Spanos, R. Olfati-Saber, and R. M. Murray. Distributed sensor fusion using dynamic consensus. *Proc. 16th IFAC World Congress*, 2005.

[50] M. V. Srinivasan and M. Davey. Strategies for active camouflage of motion. *Proc. R. Soc. B*, 259:19–25, 1995.

[51] V. A. Tucker, A. E. Tucker, K. Akers, and J. H. Enderson. Curved flight paths and sideways vision in peregrine falcons (falco peregrinus). *Journal of Experimental Biology*, 203:3755–3763, 2000.

[52] W. T. Tutte. *Graph Theory.* Addison-Wesley, Menlo Park, CA, 1984.

[53] T. Vicsek, A. Czirok, E.B. Jacob, I. Cohen, and O. Shochet. Novel type of phase transitions in a system of self-driven particles. *Phys. Rev. Lett.*, 75:1226–1229, 1995.

[54] E. Wei, E. W. Justh, and P. S. Krishnaprasad. Pursuit and an evolutionary game. *Proc. R. Soc. A*, 465:1539–1559, 2009.

[55] L. Xu. Least mean square error reconstruction principle for self-organizing neural-nets. *Neural networks*, 6:627–648, 1993.

[56] R. Yang, P. S. Krishnaprasad, and W. Dayawansa. Optimal control of a rigid body with two oscillators. In W. F. Shadwick, P. S. Krishnaprasad, and T. S. Ratiu, editors, *Mechanics day*, pages 233–260. AMS Press, 1996.

[57] F. Zhang. *Geometric cooperative control of robot formations*. PhD thesis, University of Maryland, College Park, 2004.